

THE ROLE OF MICRORNAS IN SKIN DEVELOPMENT

Maximilian Edmond Pickup



A thesis submitted in partial fulfilment of the
requirements of Nottingham Trent University for
the degree of Doctor of Philosophy.

July 2022

The copyright in this work is held by the author. You may copy up to 5% of this work for private study, or personal, non-commercial research. Any re-use of the information contained within this document should be fully referenced, quoting the author, title, university, degree level and pagination. Queries or requests for any other use, or if a more substantial copy is required, should be directed to the author.

Acknowledgements

Firstly, I would like to thank Dr. Mohammed Ahmed for his teaching, support, encouragement, and guidance during my Ph.D. I am incredibly grateful for the opportunity to complete a Ph.D. in your lab, and I hope I can live up to the scientist you have sought to teach me to be.

I would like to thank the rest of the members of the Dr. Ahmed lab: Anhua Hu and Hetal Patel for creating a friendly and enjoyable working environment within the lab. I am especially grateful for Anhua's experimental support, troubleshooting, and expertise during FACS and CFA aspects of this project.

I would also like to thank Dr. Graham Hickman for his expertise with microscopy, Dr. Stephen Reed for his expertise and help with FACS, Dr. Andrew Marr and his team for animal work, and Dr. Biola Egbowon for lab support in IBRC.

I would like to thank my parents, Mr. Martin Pickup and Mrs. Iulia Pickup for their unwavering support and encouragement and teaching me valuable skills which have made me the person I am today.

I am so grateful for my friends throughout the PGR community in IBRC, ERD, IStEC, CELS and JvG, as well as friends from outside university, all of whom have made this Ph.D. journey an enjoyable one.

Lastly, I would like to thank my partner, Miss. Chloe Bicknell for her love, encouragement, and patience during my Ph.D. Without your sacrifices, understanding and support, I would not have been able to complete this, for which I am truly grateful.

Abstract

Skin development and hair follicle (HF) cycling are governed by diverse programs of gene modulation through activation and silencing. Post-transcriptional gene expression modulation by microRNAs are another regulatory mechanism to maintain normal skin and HF development and cycling. Here, we identify that miR-148a plays an important role in the regulation of skin homeostasis and HF cycling. RNA and protein analysis of miR-148a and its targets were analysed using both *in vitro* and *in vivo* experiments. Spatiotemporal expression analysis of miR-148a during hair cycling revealed an increase in miR-148a expression during the telogen stage, in the bulge and hair germ stem/progenitor cell compartments, and the differentiated, suprabasal layers of the epidermis. We demonstrate that miR-148a can control proliferation and differentiation programs in primary mouse epidermal keratinocytes. Administration of anti-sense miR-148a inhibitor into dorsal mouse skin during telogen stage of HF cycling accelerated telogen-anagen transition and altered stem cell activity, *in vitro* and *in vivo*. RNA and protein analysis revealed that miR-148a may control these cellular processes, in part, through modulation of Rock1 and Elf5. This data identifies a previously unknown role of miR-148a and novel gene targets in the control of skin and HF homeostasis and modulating stem/progenitor cell populations. This provides a potential target for stem cell biology research and therapeutic targets for the treatment of skin disorders.

Abbreviations

3,3',5-Triiodo-L-thyronine sodium salt	T3
3'-untranslated region	3'UTR
Alkaline phosphatase	AP
alpha-smooth muscle actin	α SMA
Argonaute	Ago
Arrector pili muscle	APM
Atypical protein kinase C	PKC- ζ
Basement membrane	BM
BMP receptor 1 a	BMPR1a
Bone morphogenic protein	BMP
Bovine serum albumin	BSA
Bulge	B
Chondroitin sulfate C	CSC
Complimentary DNA	cDNA
Connective tissue sheath	CTS
Cyclin B2	Ccnb2
Cyclin D1	Ccnd1
Cyclin D2	Ccnd2
Cyclin dependant kinase regulatory subunit 1 / Cdc28 Protein Kinase Regulatory Subunit 1B	Cks1b
Cyclin dependent kinase	Cdk
Cyclin E1	Ccne1
Cytokeratin	Krt

Day	D
Delta Np63	Δ Np63
Dermal papilla	DP
Dermal sheath	DS
Dickkopf 4	Dkk4
DiGeorge critical region 8	Dgcr8
Digoxigenin	DIG
Distal-less homeobox 3	Dlx3
E26 transformation specific	Ets
E74 Like Transcription Factor 5	Elf5
Ectodysplasin A	Eda
Embryonic day	E
Epidermal growth factor	EGF
Exportin-5	Exp5
Extracellular matrix	ECM
Fibroblast growth factor	Fgf
Fluorescent activated cell sorting	FACS
Green fluorescent protein	GFP
Hair follicle	HF
Hair follicle stem cells	HF-SCs
Hair stem	HS
Hairy enhancer of split family member 1	Hes1
Hanks balanced salt solution	HBSS
Inner root sheath	IRS

Involucrin	Ivl
LIM homeobox 2	Lhx2
Matrix	M
Mesoderm	Me
MicroRNA	MiR/miRNA
Minor groove binder	MGB
MiRNA-RISC	MiRISC
Mitomycin C	MMC
Neural tube	NT
N-terminal Transactivating domain p63 alpha	TAp63 α
Nuclear factor kappa B	NF-K β
Nucleotide	Nt
Outer root sheath	ORS
P-cadherin	P-cad
Protein activator of PRK	PACT
Piwi-interacting RNA	piRNA
Planar cell polarity	PCP
Platelet-derived growth factor A	PDG-A
Post-natal day	P
Principal component analysis	PCA
Primary mouse keratinocytes	PMEKs
Protein kinase C	PKC
Rho-Associated Kinase	Rock
RISC loading complex	RLC

RNA induced silencing complex	RISC
RNA interference	RNAi
Room temperature	RT
Sebaceous gland	SG
Secondary hair germ	SHG
Sex-determining region Y-box 9	Sox9
Short interfering RNAs	SiRNA
Smoothened	Smo
Sodium dodecyl sulphate	SDS
Sonic hedgehog	Shh
Stem cell	SC
Stem cell antigen-1	Sca-1
Surface ectoderm	SE
Tar RNA binding protein	TRBP
Transforming growth factor	TGF
Transglutaminase	TG
Transit-amplifying cell	TAC
Tumour necrosis factor	TNF
Uracil-N-glycosylase	UNG
Vitamin D receptor	VDR
Wingless and Int-1	Wnt
Wntless	Wls

Publications

1. PICKUP, M. E., HU, A., PATEL, J. H., AHMED, M. I., 2023. MicroRNA-148a Controls Epidermal and Hair Follicle Stem/Progenitor Cells by Modulating the Activities of ROCK1 and ELF5. *J Invest Dermatol*, 143, 480-491.e5.
2. PICKUP, M. E. & AHMED, M. I. 2020. Detection of MicroRNAs by In Situ Hybridization in Skin. *Methods Mol Biol*, 2154, 187-196.
3. AHMED, M. I., PICKUP, M. E., RIMMER, A. G., ALAM, M., MARDARYEV, A. N., POTERLOWICZ, K., BOTCHKAREVA, N. V. & BOTCHKAREV, V. A. 2019. Interplay of MicroRNA-21 and SATB1 in Epidermal Keratinocytes during Skin Aging. *J Invest Dermatol*, 139, 2538-2542.e2.

Contents

1.0 Introduction	1
1.1 Skin Function, Morphology and Signalling Pathways	1
1.1.1 The Epidermis	2
1.1.1.1 The Basal Layer	4
1.1.1.2 The Spinous Layer	7
1.1.1.3 The Granular Layer	8
1.1.1.4 The Stratum Corneum	9
1.1.2 The Dermis	11
1.1.3 Appendages of the Skin	12
1.2 The Hair Follicle	14
1.2.1 The Hair Shaft	16
1.2.2 The Inner Root Sheath	18
1.2.3 The Outer Root Sheath	19
1.2.4 The Hair Bulb	20
1.2.5 The Connective Tissue Sheath	22
1.3 Hair Follicle Morphogenesis	23
1.3.1 Induction	24
1.3.2 Organogenesis	27
1.3.3 Cytodifferentiation	30
1.4 Hair Follicle Cycling	31

1.4.1 Telogen	34
1.4.2 Anagen	37
1.4.3 Catagen	41
1.4.4 Exogen	43
1.5 Hair Follicle Stem Cells	44
1.6 MicroRNAs	51
1.6.1 MiRNA Biogenesis	52
1.6.2 Post-transcriptional Regulation of Gene Expression	58
1.6.3 Regulation of MiRNAs	59
1.6.4 MiRNAs in Skin and Hair Follicle Development	61
1.6.5 MiRNAs in Hair Follicle Cycling	63
1.6.6 MiRNAs in Skin Disease	65
1.7 E74 Like Transcription Factor 5 (Elf5)	67
1.8 Rho-Associated Kinase (Rock) 1	68
1.9 Aims	71
2.0 Materials and Methods.....	72
2.1 Materials Used in the Investigation	72
2.1.1 Reagents and Chemicals Used During the Investigation	72
2.1.2 Transfection and Transduction Regents Used During the Investigation ..	75
2.1.3 Plasticware and Tools Used During the Investigation	75
2.1.4 Kits Used During the Investigation	76

2.1.5	Machines Used During the Investigation	77
2.1.6	Antibodies Used During the Investigation	78
2.1.7	Primers Used During the Investigation	79
2.2	Methods Used in the Investigation	81
2.2.1	Animals	81
2.2.2	MicroRNA Microarray	81
2.2.3	Cell Culture and Transfection	82
2.2.4	Flow Cytometry	83
2.2.5	Real-Time Quantitative PCR (RT-qPCR)	83
2.2.6	Western Blotting	85
2.2.7	<i>In Situ</i> Hybridisation	86
2.2.8	Fluorescent <i>In Situ</i> Hybridisation	87
2.2.9	RNA Sequencing Analysis	87
2.2.10	MiRNA-148a Gene Target Prediction	88
2.2.11	Luciferase Reporter Assay	88
2.2.12	Pharmacological Treatment of Mouse Skin	89
2.2.13	Alkaline Phosphatase Staining	90
2.2.14	Immunohistochemistry	90
2.2.15	Immunocytochemistry	91
2.2.16	Fluorescence Activated Cell Sorting (FACS)	91

2.2.17	Production of Anti-miR-148a and Control Expressing Lentiviruses	92
2.2.18	Colony Forming Assay	93
2.2.19	Image Fluorescence Quantification Analysis	93
2.2.20	Statistical Analysis	94
3.0	Results	95
3.1	Spatiotemporal Expression Analysis of MiRNA-148a During Hair Follicle Cycling	95
3.2	Identification of Novel Targets of MiRNA-148a In Epidermal Keratinocytes	103
3.3	MiRNA-148a Modulation of Cellular Proliferation and Differentiation Processes, <i>In Vitro</i>	112
3.4	Functional Analysis of MiRNA-148a Expression on Stem Cells <i>In Vitro</i> and <i>In Vivo</i>	120
3.5	Analysis of the Effects of MiRNA-148a Inhibition During Skin Homeostasis, <i>In Vivo</i>	128
4.0	Discussion	135
4.1	MiRNA-148a is Highly Expressed in Stem Cell Regions of Telogen Hair Follicles	135
4.2	Rock1 and Elf5 are Direct Targets of MiRNA-148a	138
4.3	MiRNA-148a Alters Proliferation and Differentiation Programs in Primary Mouse Epidermal Keratinocytes, <i>In Vitro</i>	142

4.4 Inhibition of MiRNA-148a Accelerates Telogen-Anagen Transition, and Modifies Stem Cell Activity, <i>In Vitro</i> and <i>In Vivo</i>	147
4.5 Inhibition of MiRNA-148a Leads to Increased Activity of Rock1 and Elf5, <i>In Vivo</i>	149
5.0 Conclusion	153
6.0 Future Directions	155
7.0 Appendix	157
Appendix 1. MicroRNA Microarray	157
Appendix 2. Cell Culture and Transfection	157
Appendix 3. Cell Cycle Analysis by Flow Cytometry	160
Appendix 4. Transcriptomic Analysis of Total RNA	160
Appendix 5. Transcriptomic Analysis of TaqMan Targets	165
Appendix 6. Proteomic Analysis by Western Blot	167
Appendix 7. <i>In Situ</i> Hybridization	173
Appendix 8. RNA Sequencing Analysis	174
Appendix 9. Generation of MiR-148a Binding Site Clones	177
Appendix 10. Generation of MiR-148a Binding Site Mutated Clones	182
Appendix 11. Validation of Clones by Sanger Sequencing	183
Appendix 12. Luciferase Bioluminescence Reporter Assay	185
Appendix 13. Pharmacological Inhibition of MiR-148a <i>In Vivo</i>	186
Appendix 14. Alkaline Phosphatase Staining for Morphological Analysis	186

Appendix 15. Immunofluorescent Analysis	187
Appendix 16. Fluorescence activated cell sorting of hair Follicle Bulge Stem Cells	187
Appendix 17. Lentiviral Production and Transduction of Hair Follicle Bulge Stem Cells	188
Appendix 18. Statistical Analysis	192
8.0 References	194

List of Figures

Figure. 1 The Structure of the Skin	3
Figure. 2 Epidermal Development in Mice	10
Figure. 3 The Structure of the Mature Hair Follicle	15
Figure. 4 Induction Stage of Hair Follicle Morphogenesis	27
Figure. 5 Organogenesis stage of Hair Follicle Morphogenesis	30
Figure. 6 The Post-natal Hair Cycle	33
Figure. 7 Stem Cell Compartments and markers in the Telogen Hair Follicle	51
Figure. 8 Schematic Depiction of MiRNA Transcription	53
Figure. 9 MicroRNA Biogenesis Pathway	55
Figure. 10 MicroRNA Strand Selection	57
Figure. 11 Analysis of MiR-148a Expression in Skin and During Hair Follicle Cycling	98
Figure. 12 Expression Analysis of MiRNA-148a in Stem Cell Populations in Skin and Hair Follicles	101
Figure. 13 Global Gene Expression Profiling after MiRNA-148a Overexpression in Primary Mouse Epidermal Keratinocytes	105
Figure. 14 MiRNA-148a Target Analysis Revealed Rock1 and Elf5 are Inversely Expressed to MiRNA-148a.....	107
Figure. 15 Co-localisation of MiRNA-148a and Gene Targets Rock1 and Elf5 Within the Epidermis and Hair Follicle Stem Cell Compartments	109

Figure. 16 MiRNA-148a Regulates Proliferation of Primary Mouse Epidermal Keratinocytes, <i>In Vitro</i>	113
Figure. 17 MiRNA-148a Regulates Differentiation of Primary Mouse Epidermal Keratinocytes, <i>In Vitro</i>	115
Figure. 18 Overexpression of miRNA-148a Inhibits Nuclear Localization of Rock1 and Elf5 in Differentiated Primary Mouse Epidermal Keratinocytes	117
Figure. 19 MiRNA-148a Inhibition Promotes Colony Forming Abilities of Hair Follicle Stem Cells, <i>In Vitro</i>	122
Figure. 20 MiRNA-148a Inhibition Accelerates Telogen to Anagen Transition, <i>In Vivo</i>	124
Figure. 21 MiRNA-148a Inhibition Alters Stem Cell Activity in Skin, <i>In Vivo</i>	126
Figure. 22 Loss of MiRNA-148a Alters Expression of Cytokeratin 1, But Not Ki67, <i>In Vivo</i>	129
Figure. 23 MiRNA-148a Inhibition Alters Rock1 and Elf5 Expression During Skin and Hair Follicle Development, <i>In Vivo</i>	132
Figure. 24 Working Model: The Mechanism of Action of MiR-148a in Modulating Stem/Progenitor Cells during Skin development and Hair Follicle Cycling	154
Figure. 25 Example of an RNA Integrity Analysis by Gel Electrophoresis	162
Figure. 26 Example of a BCA Calibration Plot for Determining Protein Concentration	168
Figure 27. Example of a Ponceau Stained Protein Transferred Nitrocellulose Membrane	171

Figure 28. A Chromatogram of Sanger Sequenced PsiCHECK-2 Cloned with MiR-148a Binding Site from Elf5 3'UTR and its Corresponding Mutation 184

List of Tables

Table 1. Laboratory Regents/Chemicals Used in the Investigation	72
Table 2. Transfection/Transduction Reagents Used in the Investigation	75
Table 3. Plasticware and Tools Used in the Investigation	75
Table 4. Kits Used in the Investigation	76
Table 5. Machines Used in the Investigation	77
Table 6. List of Antibodies Used in the Investigation	78
Table 7. List of Primers Used for RT-qPCR in the Investigation	79
Table 8. Volumes of Reagents for Cell Transfection Using MiRNAs or Plasmids in Different Sized Cell Culture Plates	159
Table 9. 43 potential gene targets of miR-148a were identified from overlapping of analysed RNA-seq data and online target prediction tools	175

1.0

Introduction

1.1 Skin Function, Morphology and Signalling Pathways

The skin is a multi-layered, stratified, and self-renewing organ that provides a protective layer around the body. The skin is the human body's largest organ and is indispensable for normal bodily functions and homeostasis, and a dynamic and multifaceted tissue (Tobin, 2006). The main functions of skin are to protect organs from water loss, pathogens, and UV radiation damage from the sun (Tobin, 2006, Fuchs, 2007, Proksch et al., 2008, Blanpain and Fuchs, 2009, Serre et al., 2018).

The skin consists of three main layers: 1, The outermost epidermis, a keratinized epithelium that forms a tough first line of defence against external insult. 2, The layer beneath the epidermis, is the dermis, which contains many of the skin's appendages such as hair follicles (HFs) and sweat glands, and 3, The hypodermis, located beneath the dermis, is a connective network of adipose tissue and vascular vessels that support and supply the dermal appendages (Figure. 1) (Fuchs and Raghavan, 2002).

The epidermis derives from the ectodermal germ layer of the blastula during mouse embryonic development where a single epidermal layer forms between embryonic day (E) 9.5 – E12.5 (Fuchs and Raghavan, 2002, Blanpain and Fuchs, 2009). The dermis is derived from the mesoderm, with dorsal skin deriving from the dermomyotome, and first forms at approximately E11.5 in mice (Atit et al., 2006, Fuchs, 2007).

Mouse skin is one of the best models for analysis of the mechanisms of skin and hair development/regeneration, wounding, and ageing. Both humans and mice share

similar developmental and healing mechanisms in the skin, which is controlled by conserved growth factor/signalling pathways, although, there are species specific gene expression profiles that indicate the limitations of the mouse model (Gerber et al., 2014). However, genetic tractability of mice permits generation of the complex transgenic mice and *in vivo* modulation of gene expression, mice provide a valuable model for functional analysis and experiments that are not possible in humans, whilst maintaining relevant insights into skin regulatory pathways and homeostasis.

The Epidermis

The epidermis is the outermost layer of the skin and is the 'first-line of defence' against external pathogens and radiation. The epidermis is characterised by several layers and contains distinct stem cell (SC) populations, which give rise to the other cell types of the epidermis and located in the lowest basal layer. Above the basal layer resides the spinous layer, followed by the granular and lastly, the outermost layer is the stratum corneum, a keratinized dead layer of cells, forming the outer barrier of the skin (Figure. 1) (Fuchs, 2007).

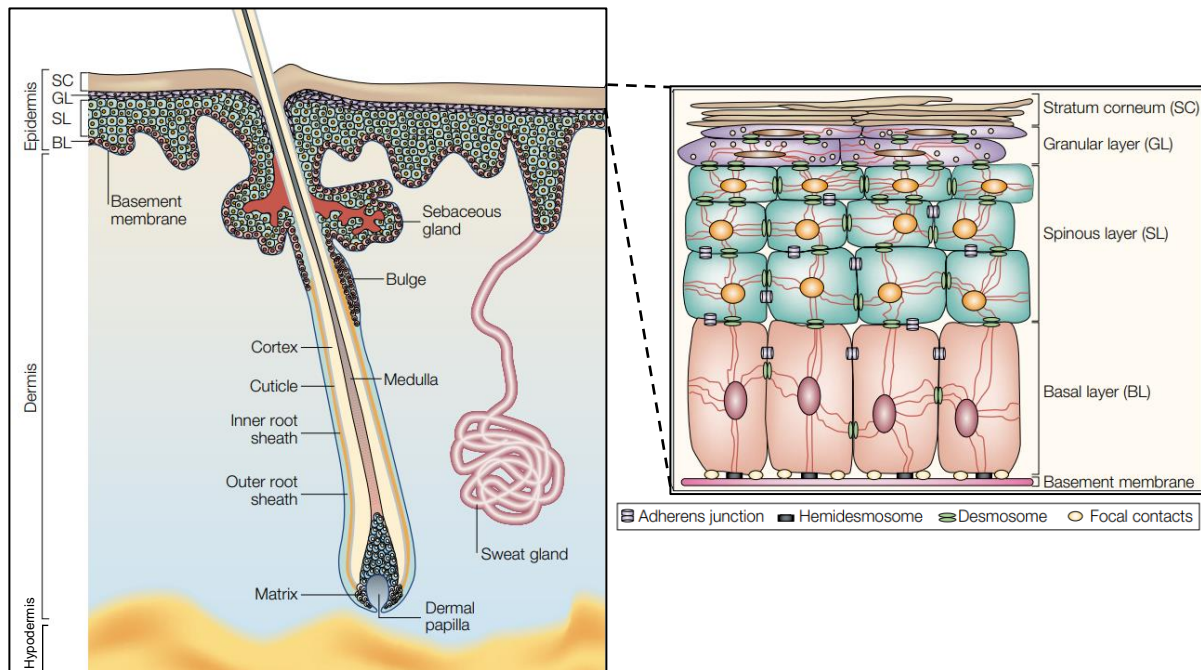


Figure 1. The Structure of the Skin.

The Skin contains three layers, the innermost hypodermis, the dermis, and the outermost epidermis. The dermis contains many of the appendages found in the skin including the HF. The epidermis is a stratified epithelium which derives from proliferating basal stem cells in the basal layer (BL), which transition through the spinous layer (SL) and granular later (GL) to form the outer barrier of dead, keratinized cells of the stratum corneum (SC). Adapted from (Fuchs and Raghavan, 2002).

Cytokeratins (Krts) are intermediate filaments that form structural components of cells. There are two types of cytokeratin filaments, type I and type II, each deriving from distinct proteins. Type I cytokeratins include Krt9-20 and type II cytokeratins include Krt1-8 (Fuchs and Weber, 1994). Basal cells are characterised by Krt5, Krt14 and Krt15 expression. Cells from the basal layer terminally differentiate into the spinous and granular layer, where cytokeratin markers, Krt1, Krt10 are expressed. The stratum corneum is characterised by loricrin and filaggrin expression, essential for formation

of an impermeable cell scaffold (Fuchs and Green, 1980, Dale et al., 1985, Byrne et al., 1994, Fuchs, 2007).

Epidermal morphogenesis is primarily initiated by wingless and Int-1 (Wnt) signalling during embryogenesis by blocking ectodermal response to fibroblast growth factors (Fgfs), causing ectodermal progenitor cells to express bone morphogenic proteins (BMPs) and commit to an epidermal fate. BMP4 has been shown to inhibit neural development and cause ectodermal progenitors to develop into Krt8 and Krt18 expressing surface ectodermal cells, which give rise to the epidermis at approximately E8.5 in mice (Wilson and Hemmati-Brivanlou, 1995, Wilson et al., 2001, Lim and Nusse, 2013, Liu et al., 2013). These surface ectodermal progenitors are protected by the periderm which is shed once the basal cells begin to stratify into other epidermal cells (Figure. 2) (M'Boneko and Merker, 1988, Hu et al., 2018a). Along-side early epidermis formation, the basement membrane which defines the bottom-most part of the epidermis, which separates the epidermis from the dermis, is formed. Integrins anchor the basal cells to the basement membrane, namely $\alpha_6\beta_4$ integrins in hemidesmosomes and $\alpha_3\beta_1$ integrins in focal adhesion complexes, binding to keratin and actin filaments respectively with both binding to the extracellular matrix (ECM) of the basement membrane *via* laminin 5 (Watt, 2002, Fuchs, 2007).

1.1.1.1 The Basal layer

The basal layer resides just above the dermis and contains a distinct SC population (Figure. 1). It is characterised by expression of cytokeratin filaments Krt5 and Krt14 and is formed at approximately E8.5-9.5 in mice (Figure. 2) (Fuchs and Green, 1980, Koster and Roop, 2007). Basal cells self-renew and maintain their own distinct SC population by symmetric cell division, maintain attachment to the basement membrane

and are highly proliferative. Basal cells also give rise to the other cell types of the epidermis through the commitment process of epidermal stratification, beginning at E8.5 in mice (Fuchs, 2007, Koster and Roop, 2007).

During epidermal stratification, basal cells divide asymmetrically, perpendicular to the basement membrane and is characterised by a commitment to terminal differentiation program and restriction of proliferation (Lechler and Fuchs, 2005, Fuchs, 2007, Ray and Lechler, 2011). At the beginning of epidermal stratification, basal cells differentiate into spinous cells (although basal cells first differentiate into a Krt1/10 expressing intermediate layer during skin morphogenesis, Figure. 2), in part through tumour protein p63 isoform expression gradient (Koster et al., 2004, Koster et al., 2007, Fuchs, 2007).

P63 family of proteins have shown to be essential in skin development and homeostasis, with knockout mice models resulting in a failure of epidermal differentiation (Mills et al., 1999, Yang et al., 1999). P63 isoform; N-terminal transactivating domain p63 alpha (TAp63 α) is required for initial commitment of ectodermal progenitors into Krt14 expressing basal cells (Koster et al., 2004, Romano et al., 2007). Although TAp63 α is required for initial cell commitment, p63 isoform Delta Np63 (Δ Np63) is required for maintenance of Krt14 expressing basal cells and maintenance of basement membrane integrity (Koster et al., 2004, Koster and Roop, 2007).

Δ Np63 expression during dividing epidermal basal cells is induced by BMP2, BMP7 and Fgf10 expression (Koster et al., 2004, Laurikkala et al., 2006). Δ Np63 along with E26 transformation specific (Ets) and other transcription factors, bind to a conserved motifs in the Krt14 enhancer region, where Δ Np63 plays an important role in

maintaining basal cell identity (Romano et al., 2007). In *p63*-null embryos, the skin does not stratify and express *Krt8* and *Krt18* – markers for early ectodermal progenitors (Koster and Roop, 2004, Hu et al., 2018a). Notably, *p63*-null embryos resulted in a lack of mInsc-LGN-Par3 accumulation on the apical side of basal cells, preventing asymmetric division and epidermal stratification (Lechler and Fuchs, 2005).

P63 has also been shown to regulate *Satb1* during epidermal morphogenesis. Knockout of *Satb1* or *p63* in mice resulted in abnormal epidermal morphology, altered chromatin structure, and a decrease in expression of differentiation related genes, including *loricrin* and *Involucrin*. Gain of *Satb1* partially rescued the epidermal phenotype of *p63* deficient mouse skin and *Satb1* was shown to be a direct target of *p63* (Fessing et al., 2011).

Cbx4 has also been shown to be a direct target of *p63*. *Cbx4* functions to control epidermal proliferation and differentiation during epidermal stratification. *Cbx4* knockout resulted in a decrease in epidermal thickness, cellular proliferation, and an increase in neuronal specific genes, whereas gain of *Cbx4* expression partially rescued the epidermal phenotype of *p63* deficient mouse skin (Mardaryev et al., 2016). Together these show the importance of *p63* regulation programs in epidermal morphogenesis and stratification during skin development.

Asymmetric division of basal cells has been shown to be essential for epidermal stratification (Smart, 1970, Lechler and Fuchs, 2005). Basal cell asymmetric division is driven by α -catenin recruitment of atypical protein kinase C (PKC- ζ) and mInsc-LGN-Par3 complex, which align at the apical side of the basal cell. PKC- ζ is apically orientated from the basement membrane by β_1 integrin expression (Lechler and Fuchs, 2005, Ray and Lechler, 2011). Asymmetric basal cell division and epidermal

stratification gives rise to the spinous layer and subsequent granular layer and the stratum corneum, however, there are several other cell types found within the basal layer that contribute to maintaining homeostasis in healthy skin (Tobin, 2006).

Within the basal layer, several other cell types are located. These include melanocytes, which are neural crest derived cells produce melanin granules called melanosomes that protect skin from UV radiation (Tobin, 2006, Cichorek et al., 2013), and Merkel cells which function as mechanoreceptors for touch sensation of the skin (Tobin, 2006, Morrison et al., 2009).

1.1.1.2 The Spinous Layer

The spinous layer is characterised by expression of Krt1, Krt10 and Involucrin, and forms a network of cells joined by desmosomes in order to strengthen the skin to physical insult (Figure. 1) (Byrne et al., 1994, Li et al., 2000, Fuchs and Raghavan, 2002). Spinous cells develop at approximately E15 in mice (Figure. 2) (Liu et al., 2013). This layer also consists of specialised Langerhans cells which function as immunological cells against pathogens. Langerhan cells are dendritic cells that extend throughout the stratified epidermis to sense pathogen infection throughout the epidermis and initiate an appropriate immune response, to protect the rest of the body (Kubo et al., 2009, Clayton et al., 2017).

The spinous layer develops from a feedback mechanism of epidermal Wnt signalling. Wnt signalling in the basal layer regulates the Δ Np63 expressing proliferative basal cells and causes a feedback cascade through dermal BMP2/4 - Smad1/5/8/ - Fgf7/10 pathways resulting in Δ Np63 expressing cells to undergo terminal differentiation into the spinous layer (Zhu et al., 2014).

Notch signalling has been implicated to play an important role in promoting epidermal terminal cell differentiation from basal cells into the spinous layer and a switch from Krt5/14 expression to Krt10/1. Notch signalling in differentiating keratinocytes has a complex relationship with p63 expression. Generally, Notch signalling is upregulated as cells differentiate from the basal layer and p63 is downregulated. P63 directly targets and inhibits notch promoted transcription factor, hairy enhancer of split family member 1 (Hes1), which is required for maintenance of spinous cells and prevents premature differentiation into the granular layer (Blanpain et al., 2006, Moriyama et al., 2008). Hes1 could be used as a relay for gradual switching of p63 mediated proliferative cells to Notch mediated differentiating cells (Nguyen et al., 2006a, Tadeu and Horsley, 2013).

1.1.1.3 The Granular Layer.

The Granular layer differentiates from the spinous layer (Figure. 1) at E16.5 in mice (Liu et al., 2013). This layer is characterised by expression of loricrin, filaggrin and transglutaminase (TG) (Figure. 2) (Koster and Roop, 2007). The granular cell layer and overlying stratum corneum cell layer become differentiated by an increasing extracellular calcium (Ca^{2+}) gradient, resulting in protein kinase C (PKC) activation (Koster and Roop, 2007, Fuchs, 2007, Liu et al., 2013). PKC contributes to downregulation of Krt1 and Krt10 as well as induction of loricrin, filaggrin and TG (Koster and Roop, 2007). PKC has been shown to target distal-less homeobox 3 (DLX3) in driving keratinocyte differentiation through Ca^{2+} mediated differentiation (Palazzo et al., 2017). PKC activates TG and in turn, loricrin expression, which by generating γ -glutamyl ϵ -lysine crosslinks, forms keratin vesicles/lamellar bodies which form tough keratin macrofibril scaffold (Fuchs, 2007, Bains, 2013). Granular cells produce keratohyalin granules, made up mainly of profilaggrin protein that is required

for crosslinking with keratins and creating the final barrier of the epidermis (Sandilands et al., 2009).

1.1.1.4 The Stratum Corneum

The stratum corneum is the outermost layer of the epidermis, a keratinized layer of flat, cornified keratinocytes that serves as the first line of defence against external microbes and insult (Figure. 1). It is formed by E18.5 in mice and is continuously shed as keratinocytes from the basal layer differentiate towards the stratum corneum to replace the continuously lost cells (Figure. 2) (Fuchs, 2007, Liu et al., 2013). As cells from the granular layer are pushed towards the surface of the epidermis, Keratohyalin granules are broken down and profilaggrin dephosphorylated and cleaved by serine proteases into filaggrin (Sandilands et al., 2009). Lamellar bodies/granules are produced from acidification of the Golgi apparatus. These granules provide lipid membrane and along with cell death and degradation of cellular organelles help to form the cornified wall (Tarutani et al., 2012). Loricrin, a substrate of the enzyme TG-1, makes up about 70% of the cornified envelope (Tharakan et al., 2010). Together, TGs catalyse the components: filaggrin, loricrin, Involucrin, lipid bilayers, keratins and other proteins to form a tight cornified cytoskeleton that blocks entry of foreign pathogens into the epidermis (Bickenbach et al., 1995, Fuchs and Horsley, 2008, Nithya et al., 2015).

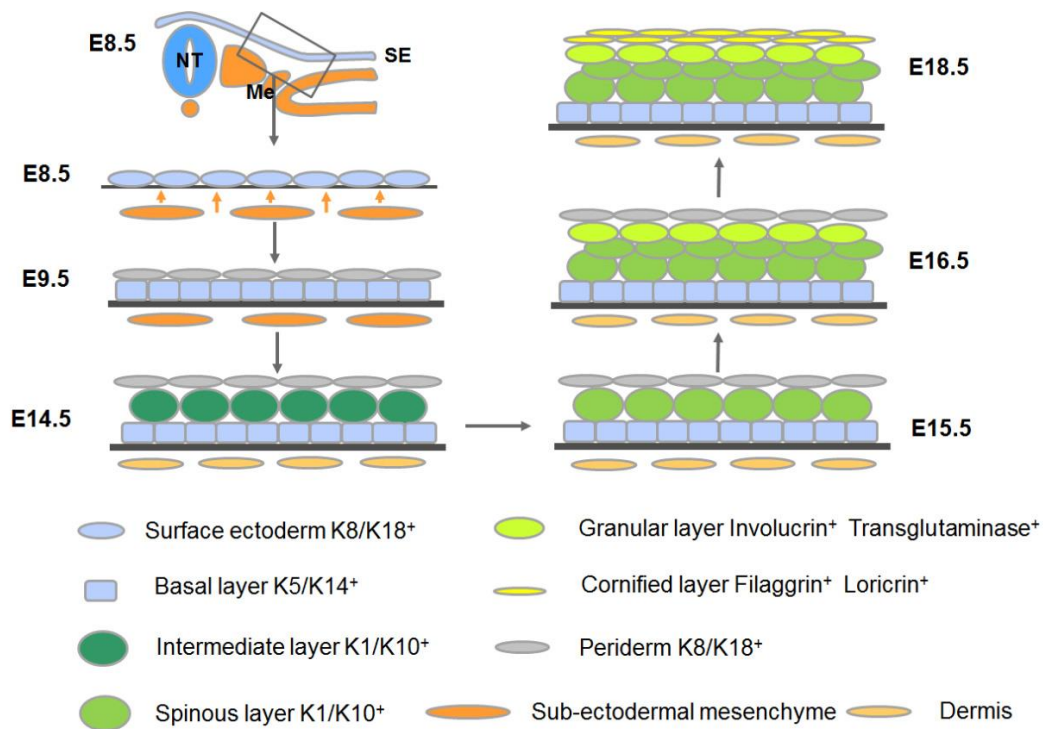


Figure 2. Epidermal Development in Mice.

The epidermis derives from *Krt8/Krt18* expressing surface ectodermal (SE) cells, whereas the dermis derives from the mesoderm at embryonic day (E) 8.5. Stratification begins at E8.5-9.5 with the formation of *Krt5/14* expressing basal layer and *Krt8/18* expressing periderm which protects the early epidermal cells. The *Krt1/10* expressing intermediate layer forms from asymmetrically dividing $\Delta Np63$ expressing basal cells at E12.5-14.5. The spinous layer differentiates from the intermediate layer with inhibited expression of $\Delta Np63$ and increase expression of *Notch1*. The granular layer characterised by PKC activation and along with TG activation and *DLX3* targeting, forms keratohyalin granules, lamellar bodies and loricrin expression. The stratum corneum are keratinized layers of flattened, dead keratinocytes, tightly joined by a cytoskeleton comprised of filaggrin, Involucrin, loricrin, keratins and lipid bilayers. NT: neural tube, Me: mesoderm, SE: surface ectoderm (Liu et al., 2013).

1.1.2 The Dermis

The dermis is a connective layer of the skin and primarily made up of fibrous components in order to support the main appendages found in this layer (Tobin, 2006). It is separated from the epidermis by the basement membrane and is derived from the mesoderm in developing embryos (Atit et al., 2006). Lineage tracing in mice has shown that fibroblasts derive from two distinct lineages which make up the two sublayers of the dermis, the upper papillary layer, and the lower reticular layer. The upper papillary layer is involved in hair growth, whereas the reticular layer forms the bulk of the dermal cell type and adipocytes found in the hypodermis (Driskell et al., 2013). Both layers are rich in collagen I and III fibres with the reticular layer containing a dense fibrous network connecting the lower dermis to the fatty layer of the hypodermis. Both layers have the ability to undergo adipogenic differentiation, and required for synthesis of the extracellular matrix, which plays an important role in controlling cell behaviour through growth factors and signalling pathways as well as a scaffold for cell adhesion (Krieg and Aumailley, 2011, Korosec et al., 2019, Rippa et al., 2019). Markers for the two layers has been established in human skin, FAP⁺CD90⁻ upper papillary fibroblasts and FAP⁻CD90⁺ lower reticular fibroblasts, however the two cell populations are not completely separated, with a gradient of cell types across the dermis (Korosec et al., 2019). From E16.5 in mice, markers for papillary fibroblasts CD26 and Blimp1 and marker for reticular fibroblasts Sca1 were established (Driskell et al., 2013, Rippa et al., 2019). The papillary and reticular layer are separated by a rete subpapillare, a vascular plexus of fibroblasts, which contain capillaries for supply to the upper dermis. A second, lower vascular plexus, the rete cutaneum, forms a barrier between the reticular layer and the hypodermis (Sorrell and Caplan, 2004).

Fibroblasts make up the majority of cells within the dermis and play distinct roles in both skin structural integrity by producing collagen and regeneration during wound healing (Woodley, 2017, Rippa et al., 2019, Korosec et al., 2019). There are also other cell types found in the dermis, which include mast cells, that release histamine to promote immunological response, and macrophages and neutrophils can also be found in the lower dermis which help to maintain skin as a barrier to the body against infection (Tobin, 2006, Forni et al., 2012). Another specialized fibroblast population of the developing epidermis are dermal papilla (DP) cells. These act as SC-like cells and play an integral part during HF cycling (Driskell et al., 2011).

1.1.3 Appendages of the Skin

The dermis contains many important appendages found in the skin. The sebaceous gland is populated with sebocytes and is a sebum producing gland located in the reticular layer of the dermis. These glands functions to keep the skin lubricated and hydrated (Tobin, 2006, Sakuma and Maibach, 2012). Growth of the DP initiates generation and differentiation of the pilosebaceous gland. The sebaceous gland is developed from initial HF morphogenesis by SRY (Sex-determining region Y)-box 9 (Sox9) expressing progenitor cells of the invaginating HF (Nowak et al., 2008). The sebaceous gland is populated by migrating multipotent bulge SCs in the post-natal HF. Blimp1 expressing unipotent progenitor sebocytes control the production and differentiation of progenitor sebocytes into mature, sebum secreting sebocytes. These Blimp1 expressing progenitor cells are also capable of self-renewing, indicating another sub population of progenitor cells within the skin (Horsley et al., 2006, Tóth et al., 2011).

Eccrine sweat glands are other appendages of the skin and their main role is thermoregulation (Tobin, 2006). They are restricted to the footpads of mice and develop at E17.5 in mice and are comprised of a secretory coil with a duct leading to where the sweat is excreted (Lu et al., 2012, Hu et al., 2018b). Eccrine sweat glands are located in the upper dermis with a long thin duct that secretes sweat directly on the surface of the skin (Cui and Schlessinger, 2015).

Development of eccrine sweat glands occurs at E17.5 from Krt14 expressing ectodermal progenitor cells (Lu et al., 2012). Wnt signalling is required for initial development, followed by ectodysplasin A (Eda) and Sonic hedgehog (Shh) signalling with inhibition of Wnt, Eda and shh signalling resulting in a block in initial pre-germ gland development, duct formation and final duct formation respectively (Cui et al., 2014).

In humans, apocrine glands are much larger than eccrine and located in the fatty layer of the hypodermis with short ducts that secrete sweat into the HF canal. They are naturally numerous around hairier regions of the body such as the axilla and perineum (Lu and Fuchs, 2014). Apocrine glands are absent in mice and little is known about their development in humans, however, using sheep models, it is suggested that apocrine sweat glands develop from the outer root sheath (ORS) of the HF, initially by Wnt signalling and then positively regulated by BMP signalling (Lu and Fuchs, 2014, Li et al., 2018). The HF is another key appendage of the skin. It has been described as a 'dynamic mini organ' due to its multi cellular components working together in a cyclic fashion with bouts of growth and regression from its own distinct stem/progenitor cell populations, and an integral part of healthy homeostatic skin (Schneider et al., 2009).

1.2 The Hair Follicle

The HF plays a wide functional role within skin and is the only permanently regenerative organ of the human body (Tobin, 2006, Schneider et al., 2009). The 'mini-organ' undergoes cycles of growth, regression and quiescence throughout life creating new hair shafts with every bout of HF cycling (Tobin, 2006). The base of the mature HF is found in the dermis, with hair shafts that protrude through the epidermis and outside the surface of the skin (Muller-Rover et al., 2001).

The HF is divided into several regions (Figure. 3). The infundibulum is the upper, opening portion of the HF and is characterised by Krt79 expression. It is derived from the developing hair germ during HF morphogenesis and replenished by Lrig expressing stem progenitor cells during HF cycling (Jensen et al., 2009, Veniaminova et al., 2013, Schneider and Paus, 2014). Just below the infundibulum is the isthmus, a part of the HF between the sebaceous gland duct opening and arrector pili muscle (APM) attachment to the HF bulge region (Paus et al., 1999). The APM functions to pull the hair shaft erect in order to trap warm air and increase body temperature (Schneider et al., 2009), however, the APM can also stimulate bulge SCs through APM-sympathetic nerve niche, playing a role in homeostatic hair (Shwartz et al., 2020). The bulge region contains a SC population that is instrumental to the cycling nature of HFs and in regeneration during wound healing (Blanpain et al., 2004, Fuchs, 2007, Blanpain and Fuchs, 2009, Schneider et al., 2009). The infundibulum and isthmus are part of the permanent portion of the HF, with a transient, cycling portion residing below, including the hair bulb, in which the new hair shafts, ORS, inner root sheath (IRS) derive from, driven by bulge SC migration and interaction with the DP (Figure. 3) (Schneider et al., 2009).

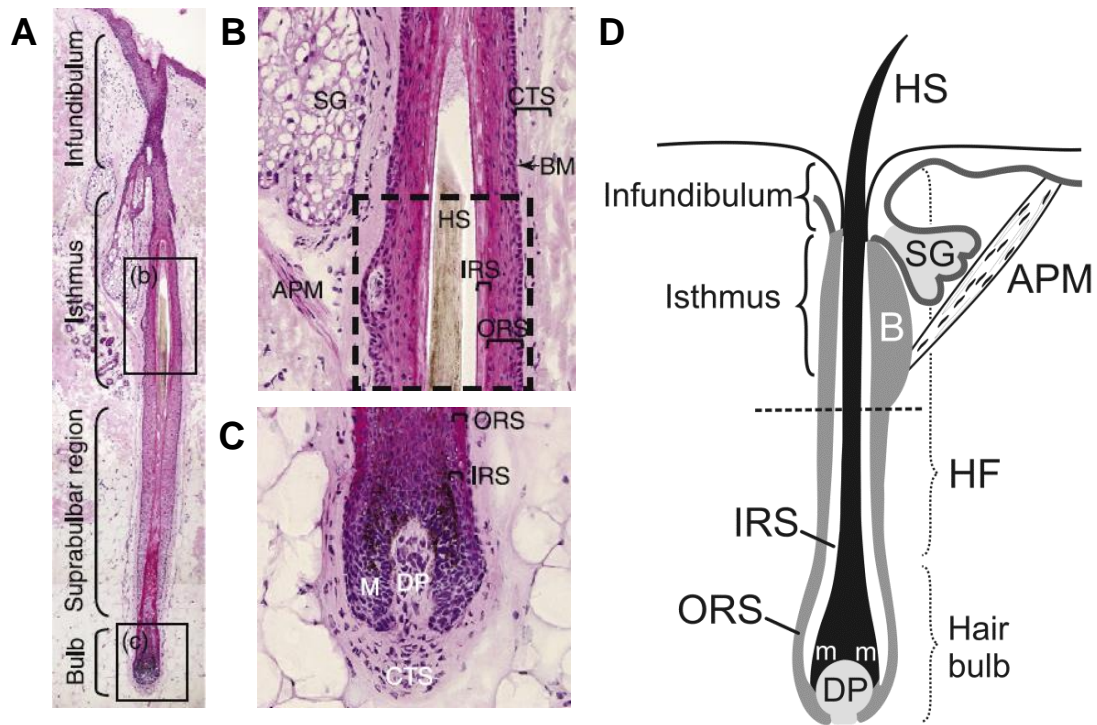


Figure 3. *The Structure of the Mature Hair Follicle.*

(A) Haematoxylin and eosin stained anagen HF. The HF is made up two main regions, the upper permanent portion containing the infundibulum and the isthmus, and the lower, cycling portion of the HF including the hair bulb and suprabulbar region. **(B)** The isthmus contains the SC residing bulge region (denoted by dashed box) and the arrector pili muscle. The sebaceous gland can also be seen towards the upper part of the isthmus. The hair shaft, ORS, IRS and CTS are identified from this section also. **(C)** The hair bulb contains the DP which is instrumental in signalling pathways involved in hair growth and cycling and promoting matrix cell differentiation. **(D)** A schematic image of the mature HF showing the various components of the HF. The dotted line separates the permanent upper portion and the lower cycling portion of the HF. (SG: Sebaceous gland, APM: Arrector pili muscle, CTS: Connective tissue sheath, BM: Basement membrane, HS: Hair stem, IRS: Inner root sheath, ORS: Outer root sheath, M: Matrix, DP: Dermal papilla, B: Bulge) Image adapted from: (Schneider et al., 2009, Rishikaysh et al., 2014).

1.2.1 The Hair Shaft

The hair shaft is made up of multiple different cells and is the part of the HF that we can see protruding out of the skin, extending from the hair bulb at its base. The hair shaft is required for initial protection of the skin from sensing external stimuli to thermoregulation through contraction of the arrector pili muscle (Schneider et al., 2009).

The hair shaft is made up of multiple cell types. The innermost medulla is comprised of keratinized keratinocytes and expresses Krt75 (Schweizer et al., 2007). The medulla is surrounded by the cortex which makes up the bulk of the hair shaft and made up of tightly packed keratinized cells expressing Krt81/86/83 of type II keratins and Krt39/34/36 of type I keratins in humans (Schweizer et al., 2007). This layer also contains melanin granules which are present in pigmented hair shafts. The last layer surrounding the cortex is the hair cuticle comprised of keratinized cells that protect the rest of the hair shaft and express Krt85 (Moll et al., 2008, Schneider et al., 2009).

There are several types of HFs in mice: Guard, awl, auchene and zigzag hairs. Guard hairs begin development at E14, awl at E16 and auchene and zigzag at E17 and E18/P1 respectively (Duverger and Morasso, 2009). Auchene hairs have a single bend in their hair shafts and zigzag, as their name suggests, contains 3-4 bends (Chi et al., 2013). The two straight hair shafts; the guard and awl are thicker than the thinner bent hair shafts with zigzag being the thinnest and awl the thickest (Chi et al., 2013). Guard hairs function as sensory hairs and make up 1-3% of the mouse coat. Awl hairs make up 30%, and undercoat residing zigzag, 65-70%. Auchene hairs make up only approximately 0.1% of total hairs on mice (Duverger and Morasso, 2009).

There are several main hair types on the human body, which can be classified as androgen-independent HFs such as eyelashes and eyebrows, and hormone-dependent HFs such as scalp, chest, and public regions. These consist of long and thick terminal hair shafts. Most of the body however is covered with vellus hair, non-pigmented, short hair shafts, which are androgen independent (Paus and Cotsarelis, 1999, Buffoli et al., 2014). The structure of hair shafts is similar between human and mice with both made up of a cuticle, cortex and medulla layer, however, human hair types can exist in a transitional phase between terminal and vellus hair types whereas mouse hair types remain in a committed state (Buffoli et al., 2014).

Hair shaft formation has been shown to be tightly regulated by Wnt and BMP signalling pathways. BMP signalling is required in the DP to maintain a progenitor population, whilst Wnt signalling is required for differentiation of matrix cells into hair shaft cells (Rendl et al., 2008, Enshell-Seijffers et al., 2010). Wnt/BMP crosstalk is essential in hair shaft growth where in overexpressing beta-catenin mouse model, hair shaft formation was greatly impaired and hair shafts were much shorter than the wild type controls. Wnt signalling is required for initial morphogenesis of the HF placode, but overexpression leads to disruption in BMP/Wnt signalling crosstalk and abnormal development of the hair shaft (Närhi et al., 2008). In BMP receptor 1 a (*BMPR1a*) knockout mice, HFs failed to grow a hair shaft (and IRS) and failed to activate Wnt responsive genes due to defects in beta-catenin accumulation (Kobielak et al., 2003). The relationship between BMP/Wnt signalling is essential for normal hair shaft formation.

Another important regulator of hair shaft formation is transcription factor Foxn1, which has been shown to be expressed in the bulbar matrix region where cells differentiate to form into the hair shaft and IRS during HF morphogenesis, and expressed in the

hair shaft of post-natal HFs (Lee et al., 1999, Bukowska et al., 2018). *Foxn1* has also been shown to be downregulated in *BMPR1a* knockout mice (Andl et al., 2004b). *Foxn1/Msx2* double knockouts resulted in complete lack of hair production but only *Foxn1* knockout resulted in an absence of *Notch1* in the matrix indicating it is downstream of *Msx2* (Cai et al., 2009). *Notch1* knockout models has shown impaired IRS and hair shaft medulla formation (Pan et al., 2004, Cai et al., 2009). Together, these indicate a signalling hierarchy of BMP-*Msx2*/*Foxn1*-*Notch1* signalling in hair shaft development (and IRS) from differentiating matrix cells (Cai et al., 2009).

1.2.2 The Inner Root Sheath

The IRS surrounds the hair shaft and is comprised of several cell types; the innermost IRS cuticle, the inner Huxley's layer and outer Henley's layer (Schneider et al., 2009). The IRS functions to protect the emerging hair shaft and channels the hair shaft through the HF (Fuchs, 2007). During active growth phase of HF cycling, type II keratin marker *Krt6* is expressed in the IRS in humans and mice (Porter et al., 2001).

Gata3 plays a key role in IRS development, identified through knockout studies in mice which led to the inability of the cuticle layer and Huxley's layer to form, resulting in an abnormal hair structure (Kaufman et al., 2003). *Gata3* is downstream of BMP signalling, with *BMPR1a* knockout mice models resulting in a downregulation of *Gata3*, *Foxn1* and *Mxs2* expression, and loss of IRS and hair shaft formation (Kobielak et al., 2003, Andl et al., 2004b). An additional study of *BMPR1a* and *Gata3* knockout models demonstrated that *Gata3* was localized to the lower matrix progenitor IRS transit-amplifying cells (TACs) (Genander et al., 2014).

Another important regulator of IRS formation is transcription factor, *Cutl1*, which has been shown to result in reduction of all IRS specific cell types after knockout (Ellis et

al., 2001). However, development of the companion layer was shown to develop independently of the IRS formation after *Gata3* and *BMPRa* knockout (Kaufman et al., 2003, Andl et al., 2004b, Mesler et al., 2017).

Also playing a role in IRS and hair shaft formation is *Foxn1*, which is present in the early developing IRS in matrix progenitors (Lee et al., 1999, Bukowska et al., 2018). In nude mouse phenotype (*Foxn1* knockout), the Hair shaft and IRS failed to form. In heterozygous *Foxn1* knockout, *Foxn1* was observed in the matrix progenitor cells and early IRS progenitors but not in the differentiating IRS cells further up the HF (Lee et al., 1999). Much like the hair shaft development, Notch signalling is involved in IRS formation, and ablation resulted in lack of IRS formation as well as hair shaft (Pan et al., 2004, Blanpain et al., 2006). Together, these studies demonstrate the important relationship between IRS and hair shaft as well as the importance of *Gata3*, *Cutl* and Notch/*Foxn1* signalling leading to normal IRS and hair shaft development.

1.2.3 The Outer Root Sheath

The ORS is the outermost epithelial layer of the HF and is an extension of the basal layer of the epidermis, surrounding the HF (Fuchs and Horsley, 2008). The bulge region is contained within the ORS just below the sebaceous gland and functions as SC pool for progenitors to migrate down the ORS to the base of the HF (Blanpain et al., 2004). Quiescent, pluripotent SCs have been found residing in the human ORS expressing nestin, fibronectin and CD34. These cells have been shown to be able to differentiate into neural cells *in vitro* (Amoh et al., 2005).

The ORS can be divided into upper, slow cycling and lower fast cycling cells, with slow cycling ORS cells surviving catagen and give rise to new bulge and a progenitor population of the secondary hair germ (SHG). Faster cycling ORS cells also give rise

to bulge SCs and function in part to produce quiescent promoting signals during telogen, showing a feedback mechanism of bulge SCs and their progeny (Hsu et al., 2011).

One of the key regulators of ORS progenitor cells is Sox9. Sox9-null mice results in impaired early hair bulb, matrix and hair shaft formation caused by the inability of stem/progenitor cells to migrate down the ORS. In Sox9-null mice, the ORS becomes thicker, and expresses markers such as Krt1/10 and Gata3, specific to the suprabasal epidermal layer, IRS and early ORS. The SC niche also fails to form in Sox9-null mice. (Vidal et al., 2005).

Another key regulator of ORS is Shh signalling which is required for maintaining normal ORS function. Conditional knockout of smoothed (a component of Shh signalling) resulted in lack of expression of ORS markers Sox9 and Krt17 but expression of Krt1 was noted, indicating a switch of ORS to epidermal lineage commitment (Gritli-Linde et al., 2007).

Another regulator of ORS development is Epidermal growth factor (EGF). EGF has been shown to promote cell proliferation and migration in the ORS during anagen growth phase, and overexpression of EGF resulted in increased expression of β -catenin, Wnt10b and Sox9, genes associated with differentiation and proliferation in the active HF (Zhang et al., 2016). These studies indicate the importance of the ORS maintaining a more undifferentiated state for the migration of bulge SCs during HF cycling.

1.2.4 The Hair Bulb

The bulb of the HF is the base of the hair shaft and resides close to the DP. The bulb is comprised mainly of matrix cells, stem/progenitor cells which migrate from the bulge

region to form the new hair during HF cycling (Blanpain et al., 2004). The matrix organises into distinct layers depending on the future cell lineage commitment. Matrix cells close to the DP are self-renewing, TACs from the bulge and are categorized as the germinative layer (Legué and Nicolas, 2005). The layer around the germinative layer are transient progenitor populations and the layer around that are the post-mitotic cells that give rise to the cell types of the hair shaft and IRS. Differentiation and commitment of matrix cells increase the further they are from the DP (Legué and Nicolas, 2005). Matrix cells at the centre of the growing bulb form the inner hair shaft and the peripheral matrix cells form the IRS and companion layer (Sequeira and Nicolas, 2012, Mesler et al., 2017).

The DP makes up an integral part of the hair bulb which is of mesenchymal origin made up of specialised fibroblasts. The DP functions to provide growth and differentiation inducing signals during HF growth phase for the matrix cells in the hair bulb but also stimulate the bulge SC region *via* the hair germ to proliferate and activate the next growth cycle (Greco et al., 2009, Driskell et al., 2011). The importance of DP in hair growth has been shown by transplant experiment of cultured DP cells implanted into mouse footpad epidermis (a region that does not grow HFs) which resulted in HF and hair shaft growth (Jahoda et al., 1984). Similar results were observed when DP cells were implanted into mouse ear wound (Jahoda et al., 1993). Implantation of spheroid DP cultures in human skin has also been shown to induce HF formation (Higgins et al., 2013). These studies indicate the essential role of the DP in normal HF growth.

BMP and Wnt signalling play key roles in the development and homeostasis of the DP. During DP development, Sox2 is expressed in guard, awl and auchene hairs but not in zigzag hairs (Driskell et al., 2009). Sox2 knockout studies resulted in slower but

normal hair shaft growth because of impaired matrix progenitor migration in the Sox2 negative hairs. This was attributed by increase in BMP6 and a decrease in BMP inhibitor Sostdc1 (Clavel et al., 2012). During HF cycling, Wnt signalling is a key signalling pathway in the control of DP induction of anagen growth phase. Knockout of β -catenin in DP cells of developed HFs resulted in premature catagen entry and prevention of HF cycling re-entry due to reduction of proliferative and differentiation stimulation of hair follicle stem cells (HF-SCs) (Enshell-Seijffers et al., 2010).

Along-side Wnt/BMP signalling control of DP cells, Alkaline phosphatase is an important marker of the DP and shown to be extensively expressed throughout the hair cycle (Handjiski et al., 1994). Studies have shown that alkaline phosphatase levels vary during the hair cycle with highest levels during active anagen growth phase and lowest levels during catagen regression phase (Iida et al., 2007).

In addition to the transit-amplifying stem/progenitors and the DP, the hair bulb contains melanocytes (pigmentary units) (Slominski et al., 2005). The melanocytes reside in the upper matrix region and transfer melanin to medulla and cortex keratinocytes, pigmenting the hair shaft during anagen stage of HF cycling (Slominski et al., 2005, Schneider et al., 2009).

1.2.5 The Connective Tissue Sheath

The connective tissue sheath, or dermal sheath (DS), is of mesodermal origin and surrounds the DP and ORS during anagen, but is restricted to surrounding the DP during telogen, where they self-renew during HF cycling (Martino et al., 2021). It is made up of connective collagen producing fibroblasts and stromal cells and functions to provide connection and anchorage of the HF to the dermis (Schneider et al., 2009). It is separated from the ORS by a basal lamina and collagen fibres (Martino et al.,

2021). The DS also functions as a smooth muscle niche, expressing alpha-smooth muscle actin (α SMA) that brings the DP into close proximity to the bulge by contraction during catagen-telogen transition by calcium/calmodulin/myosin light chain kinase pathway (Rahmani et al., 2014, Heitman et al., 2020).

The DS may play a role with the DP in directing hair growth and proliferation and the increase in size of the hair bulb during HF cycling. The DS surrounding the DP consists of Sox2⁺ and Blimp1⁺ cells and expresses α SMA (Driskell et al., 2013, Rahmani et al., 2014). During anagen growth phase, the DP increases in size which could be partly attributed to proliferation and migration of dermal sheath cells (Tobin et al., 2003). Implantation studies of DS cells transplanted to mouse footpads and ears resulted in growth of a HF, suggesting a similar functional role to DP cells (McElwee et al., 2003, Chi et al., 2010). In addition, pharmacological inhibition of DS contraction during anagen-catagen transition of the hair cycle results in a failure of the HF to contract and retains the hair shaft, showing that DS contractibility is a major driver of catagen regression stage of HF cycling (Heitman et al., 2020).

1.3 Hair Follicle Morphogenesis

HF morphogenesis begins following stratification of the epidermis at E14-18. Beneath the epidermis forms a dermal condensate, specialised dermal fibroblasts that through signalling to the upper epidermal cells regulates HF downward growth and DP formation (Noramly et al., 1999, Fuchs, 2007). The initiation of HF morphogenesis is characterised by a downward growth of a placode, epidermal basal cells begin invagination into the dermis upon signalling from the dermal condensate (Fuchs, 2007). The hair placode continues to invaginate into the dermis and forms the hair germ, followed by the hair peg and through vast cellular specification and lineage

commitment, the mature HF is formed. HF morphogenesis can be divided into three key developmental phases: The induction phase, the organogenesis phase, and the cytodifferentiation phase (Figures. 4-6) (Schneider et al., 2009).

1.3.1 Induction

HF morphogenesis begins by the formation of the placode, thickening of overlying epidermal cells at E14 for guard hairs, E16 for Awl, and auchene and zigzag at E17 and E18/P1 respectively (Duverger and Morasso, 2009). The overlying epidermal keratinocytes align above a dermal condensate at specific points of the skin, regulated by signalling crosstalk from the underlying dermis and epidermis. Dermal Wnt signalling is required for the formation of the early HF placode. This is characterised by the 'first dermal signal' from early dermal fibroblasts. Broad Wnt activity in the dermis causes localised β -catenin expression in the overlying epidermis is required for placode formation (Figure. 4) (Noramly et al., 1999, Botchkarev et al., 1999, Andl et al., 2002, Chen et al., 2012). Ectopic expression of Wnt inhibitor Dickkopf 4 (Dkk4) in early developing mouse skin resulted in failure of placode and subsequent HF formation. Dermal Wnt signalling induces epidermal Wnt signalling and then subsequent Wnt signalling in the dermis induced formation of a dermal condensate and activation of other signalling pathways essential in HF morphogenesis (Zhang et al., 2009b).

Tumour necrosis factor (TNF) family member Eda is essential for the developing placode and its downstream transcription factor, nuclear factor kappa B (NF- κ B). NF- κ B expression has been shown to be confined to the placode at approximately E14, just after activation of epidermal Wnt signalling (Zhang et al., 2009b). Knockout of *NF- κ B* is embryonic lethal but reduced expression results in failure to develop the placode

(Schmidt-Ullrich et al., 2001). Mutations in *Eda* have also resulted in impaired HF formation in humans and mouse (Ferguson et al., 1997, Srivastava et al., 1997, Saxena et al., 2019). Wnt signalling is required for NF- κ B expression and *Eda* has been identified as a downstream target of Wnt signalling (Zhang et al., 2009b). NF- κ B/*Eda* signalling have been implicated to control Wnt signalling patterning, this is demonstrated by NF- κ B inhibition and observed irregular boarder patterning in the developing placode. Secondary Wnt signals, Wnt10b and Wnt10a are absent when NF- κ B is inhibited and Wnt10b/10a are identified targets of *Eda* signalling (Zhang et al., 2009b). Wnt10a and Wnt10b, secondary Wnt signals has been shown to be expressed in the early HF placode and later in the lower matrix precursor cells of the placode and has a role in HF development after initial induction (Andl et al., 2002, Ouspenskaia et al., 2016).

Fgf20 signalling is required for initial dermal condensate formation and is downstream of Wnt and *Eda*/NF- κ B signalling in the epidermal cells (Huh et al., 2013). Fgf20 mutant mice exhibited hair placode formation but no condensing of dermal cells and progression to hair germ. Early dermal condensate markers Sox2 and Foxd1 were used to track the formation of dermal condensate in Fgf20 mutant mice, and showed that condensed fibroblasts (pre-dermal condensate) forms but remain unspecified and unable to continue with hair germ formation from the placode (Driskell et al., 2009, Sennett et al., 2015, Mok et al., 2019). Together, these activator pathways show a diverse regulatory signalling pattern for successful early placode development.

At E15, asymmetric division of Wnt expressing basal placode cells occurs and subsequent suprabasal, low Wnt expressing, Sox9 expressing HF progenitor cells arise (Ouspenskaia et al., 2016). Polarisation of the early placode continues with Shh expression in the lower, leading edge of the invaginating HF that are matrix precursor

cells, and Sox9 expressing HF precursor SCs are expressed in the upper germ (Cetera et al., 2018). Shh has been shown to be essential in the maintenance of suprabasal Sox9 expressing precursor SCs. *Shh*-null mice resulted in a decrease in Sox9 expressing suprabasal cells, which are responsible for giving rise to progenitor cell populations essential for homeostatic HF development (Ouspenskaia et al., 2016).

BMP and other inhibitory pathways are also involved in the regulatory signalling pattern of placode formation. BMP2 is expressed in the overlying hair placode and BMP4 along with its inhibitor Noggin are expressed in the dermal condensate. Increased expression of noggin resulted in increased induction of hair placode formation (Plikus et al., 2004, Botchkarev and Sharov, 2004). This converse signalling structure between BMP and its antagonist may function to fine tune regulatory pathways involved in placode formation. Eda/NF- κ B signalling inhibits BMP signalling and its placode forming inhibitory role. BMP signalling is inhibited by Ccn2 and follistatin which are both upregulated by the Eda/NF- κ B pathway (Pummila et al., 2007). Inhibition of Eda expression in mice results in inhibition of placode formation which can be rescued by exogenous noggin expression. In addition, overexpression of Eda in mice resulted in enlarged hair placodes, *in vivo* (Pummila et al., 2007).

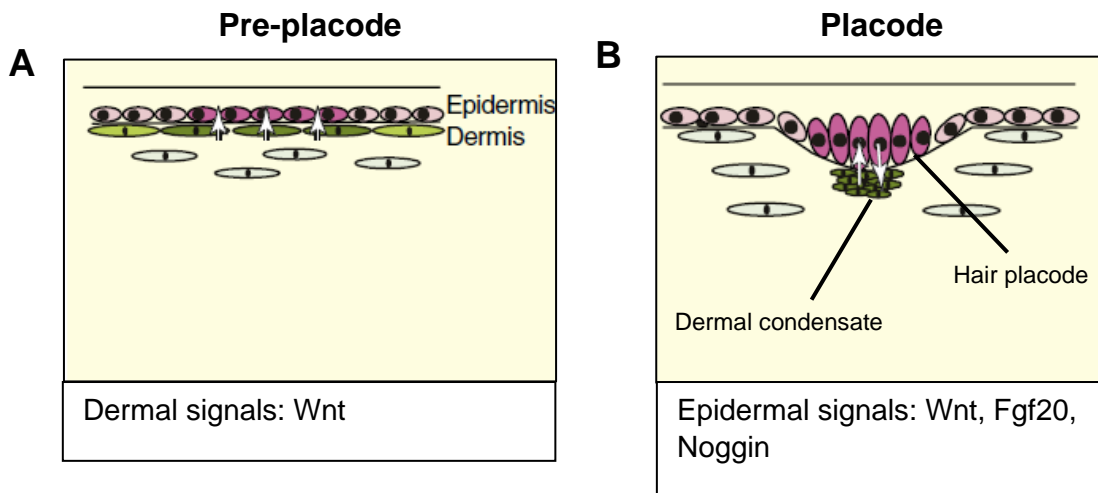


Figure 4. Induction Stage of Hair Follicle Morphogenesis.

(A) *Pre-placode: Early dermal fibroblast Wnt signals (arrows) stimulate epidermal Wnt signalling and alignment of the epidermal basal keratinocytes. Epidermal Wnt signalling activates downstream Eda/NF- κ B and Fgf20 signalling subsequent epidermal Wnt, Fgf20 signalling.* (B) *Placode: Epidermal Wnt and Fgf20 signalling relays to dermal Wnt signalling for formation of the dermal condensate (arrows). Asymmetric division of the basal keratinocytes leads to low Wnt, high Sox9 expressing suprabasal cells that will go on to form the HF-SCs. Adapted from (Schneider et al., 2009).*

1.3.2 Organogenesis

Following placode formation, the downgrowth of the HF is initiated and the hair germ forms from invaginating epidermal cells into the dermis. This stage is initiated at approximately E15 in mice (Saxena et al., 2019). At the latter stages of organogenesis, with the formation of the hair peg, the invaginating HF delves deeper into the dermis and begins to encircle the dermal condensate which will become the DP (Schmidt-Ullrich and Paus, 2005). Matrix progenitor cells surrounding the dermal condensate have been shown to initiate differentiation and express Krt79 before beginning to

surround the dermal condensate (Mesler et al., 2017). In subsequent hair peg development, the developing ORS expresses *Krt5* and the HF stem/progenitors express *Sox9* and *Lrig1* (Figure. 5) (Millar, 2002, Frances and Niemann, 2012).

Shh signalling is key in the HF downward growth, formation of the hair germ and the formation of the DP. In *Shh*-null mice, HF development is arrested after initiation of the downward growth of the placode forming the hair germ (St-Jacques et al., 1998). *Shh* has been determined as a target of *Eda/NF-K β* signalling and *NF-K β* inhibited mice exhibit inhibition of *Shh* expression and prevented hair germ downward growth (Schmidt-Ullrich et al., 2006, Zhang et al., 2009b, Pummila et al., 2007). *Wnt10b* activates *Shh* signalling in placodes (through *Wnt* activated *Eda* signalling). *Shh* in the hair placode increases expression of *Wnt5a* in the underlying dermis. This provides a second dermal signal for the downward growth of the hair placode into the hair germ (Reddy et al., 2001, Rishikaysh et al., 2014). This is further outlined by *Shh* inhibition by targeting *Smoothed (Smo)*, a mediator of *Shh* signalling, resulting in hair germ development arrest and loss of dermal condensate, outlining the essential role of *Shh* in HF morphogenesis (Woo et al., 2012).

Shh is also partly responsible for the angle of which HFs grow, pointing from anterior to posterior direction. The polarity of lower *Shh* expressing matrix precursor cells and the upper *Sox9* expressing progenitors causes shifting of the HF angle from the perpendicular placode. This is supported by *Shh* knockout in chicks showing abnormal HF orientation (Ting-Berreth and Chuong, 1996, Millar, 2002). However, other studies have shown that HF orientation is not only mediated by *Shh*.

In addition, planar cell polarity (PCP) genes are involved in aligning body structure in an anterior to posterior direction. PCP proteins have been shown to act on basal cells

in a planar fashion as the epidermis undergoes stratification (Devenport and Fuchs, 2008). Core PCP proteins: Vangl2, Celsr1 and Fzd6 are polarized in the basal epidermal layer and contribute to HF orientation. This is demonstrated by loss of function mutations in each of the genes resulted in global dysregulation of HF orientation, but some local areas demonstrated correct orientation indicating that polarization can be initiated by neighbouring HFs (Devenport and Fuchs, 2008, Chen and Chuong, 2012).

Platelet-derived growth factor A (PDGF-A) is required for placode downgrowth and hair germ formation. PDGF-A is expressed in the overlying epidermis and its receptor, PDGF-R α in the underlying mesenchymal structures in the dermis. *PDGF-A*-null mice resulted in a thinner dermis formation, reduced DP size, thinner hair sheath and misshapen HFs (Karlsson et al., 1999). Upon Shh ablation, PDGF-A becomes abnormally dispersed within the dermis although PDGF-A ligand is expressed normally, this may indicate a link between Shh targets and PDGF responsiveness for normal hair germ and DP formation (Karlsson et al., 1999, Sennett and Rendl, 2012). Another study knocked out *PDGF-R α* and *PDGF-R β* in the dermis and reported normal HF induction and formation but a thinner dermis (Rezza et al., 2015). These indicate PDGF signalling is not essential for HF induction but required for healthy HF formation in the later stages of development.

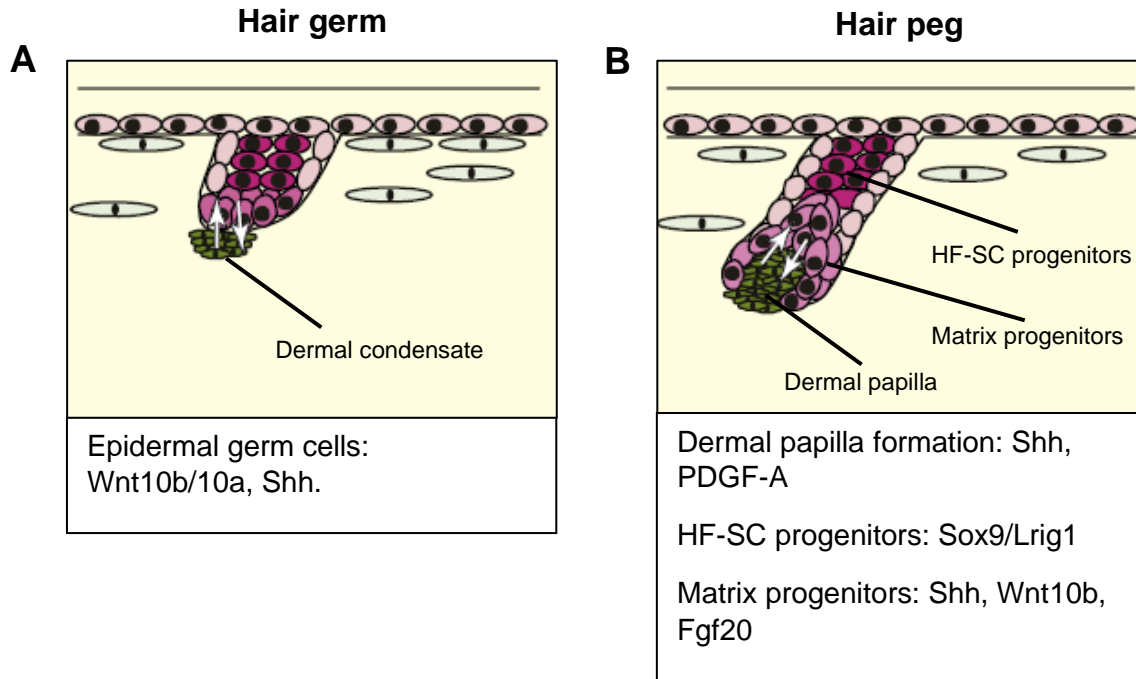


Figure 5. Organogenesis stage of Hair Follicle Morphogenesis.

(A) Invagination of the placode into the dermis leads to formation of the hair germ. Epidermal-dermal signalling crosstalk from Shh and PDGF with secondary dermal signals which are currently unknown. Shh signalling is also key in the subsequent surrounding of the dermal condensate. **(B)** The hair peg is formed from further downgrowth of the hair germ and separation of the two precursor cells for HF-SCs and matrix precursors. The DP is formed and is surrounded by matrix precursor cells. Sox9 and Lrig1 expressing cells go on to form HF bulge and sebaceous gland SCs respectively whereas shh, Wnt10b and Fgf20 control the downgrowth of matrix progenitor cell population. (HF-SC: Hair follicle stem cells) Adapted from (Schneider et al., 2009).

1.3.3 Cytodifferentiation

Cytodifferentiation can also be classified as the maturation phase of HF morphogenesis (Schneider et al., 2009). Following the formation of the hair peg, the IRS begins to form. The pre-HF-SCs separate into Lrig1 expressing pre-sebaceous

gland SCs and Sox9 expressing pre-bulge SCs. As HF maturation continues, the IRS elongates, and the HF delves deeper into the dermis. The end of HF morphogenesis is the generation of the mature HF with completely grown hair shaft, IRS, ORS and mature sebaceous gland and bulge region (Saxena et al., 2019).

As mentioned above, a vast array of signalling pathways are required for the maturation and development of the HF. Generation of the hair shaft requires BMP signalling through BMPR1a activation from DP signals. Knockout of *BMPR1a* in mice resulted in lack of formation of IRS and hair shaft. BMP-Msx2/Foxn1-Notch1 signalling pathway as well as Gata3 have all been shown to be essential in IRS and hair shaft formation from DP signals (Cai et al., 2009, Kobiela et al., 2003). Lrig1 expressing progenitors give rise to the sebaceous gland, while Sox9 positive HF-SCs become the bulge SC niche (Frances and Niemann, 2012, Kadaja et al., 2014). Blimp1 expressing cells are found in the sebaceous gland and serve as a unipotent sebocyte progenitor population, regulating proliferation and sebaceous gland homeostasis. Notably, in *Blimp1* conditional knockout mice, bulge SCs have been shown to migrate and repopulate Blimp1 sebaceous gland progenitors (Horsley et al., 2006). Once HF morphogenesis is complete, the HF begins to cycle (Figure. 6).

1.4 Hair Follicle Cycling

Following HF morphogenesis, HFs undergo cycling: periods of growth, rest, and regression (Figure. 6). After morphogenesis, the mature HF undergoes a short period of rest, where, approximately 17 days after birth, the HF cycle begins (Schneider et al., 2009). After skin morphogenesis, the HF cycle begins with catagen, the destructive, apoptotic and DS contraction stage, followed by telogen, the quiescent

phase, and anagen, the growth phase. This cycle is repeated throughout life and takes approximately 4-5 weeks in mice following morphogenesis (Muller-Rover et al., 2001).

HF cycling occurs in the lower, suprabulbar region of the mature HFs whereas the upper infundibulum and isthmus remain permanent. The lower portion undergoes changes in morphology from one stage of HF cycling to the next (Schneider et al., 2009). HF cycling is synchronised as demonstrated by hair cycling domains. Hair cycling domains are regions of HFs that cycle in unison with one another and can vary throughout adult life. Dermal BMP signals in a cyclic manor can regulate large populations of HFs and therefore control hair cycle domains. As mice age, more domains form leading to a more areas with their own cyclic rhythm (Plikus et al., 2008).

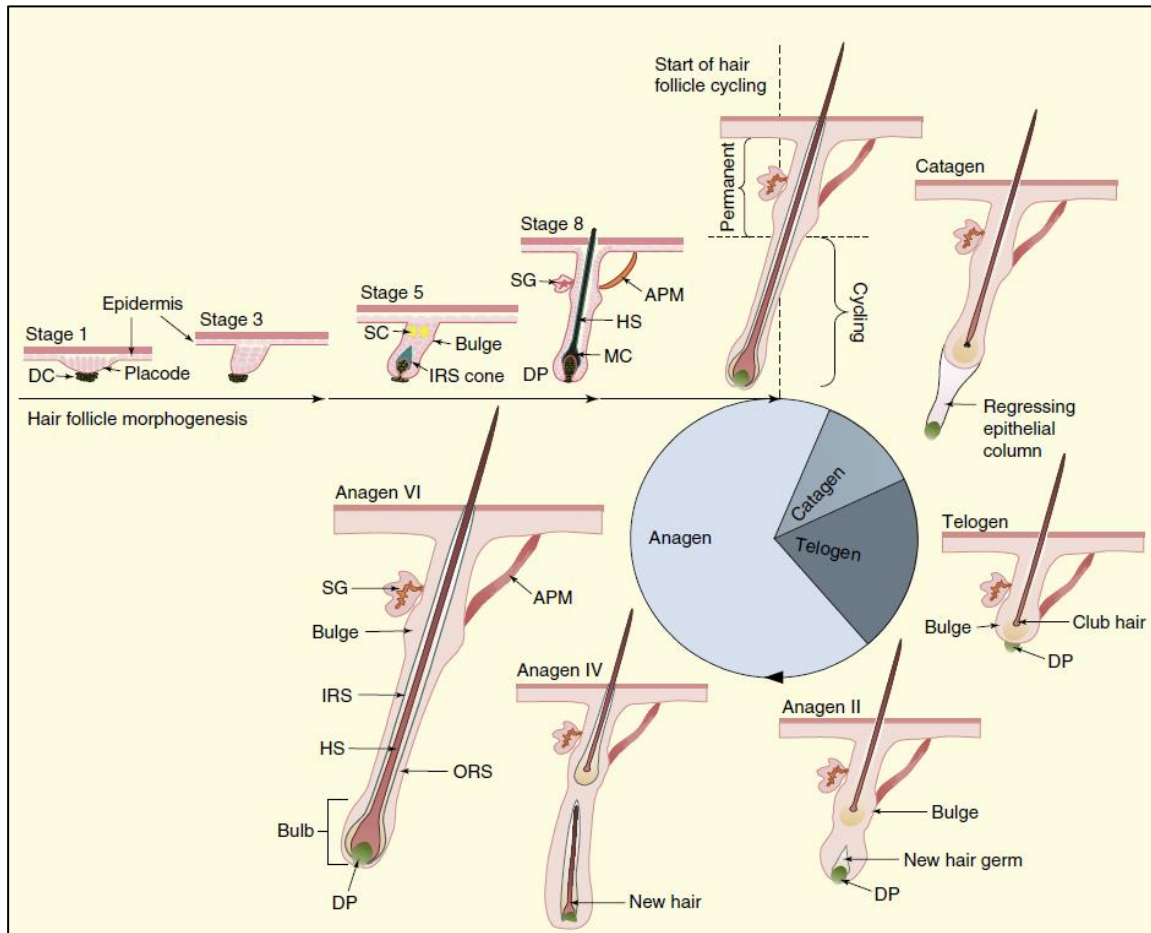


Figure 6. The Post-natal Hair Cycle.

The hair cycle is divided into the anagen growth phase, catagen regression phase and telogen quiescent phase. Following HF morphogenesis, the HF goes through catagen phase followed by resting telogen phase. The first telogen lasts only a few days. Then the anagen phase is initiated and the new IRS and hair stem grow from differentiating matrix cells and progenitor SCs under the control of the DP. Migrating bulge SCs repopulates the secondary hair germ and matrix progenitors during mid anagen. Exogen (not shown), the shedding of the previous club hair occurs during anagen of the next HF growth in subsequent cycles. (IRS: inner root sheath, SG: sebaceous gland, HS: hair shaft, MC: matrix cells, DP: dermal papilla, ORS: outer root sheath) (Schneider et al., 2009).

1.4.1 Telogen

Telogen is the resting phase of the hair cycle and a period of little activity. The first telogen following HF morphogenesis occurs at post-natal day (P)19-21 in mice and lasts a few days but in subsequent cycles, telogen can last several weeks (Muller-Rover et al., 2001). The length of the telogen HF is much shorter than the anagen HF with the DP coming to a rest just below the bulge region. The DP is instrumental in growth signalling for HF cycling and its proximity to the bulge region aids in growth by signalling to the SC regions. (Schneider et al., 2009, Driskell et al., 2011). These SC populations are the key to progressive stages of HF cycling and their activation and inhibition is tightly regulated throughout. In telogen, SC maintenance and inhibition of growth signalling gives the HF its quiescence but progression into growth after telogen relies on a switch in signalling so the hair cycle can progress (Schneider et al., 2009). In telogen HFs, the entire HF is located in the dermis and shows no IRS (Muller-Rover et al., 2001).

Telogen can be divided into two stages, (i) a refractory stage, and (ii) a competent phase. The refractory stage is a period of SC resistance to activation and promotion of HF quiescence. The competent phase is defined as SC susceptibility and increased sensitivity of bulge SCs to anagen promoting signals (Plikus et al., 2008, Schneider et al., 2009). Inhibitory BMP signalling is inversely expressed with the Wnt signalling pathway. The refractory phase is characterised by high dermal BMP2/4 expression whereas the competent has low BMP2/4 expression. Overexpression of BMP inhibitor Noggin resulted in a shortened refractory stage and quicker progression into anagen stage of the HF cycle (Plikus et al., 2008). This is demonstrated in physiological healthy HFs, at the onset of anagen, Noggin expression is increased and BMP4 expression is decreased. Noggin also increases Shh signalling which is inhibited by

BMP4. Dermal BMP signalling therefore may act on the DP which propagates signalling induction of a new hair cycle through Shh signalling (Botchkarev et al., 2001a). BMP6 is also implicated as a growth inhibitory signal and along with BMP2 and BMP4, are expressed in adipocytes to maintain SC quiescence (Plikus et al., 2008, Woo and Oro, 2011). Adipocytes also maintain control over HF-SC activation and quiescence. *Ebf1*-null mice result in decrease in mature adipose tissue and resulted in prolonged telogen, showing a lack of bulge SC activation. Inhibition of PPAR γ positive adipocyte precursor cells confirmed that pre-adipocytes are required to activate bulge SCs for progression into growth phase. It was identified that the activation of bulge SCs can occur through pre-adipocyte PDGF signalling to the DP (Festa et al., 2011).

During the refractory stage of telogen, inhibition of Wnt signalling was identified in bulge SCs by lack of nuclear β -catenin in telogen bulge SCs (DasGupta and Fuchs, 1999). Tcf-3 is involved in maintaining SC quiescence in the absence of Wnt signalling (Nguyen et al., 2006b). Ablation of BMPR1A causes bulge SC activation and increased proliferation, as well as activation of Wnt signalling through increase in β -catenin and Lef1 (Kobielak et al., 2007). Therefore, maintenance of SC quiescence can be mediated by cross talk with these signalling pathways in order to maintain the refractory stage of telogen.

Although inhibition of Wnt signalling primarily leads to lack of SC activation, Wnt5a is expressed in the bulge and secondary hair germ during telogen. Overexpression of Wnt5a in dorsal mouse skin led to elongation of the telogen stage and similar phenotype to β -catenin knockdown. Over an extended period of time however, Wnt5a induced normal hair growth (Xing et al., 2013). A later study from the same group showed that Wnt5a growth inhibitory effect can be rescued by addition of Wnt3a and

that Wnt5a suppresses β -catenin (Xing et al., 2016). β -catenin is required for HF-SC proliferation and progression from telogen into the anagen growth phase. β -catenin is expressed in the bulge and secondary hair germ during anagen and increased as BMP signalling is downregulated. Deletion of β -catenin or expression of Wnt inhibitor Dkk1 during anagen resulted in an arrest of proliferation and progression into catagen (Choi et al., 2013).

Throughout the competent phase, anagen inducing signals increase and stimulate the bulge SCs to proliferate and differentiate. A minimum threshold of anagen inducing signals must be reached for the HF to enter anagen (Plikus, 2012). Wnt/BMP signalling has been shown to be expressed competitively during skin morphogenesis and the same has been found during hair cycling: Wnt10b acts competitively with BMP6 during telogen, with BMP6 promoting SC quiescence and Wnt10b promoting anagen transition (Wu et al., 2019). This shows that Wnt/BMP signalling maintains its antagonistic relationship in hair cycling. Transforming growth factor (TGF) β 2 is not expressed during the refractory phase but highly expressed during the competent phase and anagen transition. TGF signalling activates its pathways through phosphorylation of Smad2/3 whereas BMP signalling activates its signalling through phosphorylation of Smad1/5/8 (ten Dijke and Arthur, 2007). TGF- β 2/Smad2/3 is shown to antagonise BMP signalling by targeting Tmeff1 and 'dampening' BMP inhibitory signalling, promoting telogen to anagen transition (Oshimori and Fuchs, 2012).

Fgf18 has been shown to be expressed in the bulge SC region during telogen. Fgf18 expressing bulge SCs are also positive for Krt15 and co-localise with CD34. Knockout of *Fgf18* resulted in a shortened telogen and subsequent progression into the growth phase of the hair cycle. Fgf18 is expressed in the DP in early telogen but expression

is diminished in late telogen (Greco et al., 2009). Fgf18 acts as a growth inhibitory signal and helps maintain stem/progenitor cell quiescence during telogen, which is demonstrated by Fgf18 injection into anagen HFs which resulted in suppressed proliferation of matrix cells (Kimura-Ueki et al., 2012). Other fibroblast growth factors are involved in telogen to anagen transition. Fgf7/10 has been shown to increase in expression in the DP during telogen. Fgf7/10 stimulates secondary hair germ cells to proliferate through the Fgf receptor IIIb found in both the bulge and secondary hair germ (Blanpain et al., 2004, Greco et al., 2009).

During anagen, Krt6⁺ bulge SCs arise to form the companion layer from the matrix and have a population in the bulge region, although these derive from the ORS. These inner Krt6⁺ niche bulge cells function to promote bulge SC quiescence by promoting BMP6 and Fgf18 signalling to the rest of the bulge cells. Ablation of Krt6⁺ bulge cells drastically reduces the threshold for anagen induction by anagen inducing signals to the bulge SCs and initiates anagen, whilst subcutaneous injection of Fgf18 or BMP6 can block anagen initiation/progression (Greco et al., 2009, Hsu et al., 2011, Takeda et al., 2013, Daszczuk et al., 2020).

1.4.2 Anagen

Anagen is the growth stage of HF cycling in which a new HF is formed (Muller-Rover et al., 2001). In this stage, activation of SC populations occurs through the activation threshold of anagen inducing factors. Early anagen is initiated by secondary hair germ cells, in which matrix progenitors give rise to the new IRS and hair shaft, while in mid anagen bulge SCs migrate down the ORS and repopulate the secondary hair germ and matrix progenitors (Panteleyev et al., 2001, Blanpain et al., 2004). However, this is a general view and anagen stage can be separated into six distinct stages as proposed by Muller-Rover and authors (Muller-Rover et al., 2001).

Stage 1 of anagen is similar to telogen HF but the DP begins to enlarge. In stage 2, the DP continues to enlarge and is surrounded by matrix cells and located at the lower subcutis boarder of the hypodermis. Stage 3 anagen can be further split into 3 sub sections. Firstly, matrix cells begin to surround the DP, and begin to differentiate into the IRS. Secondly, the IRS contains all its layers, the hair shaft begins to form, and the hair bulb delves into the subcutis. Lastly, the hair bulb reaches the maximum size and the IRS and hair shaft reach the sebaceous gland of the previous hair shaft. Stage 4 is characterised by the continued thinning of the DP and the IRS and hair shaft reach the hair canal of the previous hair. In stage 5 the tip of the hair shaft emerges from the hair canal and the previous hair (club hair) is lost. Lastly, stage 6 is the emergence of the new hair shaft from the skin (Figure. 6) (Muller-Rover et al., 2001).

Pigmentation of the hair shaft occurs during anagen and melanin production is absent during telogen and catagen (Slominski et al., 2005). Melanogenesis occurs with interactions between melanocytes and the DP, matrix and bulge regions. Melanogenesis is partly controlled by enzymes tyrosine related protein (TRP) 1 and 2 (Slominski et al., 2005). Melanocyte SCs are originally derived from the neural crest and are found in the bulge region and their activation is closely associated with that of bulge SCs and HF cycling. Melanocyte SCs are inactivated and maintained in an immature sate by TGF- β signalling, which is maintained during hair cycling, apart from a window of activation during early anagen (Nishimura et al., 2010). Activation of the melanocyte SCs due to reduction in TGF- β signalling and signals from the DP (KIT ligand) and matrix (endothelins), promote melanocyte SC differentiation into melanocytes. Melanocytes reach S phase in cell cycle progression by anagen 2, and by anagen 3 are significantly proliferating, coinciding with the subsequent growth and pigmentation of the new hair shaft (Slominski et al., 2005). During the later stages of

HF cycling, the hair elongates and the differentiation signals from the DP and matrix cease to have an impact on the melanocyte SCs (Nishimura et al., 2002, Hsu et al., 2014).

Wnt signalling is important in anagen induction and progression. Wnt signalling in the epidermis was shown to initiate Wnt signalling in the dermis. Deletion of *Wntless* (*Wls*) gene (required for Wnt ligand secretion) in the epidermis resulted in hair cycle arrest, reduced Wnt and β -catenin activity in the DP and reduced SC proliferation (Myung et al., 2013). Wnt signalling through *Wnt10a* and *Wnt10b* expression in the secondary hair germ and DP during early anagen have been shown, and both are absent during telogen (Reddy et al., 2001). β -catenin has been shown to be essential in anagen onset. With knockout of β -catenin in the epidermis and follicular epithelium, anagen onset fails to initiate (Huelsenken et al., 2001). Another study has shown the proliferative activating nature of Wnt signalling in HFs. Overexpression of *Wnt1* resulted in premature entry into, and a prolonged anagen stage, SC depletion and thus eventual hair loss (Castilho et al., 2009, Lim and Nusse, 2013). Another study knocked out β -catenin globally in skin, along-side in the inner follicular epithelium, and HF-SCs and compared each knockout with ectopic expression of *Dkk1*. The result of β -catenin ablation was hair cycle arrest and blocking anagen onset (Choi et al., 2013). These studies indicate the essential role of Wnt signalling in anagen onset and progression.

Shh plays a role in anagen. Exogenously administered Shh to telogen HFs resulted in activation of the anagen phase as well as increased HF size (Sato et al., 1999). In another study, Blocking Shh with anti-Shh antibodies in postnatal skin resulted in a blocking of the growth of hair during anagen (Wang et al., 2000). During anagen, Shh, and components of the Shh pathway: *Ptc1*, *Gli1* and *Gli2* are all highly expressed, and expression was reduced during catagen and telogen (Paladini et al., 2005). Topical

application of hedgehog agonist on telogen mouse skin stimulated telogen to anagen transition indicating Shh signalling as a modulator of telogen to anagen transition (Paladini et al., 2005). Gli1 expressing cells are, however, present in the lower bulge region co-expressing with Lgr5. This population may be present as an inducer for anagen phase locally to the bulge SC region (Brownell et al., 2011, Abe and Tanaka, 2017). These studies indicate that Shh plays an important role in anagen phase and maintaining matrix progenitor proliferation to produce the new hair shaft and IRS.

NF- κ B signalling helps to induce anagen and promote its progression. Strong NF- κ B expression was observed in the secondary hair germ during late telogen to early anagen transition and in the matrix and IRS in mid anagen. After induced suppression of NF- κ B, guard hairs were lost indicating the essential role of cycling in this hair type (Krieger et al., 2018). In another study EDAR in humans was shown to be present in the areas of NF- κ B activity during anagen (Kloepper et al., 2014). Also Eda-A1 overexpression in mice resulted in a prolonged anagen phase (Mustonen et al., 2003). In human scalp HFs, addition of pharmacological NF- κ B inhibitor BAY resulted in promotion of apoptosis and progression into catagen (Kloepper et al., 2014). Together, these suggest EDA-1/EDAR to regulate NF- κ B in inducing and maintaining anagen HF growth.

Inhibitory BMP signalling plays an important role in preventing ectopic growth, but during anagen, the HF needs to grow in a controlled manner, balancing activating Wnt signalling. Overexpression of BMP inhibitor Noggin in bulge SCs lead to activation of the anagen phase. BMPR1A inactivation also led to matricoma formation and coincided with an increase in β -catenin, demonstrating the antagonistic relationship between BMP and Wnt signalling (Zhang et al., 2006). Wnt10b and BMP6 have been shown to play a major role in anagen induction and have an antagonistic relationship

with one another. Wnt10b adenovirus overexpression in telogen HFs led to suppression of BMP6 expression. Equally, with adenovirus overexpression of BMP6, Wnt10b expression was suppressed and the telogen HF failed to enter anagen (Wu et al., 2019). TGF- β /Smad/2/3 signalling has been shown to antagonise BMP signalling and shown to be upregulated in the DP during anagen onset to promote active growth of the new HF through interaction with the secondary hair germ and stem/progenitor cells (Oshimori and Fuchs, 2012).

1.4.3 Catagen

Catagen is the regression phase of HF cycling in which the growing HF undergoes apoptosis of its cycling region and contraction of the dermal sheath. The first catagen stage in mice occurs at P16-18 and can be categorised into 8 distinct stages as proposed by Muller-Rover and authors (Muller-Rover et al., 2001). Stage 1 of catagen follows the end of anagen in which growth signals cease to be expressed. Stage 2 consists of the narrowing of the hair bulb by apoptosis of the hair matrix, to the approximate width of the hair canal. Stage 3, the DP begins to condense, and the hair shaft moves proximately toward the skin surface. During this stage and continuing until the end of catagen, the dermal sheath contracts, shortening the hair shaft (Heitman et al., 2020). Stage 4, 50% of the DP is surrounded by the bulb and the hair shaft continues to shorten. The club hair begins to form at the base of the hair shaft. The club hair is not pigmented. In stage 5, the hair shaft continues to move towards the skin surface and the club hair continues to develop. The ORS forms the 'germ capsule' around the club hair and the IRS becomes opaque. In stage 6, a glassy membrane of apoptotic keratinocytes connects the DP and the germ capsule. The hair shaft continues to move out towards the skin surface and the club hair grows. Stage 7-8, the DP moves towards the subcutis-dermis boarder leaving behind a streak of

connective tissue sheath fibroblasts. The IRS is the approximate level of the sebaceous gland, and the club hair and germ capsule are in the dermis, with the hair shaft at the surface skin level (Figure. 6) (Muller-Rover et al., 2001).

A key inducer of the catagen phase is Fgf5 which is expressed in the ORS during late-anagen. *Fgf5*-null HFs had abnormally long hair shafts, indicating a prolonged anagen stage (Hebert et al., 1994). This was confirmed in another study which found two isoforms of Fgf5 (a long and short protein, Fgf5 and Fgf5-S) that function to counterbalance one another, with Fgf5-S antagonising anagen to catagen transition. Through subcutaneous injection of Fgf5 during induced hair cycle, inhibition of hair growth, a promotion of apoptotic activity and transition to catagen was observed. Fgf5-S was found to be highly expressed in anagen and found to inhibit catagen transition (Suzuki et al., 2000).

Another important regulator of catagen phase is TNF- α . Subcutaneous injection of TNF- α into mouse skin resulted in a large increase in apoptosis (Rückert et al., 2000). TNF- α signalling has been shown to be regulated in part by Krt17. Krt17 is an anagen promoter and in *Krt17*-null skin, downstream TNF- α target, NF- κ B expression increases (McGowan et al., 2002, Tong and Coulombe, 2006). *Krt17*-null mice developed alopecia soon after birth due to apoptosis of the hair bulb. Krt17 interacts with TNF receptor 1 (TNFR1)-associated death domain protein (TRADD), an important component of the TNF- α /NF- κ B signal transduction and therefore may regulate TNF- α signalling and prevent the entry of the HF into catagen *via* TNF- α /NF- κ B signalling (Mustonen et al., 2003, Tong and Coulombe, 2006).

Furthermore, TGF- β 1 also plays a functional role in catagen phase. *TGF- β 1*-null mice resulted in a prolonged anagen with early entry to catagen, alongside an increase in

Ki67 expressing proliferating cells (Foitzik et al., 2000). However, injection of TGF- β 1 into dorsal mouse skin resulted in premature entry into catagen. Colocalization of TGF- β type II receptor and apoptotic TUNEL⁺ cells in the lower bulge was observed, showing that catagen entry and control can be finetuned in part by TGF- β 1 (Foitzik et al., 2000).

An additional controller in catagen and key regulator of tumour suppression in the body is tumour protein p53 (Botchkarev and Flores, 2014). P53 is expressed in the ORS and hair matrix of mature HFs and p53 expression is increased at the onset and throughout catagen. P53 knockout showed a retardation of catagen phase and decrease in apoptotic markers Bax and Bcl-2, indicating a role of p53 in controlling apoptosis during catagen (Botchkarev et al., 2001b). P63 has also been implicated in catagen although not well defined. Overexpression in transgenic mice resulted in a prolonged anagen and failure to enter catagen (Romano et al., 2010). P63 may act inversely to p53 in the skin but more research is needed (Botchkarev and Flores, 2014).

1.4.4 Exogen

Exogen is the release of the club hair, previous hair shafts that have completed cycling. Club hair shedding is coupled with anagen and found to be morphologically distinct from a telogen hair shaft with surrounding cells with deteriorated nuclei (Milner et al., 2002). Release of the club hair occurs so the new hair can take precedence in the HF although how this occurs is debated. One theory is that the club hair is pushed out by the growing hair shaft but this is considered unlikely, based on that fact the club hair resides in a separate region of the HF to the growing hair (Milner et al., 2002). Another possible explanation is regulatory signalling pathways involved in club hair retention. Overexpression of anti-apoptotic gene Bcl-xL results in a prolonged retention of the

club hair. This could mean that apoptotic regulation in the surrounding club hair results in club hair loss (Pena et al., 1999, Higgins et al., 2009). This mechanism is supported by Milner's and authors observation in deteriorated nuclei surrounding the shed club hair (Milner et al., 2002). Interestingly, plucking a resting club hair during competent telogen results in the initiation of a new anagen phase. However, knockout of cell adhesion protein, desmoglein-3 results in premature loss of the club hair but delayed entry into the new anagen indicating a timed and coordinated mechanism for the formation and shedding of the club hair (Higgins et al., 2009).

1.5 Hair Follicle Stem Cells

The HF is described as a 'dynamic mini-organ' due to its ability to self-renew (Schneider et al., 2009). HFs undergo cycles of growth and regression by signalling pluripotent SCs and multipotent progenitors to migrate, differentiate, and proliferate into the new cells that make up the HF. These SC regions have also been shown to contribute to re-epithelialization upon wounding (Fuchs and Horsley, 2008). There are several distinct and independent SC populations in the adult HF and skin, the bulge region, the sebaceous gland, and epidermal basal layer. In addition, the matrix, SHG and ORS contain progenitor populations committed to HF lineage (Figure. 7) (Blanpain et al., 2004, Ito et al., 2004, Horsley et al., 2006, Nowak et al., 2008, Kanno et al., 2013).

The bulge region of the HF was first identified to contain SCs in 1990. The niche was characterised as 'slow cycling label retaining cells' (Cotsarelis et al., 1990). The bulge region has since been identified to be present throughout the HF cycle in adult life and has been shown to give rise (through progenitor populations) the whole of the HF as well as promote wound healing (Ge et al., 2017). Chase studies using transgenic

animals were used to label bulge SCs, allowing lineage tracing of bulge SCs during HF cycling. Most of the labelled SCs remain in bulge region, indicating the self-renewal capability of the bulge niche. However, upon anagen growth phase initiation, bulge cells proliferate and migrate to the HF base down the ORS and form the new matrix, of which the IRS and hair shaft develop from (Tumbar et al., 2004).

Interestingly, after wounding, the labelled bulge SCs migrated and differentiated into infundibulum and epidermal cells showing the high lineage capacity of bulge SCs (Tumbar et al., 2004). In addition, another bulge SC lineage tracing study showed that bulge SC could lead to generation of all other cell types in the HF (e.g.: IRS, ORS, matrix and hair shaft) (Morris et al., 2004). Furthermore, *LacZ* containing bulge SCs from vibrissae (whisker) HFs from Rosa-26 mice were transplanted on to partial bulge amputated adult Rosa-26 mouse HFs, which resulted in β -galactosidase observed in the ORS, followed by the hair bulb and eventually throughout the HF within 10 weeks (Oshima et al., 2001). These studies highlight the importance of the bulge SC population which gives rise to the whole of the mature HF through migration and progenitor populations, as well as contributing to wound healing.

Two SC populations have been identified in the bulge region during telogen-anagen stage of HF cycling. A $Krt5^+$, $Krt14^{High}$, $\alpha6^{High}$, $CD34^{High}$ population maintains basal lamina contact and anchorage of the club hair, the second, $Krt5^+$, $Krt14^{Low}$, $\alpha6^{Low}$, $CD34^{High}$ population is found in the suprabasal region of the bulge, between the new hair shaft and club hair. These can be defined as the old and new bulge region respectively (Blanpain et al., 2004). Both populations had the ability to self-renew *in vitro*, repress terminal differentiation markers as well as lead to growth of new HFs when grafted onto nude mice, indicating that bulge SCs maintain their self-renewal capability and stemness throughout the HF cycling (Blanpain et al., 2004). *Lgr5* is

another key SC marker expressed in the bulge region as well as progenitor populations in the ORS and the matrix region (Jaks et al., 2008). *Lgr5* expressing cells and their progeny have been shown to actively proliferate during anagen and populate the bulge and SHG (Jaks et al., 2008). *Lgr5* expressing cells and their progeny are not only able to give rise to all new cell types of the HF, but also re-populate other SC residing areas including the bulge region. During HF cycling, CD34⁺ and Krt15⁺ expressing bulge cells do not overlap with *Lgr5* population, however, during telogen *Lgr5*⁺ and CD34⁺ cells overlap, indicating *Lgr5* in as being distinct marker of stem progenitor population during HF cycling (Jaks et al., 2008). Analysis of *Lgr5*⁺/*LacZ* cells during anagen stage of HF cycling showed cells migrating down the ORS and contribution of growth of the anagen HF (Jaks et al., 2008). *Lgr5* has also been shown to play a role in skin development. Induced expression of *Lgr5* in mice resulted in sparse fur coat and degeneration of sebocytes alongside with increase in expression of *Wnt5a* and *Gli1* (Norum et al., 2015). These populations show the dynamic nature of the bulge SC region in maintaining SC quiescence and self-renewal, but also committing to proliferation and differentiation during growth stage of HF cycling through cell migration down the ORS.

Markers for bulge SCs have been identified and have provide a more in-depth characterisation of the bulge SC niche through methods such as isolation and characterisation, lineage analysis and knockout studies (Morris et al., 2004, Fuchs, 2007, Blanpain and Fuchs, 2009). CD34 alongside integrin alpha 6 ($\alpha 6$ /CD49f) expressing keratinocytes were identified as slow cycling quiescent bulge SCs (Trempe et al., 2003). $\alpha 6$ has been shown to be important in cell adhesion and intracellular signalling (Krebsbach and Villa-Diaz, 2017). $\alpha 6$ expression is also promoted by transcription factors Oct4 and Sox2 and so may play a role in maintaining

SC 'stemness' through this mechanism (Yu et al., 2012). Krt15 and Krt19 have also been identified as bulge SC markers. Expression of both was observed in the ORS and hair bulb suggesting a Krt15⁺ and Krt19⁺ progenitor SC populations in the lower HF (Lyle et al., 1998). Krt15 expression is also colocalised with CD34 and α 6 expression in isolated bulge SCs (Trempeux et al., 2003) allowing them to be used as markers for specific bulge SC isolation (Villani et al., 2013). Other bulge SC markers include Gli1, a transcription factor that activates hedgehog signalling, can induce SC markers Krt15 and Krt19 in keratinocytes *in vitro* (Rittié et al., 2009). Gli1 expression is primarily located in the bulge region, the secondary hair germ and DP (Abe and Tanaka, 2017). A secondary stem/progenitor cell population was found near the bulge region, in the upper isthmus/lower infundibulum. These cells express α 6, is negative for CD34 but expresses stem cell antigen-1 (Sca-1) marker and have been shown to self-renew and give rise to epidermal, follicular, and sebaceous gland lineages *in vivo* (Jensen et al., 2008).

Lgr6, a close relative of Lgr5, has been found to be one of the earliest SC markers in the developing hair placode and found in the upper bulge region of the HF. It does not co-express with CD34⁺/Krt15⁺ bulge SCs and functions primarily in the formation of the sebaceous gland and interfollicular epidermis and is Wnt signalling independent, unlike Lgr5 (Snippert et al., 2010). This SC population can potentially renew sebaceous gland and epidermis in adult skin (Fuchs and Horsley, 2008, Snippert et al., 2010).

Sox9 is another important regulator of the HF and ORS formation, and is also involved in early HF placode growth, early bulge region development and adult bulge region homeostasis (Vidal et al., 2005, Nowak et al., 2008). Embryonic knockout of Sox9 led to partial HF and bulge formation, and failure to maintain transit-amplifying matrix cells

population (Nowak et al., 2008). Knockout of *Sox9* in adult HFs also showed similar results with reduction of bulge SCs and transition into epidermal cells. Furthermore, the ORS layer is not maintained, and HF growth is halted (Kadaja et al., 2014). These studies highlight the essential role of *Sox9* in formation and maintenance of bulge stem/progenitor cell populations.

Along with *Sox9*, LIM homeobox 2 (*Lhx2*) is expressed in early HF formation, in the bulge SC region, ORS and secondary hair germ (Daszczuk et al., 2020). In β -catenin and *Shh* knockout models, *Lhx2* expression is dramatically reduced, indicating *Lhx2* as a down-stream effector of Wnt and *Shh* signalling. It was also noted that loss of *Lhx2* resulted in loss of CD34 expression in bulge SCs (Rhee et al., 2006). Specific knockout of *Lhx2* in skin resulted in several phenotypes. Firstly, bulge SC adhesion and maintenance of the cytoskeleton of the bulge niche were compromised during regeneration of the new HF, resulting in the premature loss of the telogen hair shaft. Secondly, with ageing and successive hair cycling, some of the bulge SCs differentiated into sebocytes resulting in the slow degradation of the ORS and resulting in several sebaceous gland structures and a shortened HF (Folgueras et al., 2013). These studies indicate *Lhx2* to be crucial in stem/progenitor cell commitment and anchorage and maintenance of the bulge region. *Lhx2* has also been shown to play an important role in wound healing. *Lhx2* has been shown to regulate *Sox9* and *Tcf4* in the bulge SC region, promoting proliferation and re-epithelialization, whereas *Lhx2* negatively regulates *Lgr5* in the SHG, inhibiting HF cycling. These indicate the important role of *Lhx2* in controlling wound healing by modulating HF stem/progenitor cell proliferation and HF cycling (Mardaryev et al., 2011).

Several other SC markers have been identified: *Nfatc1*, which balances SC quiescence and colocalises with CD34⁺, *Sox9*⁺ and *Lhx2*⁺ cell populations (Horsley et

al., 2008). Vitamin D receptor (VDR) plays a role in ion transport and *VDR* knockout results in alopecia phenotype (Cianferotti et al., 2007). Lastly, Tcf3 is involved in maintaining SC quiescence in the absence of Wnt signalling and directing lineage commitment through Wnt signalling (Nguyen et al., 2006b). Pw1/Peg3 co-expresses with Sox9 during skin development before committing to bulge SC lineage. Pw1/Peg3 is co-expressed with CD34 and $\alpha 6$ in the anagen bulge region, and when isolated, is capable of giving rise to new HFs (Besson et al., 2017). These show a complex and diverse signalling network in SCs that fine tune gene expression, balancing activation and proliferation with quiescence and self-renewal.

The sebaceous gland resides just above the bulge region and maintains its own distinct SC population, producing sebocytes that hydrates and lubricates the skin through sebum secretion (Tobin, 2006, Sakuma and Maibach, 2012). During morphogenesis, precursor cells co-express Sox9 and Lrig1 and then split into Sox9⁺ bulge SC region and Lrig1⁺ sebocytes lineage giving rise to the early sebocytes (Frances and Niemann, 2012). Lrig1 plays a role in maintaining SC quiescence in interfollicular epidermal cells of the HF junctional zone, a region adjacent to the infundibulum and sebaceous gland. These cells also express Blimp1 (Jensen et al., 2009). Blimp1 has been identified as progenitor sebaceous gland population and are able to differentiate into sebocytes as well as self-renew. In *Blimp1* knockout mouse model, an increase in bulge SC activity was observed, which was attributed to bulge SCs repopulating the sebaceous gland stem/progenitor population (Horsley et al., 2006).

The Secondary hair germ (SHG) is a distinct progenitor population during HF cycling located between the hair bulb and DP. The SHG has been shown to be derived from migrating bulge SCs and through ORS progenitors during late catagen and present

throughout the resting quiescent telogen HF (Panteleyev et al., 2001, Panteleyev, 2018). The function of this progenitor SC pool is during initiation and growth of the next hair in the HF cycle. The SHG is thought to function to maintain the quiescence of bulge SCs from anagen activating signals from the DP as well as form hair synchronisation in mice due to partial pre-commitment to cell differentiation (Panteleyev et al., 2001, Panteleyev, 2018). Markers for SHG in telogen mouse HFs include P-cadherin (P-cad), an adhesion protein which is expressed around the DP, in the lower hair matrix and SHG during telogen. P-cad is also expressed the innermost hair matrix and ORS during active hair cycling (Müller-Röver et al., 1999). Dnmt1, P16 and Gata6 are also expressed in the SHG in telogen mouse HFs (Li et al., 2012, Wang et al., 2017, Panteleyev, 2018). In telogen HFs, Δ Np63 expression was noted in the bulge region as well as the SHG, where it is suggested to play a role in promoting self-renewal and growth during HF cycling (Romano et al., 2010). Krt15, Sox9 and Lgr5 are expressed in the SHG although it is diminished compared to the bulge region, while the SHG cells are negative for bulge SC markers CD34 and Nfatc1 (Greco et al., 2009, Panteleyev, 2018, Trempus et al., 2003). It is also interesting to note that upon wounding, the SHG can repopulate the bulge region and express bulge SC markers (Ito et al., 2004).

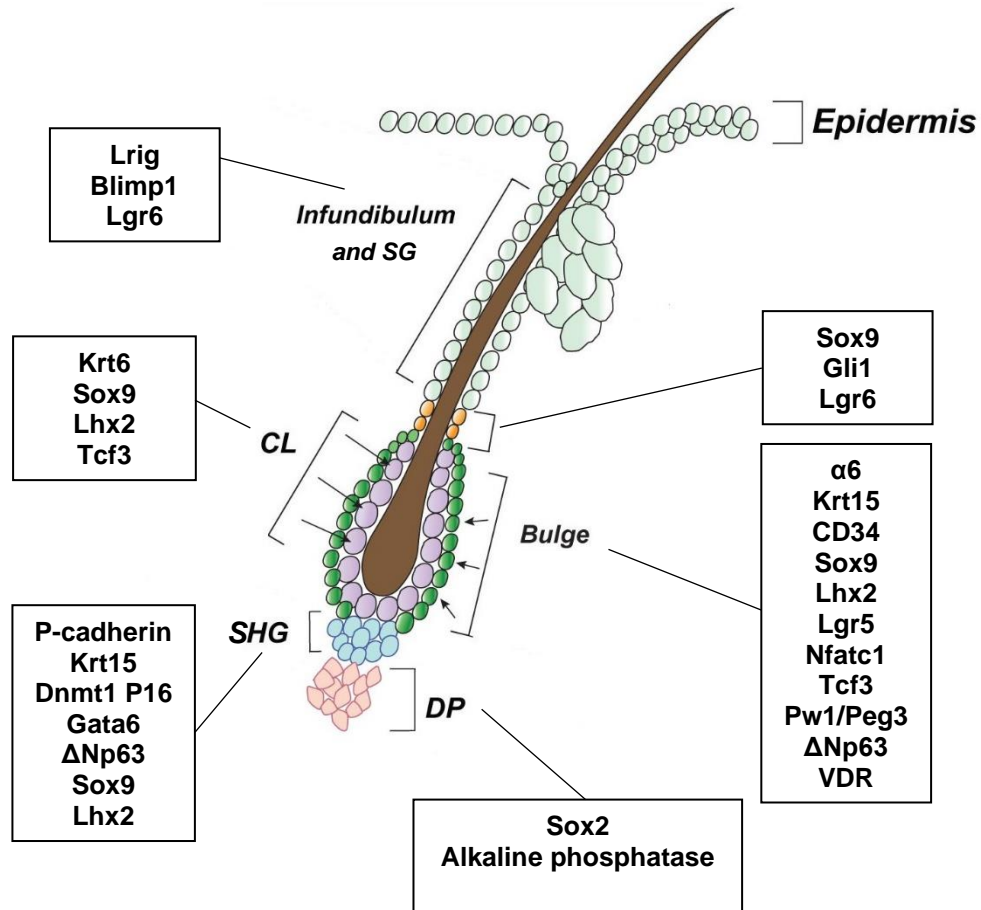


Figure 7. Stem Cell Compartments and Markers in the Mouse Telogen Hair Follicle.

Distinct SC and progenitor populations in the resting mature telogen HF. Bulge SCs give rise to the SHG and DP which signal and produce the actively growing HF during cycling. Sebaceous gland SCs function to renew sebocytes in the sebaceous gland. Key markers are given in the labelled boxes. (SG: sebaceous gland, CL: club hair, SHG: secondary hair germ, DP: dermal papilla). Adapted from (Daszczuk et al., 2020).

1.6 MicroRNAs

MicroRNAs (miRNAs/miRs) are small non-coding RNAs typically ~19-24 nucleotides (nt) in length and function to regulate genes post-transcriptionally (Yi and Fuchs, 2010, Schneider, 2012). The first miRNA to be discovered in 1993 was Lin-4, a 22nt RNA by the Ambros group (Lee et al., 1993). They found that Lin-4 did not produce a protein but a short RNA that targeted the 3'-untranslated region (UTR) of *Lin-14* and regulated

it in this manner (Lee et al., 1993). It was not until 2000 that the second miRNA; Let-7, was discovered by the Ruvkun's group (Reinhart et al., 2000). Using the same model, *C. elegans*, they found that the twenty-one nucleotide RNA Let-7 regulated larval development and targeted *Lin-41* at the 3'-UTR (Reinhart et al., 2000). Since these discoveries, many more miRNAs have been discovered and their functional roles and targets investigated. There are over two-thousand miRNAs discovered in humans which are estimated to regulate a third of the genome through messenger RNA (mRNA) degradation (Valencia-Sanchez et al., 2006, Hammond, 2015, O'Brien et al., 2018).

The mechanism by action of miRNAs in targeting mRNA for post-transcriptional genetic regulation is termed RNA interference (RNAi). The RNAi phenomena was elucidated by the Mello group in 1998 (Fire et al., 1998).

Since miRNAs discovery, other interfering RNAs have been discovered and classified as having an RNAi mechanism. Short interfering RNAs (siRNAs) were discovered in 1999. In 2001, synthesised siRNA was shown to induce RNAi *in vitro* (Hamilton and Baulcombe, 1999, Elbashir et al., 2001). Piwi-interacting RNA (piRNA) is another class of RNAi and derived from single stranded precursor transcripts unlike miRNAs and siRNAs (Ozata et al., 2019). MiRNAs differ from other RNAi players in their biogenesis.

1.6.1 MiRNA Biogenesis

MiRNAs are made through a series of proteolytic steps from a larger RNA transcript. The first step is transcription: In the canonical miRNA biogenesis pathway, this is performed by RNA polymerase II, or III to form the pri-miRNA (Lee et al., 2004, Borchert et al., 2006). The transcription of the pri-miRNA can be intergenic or intronic. Intergenic miRNAs are transcribed as independent units whereas intronic miRNAs are

transcribed from introns of their hosting transcriptional unit and therefore have a common expression pattern as the gene which hosts them. MiRNAs can also be exonic, coded within a gene's exon and like intronic miRNAs, display a close relationship with their hosting gene (Figure. 8) (Slezak-Prochazka et al., 2013). Within each transcript location, miRNAs can also be clustered with several others under control from a shared promoter (Ramalingam et al., 2014). Large clusters of miRNAs within a genomic loci make up a polycistronic units, multiple miRNAs are co-transcribed and then spliced later in the processing network (Figure. 8) (Lee et al., 2002).

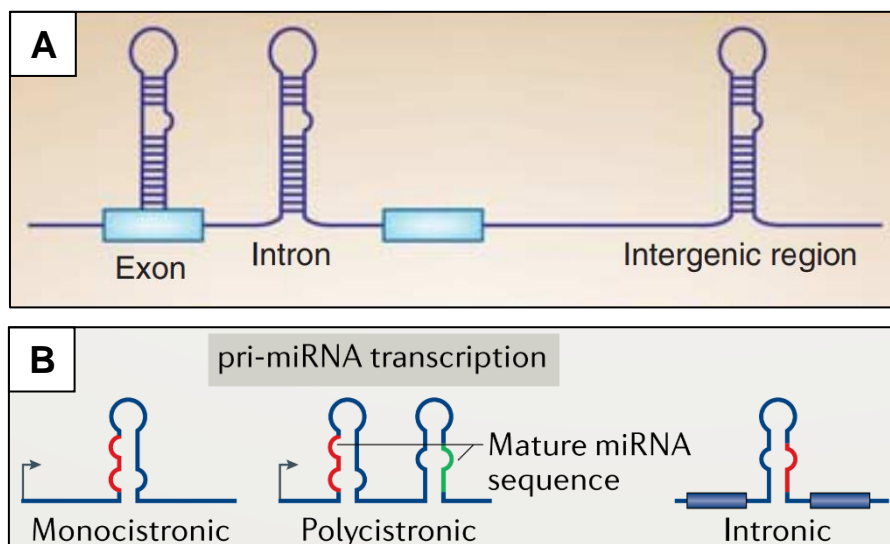


Figure 8. *Schematic Depiction of MiRNA Transcription.*

(A) MiRNAs are found throughout the genome, coded within exon and introns of genes under the control of the associated gene promoter, or as independent units with their own promoter, termed intergenic miRNAs. (B) Single coded miRNAs are termed monocistronic whereas multiple miRNAs within a cluster are termed polycistronic and can contain miRNAs of the same family. Adapted from (O'Carroll and Schaefer, 2013) and (Treiber et al., 2018).

Following transcription, the pri-miRNA is cleaved by RNase III enzyme Drosha and the DiGeorge critical region 8 (Dgcr8) protein complex into a ~seventy nucleotide stem loop structure pre-miRNA. Dgcr8 contains two double stranded RNA binding domains which recognise the pri-miRNA, while Drosha contains two RNase III domains which interact and cleave the pri-miRNA 5' and 3' strands, leaving approximately eleven Base pairs from the miRNA sequence and a two-nucleotide overhang (Lee et al., 2003, Han et al., 2004, Han et al., 2006, Ha and Kim, 2014). After cleavage, the pre-miRNA is exported from the nucleus to the cytoplasm by Exportin-5 (Exp5) coupled with Ran-GTP cofactor (Figure. 9) (Yi et al., 2003).

Once the pre-miRNA is in the cytoplasm, it is processed by RNase III enzyme Dicer (Zhang et al., 2004). Dicer recognises the 2-nucleotide overhang left by Drosha-Dgcr8 cleavage. For Dicer to correctly cleave the pre-miRNA, Dicer recognises the 3' end of the antisense strand and 5' phosphorylated end of the sense strand. The cleavage site is usually a set distance from the 3' end of the Dicer binding site with length depending on the type of Dicer and species and distance between Paz (PIWI-Argonaute-ZWILLE) and RNase III domains of Dicer (Zhang et al., 2004, Macrae et al., 2006). In mammals, Dicer cuts from a specific distance from the phosphorylated 5' end binding site providing another regulatory mechanism for correct Dicer cleavage (Park et al., 2011). The loop structure of pre-miRNA is cleaved leaving behind a miRNA duplex (Figure. 9). Alternate splicing of the pre-miRNA loop by Dicer can lead to isomirs of a miRNA which can differ in length or sequence leading to an increased repertoire for the miRNA and contributes to evolutionary stability (Tan et al., 2014). The Dicer cleaved miRNA duplex is coupled with an Argonaute (Ago) protein which then forms an RNA induced silencing complex (RISC) with other proteins, forming a mature miRNA-RISC (miRISC), which mediates the RNAi function of the miRNA (Hammond et al., 2001).

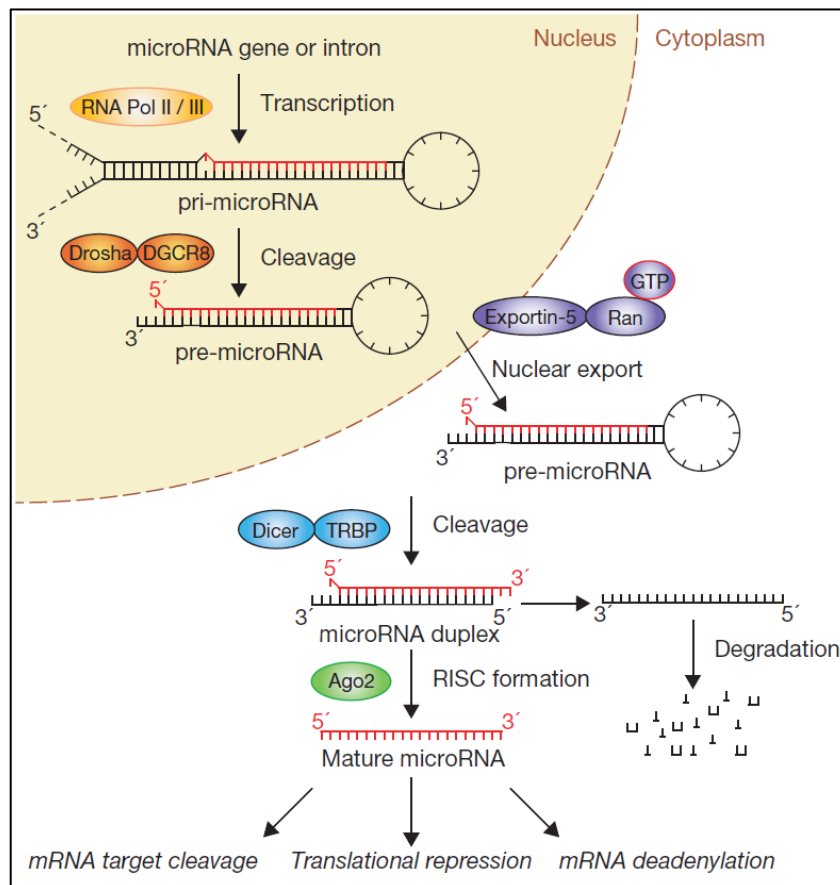


Figure 9. MicroRNA Biogenesis Pathway.

MiRNAs are transcribed by RNA polymerase II/III into pri-miRNA. Pre-miRNA is made in the nucleus through cleavage of pri-miRNA by Drosha-Dgcr8 complex before it is exported to the cytoplasm by Exportin-5. The pre-microRNA is further cleaved into mature microRNAs by Dicer complex. The mature microRNA forms an RNA Induced Silencing Complex (RISC) with argonaut proteins where the complex can bind to messenger RNA 3'-UTR and prevent protein expression through target cleavage, repression or deadenylation (Winter et al., 2009).

The miRNA duplex bound to the RISC is then unwound, and cleavage of the passenger strand (miR*) occurs, leaving behind a single-stranded guide miRNA strand. Selection of the guide strand is driven by thermodynamic stability of the strands. The strand with the less thermodynamically stable 5' end is generally selected

as the guide strand whereas the strand with higher stability at the 5' is usually degraded (Schwarz et al., 2003, Khvorova et al., 2003). Argonaute protein strand selection also plays a role with preferential binding of uracil in the 5' end with cytosine commonly present in the 5' end of the passenger strand (Figure. 10) (Mi et al., 2008, Frank et al., 2010, Medley et al., 2021). The more active arm can however switch in different tissues and change throughout development (Chiang et al., 2010). The 5p arm (termed so as the mature miRNA derives from the 5' end of the pre-miRNA hairpin) is generally more selected in miRNA processing because of the accuracy of the processing enzymes. Drosha is a more accurate enzyme than Dicer and so the 5p arm 'seed' sequence would be more accurately cut at the 5' end, where drosha cuts (Figure. 10) (Hu et al., 2009).

Strand selection and miRISC maturation is regulated by the RISC loading complex (RLC) in humans. The RLC is comprised of Dicer, Ago2 core and RNA binding domains; TRBP (Tar RNA binding protein) and PACT (protein activator of PKR) (MacRae et al., 2008, Lee et al., 2006, Winter et al., 2009). TRBP and PACT function to aid Dicer in pre-miRNA cleavage and assembly of the RISC. Knockout of both resulted in a significant reduction in gene silencing capability (Chendrimada et al., 2005, Lee et al., 2006). Ago proteins are key members of the RISC. There are 4 human Ago proteins but the Ago2 is the main protein that mediates the mRNA targeting and cleavage effects of the RISC (Liu et al., 2004). However, more recently, Ago3 has been shown to have this function with certain miRNAs (Park et al., 2017). Upon RISC assembly, the Ago protein undergoes conformational changes in miRNA duplex binding and unwinding before selection of the specific strand (Wang et al., 2009). Once the RISC is assembled, the 'seed' region, placed at position 2-8nt of the miRNA known as the 'seed' sequence, binds through complimentary base pairing usually to the

3'UTR of the target mRNA where the miRISC mediates its effect (Djuranovic et al., 2012).

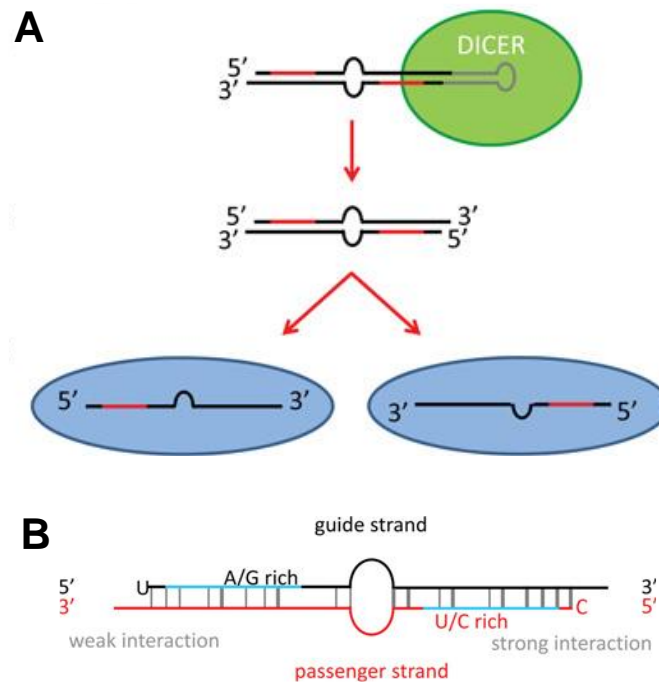


Figure 10. MicroRNA Strand Selection.

(A) Cleavage of pre-miRNA by Dicer leads to a miRNA duplex. The duplex is split into a guide and passenger strand. Either or both strands can be selected and present in a miRISC (red highlighted segment is the 'seed' sequence; blue circles are Ago proteins). **(B)** The guide strand is selected by the less thermodynamically stable 5' end. In human miRNA, 5' end of the guide strand usually starts with a Uracil base and its 'seed' sequence is generally Adenosine/Guanine rich as this leads to lower thermodynamic stability compared to Uracil/Cytosine rich passenger strand. Adapted from (Meijer et al., 2014).

Most miRNAs are synthesised through the described canonical biogenesis pathway, however, non-canonical miRNA biogenesis is also emerging as a regulatory subset of miRNAs. Non-canonical biogenesis bypasses one or more steps of the canonical biogenesis pathway. These pathways can be Drosha/Dgcr8 or Dicer independent and

have a variety of starting transcripts, not necessarily from introns (Abdelfattah et al., 2014, Ha and Kim, 2014). For example, miR-451 biogenesis does not require Dicer and is cleaved by Ago-2 (Yang et al., 2010). Short hairpin duplexes can be produced from introns independently from Drosha. These mimic pre-miRNA structures and can enter the cleavage step at Dicer. An example of this is miR-1003 in *D. melanogaster* (Ruby et al., 2007).

1.6.2 Post-transcription Regulation of Gene Expression

Binding of MiRISC 'seed' sequence to mRNA 3'UTR *via* complimentary base pairing results in a variety of outcomes, such as: unloading of the miRNA to its target, cleavage of the target, stable target binding or transient target binding (Jo et al., 2015). The selection of one of these outcomes depends on the miRNA:mRNA interaction through their sequences and also thermodynamic stability. 'Seed' sequences and their target are not always perfect matches. Complimentary pairing of nucleotide 12-16 can aid target stability and even non-'seed' target sites exists. This variety can give rise to a range of targets, so miRNAs have a wider range of influence and can fine tune gene expression (Grimson et al., 2007, Brodersen and Voinnet, 2009, Wang et al., 2009).

MicroRNA 'families' are categorised based on their 'seed' sequence similarity and can therefore be predicted to have similar targets and function during gene targeting (Bartel, 2009). MiRNA families allow target site multiplicity can aid in effective mRNA targeting and also result in a single miRNA with a variety of targets due to lack of requirement for perfect base pair matching to the target (Brodersen and Voinnet, 2009). Examples include: *p21*, a modulator of cell cycle and DNA repair, can be targeted by 28 different miRNAs (Wu et al., 2010a). Whilst knockout of 83% of miRNAs in *C. elegans* did not result in detrimental phenotype and normal development due to

miRNA family members filling in for the role in a redundancy mechanism (Miska et al., 2007). These studies indicate the complexity of miRNA networks where redundancy and multiplicity of targeting gives mutation and evolutionary protection of regulation and potential for form new regulatory networks.

It is believed that miRNA-target cleavage is dependent on central binding regions of the 'seed' sequence with single mutations in the centre of the 'seed' sequence drastically reducing cleavage activity (Martinez and Tuschl, 2004, Brodersen and Voinnet, 2009). The miRNA is held in a position optimal for target binding and nucleation (Parker et al., 2009, Lambert et al., 2011, Jo et al., 2015). The outcome of the miRISC-target interaction is potentially dependant on the nucleation and thermodynamic stability, as well as Ago-2 cleavage of the target using Mg^{2+} ions (Wang et al., 2009, Jo et al., 2015). A study in human AGO2 bound to small RNA guide sequence revealed multiple actions upon target binding. Despite perfect 'seed' region matches with the target, 72% of target binding events resulted in stable binding or miRNA-mRNA unloading, but not cleavage, which is dependent on the argonaute protein and target RNA strand, along-side thermodynamic kinetics of binding. In addition, target cleavage probability was lowered with mismatches in the 'seed' sequence (Jo et al., 2015).

1.6.3 Regulation of MiRNAs

Regulation of miRNAs is an essential step in the gene regulatory network to ensure homeostasis. Transcription of miRNAs are under control from their promoters. However, promotor mapping for miRNAs has not yet been established and various promotor prediction theories have arisen from analysing histone markers, analysing RNA pol II binding region, ChIP and RNA sequencing (Zhao et al., 2017). Intrinsic

regulation of miRNAs are changes in its sequence that effects the biogenesis and mature production of the miRNA. MiRNA tailing is the addition of nucleotides to the 3' end of the RNA to tag them for degradation (Ha and Kim, 2014). RNA binding proteins Lin28a and Lin28b cause uridylation of pre-Let-7 which then fails to undergo Dicer processing and is broken down (Heo et al., 2008). As well as tailing, miRNAs can undergo editing which converts adenosine base into an inosine base. Editing of pre-miR-151 produces a similar effect as tailing, with failure to undergo Dicer cleavage and thus degradation (Kawahara et al., 2007). Another regulatory mechanism in miRNA processing is methylation. Highly methylated miRNA transcripts or miRNA transcript flanking regions lead to higher miRNA expression and lower methylation lead to lower miRNA expression (Glaich et al., 2019). However, methylation of partially processed miRNAs can lead to degradation. RNA-methyltransferase, BCDIN3D, methylates pre-miR-145 resulting in reduced processing by Dicer (Xhemalce et al., 2012). MiRNA methylation has been implicated in cancer, with miR-17, miR-21 and miR-200C all harbouring increased methylation in gastrointestinal cancers compared to healthy tissues, affecting their mechanism as post-translational regulators (Konno et al., 2019).

Stability and half-life of a miRNA can be influenced by developmental cues. During cell cycle arrest at G₀, the miRNA-16 family expression level drastically increases, but quickly decreases during G₁ re-entry. This quick change in expression levels is due to the instability of some of its family members (Rissland et al., 2011). This instability can lead to quick temporal changes in miRNA levels in response to biological cues. Stability of miRNAs could be attributed to the nucleotide additions and amendments through tailing and uridylation. Specific interaction with the target could influence miRNA stability and therefore abundance. MiRNAs can bind to multiple targets before

they are degraded, and their stability influences how many targets the miRNA can bind. Perfect binding of miR-233 to its target has shown to decrease its stability and promote its degradation (Baccarini et al., 2011). Equally, binding to certain targets can increase the stability of the miRISC. MRNAs can protect miRNAs from degradation in *C. elegans* through studies with Let-7(n2853) mutation which destabilised mature let-7 miRNA, although the mechanism of its protection was not clear (Chatterjee et al., 2011).

Exoribonucleases are partly responsible for miRNA degradation and clearance once they are released from the RISC. For example, In *C. elegans*, let-7 is degraded by exoribonuclease XRN-2 (Chatterjee and Grosshans, 2009). In addition, loss of exonuclease Eli1 in mouse lymphocytes resulted in an increase in miRNA abundance (Thomas et al., 2012).

1.6.4 MiRNAs in Skin and Hair Follicle Development

The diverse network of miRNAs provides an important regulatory role in skin and HF development. The role of miRNAs has been shown to be essential in mice with *Dicer* knockout resulted in embryonic lethality (Bernstein et al., 2003). Conditional *Dicer1* knockout in embryonic skin progenitors resulted in severe defective skin and HF development with HF placodes evaginating into the epidermis and forming cysts (Yi et al., 2006). Epidermal specific *Dicer* knockout resulted in loss of Shh and Notch signalling in post-natal developing HFs resulting in evagination of the DP, failure of hair shaft to form, lack of SC markers Krt15 and CD34 expression, and a reduction of Sox9⁺ progenitor cells (Andl et al., 2006, Yi et al., 2006). In addition, miRNA processing enzyme *Dgcr8* knockout showed similar defects to conditional *Dicer1* knockout mice models (Yi et al., 2009). These studies indicate the vital importance of miRNAs in skin

development. More specifically, Yi and authors classified the spatial expression patterns of several miRNAs in the skin and HF, for example miR-203, 205 and 200a were all highly expressed in the epidermis compared to miR-199a, 214 and 152 that were highly expressed in the HF (Yi et al., 2006). These indicate that the spatial and temporal expression of miRNAs is essential for normal skin development.

Specific miRNAs have been identified and their roles in skin and HF development classified over the years. Approximately seventy miRNAs have been shown to be dynamically expressed in embryonic skin, as well as greater than two-hundred miRNAs identified to be differentially expressed during the different stage of HF cycling through microRNA microarray analysis (Andl et al., 2006, Yi et al., 2006, Mardaryev et al., 2010). MiRNA-203 has been shown to be important in regulating keratinocyte differentiation. Knockout of miR-203 resulted in thinner skin compared to control, a depletion of basal SCs, and a decrease in their proliferation (Yi et al., 2008). *P63* was identified as a target of miR-203. P63 expression has been shown in the basal layer of the epidermis and is downregulated when the epidermis becomes stratified (Koster et al., 2004). MiR-203 knockout results in ectopic expression of p63 and premature miR-203 expression results in loss of basal p63 expression (Yi et al., 2008), suggesting that miRNA-203 is involved in promoting differentiation of keratinocytes during epidermal stratification.

MiR-34b and miR-34c have been shown to be targeted by *p63* in order to progress through the cell cycle and proliferate as the epidermis becomes stratified. MiR-34b and miR-34c are both expressed in the suprabasal, differentiating keratinocytes of the epidermis, to control cell cycle progression in the differentiating and proliferating epidermis (Antonini et al., 2010). These shows the importance of a miRNA as a

mediator of skin development and relationship with p63 for cell cycle progression and differentiation during epidermal stratification.

In addition, miR-214 is expressed in differentiating epidermal keratinocytes during skin development and hair matrix cells in developing HFs. MiRNA-214 was found to directly target *β-catenin* (Ahmed et al., 2014). Wnt signalling has been implicated in promoting differentiation of developing epidermal keratinocytes from the basal layer, initiation of HF placode formation and progressive HF formation (Andl et al., 2002, Zhang et al., 2009b, Zhu et al., 2014). The reduction in HF formation and decreased proliferation after induced overexpression of miR-214 is linked to modulation of the diverse regulatory Wnt signalling pathway.

MiRNA-205 was found to be highly expressed in the basal layer of the epidermis and in SC compartments during skin and HF development (Yi et al., 2006, Wang et al., 2013a). Knockout of miR-205 is neonatal lethal by post-natal day 10 and resulted in a thinner epidermis and mis-angled HFs at P4.5. Proliferation of the interfollicular progenitors and HF-SCs were impaired but not in the matrix cells (Wang et al., 2013a). This indicates miRNA-205 plays a role in controlling the proliferation of SCs in development.

1.6.5 MiRNAs in Hair Follicle Cycling

To determine whether miRNAs are essential during HF cycling, inducible deletion of *Dicer* or *Drosha* was performed during anagen (Teta et al., 2012). Induced deletion of *Dicer* or *Drosha* during anagen stage of HF cycling resulted in failure to enter the subsequent catagen phase and loss of bulge SCs. Anagen induction by plucking resting HFs in induced *Dicer* or *Drosha* knockout resulted in the production of transit-amplifying matrix-like cells but with increased apoptosis and increase in DNA damage

(Teta et al., 2012). This indicates that miRNAs are essential in HF cycling and maintenance of SC populations for progressive cycles.

In another study, global miRNA microarray profiling in the skin was performed at distinct stages of the hair cycle and differential expression pattern for a wide range of miRNAs was revealed (Mardaryev et al., 2010). MiRNA-31 was shown to be upregulated during anagen and markedly downregulated during catagen and telogen and inhibition of miR-31 resulted in accelerated anagen development. It was revealed that miR-31 regulated anagen stage through direct regulation of *Fgf10* and negatively regulates Wnt and BMP signalling components: Sclerostin and BAMBI. MiR-31 was also shown to directly target *Krt16*, *Krt17*, *Dlx3* and *Fgf10* (Mardaryev et al., 2010). Another miRNA, miR-148a was shown to be differentially expressed during hair cycling. MiR-148a expression was upregulated during telogen stage of HF cycling with downregulation of miR-148a expression during anagen and catagen stage, however, the role of miR-148a has not been established in hair cycling (Mardaryev et al., 2010). This microarray analysis shows the diverse regulatory control miRNAs have on controlling HF cycling.

An additional miRNA, miR-125b was found to be expressed in HF-SCs and decreased in the progenitor populations (Zhang et al., 2011). Overexpression of miR-125b was found to increase epidermal thickness, enlargement of sebaceous gland and development of alopecia with *Blimp1* and *VDR* identified as direct targets of miR-125b. (Zhang et al., 2011). *Blimp1* is required for sebaceous gland development and expressed in sebaceous gland stem/progenitor cell populations (Horsley et al., 2006). *VDR* has been shown to be essential for the anagen phase and normal HF cycling. *VDR*-null mice exhibit alopecia and significant reduction of Wnt and Shh target genes, associated with early anagen induction (Andl et al., 2002, Sato et al., 1999, Lisse et

al., 2014). Therefore, miRNA-125b most likely plays a role in fine tuning SC specification and fate involved in HF cycling by maintaining SC 'stemness' (Zhang et al., 2011).

MiR-29a/b1 is also involved in the fine-tuned control of SCs during HF cycling. MiR-29a/b1 expression patterns showed that its expression was inverse to HF-SC lineage progression, with decreased expression as SCs differentiate (Ge et al., 2019). Overexpression of miR-29a/b1 in anagen and telogen HFs resulted in shortened hair shafts and hair loss due to reduced proliferation of stem and matrix cells, whilst inhibition of miR-29a/b1 *in vivo* resulted in accelerated SC lineage progression (Ge et al., 2019). MiRNA-29a/b1 was found to target *Ctnnb1*, *Lrp6*, *Bmpr1a*, and *Ccna2*, genes associated with Wnt and BMP signalling and contribute to proliferative and differentiation regulation during HF cycling (Ge et al., 2019).

1.6.6 MiRNAs in Skin Disease

Various miRNAs have been implicated in skin disorders through either repression of tumour suppressor genes (Onco-miRs) (Esquela-Kerscher and Slack, 2006) or dysregulation of their regulatory roles. Dysregulation of signalling pathways can provide aberrant proliferation or differentiation associated with some skin disorders and failure to maintain skin homeostasis (Lim and Nusse, 2013, Lopez-Pajares et al., 2013).

MiRNA-21 plays a role in controlling skin development by modulating BMP signalling as a downstream component (Ahmed et al., 2011). MiR-21 expression is observed in the epidermis and the HF epithelium. BMP4 treatment was shown to dramatically reduce miR-21 expression in keratinocytes and miR-21 expression was increased in transgenic mouse model overexpressing BMP antagonist noggin. MiR-21 was also

shown to target BMP dependant tumour suppressor genes *Pten*, *Pdcd4*, *Timp3* and *Tpm1* (Ahmed et al., 2011). MiR-21 has also been shown to be involved in ageing. MiR-21 negatively regulates chromatin remodeler *Satb1* in both aged human and mice and serves as a directly target of miR-21 (Ahmed et al., 2019). Together, these studies show the importance of miR-21 in maintaining skin homeostasis through skin development and potentially age-related disorders.

MiRNAs have also been shown to be dysregulated in inflammatory skin disease such as psoriasis (Ichihara et al., 2011). Psoriasis is a chronic inflammatory skin disease mediated by dysregulation of inflammatory pathways that form lesions on the skin (Timis and Orasan, 2018). MiR-146a, has been shown to be upregulated in psoriasis (Sonkoly et al., 2008). After miR-146a inhibition, Interleukin-7 expression was increased, hyperproliferation was observed, and psoriasis onset (Ichihara et al., 2011, Srivastava et al., 2017). MiR-146a was found to target genes involved in the TNF- α signalling which have been shown to mediate immune responsive genes (Taganov et al., 2006). Another miRNA involved in psoriasis is Let-7b. Let-7b overexpression was shown to increase epidermal differentiation in psoriasis. Let-7b was found to directly target Interleukin-6 and regulate differentiation through modulation of the Erk1/2 pathway (Choi et al., 2014, Wu et al., 2018).

Taken together, these indicate the importance of miRNAs in the control of normal skin and HF development. Dysregulation of miRNAs in the skin can lead to development of skin disorders and therefore provide ideal targets for future therapeutic approaches.

1.7 E74 Like Transcription Factor 5 (Elf5)

Elf5 is a transcription factor that is a member of the ETS family of transcription factors whose membership is based on the ETS binding region which binds to A/G rich regions in gene promoters, modulating gene expression in this manner (Zhou et al., 1998).

Elf5 has been well categorised in the control of mammary gland alveolar development and is also essential for embryonic development, with *Elf5* knockout being embryonic lethal (Zhou et al., 2005). Conditional knockout of *Elf5* in mammary glands result in failure of alveologenesis during pregnancy (Chakrabarti et al., 2012b). Deletion of *Elf5* led to increase in expression of basal cell markers Krt8 and Krt14, and accumulation of mammary SCs along-side increase in Notch signalling, indicating that Elf5 plays an important role in modulating cellular differentiation from SCs in the mammary gland (Chakrabarti et al., 2012b).

Elf5 has previously been observed in the skin. Generation of Elf5-LacZ mice resulted in high galactosidase staining observed in the IRS of anagen HFs (Choi et al., 2008). In a separate study, Elf5 expression was also upregulated in keratinocyte differentiation (Tummala and Sinha, 2006).

Elf5 has also been characterised in several other tissues. During kidney development, Elf5 expression was observed in developing collecting ducts and mature principal cells, as analysed by lineage tracing. Elf5 was also found to be upregulated when Notch1 was overexpressed and is linked to promotion of principal duct cell lineage, implicating Elf5 in promoting cell differentiation and commitment (Grassmeyer et al., 2017). Elf5 is also expressed during lung development. Elf5 was observed in the distal tips of developing lungs and restricted to the epithelium. Elf5 expression was also found to be induced by Fgf7 and Fgf10 and mediated through the Akt pathway

(Metzger et al., 2007). These studies demonstrate the variety of pathways involved in modulating Elf5 expression and indicate its importance during developmental processes. However, its role in skin and HFs is currently unknown.

Elf5 has also been characterised in progression of various cancers. Elf5 has been shown to suppress breast cancer progression through acetylation and reduction in expression of Elf5 target gene Cyclin D1 (*Ccnd1*), a driver of S to G2 phase during cell cycling (Stacey, 2003). *Ccnd1* was shown to have two Elf5 binding sites in the promoter identified by ChIP analysis (Li et al., 2021). The anti-proliferative mechanism of Elf5 in breast cancer may be present in other epithelial tissue types and help to regulate proliferation in other developmental processes (Chakrabarti et al., 2012a).

To our knowledge, Elf5 has not been shown to be regulated by any miRNAs in skin or HFs. Understanding the regulation of Elf5 through miRNA targeting could elucidate the regulatory mechanisms behind keratinocyte proliferation and differentiation processes and offer a new therapeutic or research target for controlling key developmental processes in skin and HFs.

1.8 Rho-Associated Kinase (Rock) 1

Rock1 is a serine/threonine kinase and downstream effectors of GTPase Rho. There are two main mediators of Rho signalling, Rock1 and Rock2. Rock1 and Rock2 have been shown to have 92% sequence identity in their kinase domains but 66% in their PH domains, indicating similar, but distinct roles (Nakagawa et al., 1996).

Rock signalling has been shown to regulate the actin cytoskeleton and cell adhesion. Isolation of mouse embryonic fibroblasts from *Rock1* knockout mice showed increased actin cytoskeletal stability resulting in a decrease in cell shrinkage, detachment and apoptosis compared to fibroblasts isolated from *Rock2* knockout mice

resulting in impaired cell adhesion (Shi et al., 2013). In the skin, inhibition of ROCK2 signalling in human keratinocytes resulted in inhibition of differentiation and an increase in cell proliferation, whereas activation of ROCK2 resulted in increase in differentiation and a decrease in proliferation (McMullan et al., 2003). The same group showed a difference between the roles of ROCK1 and ROCK2 in human keratinocytes with ROCK1 inhibition resulting in decreased keratinocyte adhesion and increased differentiation, whereas ROCK2 inhibition resulted in the opposite (Lock and Hotchin, 2009). These studies indicate the dual mechanism of RhoA signalling in fine tuning keratinocyte differentiation and proliferation, potentially through modulation of cell adhesion and detachment required for terminally differentiating or proliferating cells.

Rock signalling has been shown to play a role in wound healing. Administration of Rock inhibitor to mouse wounds led to a significant delay in wound closure and a decrease in α -Smooth muscle actin fibre formation (Tholpady et al., 2014). Slower wound healing and re-epithelialization was observed in zebrafish wound models upon Rock inhibition and also failure for epidermal cells to undergo cell elongation to close the wound (Richardson and Hammerschmidt, 2018). Rock signalling has been shown to play a role in determining planar cell polarity to form epithelial sheets and could influence wound closure and re-epithelialization (Strutt, 2001, Caddy et al., 2010).

Several miRNAs have been shown to directly target Rock1 in cancers: MiR-145, increasing glioma cell invasion by actin cytoskeletal reorganisation, miR-124, which inhibits cell proliferation and metastasis in colorectal cancer, and miR-129-5p, suppresses proliferation and invasion in osteosarcoma (Wan et al., 2014, Zhou et al., 2016, Han and Wang, 2018). In gastric cancer cell lines, pharmacological inhibition of Rock signalling resulted in G1-S phase arrest during the cell cycle and cyclin dependant kinases (CDK) 2, 4 and 6 were downregulated, whilst upregulation of cell

cycle inhibitors: p15, p16, p18 and p19 was also observed (Zhang et al., 2009a). In non-small cell lung cancer and melanoma mouse models, conditional knockout of *Rock1* and *Rock2* resulted in defects in cell proliferation through G1 cell cycle arrest. Downregulation of CDK1, Cyclin A and cyclin dependant kinase regulatory subunit 1 (CKS1b) were also observed alongside increased cellular senescence (Kümper et al., 2016). These indicate the powerful role of Rock signalling in mediating cellular proliferation in cancer models that may have similar functional roles in developmental processes.

With *Rock1* playing a diverse role in cellular differentiation and proliferation, characterising the regulatory pathway in during skin development and HF cycling would open potential routes of investigation for novel therapies and research targets in treatment of skin related disorders.

1.9 Aims

MiRNAs form a diverse and expansive regulatory network of genetic expression in the body. The skin and HF provide a model of research that is representative of the cellular processes in the body such as, cell migration, differentiation, proliferation, and apoptosis. Using skin and HFs as research models to study miRNA regulatory networks will help elucidate the role of miRNAs and their role in regulating these cellular processes. This will improve our understanding of the important pathways involved in skin and HF development, regeneration, and homeostasis, which will lead to improved treatment and therapy for various skin disorders in the future.

Our initial miRNA microarray data has shown that miR-148a is highly expressed during telogen phase (quiescent SCs) of HF cycling (Figure. 11A). We hypothesise that miR-148a plays an important role in regulating skin development and HF cycling *via* tight regulation of gene targets and signalling pathways associated with stem/progenitor cell populations during this stage. Therefore, the aim of this study was to investigate the role of miR-148a in controlling molecular mechanisms underlying stem/progenitor cell maintenance and activation during skin and HF development.

2.0

Materials and Methods

2.1 Materials Used in the Investigation

2.1.1 Reagents and Chemicals Used During the Investigation

Table 1. *Laboratory Reagents/Chemicals Used in the Investigation.*

Reagent	Catalogue number	Company
0.25% (w/v) Trypsin-EDTA	25200-072	ThermoFisher
0.45µm nitrocellulose membrane	1620115	BIO-RAD
2-Mercaptoethanol	125470010	ThermoFisher
3,3',5-Triiodo-L-thyronine sodium salt (T3)	TT5516	Merck
30% (w/w) Acrylamide/Bis solution (37.5:1)	1610158	BIO-RAD
5X Saline-sodium citrate (SSC)	15557-044	ThermoFisher
Acetic acid	10171460	ThermoFisher
Acetic anhydride	320102	Merck
Adenine	A8626	Merck
Agarose	11496950	ThermoFisher
Ammonium persulfate (APS)	161-0700	BIO-RAD
Ampicillin Sodium Salt	BP1760	Fisher Scientific
Baphthol AS-BI phosphate	N2125	Merck
Blocking reagent	11096176001	Roche
BM Purple AP substrate	11442074001	Roche
Bovine serum albumin (BSA)	BP9702	Fisher Scientific
BT chelex 100 resin	143-2832	BIO-RAD
Calcium chloride (CaCl ₂) 0.5 M	C/1400/60	Fisher Scientific
Cholera Toxin	C8052	Merck
Chondroitin sulfate sodium salt from shark cartilage (CSC)	C4384	Merck

cOmplete ULTRA Protease inhibitor cocktail tablets, Mini EDTA-free	04906837001	Merck
DAPI	D9542	Merck
Deionised (DI) formamide	F9037	Merck
Diethyl pyrocarbonate (DEPC)	D5758	Merck
DMEM media (+4.5g/L D-glucose, -L-glut, -pyruvate)	11960-044	ThermoFisher
DMEM/F-12 Ham (3:1) High Glucose (+L-glutamine, -CaCl ₂ , -Sodium bicarbonate)	AT189	HIMEDIA
DPX mounting medium	06522	Merck
EDTA UltraPure 0.5 M, pH 8.0	15575-020	ThermoFisher
Epidermal growth factor from murine submaxillary gland	E4127	Merck
Ethanol	BP8202	Fisher Scientific
Formamide	F9037	Merck
Glycerol	G/0650/17	Fisher Scientific
Hanks' Balanced Salt Solution (HBSS) without Ca ²⁺ , Mg ²⁺	88284	ThermoFisher
Heat-inactivated Fetal bovine serum	11550356	Fisher Scientific
Hematoxylin	BP2424	Fisher Scientific
Heparin	BP2524	Fisher Scientific
HEPES	BP310-100	Fisher Scientific
Hydrocortisone	H0888	Merck
Insulin from bovine pancreas	16634	Merck
Isopropanol	BP2618	Fisher Scientific
Kanamycin Sulfate	BP906-5	Fisher Scientific
Levamisole hydrochloride	187870100	ThermoFisher
L-Glutamine (200 mM)	25030-081	ThermoFisher
Lipofectamine 3000	L3000001	ThermoFisher
Magnesium Chloride (MgCl ₂)	223210010	ThermoFisher
Milk powder		Marvel
(EMEM) Minimum Essential Medium -Eagle with Earle's BSS (with non-essential amino acids, L-glutamine, without calcium)	BE06-174G	Lonza

MiRCURY LNA miRNA Detection Probe mmu-miR-148a-3p	339112	Qiagen
Mitomycin C (MMC)	BP2531	ThermoFisher
N, N,-Dimethylformamide (DMF)	D4551	Merck
New Fuchsin	2121410000	ThermoFisher
MEM Non-essential amino acid solution 100X	M7145	Merck
Normal Donkey Serum	S30	Merck
Normal Goat Serum	191356	MP Biomedicals
NP-40 surfact-AMPs detergent solution	28324	Fisher Scientific
Nuclear fast red solution	N3020-100	Merck
OCT medium	KMA-0100-00A	ThermoFisher
Paraformaldehyde	P/0840/53	Fisher Scientific
Penicillin/Streptomycin (10,000 U/ml)	15140122	ThermoFisher
Polybrene	TR-1003-G	Merck
Ponceau S	10454915	ThermoFisher
Propidium Iodide	P1304MP	ThermoFisher
PsiCHECK-2	C8021	Promocell
PureCol Collagen Type I (Bovine)	5005	Advanced Biometrix
qPCR BIO SyGreen High ROX	PB089618-041-6	PCR Biosystems
Reduced serum OptiMEM	31985070	ThermoFisher
Rhodamine B	132311000	ThermoFisher
RiboRuler High Range RNA ladder	SM1821	ThermoFisher
RNase A	10109169001	Roche
Sheep Serum	16070096	ThermoFisher
SOC outgrowth medium	B9020S	New England Biolabs
Sodium Chloride (NaCl)	10316943	Fisher Scientific
Sodium Deoxycholate	D6750	Merck
Sodium dodecyl sulphate (SDS)	BP1311-1	Fisher Scientific
Sodium nitrite	G7398	Merck
Subcloning Efficiency DH5 α Competent Cells	18265017	ThermoFisher
SybrSafe	533102	ThermoFisher
T4 DNA ligase	M0202	New England Biolabs
TaqMan probe hsa-miR-148a-3p	4427975 (000470)	ThermoFisher
TaqMan probe U6 snRNA	4427975 (001973)	ThermoFisher
TaqMan universal mastermix II, no UNG	4440045	ThermoFisher
TEMED	161-0800	BIO-RAD
Triethanolamine (TEA)	421630010	ThermoFisher

Tris Base	BP152	Fisher Scientific
Tris-HCl	BP1758	Fisher Scientific
Triton X-100	BP151-500	Fisher Scientific
TRIzol	R050-1-50	Zymo-Research
Tween-20	BP337-500	Fisher Scientific
Vectashield antifade mounting medium with DAPI	H-1200	Vector Labs
Versene	15040-033	ThermoFisher
Filter paper, 5-13 µm pore	11445248	ThermoFisher
Xylene	534056	Fisher Scientific
Yeast RNA	AM7118	ThermoFisher
PCRBIO DNA ladder IV	PB40.14-01	PCR Biosystems
Pageruler plus pre-stained protein ladder	26619	ThermoFisher

2.1.2 Transfection and Transduction Reagents Used During the Investigation

Table 2. Transfection/Transduction Reagents Used in the Investigation.

Reagent	Catalogue number	Company
Atelocollagen, AteloGene Local use.	1492	Koken
mirVana miR-148a-3p Inhibitor	4464084	ThermoFisher
mirVana miR-148a-3p Mimic	4464066	ThermoFisher
mirVana miRNA Inhibitor Negative Control #1	4464076	ThermoFisher
mirVana miRNA Mimic Negative Control #1	4464058	ThermoFisher
MiRZIP-148a anti-miR-148a microRNA construct	MZIP148a-PA-1	Cambridge Biosciences
Scrambled shRNA control in pGFP-C-shLenti shRNA Vector	TR30021	OriGene

2.1.3 Plasticware and Tools Used During the Investigation

Table 3. Plasticware and Tools Used in the Investigation.

Item	Catalogue number	Company
1.5 ml microcentrifuge tubes	72.690.001	Sarstedt

12-well plate	CC7682-7512	StarLab
15 ml sterile tubes	62.554.503	Sarstedt
2.0 ml microcentrifuge tubes	72.695.500	Sarstedt
24-well plate	CC7682-7524	StarLab
40 µm cell strainer	22-363-547	ThermoFisher
50 ml sterile tubes	62.547.254	Sarstedt
60 mm dish	CC7682-3359	ThermoFisher
6-well plate	CC7682-7506	StarLab
70 µm cell strainer	1-800-766-7000	ThermoFisher
96 well semi-skirted PCR plates	E1403-6200	StarLab
96-well plate	83.3924	Sarstedt
96-well plate white bioluminescence plate	165306	ThermoFisher
Glass coverslips	12323148	ThermoFisher
Haemocytometer	145-0011	BIO-RAD
Petri-dishes	12654785	ThermoFisher
Polyolefin sealing film for qPCR, Self-adhesive	E2796-9895	StarLab
Serological pipettes, 10ml	86.1254.001	Sarstedt
Slide mailers	HEA15986	HeathrowScientific
SuperFrost plus microscope slides	631-0108	VWR
T75 flasks	83.3910.002	Sarstedt
Cell Scraper	08100241	ThermoFisher

2.1.4 Kits Used During the Investigation

Table 4. Kits Used in the Investigation.

Kit	Catalogue number	Company
Direct-zol RNA MiniPrep Kit	R2050	Zymo-Research
Dual-Glo Luciferase Assay System	E2920	New England Biolabs
Lenti-vpak Packaging Kit	TR30037	OriGene
Micro BCA Protein Assay Kit	23235	ThermoFisher
Mini Trans-Blot Electrophoretic Transfer Cell	1703930	BIO-RAD
NE-PER Nuclear and Cytoplasmic Extraction Reagents	78833	ThermoFisher

Nucleospin Gel and PCR Clean-up	740609.50	Machery-Nagel
Nucleospin Plasmid Mini kit for Plasmid DNA	740588.250	Machery-Nagel
Phusion Flash High-Fidelity PCR Master Mix	F548S	ThermoFisher
Q5 Site-Directed Mutagenesis Kit	E0554	New England Biolabs
qPCR Lentivirus Complete Titration Kit	LV900	Abm
qPCRBIO cDNA Synthesis Kit	PB30.11-02	PCR Biosystems
Quick-DNA Miniprep Plus Kit	D4068S	Zymo-Research
SuperSignal West Pico PLUS Chemiluminescent Substrate	34577	ThermoFisher
TaqMan MicroRNA Reverse Transcription Kit	4366596	Applied biosystems
TaqMan Reverse Transcription Kit	4366596	ThermoFisher
Zero Blunt PCR Cloning Kit	K270020	ThermoFisher

2.1.5 Machines Used During the Investigation

Table 5. Machines Used in the Investigation.

Machine	Catalogue number	Company
Automated cell counter	TC20	BIO-RAD
CLARIOStar plus plate reader	-	BMG Labtech
Compact orbital shaker-incubator	ES20	Grant Instruments
Cryostat	CM1860	Leica
DM500 microscope with EC4 camera	-	Leica
Gallios Flow Cytometer	-	Beckman Coulter
HulaMixer sample mixer	10548425	ThermoFisher
Universal oven	UN110	Memmert
iBright FL1000 Imaging system	A32752	ThermoFisher
IncuCyte S3 live cell analysis instrument	-	Sartorius

Leica Thunder 3D cell culture imaging system	-	Leica
MoFlo XDP cell sorter	-	Beckman Coulter
NanoDrop 8000	ND-8000	ThermoFisher
QuantStudio 5 Real-Time PCR system	A34322	ThermoFisher
Refrigerated Micro-Centrifuge	75002543	ThermoFisher
Thermocycler	T-100	BIO-RAD
Thermo-Shaker	HC24N	Grant-bio
Transilluminator – Blue light	13193102	ThermoFisher
Avanti Ultra-Centrifuge	JXN-26	Beckman Coulter

2.1.6 Antibodies Used During the Investigation

Table 6. List of Antibodies Used in the Investigation.

Name	Host species	Dilution used	Catalogue number	Company
Anti-Digoxigenin-Alkaline phosphatase Fab fragments	Sheep	ISH: 1:2500	11093274910	Merck
Allophycocyanin (APC) Streptavidin	Rat	FACS: 1:300	405207	BioLegend
Anti-Digoxigenin-Rhodamine, Fab fragments	Sheep	FISH: 1:100	11207750910	Roche
Anti-Guinea Pig IgG Alexa Fluor 555	Goat	IF: 1:200	A21435	ThermoFisher
Anti-Mouse IgG, HRP linked	Horse	WB: 1:3000	7076S	Cell Signaling
Anti-Rabbit IgG Alexa Fluor Plus 488	Goat	IF: 1:200	A32731	ThermoFisher
Anti-Rabbit IgG Alexa Fluor Plus 647	Goat	IF: 1:200	A32733	ThermoFisher
Anti-Rabbit IgG, HRP linked	Goat	WB: 1:3000	7074S	Cell Signaling

Anti-Rat IgG Cyanine5	Goat	IF: 1:200	A10525	ThermoFisher
CD34	Rat	IF: 1:100	ab8158	Abcam
CD34 (RAM34)	Rat	FACS: 1:50	13-0341-82	ThermoFisher
CD49f (integrin α 6)	Rat	FACS 1:50	555736	BD Biosciences
Cytokeratin 1 (Krt1)	Rabbit	WB: 1:10000 IF: 1:500	ab93652	Abcam
Cytokeratin 15 (Krt15)	Guinea Pig	IF: 1:100	BP5077	OriGene
Elf5	Rabbit	IF: 1:100, WB: 1:1000	A718	2B Scientific
GAPDH	Mouse	WB: 1:10000	ab8245	Abcam
Histone 3 (H3) XP	Rabbit	WB: 1:1000	4499	Cell Signaling
Ki67	Rabbit	IF: 1:100	Ab16667	Abcam
Lamin B1	Mouse	WB: 1:200	Sc-374015	Santa Cruz Biotechnology
Ly-6A/E (Sca-1)	Rat	FACS: 1:50	11-5981-82	ThermoFisher
Rock1	Rabbit	IF: 1;100 WB: 1:1000	MBS9610378	MyBioSource

2.1.7 Primers Used During the Investigation

Table 7. List of Primers Used for RT-qPCR in the Investigation.

Gene symbol	Gene name	Accession no.	Sense sequence (5'-3')	Anti-sense sequence (5'-3')
<i>Actb</i>	Actin, beta	NM_007393.5	CCAACCGTGAAAAGATGACC	CCATCACAATGCCTGTGGTA
<i>Atxn7l1</i>	Ataxin 7 like 1	NM_001033436.3	GTGTTTGATAGAAGGTGGGATCG	TGAAAGGCTGCAAAACGGAT
<i>Ccnb2</i>	Cyclin B2	NM_007630.2	AGCAGCAGTATTACACAGGC	GGAGGCCAGGTCTTTGATGA
<i>Ccnd1</i>	Cyclin D1	NM_001379248.1	CCCCAACAACTTCTCTCCT	CCTTGGGGTCGACGTTCT
<i>Ccnd2</i>	Cyclin D2	NM_009829.3	GCCAAGATCACCCACACTGA	ATGCTGCTCTTGACGGA
<i>Ccne1</i>	Cyclin E1	NM_007633.2	ACTCCCACAACATCCAGACC	CGCTGCTCTGCTTCTACTG
<i>Cdk1</i>	Cyclin-dependent kinase 1	NM_007659.4	GGGCACTCCTAACACGAAG	CCAGAGATTCGTTTGGCAGG
<i>Cdk16</i>	Cyclin-dependent kinase 16	NM_011049.5	GCAATCGGATCTCTGCTGA	CAGGCATAGAAGTGGACCGA

<i>Dynll2</i>	Dynein light chain LC8-type 2	<i>NM_026556.4</i>	GCAGTGATCAAGAACGCAGA	GTGCTTTGTCTCGTGTGTGA
<i>Elf5</i>	E74-like factor 5	<i>NM_010125.3</i>	GTGGCATCAAGAGTCAAGACTGTC	CTCAGCTTCTCGTACGTATCC TG
<i>Ivl</i>	Involucrin	<i>NM_008412.3</i>	TGCCTTCTCCCTCCTGTGA	CAGTCTTGAGAGGTCCTGA
<i>Ptges3</i>	Prostaglandin E synthase 3	<i>NM_019766.4</i>	TTGTCTTGAGGAAGCGATAA	GTCATCCTCCAGTCTTTCCA
<i>Krt1</i>	Keratin 1	<i>NM_008473.2</i>	CATATTAGTAGCAGTCTGA	TGAAGTCCTCTTTCAAAT
<i>Krt10</i>	Keratin 10	<i>NM_010660.2</i>	AGTTCTTGCTCTTCTGATTG	CAAGTCTGACCTGGAAATGC
<i>Rab10</i>	RAB10, member RAS oncogene family	<i>NM_016676.5</i>	TCACACCATCACAACTCCT	TGTTCTCCTTTGCCTTTGGG
<i>Rab14</i>	RAB14, member RAS oncogene family	<i>NM_026697.4</i>	AGCAGACTTGAAGCACAGA	AGACTCGGCAGCATTGAGAT
<i>Rmnd5a</i>	Required for meiotic nuclear division 5 homolog A	<i>NM_001355745.1</i>	TGTCCATTCTTCGTCAGCA	GGCATCTCCTGGACTCTGTT
<i>Rock1</i>	Rho-associated coiled-coil containing protein kinase 1	<i>NM_009071.2</i>	GACTTGATTTCCCGTGCAA	TCTTGTTGACAGCGTTGCGAG
<i>Stx3</i>	Syntaxin 3	<i>NM_152220.2</i>	CTCTCCCGAAGTTTGTGGA	CTTACGATGTCCTTGTGCCG
<i>Tbl1xr1</i>	Transducin (beta)-like 1X-linked receptor 1	<i>NM_030732.3</i>	CCAACAGGACCAGGGACAAA	AAAAGCCACACTGTACACGG
<i>Ythdc2</i>	YTH domain containing 2	<i>NM_001163013.1</i>	TAGGAAGGGAGAAGAGCCAG	AACTGTTCCCAACCTGAGG

2.2 Methods Used in the Investigation

2.2.1 Animals

Animal studies were performed in accordance with protocols approved by the UK Home office. All Animal work was conducted under licence of the Nottingham Trent University (Nottingham, UK).

C57BL/6 wild type female mice were acquired from Charles River Laboratories, UK. For hair cycle analysis, dorsal C57BL/6 skin samples were collected by liquid nitrogen snap freezing at post-natal day (P) 12-14 (late-anagen), P16-17 (catagen), and P20-23 (telogen) for RT-qPCR analysis. Depilation induced hair cycle of C57BL/6 dorsal mouse skin was performed as previously described (Muller-Rover et al., 2001, Mardaryev et al., 2010). Briefly, hair was removed by waxing 7-week-old C57BL/6 wild type dorsal mouse skin which induces HF cycle development. Depilation-induced skin samples were collected at time points day (D) 0 (telogen), D3 (anagen II), D5 (anagen IV), D8-12 (anagen VI), and D16-19 (catagen) by snap freezing in liquid nitrogen for subsequent RT-qPCR analysis and *in situ* hybridization. Consequently, \geq five mice were used for each time point.

Whole skins of C57BL/6 wild type female mice were collected at telogen stage of HF cycling (7-9 weeks old, telogen) for FACS SC sorting for colony forming assay and RT-qPCR analysis. Consequently, \geq three mice were used for each FACS sorting.

2.2.2 MicroRNA Microarray

Total RNA was extracted as described below from snap frozen C57BL/6 skin samples collected during post-natal hair cycling, P12-23. 5 μ g of RNA was used for microRNA

microarray analysis and performed by LC Sciences (Houston, US) as described previously (Mardaryev et al., 2010) (please see appendices 1.1).

2.2.3 Cell Culture and Transfection

C57BL/6 wild type mouse pups were collected between post-natal day P1 and P3 and primary mouse keratinocytes (PMEKs) were extracted for subsequent growth and modulation. The following steps were carried out for each skin. Briefly, the skin was gently removed from the mouse, leaving a single skin sheet. The skins were incubated, floating dermis-side-down (with the epidermis remaining dry and unsubmerged) in 0.25% (w/v) Trypsin-EDTA (please see materials for all catalogue numbers) at 4°C over-night. The following day, the epidermis was removed from the dermis and collected in complete primary mouse epidermal keratinocyte (PMEK) low calcium media, comprised of; EMEM calcium-free medium supplemented with 0.05 mM CaCl₂, 4% (v/v) chelated heat-inactivated fetal bovine serum, 0.4 µg/ml hydrocortisone, 5 µg/ml insulin, 10 ng/ml epidermal growth factor, 10⁻¹⁰ M cholera toxin, 2⁻⁹ M 3,3',5-Triiodo-L-thyronine sodium salt (T3), 100 U/ml penicillin, 100 µg/ml streptomycin, and 2 mM L-glutamine and minced by repeated snipping with scissors and pipetting up and down with a serological pipette for 5 minutes each (please see appendices 2.1). The resulting cell homogenate was filtered with a 70µm cell strainer. Tissue culture (TC) plates were coated with collagen coating solution (5ml of hanks balanced salt solution (HBSS), 500 µl 1 M HEPES, 100 µl 5% (v/v) BSA, 50 µl of 3 mg/ml PureCol collagen type I, excess aspirated and allowed to dry before seeding PMEKs in complete PMEK media. Cells were cultured at 33°C, 8% CO₂ until 60-70% confluent for experimental purposes (please see appendices 2.2).

PMEKs were transfected with 200 nM of synthetic miR-148a mimic (pro-miR-148a) or inhibitor (Anti-miR-148a) or miRNA negative controls using Lipofectamine 3000 in reduced serum OptiMEM for 4 hours at 33°C, 8% CO₂ before changing to complete PMEK media and subsequent culturing for 48 hours for down-stream analysis (please see appendices 2.3). 200 nM was chosen as a concentration for miRNA mimic/inhibitor transfection as previously reported (Ahmed et al., 2014, Ahmed et al., 2019). Validation of transfection efficiency was assessed by TaqMan RT-qPCR for miR-148a. For calcium-induced differentiation analysis, complete PMEK media was supplemented with 1.8 mM CaCl₂ and cultured for 48 hours at 33°C, 8% CO₂ before downstream analysis.

2.2.4 Flow Cytometry

PMEKs were cultured and treated with either pro-miR-148a, anti-miR-148a or miRNA control as described above. 48 hours post transfection, cells were trypsinized with 0.25% (w/v) Trypsin-EDTA, washed with PBS and fixed with 70% (v/v) ethanol/PBS at -20°C for 30 minutes. Fixed cells were incubated with RNase A (100 µg/ml) at 37°C for 30 minutes. The cells were subsequently stained with propidium iodide (20 µg/ml) at 4°C for 30 minutes. Analysis of cells in each distinct stage of cell cycle was evaluated using Beckman Coulter Gallios. For each sample, minimum of 10,000 events were collected and analysed on Beckman Coulter Kaluza Analysis Software (Beckman Coulter, UK, please see appendices 3.1).

2.2.5 Real-Time quantitative PCR (RT-qPCR)

Total RNA was extracted using Direct-Zol RNA MiniPrep kit (please see appendices 4.1). For first-strand cDNA synthesis, 100 ng of total RNA was used with the qPCR BIO cDNA synthesis kit (please see appendices 4.2). Gene expression was analysed using

qPCR BIO SyGreen High ROX mix and performed on a QuantStudio 5 Real Time PCR system at the following conditions: 95°C for 2 minutes followed by 40 cycles of denaturation (95°C for 5 seconds) and annealing and extension (30 seconds at temperature experimentally determined for each primer pair, please see appendices 4.3). Primers were designed using Primer3 (<https://primer3.ut.ee/>), UCSC genome browser (<https://genome.ucsc.edu/>) and NCBI primer blast (<https://www.ncbi.nlm.nih.gov/tools/primer-blast/>) (please see table 7 for primer sequences). Differences in amplification between treated samples and controls were calculated using $\Delta\Delta\text{Ct}$ method with normalisation to Actin (*Actb*). Data was normalised to Actin due to its consistent expression levels between treated and non-treated samples. Data from technical triplicates were pooled, mean standard error of the mean (\pm SEM) was calculated, and statistical analysis was performed using unpaired student's *t*-test (please see appendices 18).

TaqMan RT-qPCR was utilised for detection of microRNAs for evaluation of efficient miRNA overexpression/inhibition. TaqMan cDNA was synthesised from total RNA using TaqMan MicroRNA Reverse Transcription kit (please see appendices 5.1). Detection of miRNAs by TaqMan RT-qPCR was performed using TaqMan Real Time PCR Assay and TaqMan Universal Master Mix II, No UNG. MiR-148a/miR-148a-5p/miR-152 was amplified under the following cycling conditions: 95°C for 10 minutes, followed by 40 cycles of 95°C for 15 seconds and 60°C for 60 seconds (please see appendices 5.2). Differences between samples and controls were calculated using the $\Delta\Delta\text{Ct}$ method and normalized to the U6 snRNA values. Data from triplicates were pooled, mean \pm SEM was calculated, and statistical analysis was performed using unpaired Student's *t*-test (please see appendices 18).

2.2.6 Western Blotting

Total protein lysate was extracted from cultured cells using RIPA lysis buffer (50 mM Tris-HCl, 1% (w/v) NP-40, 0.25% (w/v) sodium deoxycholate, 150 mM NaCl, and 1 mM EDTA; pH 7.4) and cOmplete ULTRA Protease Inhibitor Cocktail and quantified using Micro BCA Protein assay kit (please see appendices 6.1). 10 µg of protein with appropriate volume of 4x sample buffer (0.25 M Tris-HCl, 0.28 M SDS, 40% (v/v) glycerol), 0.5 µl 2-mercaptoethanol and made up to equal volume with RIPA lysis buffer was run on a 7.5, 10, 12 or 15% (v/v) SDS gel depending on protein molecular weight of interest. The gel was run at 120V for approximately 90 minutes (please see appendices 6.2). The protein gel was then transferred to a 0.45 µm nitrocellulose membrane by wet transfer with ice cold transfer buffer at 90V for 90 minutes (please see appendices 6.3). The resulting membrane was blocked with 5% (w/v) milk in TBST (0.1% (v/v) Tween-20, 20 mM Tris base, 150 mM NaCl) before incubating with primary antibody in 1% (v/v) milk/TBST at 4°C overnight. The following day, horseradish peroxidase-tagged IgG antibody was used as a secondary antibody (1:3,000). Antibody binding was visualized with an enhanced chemiluminescence SuperSignal West Pico kit and iBright FL1000 GelDoc Imager (please see appendices 6.4). Antibody against protein Gapdh was used as a loading control.

Nuclear and cytoplasmic protein was extracted from cultured cells using NE-PER Nuclear and cytoplasmic extraction kit reagents (please see appendices 6.5). Nuclear and cytoplasmic Western blot procedure was conducted as described above, as per manufacturer's instructions. For nuclear Western blot, Antibodies against proteins Histone 3 or Lamin B1 were used as loading controls.

2.2.7 In Situ Hybridisation

In situ hybridization was performed on 10 µm skin cryosections fixed with 4% (w/v) paraformaldehyde at room temperature for 10 minutes. Sections were acetylated with triethanolamine buffer (300 mM triethanolamine, and 0.25% (v/v) acetic anhydride) for 10 minutes and permeabilized (1% (v/v) Triton X-100/1x DEPC treated PBS) for 10 min. Slides were incubated in hybridization buffer (50% (v/v) formamide DI, 5x saline-sodium citrate (SSC), 50 µg/ml yeast RNA, 1% (w/v) SDS, 50 µg/ml heparin) at 60°C for 1 hour. 320 nM of MiRCURY LNA miRNA mmu-miR-148a-3p double-digoxigenin detection probe in hybridization buffer was mixed and incubated at 80°C for 5 minutes followed by incubation on ice for 5 minutes. Slide sections were hybridized with probe solution at 60°C for 16-20 hours. The following day, slide sections were washed three times in wash buffer one (50% (v/v) formamide, 5X SSC and 1% (w/v) SDS) at 60°C for 15 minutes per wash, followed by three times in wash buffer two (50% (v/v) formamide and 5X SSC) at 60°C for 15 minutes per wash, followed by three times in TBST-levamisole buffer (1x tris-buffered saline, 0.05% (v/v) tween-20 and 1x levamisole) at room temperature for 10 minutes per wash. Slides were blocked at room temperature for 60 minutes in blocking solution (2% (w/v) blocking reagent, 5% (v/v) sheep serum, 1% (v/v) Tween-20 and levamisole in 1x TBST). Slides were incubated with sheep alkaline-phosphatase-conjugated anti-DIG antibody (1:2500) at room temperature for 2 hours and then washed three times at room temperature for 15 minutes per wash with NTMT buffer (100 mM NaCl, 100 mM Tris HCl (pH 9.5), 50 mM MgCl₂, 1% (v/v) Tween-20). Slides were incubated with BM purple for 12-96 hours until a purple colour reaction had occurred. Slides were washed three time with PBS for 10 minutes per wash and counterstained with nuclear fast red solution for 1 minute. Slides were subsequently washed with ddH₂O three times, once with xylene and

coverslip with DPX mounting medium. MiR-148a was imaged using Leica THUNDER imager 3D cell culture (please see appendices 7.1).

2.2.8 Fluorescent *In Situ* Hybridization

Fluorescent *in situ* hybridization was completed as per *in situ* hybridization with following modifications. Sections were blocked at room temperature for 30 minutes in blocking solution (0.1 M Tris-HCl (pH 7.5), 0.15 M NaCl, 5% (v/v) sheep serum and 0.5% (w/v) blocking reagent). Detection of miR-148a was performed using sheep rhodamine-conjugated anti-Digoxigenin antibody (1:100) and incubated at 4°C overnight alongside antibodies against Rock1, Elf5, cytokeratin 1 (Krt1), CD34 or Krt15. Slides were washed with TNT wash buffer (0.1 M Tris-HCl (pH7.5), 0.15 M NaCl and 0.05% (v/v) tween-20) at room temperature for 10 minutes per wash. Slides were incubated at room temperature with corresponding Alexa Fluor-488 antibodies or Alexa Fluor-647 (1:200) for 1 hour. Slides were then washed with TNT wash buffer at room temperature for 10 minutes per wash and mounted with Vectashield anti-fade mounting media with DAPI. Images were taken using the Leica THUNDER imager 3D cell culture. Please see appendices 7.2.

2.2.9 RNA Sequencing Analysis

Total RNA from pro-miR-148a and miRNA control treated PMEKs were collected as described above and sent to Novogene, UK for RNA sequencing using the Illumina PE150 platform. The data was uploaded to Galaxy web platform (<https://usegalaxy.org/>) for analysis. Data was aligned to *Mus Musculus* genome (mm9) and all genes that were insignificant ($p > 0.05$) were excluded from our analysis and subsequent heat map and gene ontology analysis (please see appendices 8.1).

2.2.10 MiRNA-148a Gene Target Prediction

Potential miR-148a target genes were predicted using three different prediction algorithms on default settings: TargetScan (<http://www.targetscan.org/>) which predicts biological targets of microRNAs by analysis of conserved sites that match the 'seed' region of microRNAs, miRanda (<http://microrna.sanger.ac.uk>) uses an algorithm to predict microRNA-mRNA pairs, and miRDB (<http://mirdb.org/>) uses miRNA-target interactions from high-throughput sequencing experiments. A Venn diagram of all potential miR-148a targets was made to determine consistently predicted genes from all three prediction algorithms. Gene conservation between mouse and human was assessed using NCBI homologene (<https://www.ncbi.nlm.nih.gov/homologene/>) (please see appendices 8.1).

2.2.11 Luciferase Reporter Assay

For generation of plasmids incorporating miR-148a binding sites on 3'UTR of *Rock1* and *Elf5*, forward and reverse primers containing XhoI and NotI restriction sequences were used to amplify 3'UTR miR-148a binding sequence from C57BL/6 mouse genomic DNA. C57BL/6 mouse genomic DNA was extracted using Quick-DNA Miniprep Plus kit. *Elf5* Sequences: 5'-AAAACTCGAGACACAGCATCGATCTCTTCTCT-3' and 5'-TTTTGCGGCCAGTTAGGGTTCAGGGCACTC-3', and *Rock1* sequences: 5'-AAAACTCGAGTTGGGAACTGGGAGAAGAGG-3' and 5'-TTTTGCGGCCGCGGGTAATGCAACTTCCACTGA-3' were used and PCR products were generated using Phusion Flash High-Fidelity PCR Master Mix (please see appendices 9.1). The amplified PCR products were incorporated into psiCHECK-2 plasmid using zero blunt cloning kit (please see appendices 9.2). Mutated binding

sequences were generated using Q5 site-directed mutagenesis kit, substituting 6 bases from the miR-148a binding sequence (please see appendices 10.1). Plasmids were verified to containing wild type or mutated miR-148a binding site by Sanger sequencing (Source Biosciences, UK, please see appendices 11.1).

1×10^3 HaCaT cells (ATCC, PCD-200-001) per well were grown in a 96 well bioluminescence plate with DMEM supplemented with heat-inactivated 10% (v/v) fetal bovine serum, 100 U/ml penicillin, 100 μ g/ml streptomycin and 2 mM L-glutamine in 5% CO₂ at 37°C. After 72 hours (70% confluence), HaCaTs were co-transfected with 100 ng generated plasmid and 200 nM pro-miR-148a or miRNA control mimic using lipofectamine 3000. 24-hours post transfection relative luciferase activities were measured using Dual-Glo luciferase assay system (please see appendices 12.1). Luminescence was measured using CLARIOStar plate reader. Data from five independent experiments was pooled, mean \pm SEM was calculated, and statistical analysis was performed using unpaired Student's *t*-test (please see appendices 18).

2.2.12 Pharmacological Treatment of Mouse Skin

20 μ M Synthetic miR-148a inhibitor (anti-miR-148a) or inhibitor negative control was administered subcutaneously to dorsal skin of C57BL/6 wild type mice in 20 μ M atelocollagen for their local and sustained delivery. Anti-miR-148a treatment was performed on post-natal skin days P20, P21 and P22, and skin samples were collected on P23 (Figure. 20A). In each experiment, \geq four-five mice/time point were used for analyses in both experimental and control groups. Collected samples were processed for histological, immunofluorescent, and RT-qPCR analysis, please see appendices 13.1).

2.2.13 Alkaline Phosphatase Staining

Skin cryosections (10 µm) were fixed in acetone at -20°C for 10 minutes followed by three washes with PBS at room temperature. Slides were incubated in developing solution (100 mM NaCl, pH 8.3, 100 mM Tris, pH 9.5, 20 mM HCl, 0.05% (w/v) Naphtol ASBI phosphate, 0.5% (v/v) DMF, 25 mM sodium-nitrite, and 5% (w/v) New fuchsin) for 15 min, followed by three washes with PBS. slides were immersed in Hematoxylin counterstain solution for 45s at RT and rinsed with running H₂O before dipping in xylene and mounting with DPX mounting media (please see appendices 14.1). Images were captured using Leica DM500 microscope.

2.2.14 Immunohistochemistry

Dorsal mouse skin cryosections (10 µm) were fixed with 4% (w/v) paraformaldehyde at room temperature for 10 minutes followed by washing with 0.2% (v/v) Triton-X-100/PBS. cryosections were blocked with 0.2% (v/v) Triton-X-100/PBS, 5% (v/v) fetal bovine serum, 2% (v/v) bovine serum albumin and 10% (v/v) normal goat and/or donkey serum for 1 hour at room temperature. Slides were subsequently incubated with primary antibody (see table 6) overnight at 4°C. The following day, slides were washed with 0.2% (v/v) Triton-X-100/PBS and incubated with the associated Alexa Fluor-488, Alexa Fluor-A555 or Alexa Fluor-647 (see table 6) secondary antibody at room temperature for 1 hour. slides were washed with 0.2% (v/v) Triton-X-100/PBS before counterstaining and mounting with Vectashield anti-fade mounting media with DAPI. Images were taken using Leica THUNDER imager 3D cell culture. Please see appendices 15.1.

2.2.15 Immunocytochemistry

PMEKs were grown on coverslips and transfected with either miR-148a mimic or miRNA control, as described above. PMEKs were treated with media supplemented with 1.8 mM CaCl₂ for 48 hours to induce keratinocyte differentiation. Cells were fixed with 4% (w/v) paraformaldehyde followed by washing with 0.2% (v/v) Triton-X-100/PBS. Cells were blocked with 0.2% (v/v) Triton-X-100/PBS, 5% (v/v) fetal bovine serum, 2% (v/v) bovine serum albumin and 10% (v/v) normal goat and/or donkey serum for 1 hour at room temperature. Cells were subsequently incubated with primary antibodies Elf5 or Rock1 (see table 6) overnight at 4°C. The following day, cells were washed with 0.2% (v/v) Triton-X-100/PBS and incubated with the associated Alexa Fluor-488 (see table 6) secondary antibody at room temperature for 1 hour. slides were washed with 0.2% (v/v) Triton-X-100/PBS before counterstaining and mounting with Vectashield anti-fade mounting media with DAPI (please see appendices 15.1). Images were taken using Leica THUNDER imager 3D cell culture. Arbitrary fluorescent units were measured using ImageJ (<https://imagej.nih.gov/ij>).

2.2.16 Fluorescence Activated Cell Sorting (FACS)

Dorsal and ventral skin from C57BL/6 mice were harvested and shaved during telogen stage of hair follicle cycling (7-9 weeks old). The hypodermis was removed, and skin sections were floated on 0.25% (w/v) trypsin-EDTA overnight at 4°C. The following day, the epidermis including hair follicles were removed and minced before trypsin neutralisation with EMEM calcium-free medium (as described above, with no CaCl₂) and filtered using a 70 µm and 40 µm cell strainer. The cells were pelleted by centrifugation at 300 x g for 10 minutes and suspended in 1 ml of EMEM calcium-free medium. Cells were stained with antibodies: Ly-6A/E (Sca-1), CD34 (RAM34) and

CD49f ($\alpha 6$) in 2% (v/v) bovine serum albumin/PBS staining buffer rotating in the dark for 1 hour at 4°C. Cells were then washed with FACS wash buffer (phenol-free, Ca^{2+} -free, Mg^{2+} -free HBSS containing 1% (v/v) penicillin-streptomycin, 20 mM D-glucose, and 2% (v/v) chelated heat inactivated fetal bovine serum). Cells were stained with secondary antibody APC streptavidin in the dark for 1 hour at 4°C. Hair follicle bulge stem cells ($\text{CD34}^+/\text{CD49f}^{\text{High}}/\text{Sca-1}^-$) and junctional cells ($\text{CD34}^-/\text{CD49f}^{\text{Low}}/\text{Sca-1}^-$) were sorted using MoFlo XDP cell sorter and data analysed using Summit software (Beckman Coulter, UK). Sorted cells were then used for colony forming assay or RT-qPCR analysis. Please see appendices 16.1.

2.2.17 Production of Anti-miR-148a and Control Expressing Lentiviruses

HEK293T cells were cultured in a 6-well plate with DMEM supplemented with heat-inactivated 10% (v/v) fetal bovine serum, 1% (v/v) L-glutamine and 5% (v/v) non-essential amino acids with 5% CO_2 at 37°C. At 40% confluence, HEK293T cells were co-transfected with MiRZIP-148a anti-miR-148a microRNA construct or Scrambled shRNA control in pGFP-C-shLenti shRNA Vector control with packaging plasmid using Lenti-vpak packaging kit. Per well, 1 μg of plasmid with 1.2 μg and 6.6 μl of Turbofectin transfection reagent was prepared and pipette dropwise to the HEK293T cells in media. Media was changed after 12 hours, and viral supernatant was collected 24- and 48 hours post media change. Precipitation of viral particles was achieved using 80 $\mu\text{g}/\text{ml}$ polybrene and 80 $\mu\text{g}/\text{ml}$ chondroitin sulfate C (CSC), followed by incubation for 18 hours at 4°C. Viral pellets were acquired by centrifugation at 10,000 x g for 30 minutes at 4°C (please see appendices 17.1). Titration of lentiviral particles was performed using qPCR lentivirus titration kit (please see appendices 17.2).

2.2.18 Colony Forming Assay

Swiss 3T3 cells were grown in 24 well plates with DMEM supplemented with 10% (v/v) heat-inactivated fetal bovine serum, 100 U/ml penicillin, 100 µg/ml streptomycin and 2 mM L-glutamine with 5% CO₂ at 37°C. At 70% confluence, 3T3 cells were treated with 8 µg/ml mitomycin C (MMC) for 2 hours followed by washing with PBS and replacement of media (please see appendices 17.3). Post sorting, 1000 HF-bulge SCs were seeded per well of a 24 well plate with MMC treated 3T3 cells with DMEM/F-12 (3:1) supplemented with 10% (v/v) chelated fetal bovine serum, 10 ng/ml epidermal growth factor, 0.5 µg/ml hydrocortisone, 10⁻¹⁰ M cholera toxin, 5 µg/ml insulin, 1.8⁻⁴ M Adenine, 100 U/ml penicillin, 100 µg/ml streptomycin and 0.3 mM calcium and cultured at 5% CO₂ and 32°C. 48 hours post seeding, stem cells were transduced with MiRZIP-148a or scrambled shRNA control at a MOI of 20 (4.0 x 10⁴ viral titre per ml) supplemented with 8 µg/ml polybrene directly into the cell culture media for 4 hours at 5% CO₂ and 32°C (please see appendices 17.4). Media was changed every 48 hours and cells cultured for 10 days. GFP and Phase imaging was performed using IncuCyte S3 live cell analysis instrument to determine transduction efficiency and used for calculation of difference in colony size and number.

2.2.19 Image Fluorescence Quantification Analysis

Immunofluorescence intensity analysis was determined using ImageJ software, as described previously (Ahmed et al., 2014). In brief, red or green fluorescent signals were collected from experimental tissues in RGB format using the same exposure conditions. To measure the fluorescence intensity at each pixel, the RGB images were converted to 8 or 16-bit grayscale format. Regions of interest of distinct size within the control and anti-miR-148a (epidermis and/or HFs) were selected, and the mean values

of intensity were calculated for each selected areas followed by the normalization relative to the number of DAPI+ cells and fluorescence intensity.

2.2.20 Statistical Analysis

Unpaired student's *t*-test was used for analysis of relative expression or relative fluorescence intensity in RT-qPCR data, Immunocytochemistry, and CFA measurements, where \geq four-five mice were used per *in vitro* and *in vivo* experiments. Please see appendices 18.

3.0

Results

3.1 Spatiotemporal Expression Analysis of MiRNA-148a During Hair Follicle Cycling

Aims:

The analysis of miR-148a expression patterns during skin and hair follicle (HF) development and hair cycling.

Results:

Initial analysis of global microRNAs (miRNAs, miRs) during spontaneous hair cycle from post-natal day (P) 12 (anagen) to P23 (telogen) was completed by miRNA microarray analysis (Mardaryev et al., 2010). The array data showed significant expressional changes in a number of miRNAs. One of the most dynamic and highly expressed miRNAs in telogen phase of hair cycling was miR-148a, which was further investigated. We observed in the miRNA microarray analysis that the highest expression of miR-148a was observed during telogen stage of the hair cycle (P20-21), a period of stem cell (SC) inactivity and quiescence, compared to late-anagen and catagen stages (P12-P17). MiR-148a expression was very low in late-anagen (P12) and remained low throughout late-anagen (P12-P15) and catagen (P16-P17) phases of hair cycle. MiR-148a expression markedly increased during early telogen (P20-21) and reduced expression in late telogen stages (P22-23; Figure. 11A). Due to the

distinct expression pattern of miR-148a during hair cycling, miR-148a was selected for further investigation, as to investigate its potential molecular mechanisms in controlling SC quiescence during telogen stage of HF cycling. To validate the miRNA microarray profile, TaqMan RT-qPCR was performed initially during spontaneous post-natal hair cycle. During catagen (P16-P17), miR-148a expression increased compared with late-anagen stage (P12) of HF cycling ($***P<0.001$). At telogen (P20-23), miR-148a expression increased further compared to anagen and catagen ($*P<0.05$, $***P<0.001$) and remained elevated during the rest of telogen stage (Figure. 11B). MiR-148a expression was also investigated during depilation-induced hair cycle and revealed a similar expression pattern of miR-148a during spontaneous HF cycling. During anagen, post depilation day (D) 3-12, miR-148a expression reduced ($**P<0.01$) compared to telogen (D0). During catagen stage of HF cycling (D16-D19), miR-148a expression reduced further compared with telogen and anagen stages of HF cycling ($***P<0.001$, Figure. 11C).

As we observed high levels of miR-148a expression during telogen phase of skin and HF development in spontaneous (post-natal) and induced hair cycle, we analysed the spatiotemporal expression pattern of miR-148a during HF cycling. *In situ* hybridisation was performed during depilation-induced HF cycling in C57BL/6 wild type dorsal mouse skin. In the epidermis of telogen skin, miR-148a expression was observed in the suprabasal layer, with reduced expression observed in the basal layer (Figure. 11D, Panel (i), arrowhead). In telogen HFs, expression of miR-148a was observed in the bulge and secondary hair germ (Figure. 1D, Panel (i)). During mid-anagen (D5), in the epidermis, miR-148a expression was markedly decreased compared to telogen skin (Figure. 11D, Panel (ii), arrowhead). In the HFs in early anagen, miR-148a expression was markedly reduced in the bulge region and developing hair bulb

compared to telogen HFs (Figure. 11D, Panel (ii), arrows). During late-anagen (D12) and catagen (D18) stages of HF cycling, miR-148a expression reduced further and very little expression was detected in the epidermis and HFs (Figure. 11D, Panels (iii)-(iv)). Negative control using scrambled probe showed no detectable colorimetric signal (Figure. 11E).

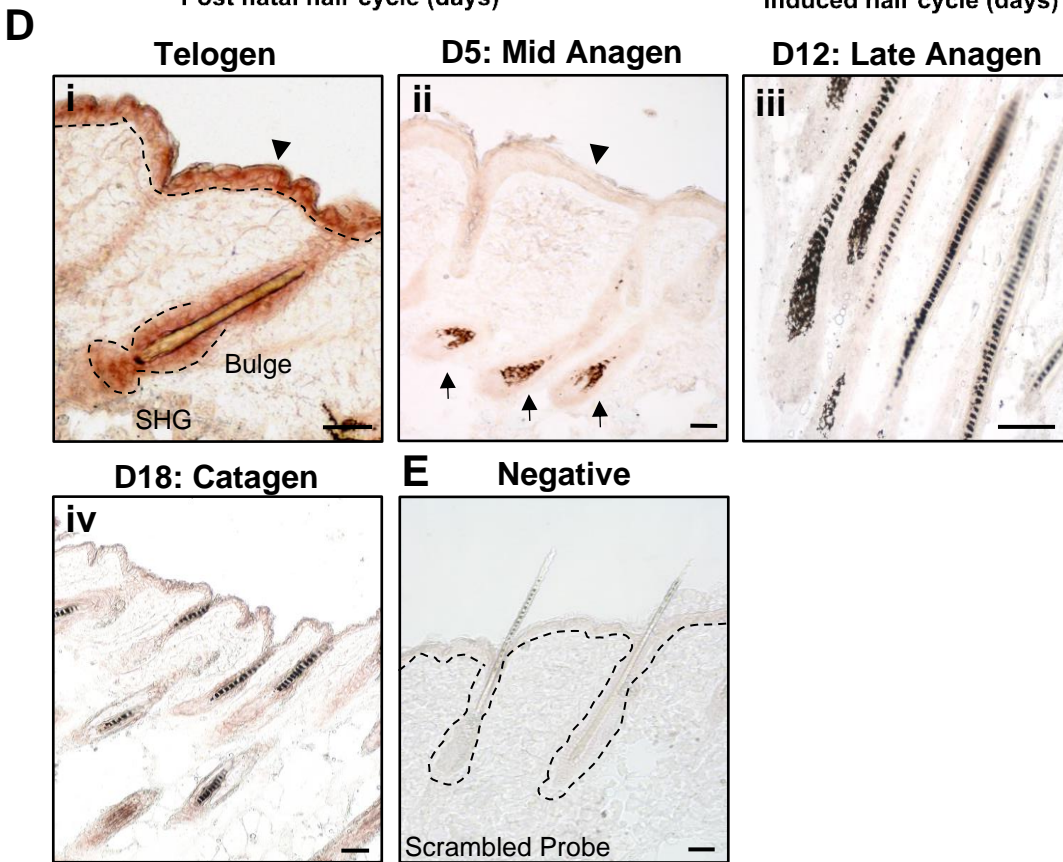
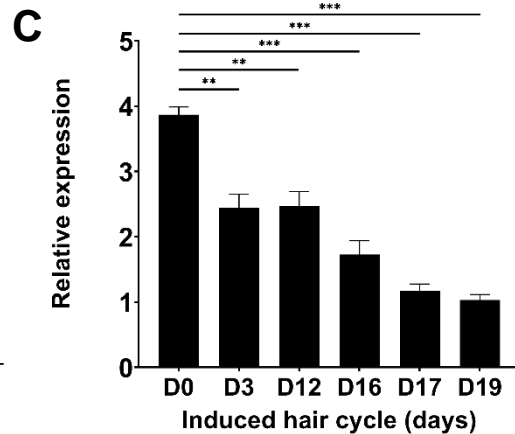
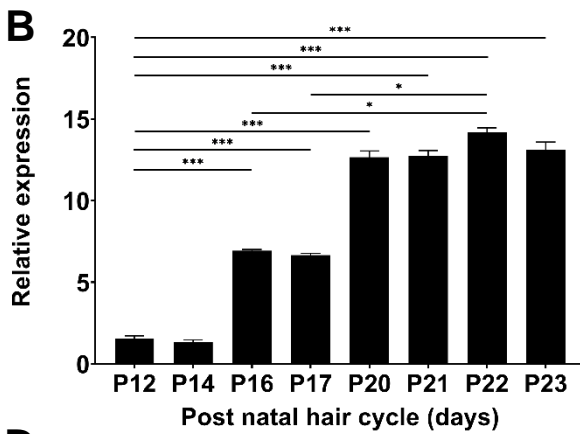
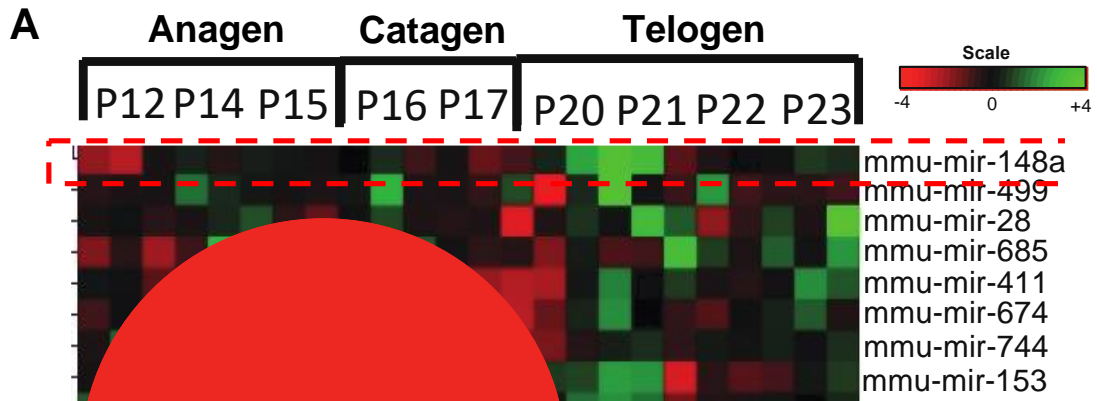


Figure 11. Analysis of MiR-148a Expression in Skin and During Hair Follicle Cycling.

(A) Microarray profile of miRNAs during post-natal HF cycling revealed dynamic expression patterns of several microRNAs. MiR-148a was shown to be one of the highest expressed miRNAs during telogen stage of hair follicle (HF) cycling compared with anagen and catagen. **(B-C)** TaqMan RT-qPCR analysis of miR-148a expression. **(B)** MiR-148a expression analysis during spontaneous HF cycling from post-natal day (P) 12-15 (late-anagen), through P16-17 (catagen) and P20-P23 (telogen). MiR-148a expression was highest during telogen stage of HF cycling (P20-23) compared with anagen and catagen. **(C)** MiR-148a expression analysis during depilation induced HF cycling from Day (D) 0 (telogen), through D3-12 (anagen), and D16-19 (catagen). MiR-148a expression was highest during telogen (D0) stage of induced hair cycle compared with anagen and catagen. **(D)** *In situ* hybridization of miR-148a during induced hair cycle. MiR-148a expression was observed in the suprabasal layer of the epidermis during telogen stage of HF cycling (Panel (i), arrowhead). In the HF, miR-148a expression was detected in the bulge and secondary hair germ stem/progenitor compartments (Panel (i), labels) during telogen stage (D0) of HF cycling. A reduction of miR-148a expression was observed during mid-anagen stage (D5) of HF cycling in the suprabasal layer of the epidermis (Panel (ii), arrowhead), and in the HF bulb (Panel (ii), arrows) and). MiR-148a expression was absent from late-anagen (D12) and catagen stages of HF cycling (D18, Panels (iii) and (iv), respectively). **(E)** Negative control using scrambled probed showed low to no detection of expression. Broken lines define epidermal-dermal boarder and HF-SC compartments. RT-qPCR data are presented as mean \pm SEM from three independent experiments. ** $P < 0.01$, *** $P < 0.001$ analysed by Student's *t*-test. Representative microphotographs of *In situ* hybridization are shown from *n* = three mice per experiment. Scale bars: 50 μ m.

As we observed high levels of miR-148a expression during telogen stage of HF cycling via TaqMan RT-qPCR and *in situ* hybridisation, we aimed to determine if miR-148a

was co-localised with SC markers in the skin and HF. Fluorescent *in situ* hybridisation (FISH) with simultaneous immunostaining was utilised to analyse the spatiotemporal expression pattern of miR-148a with stem/progenitor markers cytokeratin 15 (Krt15) and CD34. In the epidermis, FISH analysis revealed Krt15 expression in the basal layer, mutually exclusively from miR-148a expression in the suprabasal layer (Figure. 12A-B, asterisk). In the HF, Krt15 and CD34 were both co-expressed with miR-148a in the bulge region of the HF (Figure. 12A-B, arrowheads). Negative control using scrambled probe showed no detectable expression (Figure. 12C). As CD34 is uniquely expressed in and used to isolate mouse HF-bulge stem cells (SCs) (Trempeus et al., 2003, Blanpain et al., 2004), we therefore employed fluorescent activated cell sorting (FACS) to isolate mouse HF-bulge SCs and we observed significantly higher ($*P<0.05$) miR-148a expression in CD34-positive ($CD34^{+}/CD49f^{High}/Sca-1^{-}$) bulge SCs compared to CD34-negative ($CD34^{-}/CD49f^{Low}/Sca-1^{-}$) populations analysed by TaqMan RT-qPCR (Figure. 12D). In addition, analysis of FACS sorted telogen SCs by RT-qPCR showed that we had indeed successfully sorted bulge SC populations: Krt15 ($***P<0.001$), Lgr5 ($***P<0.001$) and Lhx2 ($*P<0.05$) SC markers were significantly higher in FACS sorted bulge SCs (CD34-positive) *versus* CD34-negative cells (Figure. 12E).

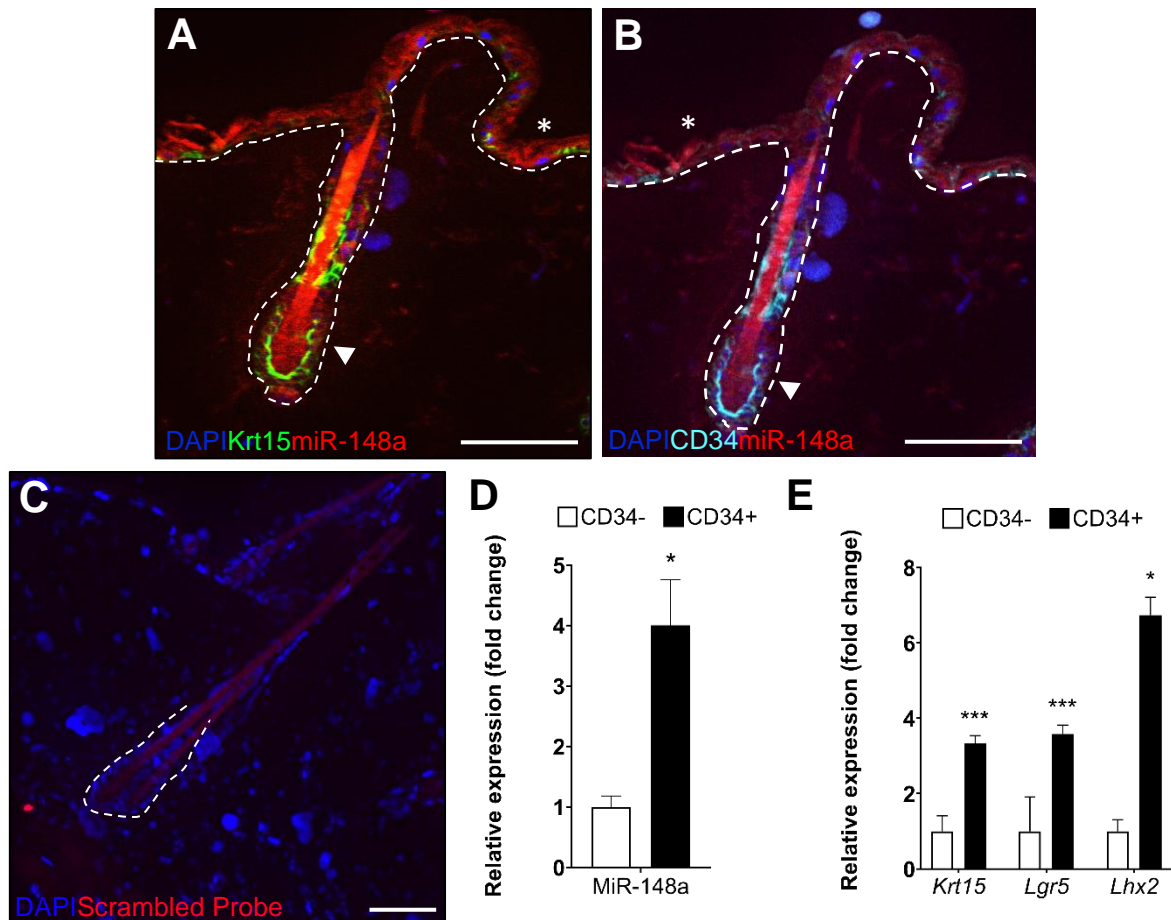


Figure 12. *Expression Analysis of miRNA-148a in Stem Cell Populations in Skin and Hair Follicles.*

(A-C) Fluorescent in situ hybridization of miR-148a expression (red) and SC markers cytokeratin 15 (Krt15, green) and CD34 (cyanine) with DAPI (blue) in C57BL/6 wild type telogen mouse skin. (A-B) MiR-148a expression was observed in the suprabasal layer, whereas Krt15 was observed in the basal layer of the epidermis. CD34 expression was not observed in the epidermis (A-B, asterisk). In the HF, miR-148a expression was observed in the bulge and secondary hair germ stem/progenitor region of the HF, co-expressed with stem/progenitor markers Krt15 and CD34 (A-B, arrowheads). (C) Negative control using scrambled probe and secondary antibodies showed no non-specific/background expression. (D) An increase in miR-148a expression was observed in HF-bulge SCs isolated from 7-9-week-old female C57BL/6 wild type telogen mouse skin by fluorescent

activated cell sorting (FACS). **(E)** Confirmatory RT-qPCR analysis of bulge SC markers revealed an increase in expression of all bulge SC markers analysed in CD34-positive populations compared to CD34-negative. Broken lines define epidermal-dermal boarder and HF. *n* = three mice were used per experiment. RT-qPCR data are presented as mean \pm SEM from three independent experiments. **P*<0.05, ***P*<0.01, ****P*<0.001 analysed by Student's *t*-test. Scale bars: 50 μ m.

From microarray analysis of miR-148a expression during hair cycling and subsequent RT-qPCR and *in situ* hybridisation analysis, we observed that miR-148a is highly expressed during the telogen stage of HF cycling, compared to anagen and catagen, specifically in the bulge SC region, progenitor SHG population and the differentiated suprabasal layer of the epidermis (Figure.11). Further analysis revealed that miR-148a was co-expressed with stem/progenitor markers CD34 and Krt15 in the bulge and SHG (Figure. 12). The expression of miR-148a in differentiated suprabasal layers of the epidermis, suggests that miR-148a may function to promote differentiation in the epidermis. However, the expression of miR-148a in the stem/progenitor regions of the HF during telogen suggests that miR-148a may play a role in modulating SC quiescence during HF cycling, potentially performing a dual role in skin.

3.2 Identification of Novel Targets of MiRNA-148a in Epidermal Keratinocytes

Aims:

To identify novel gene targets of miR-148a in primary mouse epidermal keratinocytes.

Results:

To investigate the possible regulatory mechanisms of miR-148a in primary mouse epidermal keratinocytes (PMEKs), we utilised RNA sequencing analysis. PMEKs were transfected with either pro-miR-148a (overexpression) or miRNA-controls. Using the publicly available Galaxy platform (<https://usegalaxy.org/>), we generated a heat map, gene ontology analysis (under-and/or over expressed genes) and the selection of significantly ($*P < 0.05$) downregulated genes for further analysis (Figure. 13). The heat map depicts gene expression changes based on Z-score following pro-miRNA-148a (overexpression) *versus* miRNA-control transfections in PMEKs. The Z score depicts the standard deviation of the sample, above or below the mean of the rest of the samples. Blue colour depicts up to 2 standard deviations below the mean gene expression and red colour depicts up to 2 standard deviations above the mean gene expression (Figure. 13A). Genes were then grouped into 12 functionally distinct categories and ranked, including cell differentiation and cell cycle categories and revealed many gene expression changes in these functional groups (Figure. 13B). To assess the quality of our RNA sequencing data, a principal component analysis (PCA) and volcano plot were generated (Figures. 13C-D). In our PCA-1 component, we observed 96% variance between pro-miR-148a treated PMEKs *versus* miRNA-controls and high degree of clustering of RNA samples with corresponding treatments

showing there is dramatic and reproducible effects on cells after miR-148a overexpression compared to control samples (Figure. 13C). Our volcano plot also confirmed large fold changes, which are statistically significant ($*P<0.05$), are caused by overexpression of miR-148a compared to control samples. Genes that were not significant were excluded from further analyses (Figure. 13D). To identify putative gene targets of miR-148a, online prediction tools were used: TargetScan (<http://www.targetscan.org/>), miRanda (<https://www.mirbase.org/>) and miRDB (<http://mirdb.org/>) (Ahmed et al., 2014, Ahmed et al., 2019). Four hundred and eight, overlapping, putative miR-148a gene targets were identified from all three databases (Figure. 13E). To refine our gene target list further, these four hundred and eight predicted gene targets were overlapped with genes identified from our RNA sequencing that were significantly ($*P<0.05$) downregulated (a total of eight hundred and fifty-nine genes). From this analysis, we identified forty-three potential gene targets of miR-148a (Table 9 and Figure. 13E).

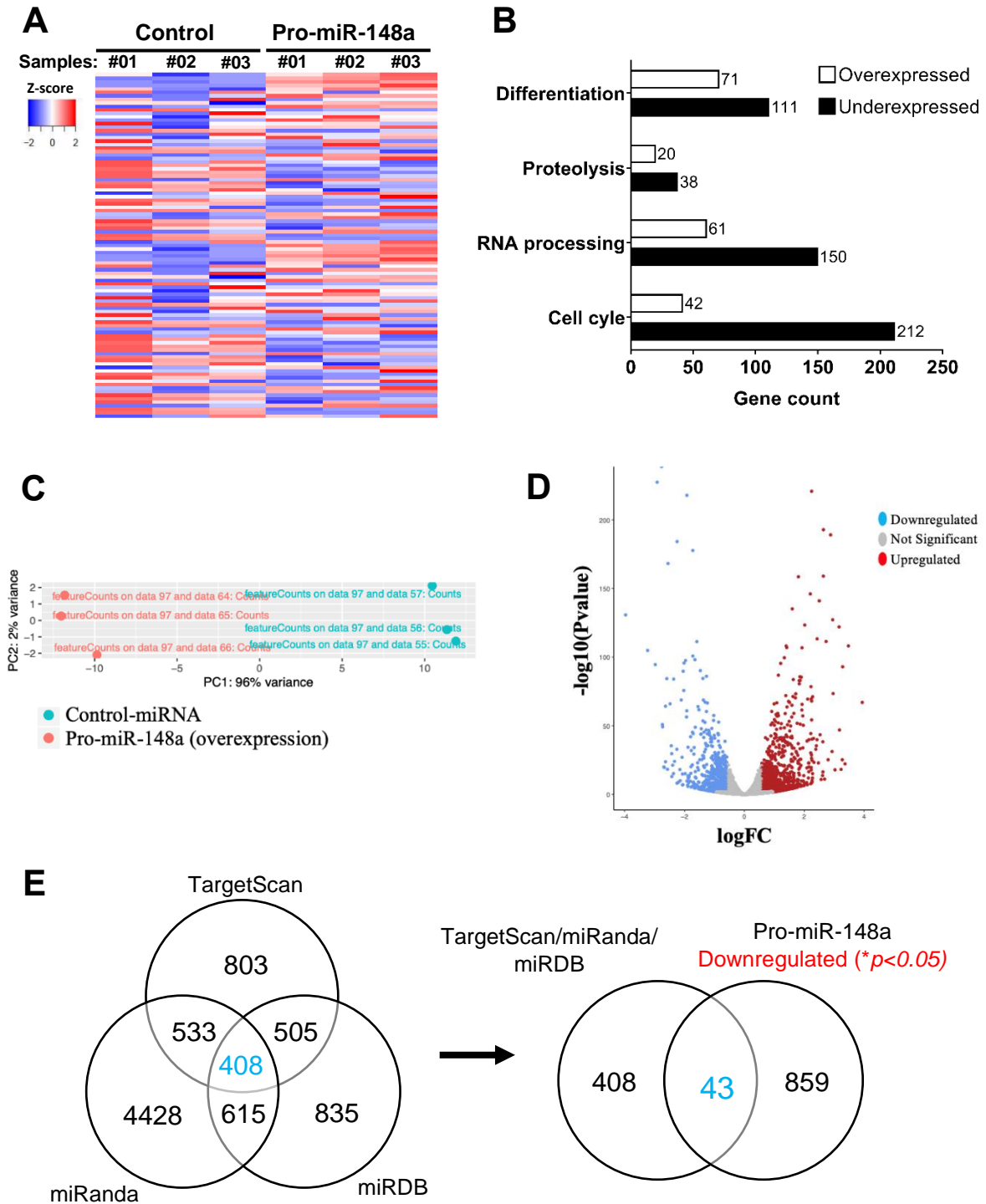


Figure 13. Global Gene Expression Profiling after MiRNA-148a Overexpression in Primary Mouse Epidermal Keratinocytes.

(A) Heat map depicting gene expression changes (Red: up to 2 standard deviations above the mean gene expression. Blue: up to 2 standard deviations below the mean gene

expression) in pro-miR-148a transfected PMEKs versus miRNA-controls following RNA-sequencing analysis. **(B)** Gene ontology bar chart of distinct functional groups depicting changes to total number of genes after pro-miR-148a transfections in PMEKs versus miRNA-control. **(C)** PCA plot depicting the variance between samples and groups. A 96% variance was achieved between pro-miR-148a treated PMEKs versus miRNA-controls. **(D)** Volcano plot depicting a significant number of gene expression changes (overexpression and inhibition) in pro-miR-148a treated PMEKs versus miRNA-controls. Genes that were not significant ($P > 0.05$) were excluded from further analyses. **(E)** Venn diagram of online miRNA target prediction tools; TargetScan, miRanda and miRDB, revealed four-hundred and eight aligned predicted targets of miR-148a. Predicted gene targets were overlapped with significantly ($*P < 0.05$) downregulated genes from our RNA-sequencing data after pro-miR-148a transfections in PMEKs, which revealed forty-three significant, potential gene targets. $*P < 0.05$ analysed by Student's t-test.

Having identified forty-three potential targets of miR-148a, we validated the top ten highly conserved genes between human and mouse as well as genes that have known regulatory roles in epithelial development (Table 9) (Lock and Hotchin, 2009, Chakrabarti et al., 2012b). From this, *Rock1* ($**P < 0.01$, $***P < 0.001$) and *Elf5* ($*P < 0.05$, $***P < 0.001$) were found to be the only significantly up and downregulated genes after anti-(inhibition) and/or pro-miR-148a transfections in PMEKs. Despite the apparent large increase in *Stx3* expression after treatment with pro-miR-148a, sample expression variation resulted in an insignificant increase in expression (Figure. 14A). No significant difference was observed in the remaining genes analysed (Figure. 14A-B). In addition, an increase and decrease in protein levels of *Rock1* and *Elf5* was observed following anti-and/or pro-miR-148a transfections, respectively (Figure. 14C-D). We therefore focussed only on *Rock1* and *Elf5* for further analysis.

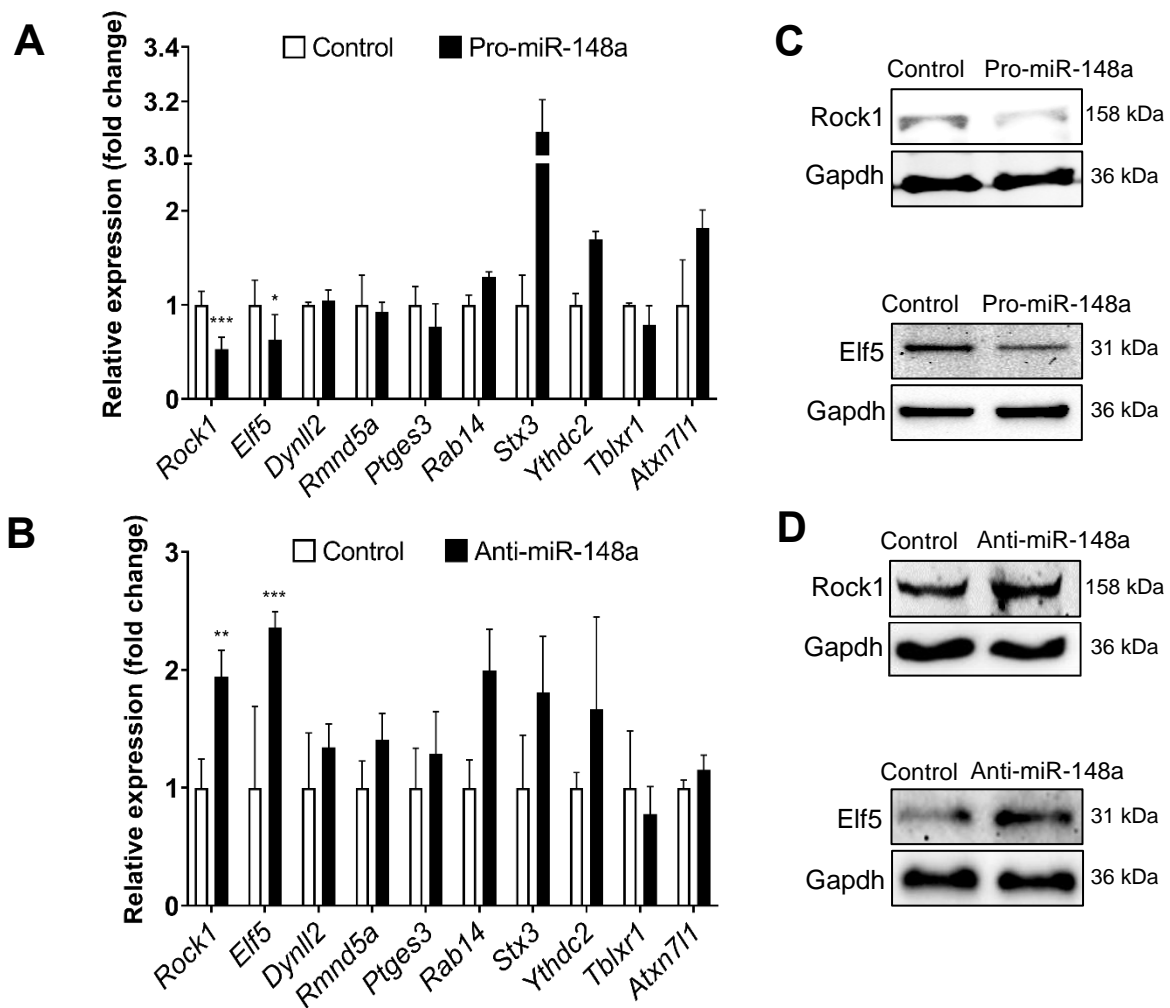


Figure 14. MiRNA-148a Target Analysis Revealed Rock1 and Elf5 are Inversely Expressed to MiRNA-148a.

(A-B) Target validation of RNA sequencing by RT-qPCR. **(A)** Pro-miR-148a transfected PMEKS resulted in a significant decrease in predicted gene targets Rock1 and Elf5, whereas no significant changes were observed in other genes analysed. **(B)** Anti-miR-148a (inhibition) transfected PMEKS resulted in a significant increase in predicted gene targets Rock1 and Elf5 whereas no significant changes were observed in other genes analysed **(C-D)** Protein analysis by Western blot in PMEKS following anti-and/or pro-miR-148a transfections in PMEKS showed an increase and decrease in Rock1 and Elf5 protein levels respectively. RT-qPCR data are presented as mean \pm SEM values from three independent

experiments. Representative Western blots shown from three experimental repeats.

* $P < 0.05$, ** $P < 0.01$, *** $P < 0.001$ analysed by Student's *t*-test.

To confirm whether Rock1 and Elf5 are indeed direct targets of miR-148a, we utilized a dual luciferase reporter assay. Reporter constructs containing miR-148a binding site in the 3' untranslated region (UTR) of *Rock1* and *Elf5* were co-transfected with pro-miR-148a in HaCaT cells. A significant (Rock1: *** $P < 0.001$, Elf5: * $P < 0.05$) reduction in bioluminescence was observed after co-transfections with pro-miR-148a and reporter constructs. No reduction in bioluminescence was observed following co-transfections with pro-miR-148a and reporter constructs containing mutated miR-148a binding sites in the 3'UTR (Figure. 15A).

Following confirmation of miR-148a as a direct regulator of *Rock1* and *Elf5*, we investigated the expression patterns of Rock1 and Elf5 in skin and HFs, in relation to miR-148a using fluorescent *in situ* hybridization (FISH) with simultaneous immunostaining: in the epidermis, miR-148a was primarily expressed in the suprabasal layer (Figure. 15B, Panel (i), asterisk) whereas Rock1 was expressed in the basal layer (Figure. 15B, Panel (i), arrow). Elf5 expression was also observed mainly in the basal layer with some expression observed in the suprabasal layer also (Figure. 15B, Panel (iv), arrow). In the HF, Rock1 and Elf5 were co-expressed with miR-148a in the bulge region and secondary hair germ stem/progenitor compartments (Figure. 15B).

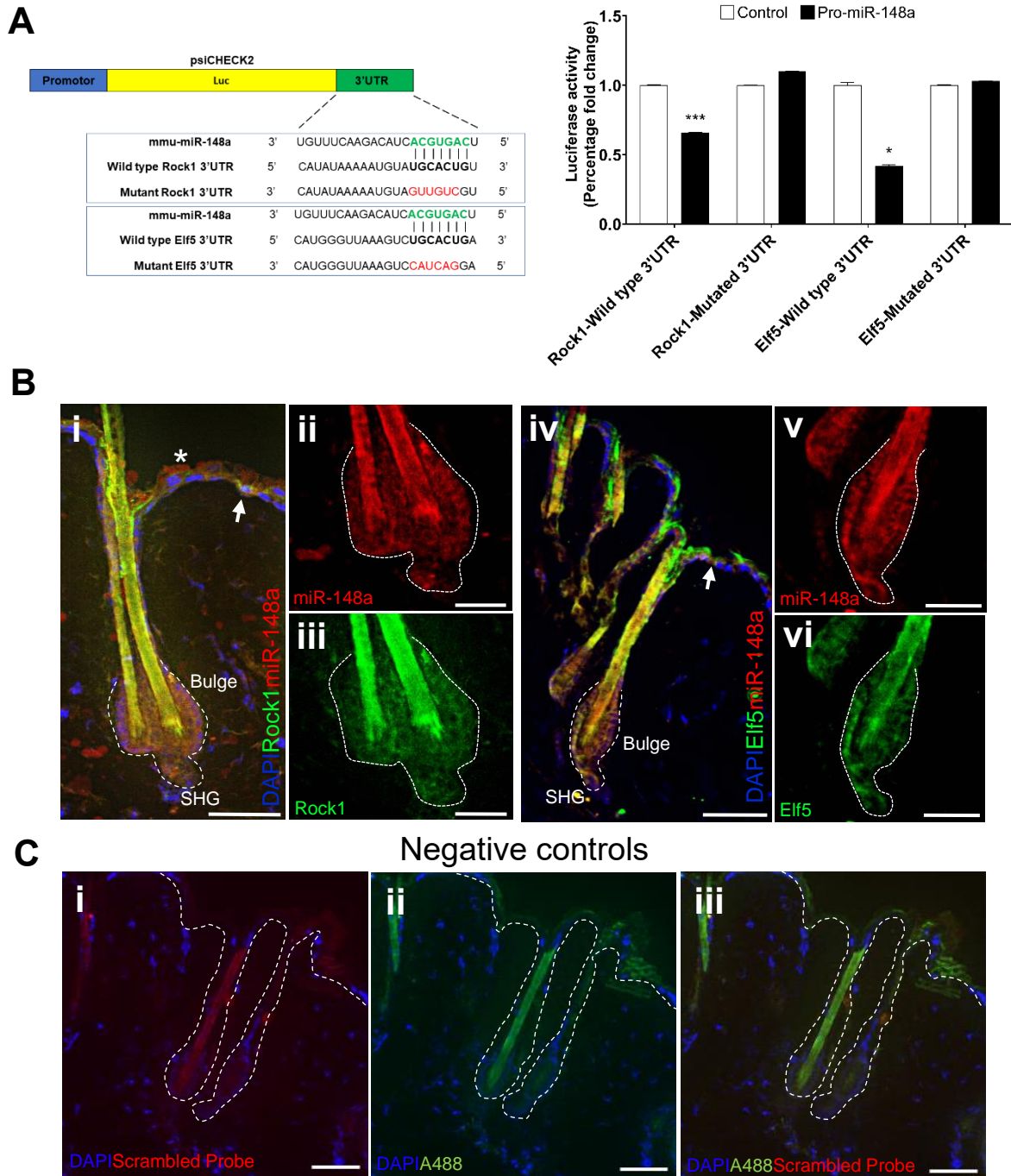


Figure 15. *Co-localisation of MiRNA-148a and Gene Targets Rock1 and Elf5 Within the Epidermis and Hair Follicle Stem Cell Compartments.*

(A) Luciferase reporter assay: Luciferase reporter plasmids were constructed containing miR-148a 3'-UTR binding sites of Rock1 and Elf5 (green letters) as well as mutated binding sites (red letters). A significant reduction in luciferase activity was measured after co-

transfections of pro-miR-148a and Luciferase reporter plasmids constructs containing miR-148a binding sites in Rock1 and Elf5 3'-UTR in HaCaTs. No reduction in luciferase activity was observed following co-transfections with pro-miR-148a and Luciferase reporter plasmids constructed containing mutated miR-148a binding sites in Rock1 and Elf5 3'-UTR. pRenilla reporter luciferase activity was normalised to pFirefly luciferase activity. **(B)** Representative microphotographs of fluorescence in situ hybridization of miR-148a (red), Rock1 (green), Elf5 (green) and DAPI (blue) in C57BL/6 wild type dorsal mouse skin during telogen stage of hair cycle. In the epidermis, miR-148a is expressed in the suprabasal layer (Panel (i), asterisk), whereas Rock1 is predominately expressed in the basal layer (Panel (i), arrow). Elf5 expression in the epidermis is observed in the basal layer and the suprabasal layer, co-expressed with miR-148a (Panel (iii), arrow). In the HF, miR-148a is expressed in the SC compartments (bulge region and secondary hair germ) of telogen HFs which is co-localised with Rock1 and Elf5 expression (Panel (i)-(vi)). **(C)** Representative microphotographs of negative control fluorescent in situ hybridisation of scrambled probe (red, Panel (i)) and Alexa fluor 488 (A488, green, Panel (ii)) and overlay (Panel (iii)). Negative controls using scrambled probe and A488 showed no detectable expression. Broken lines outline epidermal-dermal boarder. Luciferase bioluminescence data are presented as mean \pm SEM values from five independent experiments. * $P < 0.05$, *** $P < 0.001$ analysed by Student's *t*-test. In situ hybridization with subsequent immunofluorescent analysis was performed from $n =$ three mice per experiment. Figure. B, Panels (i) and (iv), and Figure. C, Panels (i)-(iii) scale bars: 50 μ m, Figure. B, Panels (ii), (iii), (v) and (vi) scale bars: 25 μ m.

In summary, bioinformatic analysis of RNA-seq data of miR-148a overexpression in PMEKs and overlapping of potential gene targets of miR-148a from online databases, revealed 43 potential gene targets of miR-148a (Figure. 13). Validation of the top genes from this list that were most conserved between human and mice, and with a

known role in epithelial tissue revealed only Rock1 and Elf5 as significantly changed in expression following modulation of miR-148a in PMEKs (Figure. 14). Following identification of Rock1 and Elf5 as potential targets of miR-148a, dual luciferase reporter assay incorporating the miR-148a binding site in the 3'UTR of Rock1 and Elf5, and mutated binding sites was performed. This revealed Rock1 and Elf5 as genuine targets of miR-148a (Figure. 15). We next investigated the expression pattern between miR-148a, Rock1 and Elf5 in telogen HF. We observed expression of miR-148a in the suprabasal layer of the epidermis, with Rock1 and Elf5 expression mainly observed in the basal layer of the epidermis. In the HF, miR-148a was co-expressed with Rock1 and Elf5 in the bulge SC region and the SHG (Figure. 15). MiRNA modulation of gene expression occurs through regulation of their gene targets. Identification of direct targets of miR-148a helps to elucidate the role of miR-148a in the skin through investigation of the roles of Rock1 and Elf5. The potential role of miR-148a in modulation of differentiation processes in the epidermis and maintenance of SC quiescence during HF cycling may occur through a miR-148a-Rock1/Elf5 mechanism.

3.3 MiRNA-148a Modulates Proliferation and Differentiation Processes, *In Vitro*

Aims:

To investigate the role of miR-148a in controlling cell proliferation and differentiation processes in primary epidermal mouse keratinocytes, *in vitro*.

Results:

Bioinformatic analysis and gene ontology analysis of our RNA sequencing (Figure. 13) revealed changes in genes belonging to cell cycle and differentiation categories (Figure. 13B). We therefore investigated the possible role of miR-148a in cell proliferation and differentiation in PMEKs, *in vitro*. RT-qPCR analysis into cell cycle gene regulators of anti-and/or pro-miR-148a transfected PMEKs revealed a significant up-or downregulation of genes: Cyclin dependant kinase 16 (*Cdk16*, * $P < 0.05$ and *** $P < 0.001$), Cyclin dependant kinase 1 (*Cdk1*, * $P < 0.05$), Cyclin B2 (*Ccnb2*, * $P < 0.05$ and ** $P < 0.01$), Cyclin E1 (*Ccne1*, * $P < 0.05$), Cyclin D1 (*Ccnd1*, * $P < 0.05$), Cyclin D2 (*Ccnd2*, * $P < 0.05$ and ** $P < 0.01$) and Cdc28 Protein Kinase Regulatory Subunit 1B (*Cks1b*, *** $P < 0.001$ and ** $P < 0.01$), respectively (Figure. 16A-B). To further analyse the potential role of miR-148a in regulating cell cycle, we subsequently utilised flow cytometry with propidium iodide staining which revealed a 6.85% decrease in cells in G0/1 phase, a 14.3% increase in cells in S phase, and a 7.78% decrease in cells entering G2/M phase following pro-miR-148a transfections *versus* miRNA-controls (Figure. 16C).

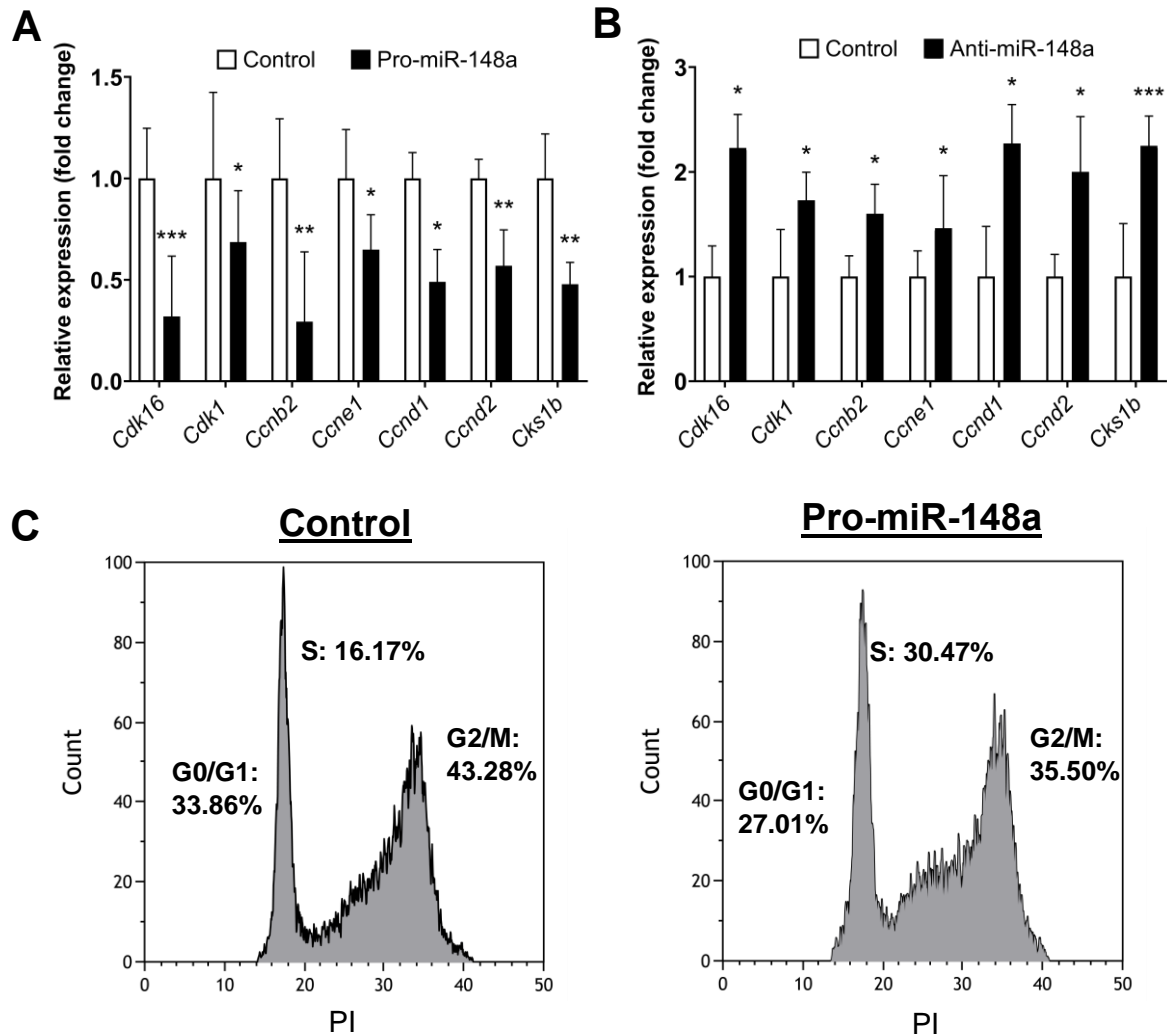


Figure 16. MiRNA-148a Inhibits Proliferation of Primary Mouse Epidermal Keratinocytes, *In Vitro*.

(A-B) RT-qPCR analysis of cell cycle gene regulators in PMEKS. An increase or decrease in expression for all cell cycle genes analysed was observed following anti-and/or pro-miR-148a transfections, respectively. Data are presented as mean \pm SEM values from three independent experiments. (C) Flow cytometric analysis of PMEKS by propidium iodide staining revealed an accumulation of cells in S phase of cell cycling in pro-miR-148a transfected PMEKS compared with miRNA-controls. Graphs shown are representatives from a single experiment. Percentages in each cell cycle stage are mean values from three independent experiments. 10,000 events were collected per experiment. * $P < 0.05$, ** $P < 0.01$, *** $P < 0.001$ analysed by Student's *t*-test.

Subsequently, we investigated the role of miR-148a during differentiation in PMEKs using calcium-induced differentiation assay. Calcium induced differentiation of keratinocytes by media supplementation with 1.8 mM Ca²⁺ is a well-established method for differentiation induction (Hennings et al., 1980, Borowiec et al., 2013). Calcium-induced differentiation of PMEKs was performed in parallel with transfection with either anti-and/or pro-miR-148a. RT-qPCR analysis revealed that differentiation markers Cytokeratin (*Krt*) 1 (***P*<0.01 and ****P*<0.001), *Krt10* (****P*<0.001) and Involucrin (*Ivl*, ****P*<0.001) were all either significantly up-and/or downregulated respectively (Figure. 17A-B). In addition to differentiation markers, miR-148a gene targets *Rock1* (***P*<0.01 and ****P*<0.001) and *Elf5* (**P*<0.05 and ***P*<0.01) were analysed, and both were up or downregulated after anti-and/or pro-miR-148a transfections, respectively (Figure. 17A-B). Furthermore, we analysed whole protein extract levels by Western blot of *Krt1*, *Rock1* and *Elf5*, which revealed up-and/or downregulation of all proteins analysed after anti-and/or pro-miR-148a transfections, respectively (Figure. 17C-D).

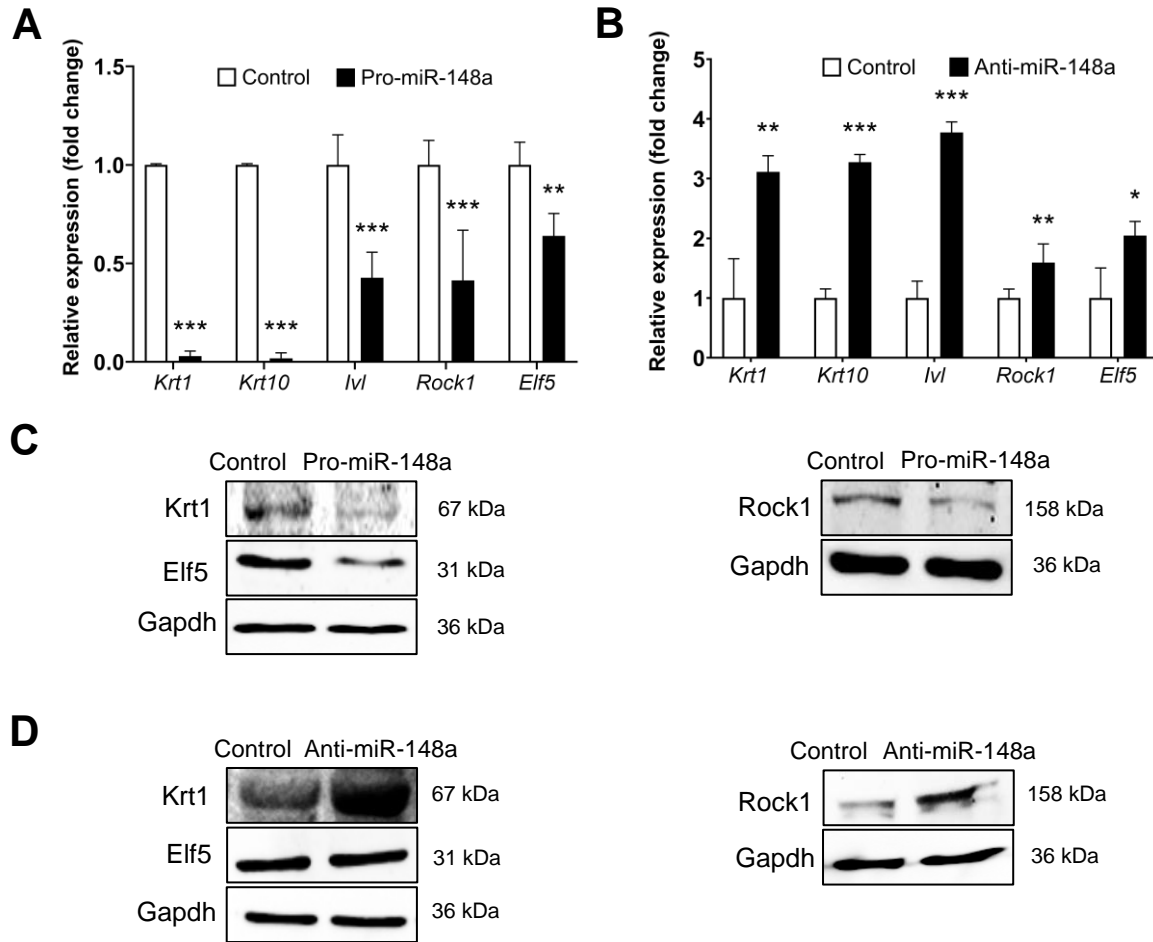


Figure 17. *MIRNA-148a Regulates Differentiation of Primary Mouse Epidermal Keratinocytes, In Vitro.*

(A-B) RT-qPCR analysis of differentiation associated genes, *Krt1*, *Krt10*, *IvI*, alongside *Rock1* and *Elf5* in calcium-induced (1.8mM) differentiation of PMEKS. An increase and decrease in expression of all genes analysed was observed following anti-and/or pro-miR-148a transfections, respectively. Data are presented as mean \pm SEM values from three independent experiments. **(C-D)** Western blot analysis of differentiation marker *Krt1* alongside *Rock1* and *Elf5* during calcium-induced differentiation of PMEKS. An increase and decrease in protein levels of all proteins analysed was observed following anti-and/or pro-miR-148a transfections, respectively. Data shown are representative images from a single experiment, of three independent repeats. * $P < 0.05$, ** $P < 0.01$, *** $P < 0.001$ analysed by Student's *t*-test.

To investigate whether differentiation of PMEKs is regulated by miR-148a through modulation of Rock1 and Elf5, we performed immunocytochemistry investigating whether miR-148a could regulate nuclear translocation/activation of Rock1 and Elf5 in differentiation induced PMEKs (Ca^{2+} : 1.8 mM), *in vitro*. Immunocytochemical staining of Rock1 and Elf5 in differentiated PMEKs was performed following pro-miR-148a or miRNA-control transfections. A decrease in expression of both nuclear and cytoplasmic Rock1 and Elf5 was observed in pro-miR-148a transfected PMEKs *versus* miRNA-controls (Figure. 18A-D). This was validated by quantitative immunofluorescence analysis, revealing a significant ($***P<0.001$) decrease in nuclear and cytoplasmic fluorescence levels of Rock1 and Elf5 after pro-miR-148a transfected PMEKs compared to miRNA-control transfected (Figure. 18E-F). We further confirmed effects on nuclear localisation using Western blot analysis from isolated nuclear protein extracts. Nuclear protein analysis after pro-miR-148a treated differentiated PMEKs revealed a downregulation of nuclear Rock1 and Elf5 protein levels compared to miRNA-controls (Figure. 18G-H).

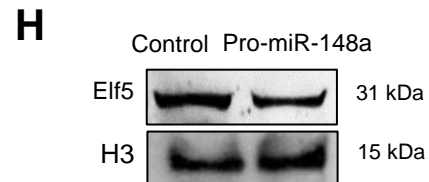
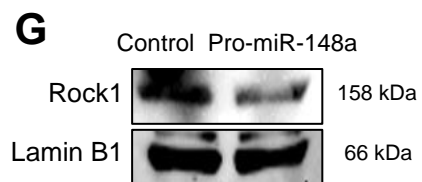
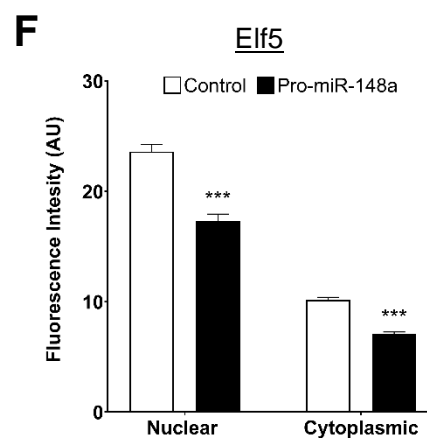
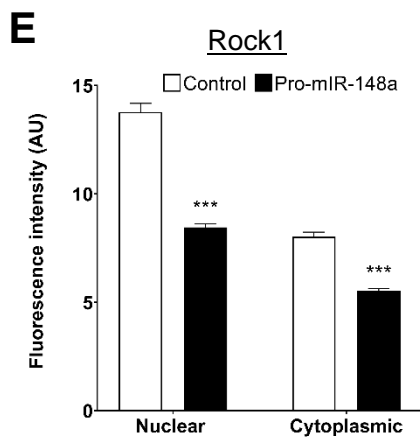
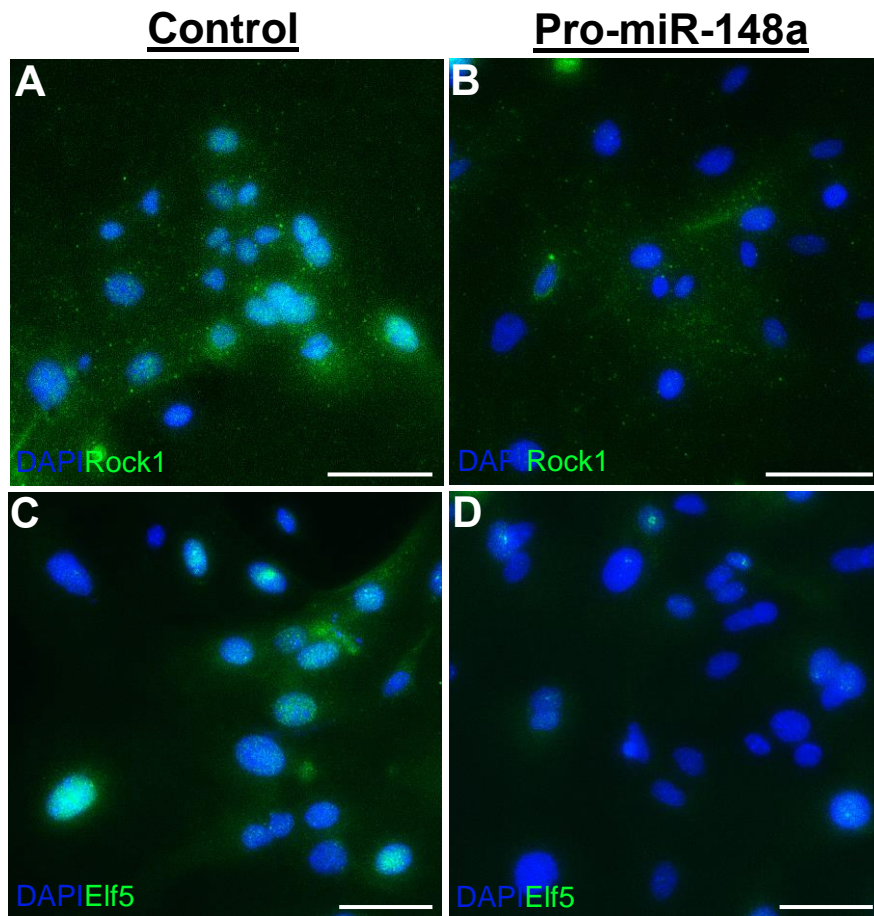


Figure 18. Overexpression of miRNA-148a Inhibits Nuclear Localization of Rock1 and Elf5 in Differentiated Primary Mouse Epidermal Keratinocytes.

(A-D) Immunocytochemistry of Rock1 (green), Elf5 (green) and DAPI (blue) in pro-miR-148a transfected differentiated PMEKs. Overexpression of miR-148a resulted in a decrease in Rock1 and Elf5 in the cytosol and nucleus of differentiated PMEKs compared to miRNA-controls. **(E-F)** Quantitative immunofluorescence analysis of Rock1 and Elf5 in differentiated PMEKs after pro-miR-148a transfection compared with miRNA-controls was analysed by ImageJ (<https://imagej.nih.gov/ij/>) and normalised to DAPI+ cells. A significant reduction in Rock1 and Elf5 fluorescence in the nucleus and cytosol was observed in pro-miR-148a transfected differentiated PMEKs compared to miRNA-controls. Data are presented as mean \pm SEM values from 100 cells counted from three independent experiments. **(G-H)** Western blot analysis of nuclear protein of Rock1 and Elf5 following pro-miR-148a transfection in differentiated PMEKs. Overexpression of miR-148a reduced the nuclear protein levels of Rock1 and Elf5 in differentiated PMEKs compared to miRNA-controls. Data shown are from a single representative experiment of three experimental repeats. *** $P < 0.001$ analysed by Student's *t*-test. Scale bars: 50 μ m.

From analysis of proliferation in PMEKs after modulation of miR-148a, we revealed that miR-148a inhibits proliferation of PMEKs and cells accumulate in the S phase of cell cycling after miR-148a overexpression, *in vitro* (Figure. 16). Analysis of PMEKs following modulation of miR-148a in calcium induced differentiation assay revealed that miR-148a inhibits differentiation of PMEKs, *in vitro* (Figure. 17). MiR-148a modulation of these processes provides a potential explanation of the role of miR-148a in skin based on its spatiotemporal expression pattern, with modulation of proliferation and differentiation processes an integral part of maintaining skin homeostasis. MiR-148a may modulate these processes to maintain SC quiescence

during telogen stage of HF cycling, and to modulate proliferation/differentiation commitment of epidermal cells.

We next investigated whether overexpression of miR-148a could prevent the nuclear translocation of Rock1 and Elf5 during in calcium induced differentiation of PMEKs. Treatment of pro-miR-148a in calcium induced differentiation in PMEKs revealed that Rock1 and Elf5 were indeed prevented from translocating to the nucleus (Figure. 18). This suggests that the role of miR-148a in modulating differentiation processes in PMEKs may be through a miR-148a-Rock1/Elf5 mechanism, preventing their nuclear translocation, and their downstream activity.

3.4 Functional Analysis of MiRNA-148a Expression in Stem Cells *In Vitro* and *In Vivo*

Aims:

To analyse the potential effects of inhibition of miR-148a on skin and HF development, through modulation of SCs.

Results:

As we have determined specific miR-148a expression in stem/progenitor compartments of telogen HFs (bulge and hair germ), as well as high expression of miR-148a in FACS sorted CD34-positive SCs (Figure. 12D), we subsequently attempted to determine whether miR-148a could impact SC populations, *in vitro*. We performed colony forming assay using FACS sorted HF-bulge SCs from C57BL/6 wild type mouse skin. Lentiviral vectors containing sequences to inhibit miR-148a or act as controls (scrambled sequence) were used for transduction of HF-bulge SCs during colony forming assay. High transduction efficiency was observed in both controls and anti-miR-148a transduced SCs as seen by GFP positive colonies, which were subsequently counted and quantified after 10 days of growth (Figure. 19A, Panels (i) and (ii)). An increase in colony size and number is a method used to determine the clonal capacity of SCs and a well establish mechanism to assess the colony forming capacity of isolated SCs (Moestrup et al., 2017). To determine if inhibition of miR-148a had any impact on colony number and size, we measured and counted all GFP positive holoclonal SC colonies. Holoclonal colonies are distinct, well bordered, circular colonies of homogenous SCs that have a high capacity of self-renewal and contain no differentiated cell types. The borders of holoclonal colonies are much

smoother and rounder compared to the 'wrinkled' and more unordered borders of more differentiated paraclone and meroclone colonies (Barrandon and Green, 1987). We observed a significant increase in both number of colonies ($**P<0.01$) and size of colonies above 50 μm in diameter ($***P<0.001$) between anti-miR-148a transduced SCs compared to controls (Figure. 19A-B). There was no significant difference observed between colonies measuring less than 50 μm in diameter (Figure. 19B). In addition, to confirm that the effects were due to loss of miR-148a, TaqMan RT-qPCR revealed a significant reduction ($***P<0.001$) of miR-148a expression in anti-miR-148a treated SCs compared to controls (Figure. 19C).

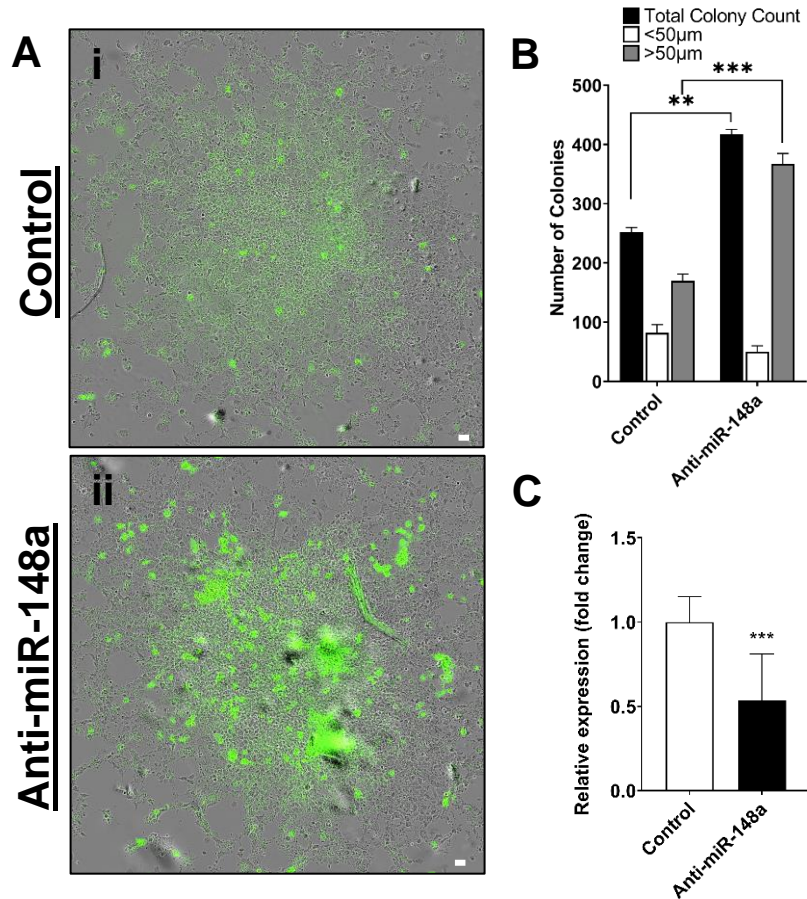


Figure 19. MiRNA-148a Inhibition Promotes Colony Forming Abilities of Hair Follicle Stem Cells, In Vitro.

(A) Colony forming assay: Anti-miR-148a lentiviral transduction of HF-bulge SCs increased the number and size of colonies formed compared to control transduced HF-bulge SCs. Efficiency of lentiviral transduction for control and miR-148a inhibition in FACS isolated HF-bulge SCs were evaluated using green fluorescent protein (GFP) incorporated lentiviral particles **(B)** Quantification of number and size of GFP positive SC colonies in anti-miR-148a lentiviral treated HF-bulge SCs versus control. A similar number of smaller colonies (<50 µm in diameter) were found in anti-miR-148a treated HF-bulge SCs compared to controls. While a significantly higher number of larger colonies (>50 µm in diameter) were observed in anti-miR-148a treated HF-bulge SCs compared to controls. **(C)** MiR-148a TaqMan RT-qPCR expression analysis of lentiviral anti-miR-148a transduced SCs and revealed a significant reduction of miR-148a expression. Data are presented as mean ±

*SEM and representative microphotographs from three independent experiments. **P<0.01, ***P<0.001 analysed by Student's t-test. Scale bars: 100 µm.*

To investigate the role of miR-148a in controlling skin and hair cycle associated tissue remodelling, miR-148a was pharmacologically inhibited with a synthetic inhibitor which specifically binds to miR-148a *via* complimentary base pairing, preventing it from binding to its gene targets. Pharmacological miR-148a inhibitor or miRNA-control was administered into dorsal skin of C57BL/6 wild type mice at post-natal day 20 through to day 22. The skin was harvested at post-natal day 23 for histomorphological and immunofluorescent analysis (Figure. 20A). Successful inhibition of miR-148a was assessed by TaqMan RT-qPCR. A significant ($***P<0.001$) reduction of miR-148a was observed in anti-miR-148a treated skin compared with miRNA-controls (Figure. 20B). Pharmacological inhibition of miR-148a revealed changes in HF stages. In miRNA-control treated skin, HF staging analysis revealed that the majority of HFs were in anagen II stage of HF cycling (Figure. 20C, Panel (i), arrows). In anti-miR-148a treated skin, significantly ($*P<0.05$) more HFs were observed in anagen stage III of HF cycling, characterised by an enlarged dermal papilla partially enclosed by keratinocytes (Figures. 20C, Panel (ii)-(iii), arrows and 20D). Skin thickening is an established factor of hair cycle progression (Hansen et al., 1984, Muller-Rover et al., 2001, Mardaryev et al., 2010), we therefore investigated whether pharmacological inhibition of miR-148a could affect skin thickness. Skin thickness was measured from the outermost epidermis to the top of the panniculus carnosus, the base of the skin in mice (Schmidt and Horsley, 2012). In anti-miR-148a treated skin, a significant ($*P<0.05$) thickening of the skin was observed compared with miRNA-controls (Figures. 20C, asterisk, and 20E).

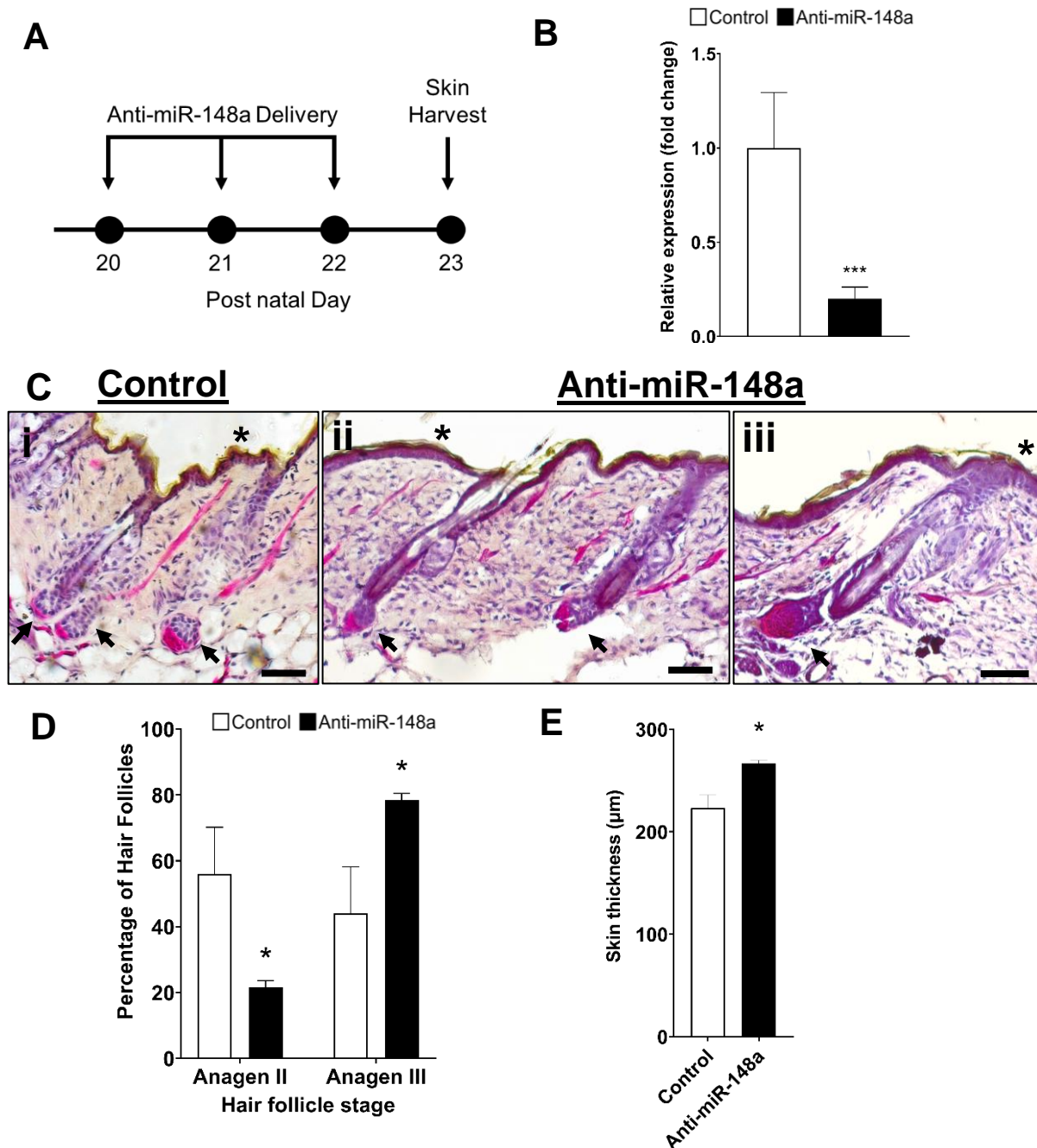


Figure 20. MiRNA-148a Inhibition Accelerates Telogen to Anagen Transition, In Vivo.

(A) Anti-miR-148a and miRNA negative control were administered subcutaneously in C57BL/6 wild type mouse dorsal skin from post-natal day 20 to 22 before harvesting on post-natal day 23. (B) TaqMan RT-qPCR analysis of miR-148a in anti-miR-148a treated skin compared to miRNA-controls showed a significant inhibition in miR-148a expression. (C) Representative microphotographs of alkaline phosphatase-stained miRNA-control and anti-miR-148a treated wild type C57BL/6 dorsal mouse skin. In anti-miR-148a treated skin,

the skin was thicker compared to miRNA-controls (Panel C, (i), (ii) and (iii), asterisk). HFs in miRNA-control treated skin were mainly observed in anagen II stage characterised by an enlarged dermal papilla close to the hair shaft (Panel C, (i), arrows). In anti-miR-148a treated skin, the HFs were predominantly in anagen III, characterised by an enlarged dermal papilla partially enclosed by keratinocytes (Panel C, (ii)-(iii), arrows). **(D)** Pharmacological inhibition of miR-148a resulted in an increase of anagen III stage HFs and a reduction of anagen stage II HFs compared to miRNA-controls. Data are presented as mean \pm SEM values of 100 HFs. **(E)** Skin thickness increased post miR-148a inhibition compared to miRNA-controls, a well-known characterisation of hair cycle progression. Data is presented of $n =$ three mice. Data of skin thickness and HF category is presented as mean \pm SEM values of 100 measurements. * $P < 0.05$ analysed by Student's t -test. Scale bars: 50 μ m.

To determine the impact of loss of miR-148a on skin and hair stem/progenitor populations, *in vivo*, immunofluorescent analysis of SC marker Krt15 was analysed in anti-miR-148a treated and miRNA-control skins. Krt15 is a well-established as a marker of basal and HF-bulge stem cells as well as the ORS (Liu et al., 2003, Cotsarelis, 2006). In the epidermis, a significant (* $P < 0.05$) increase of Krt15 expression was observed in the basal layer in anti-miR-148a treated skin, whereas expression was reduced and uneven throughout the basal layer in control treated skin (Figures. 21A, Panel (i) and (ii), asterisk, and 11B). In the HF, a significant increase (* $P < 0.05$) in expression of Krt15 was observed in the developing hair bulb and bulge region in anti-miR-148a treated skin compared to miRNA-controls (Figures. 21A, Panel (i) and (ii), arrows, and 11B).

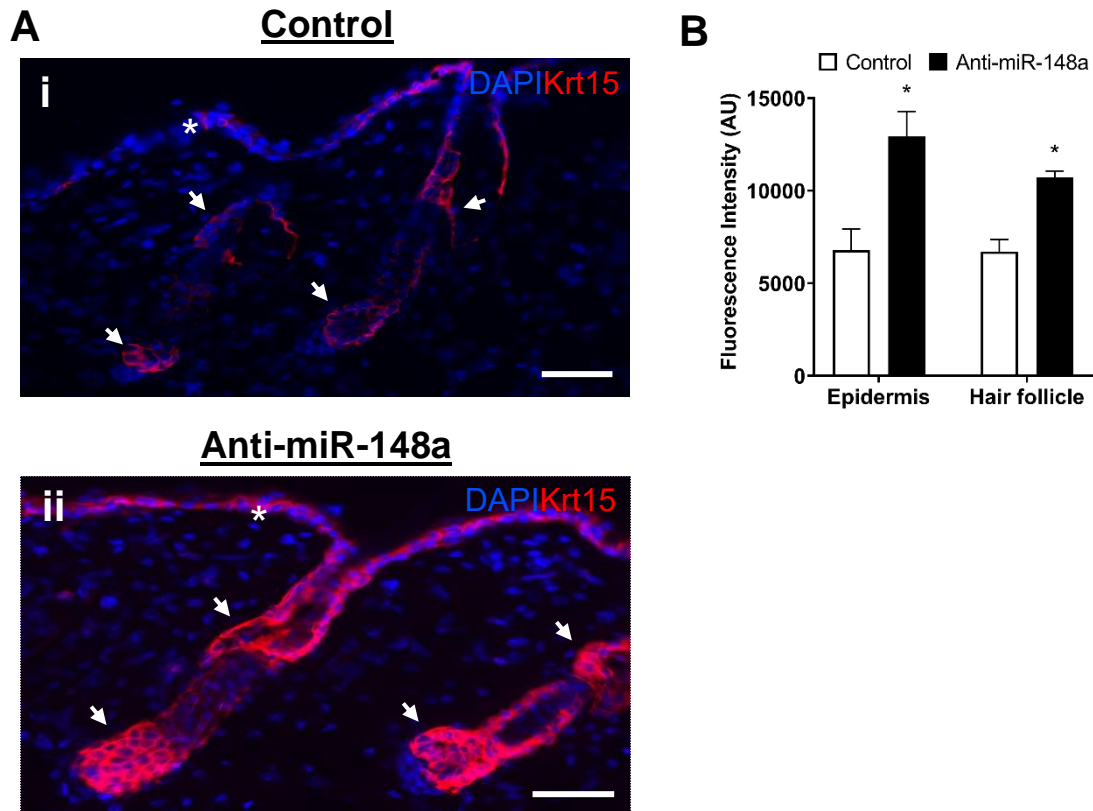


Figure 21. *MiRNA-148a Inhibition Alters Stem Cell Activity in Skin, In Vivo.*

(A) Representative microphotographs of immunofluorescent analysis of Krt15 (red) and DAPI (blue) in skin and HFs. In the epidermis, elevated Krt15 expression was observed throughout the basal layer in anti-miR-148a treated skin, whereas in control skins, Krt15 expression was reduced and uneven throughout the basal layer (Panel A, (i) and (ii), asterisk). In the HFs: elevated Krt15 expression was observed in the bulge region and developing hair bulb in anti-miR-148a treated skin compared to miRNA-controls (Panel A, (i) and (ii), arrows). **(B)** Quantitative immunofluorescence analysis: Krt15 (red fluorescence) in the epidermis and HFs of control versus anti-miR-148a treated skin samples normalised to DAPI+ cells. A significant increase in Krt15 fluorescence was observed in the epidermis and HFs in anti-miR-148a treated skins versus miRNA-controls. $n =$ three mice/treatment. Data are presented as mean \pm SEM values from three independent experiments. $*P < 0.05$ analysed by Student's t -test. Scale bars: 50 μ m.

Functional analysis of the role of miR-148a in modulating SCs, *in vitro*, was performed by colony forming assay. Inhibition of miR-148a in isolated bulge SCs by colony forming assay revealed that inhibition of miR-148a increased colony size and number of bulge SCs, *in vitro* (Figure. 19). Functional analysis of the role of miR-148a in modulating SCs, *in vivo*, was performed by subcutaneous injection of miR-148a inhibitor. Alkaline phosphatase staining and HF characterisation revealed that HFs had progressed to anagen stage III in anti-miR-148a treated skins compared to anagen stage II in control treated skins and a thickening of the skin was also observed in anti-miR-148a treated skins compared to controls (Figure. 20). Immunofluorescent analysis of stem/progenitor marker Krt15, revealed a significant increase in the activity of Krt15 in anti-miR-148a treated skins compared to controls (Figure. 21). Together, these indicate that miR-148a functions to repress SC activation and maintain SC quiescence. Abnormal activation of stem/progenitor cells after inhibition of miR-148a, *in vitro* (Figure. 19) and *in vivo* (Figure. 21) may explain the acceleration of hair cycle stage observed (Figure. 20), due to increased proliferation and differentiation processes associated with SC activation.

3.5 Analysis of the Effects of MiRNA-148a Inhibition During Skin Homeostasis, *In Vivo*

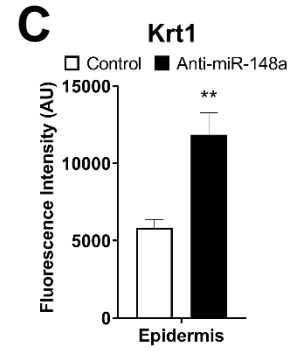
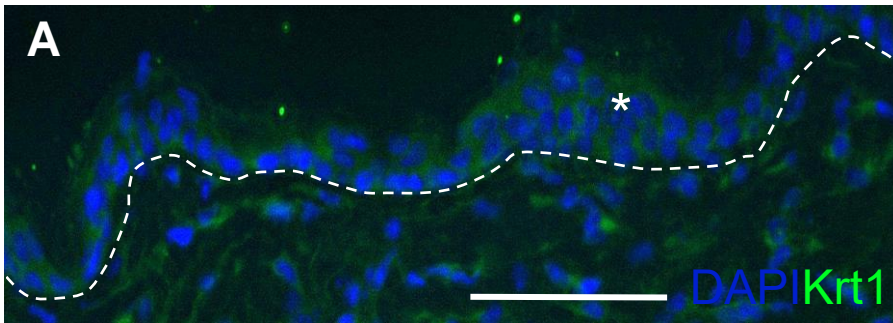
Aims:

To investigate the effects of miR-148a inhibition on Rock1 and Elf5 expression in skin and hair follicles, *in vivo*.

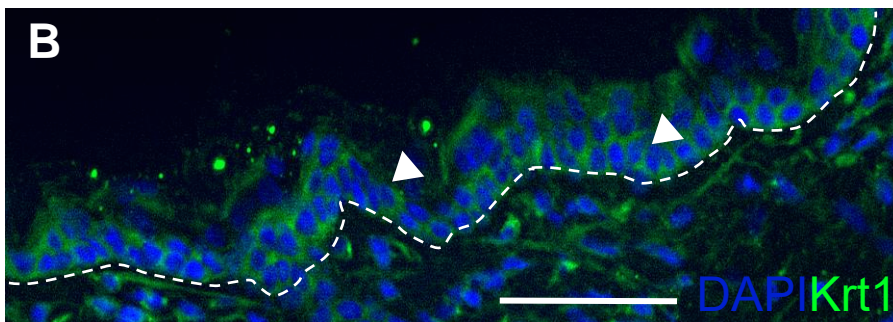
Results:

Following anti-miR-148a treatment in mouse skin, *in vivo* (Figure. 20), in the epidermis, miR-148a inhibition resulted in an increase in expression in differentiation marker Krt1 compared to controls epidermis (Figure. 22A-B). Quantitative immunofluorescence analysis of Krt1 showed a significant increase in Krt1 fluorescence observed in the epidermis in anti-miR-148a treated skin *versus* miRNA-control skins (Figure. 22C). Subsequently, to analyse the effect of miR-148a inhibition on cell proliferation, we used proliferation marker Ki67. We observed no changes in Ki67 fluorescence after inhibition of miR-148a compared to controls epidermis (Figure. 22D-E). Quantitative immunofluorescence analysis of Ki67 showed no significant change in fluorescence in anti-miR-148a treated skins *versus* miRNA-control skins (Figure. 22F).

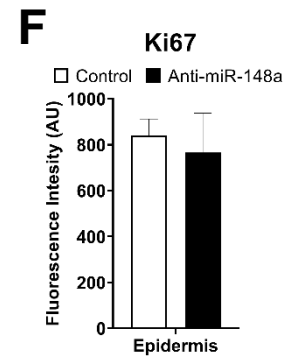
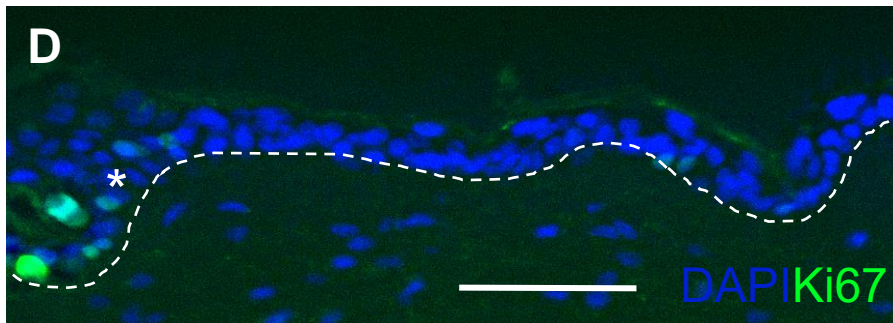
Control



Anti-miR-148a



Control



Anti-miR-148a

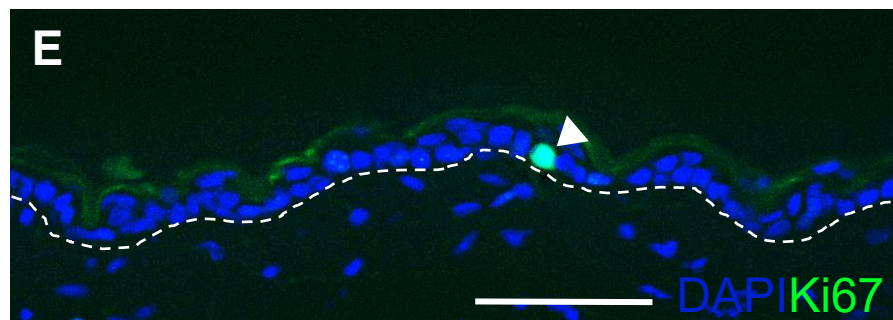


Figure 22. Loss of MiRNA-148a Alters Expression of Cytokeratin 1, But Not Ki67, In Vivo.

(A-F) Representative microphotographs of Immunofluorescent analysis of Krt1 (green), Ki67 (green) and DAPI (blue). **(A-B)** Krt1 expression was elevated in anti-miR-148a treated skin (Panel B, arrowhead) compared to controls epidermis (Panel A, asterisk). Broken line demarcates dermal-epidermal boarder. **(C)** Quantitative immunofluorescence analysis: Immunodetection of Krt1 in the epidermis of control versus anti-miR-148a treated skin samples normalised to DAPI+ cells. A significant increase in Krt1 fluorecence was observed in anti-miR-148a treated skin versus miRNA-controls. **(D-E)** No significant difference in Ki67 expression was observed in anti-miR-148a treated skin compared to controls epidermis (Panel D and Panel E, asterisk and arrowhead). Broken line demarcates dermal-epidermal boarder. **(F)** Quantitative immunofluorescence analysis: Immunodetection of Ki67 in the epidermis of control versus anti-miR-148a treated skin samples normalised to DAPI+ cells. No significant difference in Ki67 fluorecence was observed in anti-miR-148a treated skin versus miRNA-controls. $n = \text{three mice/treatment}$. ** $P < 0.01$ analysed by Student's t -test. Scale bars: $50 \mu\text{m}$.

We then analysed expression patterns of Rock1 and Elf5 in anti-miR-148a treated skins compared to control skins. In the epidermis, an increase in Rock1 expression was observed in the basal and suprabasal layer of the epidermis of anti-miR-148a treated skins (Figure. 23B, arrowheads) compared to control skins, where expression was restricted to the basal layer of the epidermis (Figure. 23A, asterisk). In the HF, an increase in Rock1 expression was observed in the bulge and hair bulb regions of the HF in anti-miR-148a treated skins (Figure. 23B, arrows) compared to control skins, where Rock1 expression was restricted to the hair bulb (Figure. 23A, arrow). In addition, Elf5 expression was increased throughout the basal and suprabasal layer of

the epidermis in anti-miR-148a treated skins (Figure. 23D, arrowheads) compared to control skins, where expression was significantly lower in the epidermis (Figure. 23C, asterisk). In the HF, Elf5 was expressed throughout the developing HF, with expression observed in the bulge and bulb regions, and ORS in anti-miR-148a treated skins (Figure. 23D, arrows) compared to control skins, where lower expression was observed in the bulge region and developing hair bulb (Figure. 23C, arrows). Quantitative immunofluorescence analysis of Rock1 (** $P < 0.01$ and *** $P < 0.001$) and Elf5 (* $P < 0.05$ and ** $P < 0.01$) showed a significant increase in fluorescence in the epidermis and HF of anti-miR148a treated skins *versus* miRNA-control skins respectively (Figure. 23E-F).

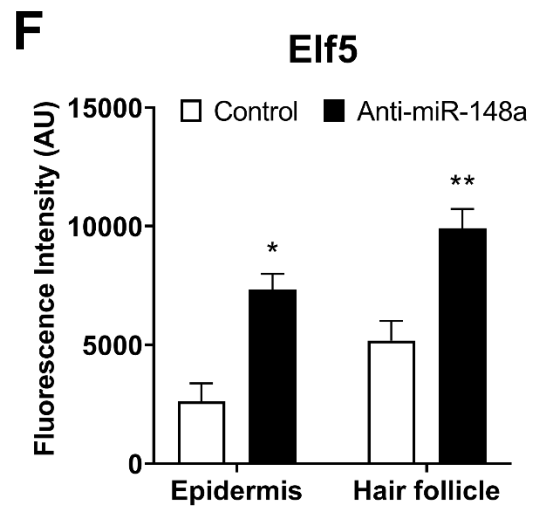
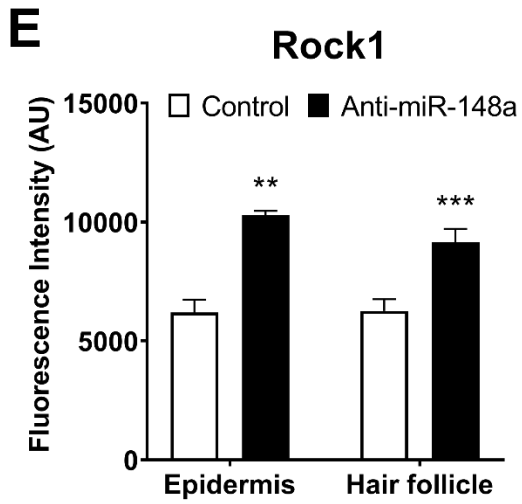
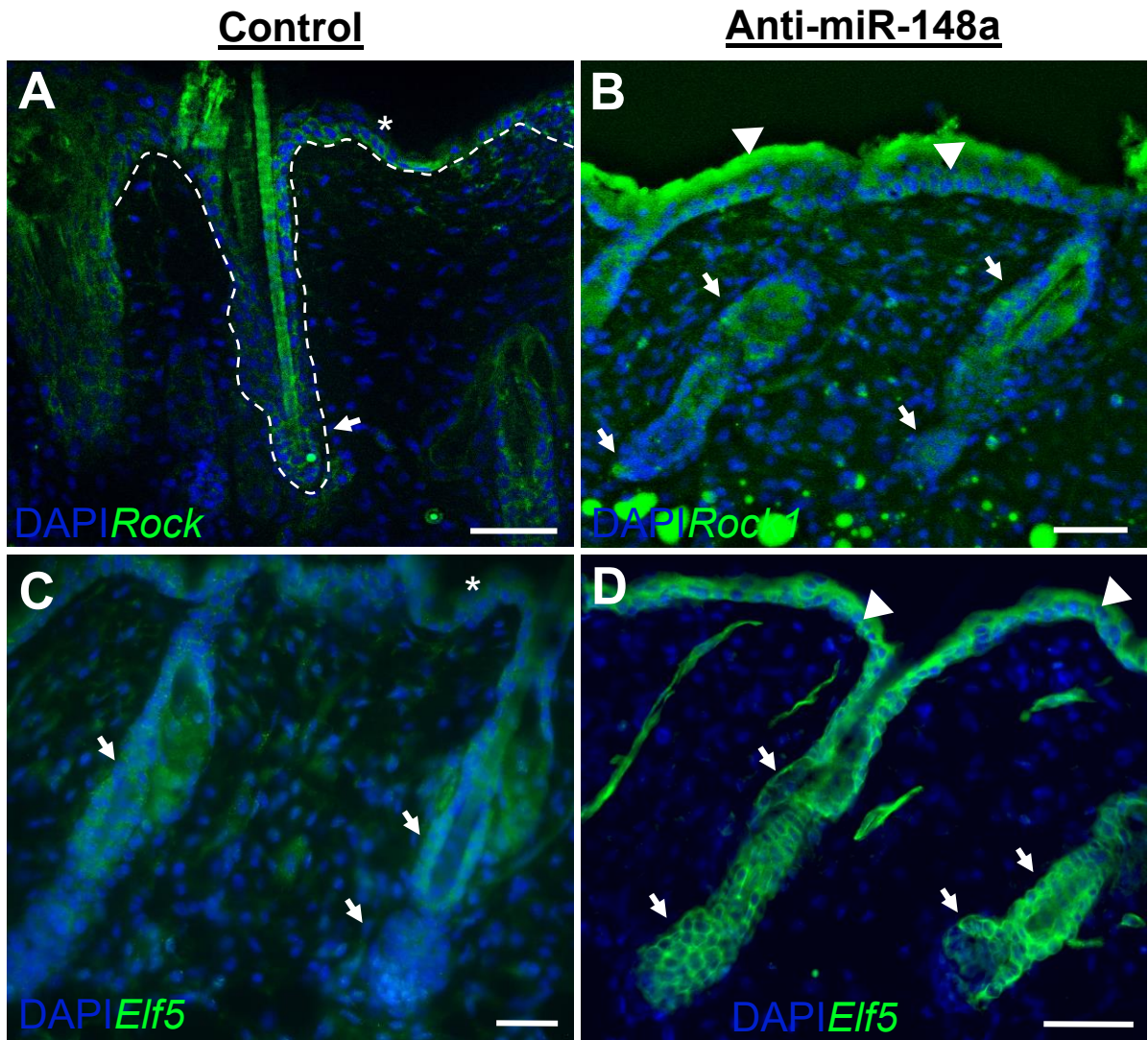


Figure 23. MiRNA-148a Inhibition Alters Rock1 and Elf5 Expression During Skin and Hair Follicle Development, In Vivo.

(A-D) Representative microphotographs of Immunofluorescent analysis of Rock1 (green), Elf5 (green) and DAPI (blue) in anti-miR-148a treated dorsal mouse skin compared to control skins **(A-B)** Immunohistochemical staining of Rock1 in the skin. An increase in Rock1 expression was observed in anti-miR-148a treated skin in the basal and suprabasal layers of the epidermis (Panel B, arrowheads) and in the bulge and developing hair bulb region of HFs (Panel B, arrows). While, lower Rock1 expression was restricted to the basal layer of the epidermis and developing hair bulb of control samples (Panel A, asterisk, and arrow respectively). **(C-D)** Immunohistochemical staining of Elf5 in the skin. Elf5 expression was elevated within the basal and suprabasal layers of the epidermis (Panel D, arrowheads) compared with control skins (Panel, C, asterisk). In the HF, an increase in Elf5 expression was observed throughout the HFs including the bulge and developing hair bulb regions, and ORS (panel D, arrows) compared to control skins where lower expression was detected in the developing hair bulb and bulge (panel C, arrows). **(E-F)** Quantitative immunofluorescence analysis: Immunodetection of Rock1 (Panel E) and Elf5 (Panel F) in the epidermis and HFs of control versus anti-miR-148a treated skin samples normalised to DAPI+ cells. A significant increase in both Rock1 and Elf5 fluorescence in the epidermis and HF was observed in anti-miR-148a treated skin versus miRNA-controls. $n =$ three mice/treatment. $*P < 0.05$, $**P < 0.01$, $***P < 0.001$ analysed by Student's t -test. Broken lines demarcate dermal-epidermal boarder. Scale bars: 50 μ m.

In summary, investigation of inhibition of miR-148a on differentiation processes, *in vivo*, revealed an increase in fluorescence of differentiation marker Krt1 in the epidermis of anti-miR-148a treated skins compared to controls (Figure. 22A-C). Investigation of inhibition of miR-148a *in vivo* on proliferation processes revealed no significant difference in fluorescence of proliferation marker Ki67 in the epidermis of

anti-miR-148a treated skins compared to control skins (Figure. 22D-F). Investigation of inhibition of miR-148a *in vivo* on Rock1 and Elf5 revealed an increase in fluorescence of Rock1 and Elf5 throughout the epidermis in anti-miR-148a treated skins compared to the basal layers in control treated skins. In the HF, an increase in fluorescence of Rock1 and Elf5 was observed in the bulge and hair bulb regions compared to control skins (Figure. 23). These results show that the effect of miR-148a modulation of differentiation and Rock1 and Elf5 expression, *in vitro* (Figure. 17-19) is sustained *in vivo*. These data indicate that miR-148a modulation of Rock1 and Elf5 may regulate skin homeostasis through modulation of differentiation processes, however, no effect was observed in proliferation after inhibition of miR-148a *in vivo*.

4.0

Discussion

4.1 MiRNA-148a is Expressed in Stem Cell Regions of Telogen Skin and Hair Follicles

MicroRNAs have been shown to play fundamental roles in modulating gene expression profiles throughout skin development and HF cycling (Mardaryev et al., 2010, Ahmed et al., 2011, Ahmed et al., 2014). Microarray analysis of miRNAs during hair cycling revealed high expression of miR-148a during telogen stage of HF cycling (Figure. 11A). Through RT-qPCR and ISH analysis, we show for the first time, miR-148a expression in the differentiated, suprabasal layer of the epidermis, as well as in the bulge and SHG stem/progenitor cell compartments of telogen HFs during cycling (Figure. 11B-D). MiR-148a expression was also shown to be enriched in CD34⁺ HF-SCs and co-expressed with SC markers Krt15 and CD34 in telogen HFs (Figure. 12).

The expression of miR-148a in differentiated suprabasal layers of the epidermis, suggests that miR-148a may function to promote differentiation in the epidermis. MiR-148a has been shown to modulate differentiation processes in other cells and tissues, suggesting that this could be a common mechanistic role of miR-148a. For example, miR-148a promotes differentiation of macrophages upon activation of Notch signalling (Huang et al., 2017). Also, during adipogenesis, differentiation of human adipose-derived mesenchymal stem cells (hMSCs-Ad) is partially regulated by miR-148a. In addition, miR-148a was shown to target Wnt1 – an inhibitor of adipogenesis, whilst inhibition of miR-148a accelerated differentiation (Shi et al., 2015). Furthermore, miR-

148a was also found to be upregulated in obese humans and mice on a high-fat diet, suggesting that miR-148a has an instrumental effect in modulating cellular processes during adipogenesis and maintaining homeostasis under changing conditions (Shi et al., 2015). These studies show that miR-148a plays an important role in cellular differentiation and suggests that miR-148a may have a similar function in the epidermis during skin development.

Of note, individual miRNAs have been shown to play a crucial role in modulating differentiation processes in skin. Examples include, miR-203 which promotes epidermal differentiation and directly targets *p63*, which is highly expressed in the basal layer of the epidermis and an important modulator for epidermal stratification during skin development (Koster et al., 2004, Lechler and Fuchs, 2005, Romano et al., 2007). Premature expression of miR-203 in basal cells resulted in a thinner epidermis and prevention of full stratification, along-side restriction of proliferation and cell cycle exit (Yi et al., 2008). MiR-203 expression has also been observed in the differentiated suprabasal layer of the epidermis during human skin morphogenesis and co-expressed with differentiation markers Involucrin and Filaggrin (Wei et al., 2010). These studies show that miR-203 functions as a promotor of differentiation in the epidermis and acts as a molecular switch between proliferating basal cells and terminally differentiating epidermal keratinocytes.

In addition, regulation of epidermal differentiation is also controlled by miR-184. MiR-184 was shown to promote epidermal differentiation and inhibit proliferation in human epidermal cells, in part through targeting *Krt15*, and inducing Notch signalling. Knockout of miR-184 resulted in skin thickening, accumulation of spinous cells and an increase in Ki67⁺ proliferating epidermal cells, indicating a role in commitment switch from proliferating basal cells to differentiating suprabasal epidermal cells.

Furthermore, inhibition of miR-184 increased the clonogenicity of epidermal stem/progenitor cells, indicating a functional role of modulating differentiation and cell commitment during skin development (Nagosa et al., 2017). We postulate that miR-148a may have a similar role as miR-184 in modulating proliferation/differentiation processes during epidermal development and of miR-203 in promoting epidermal differentiation, which requires further investigation.

Our data demonstrates that miR-148a is expressed in stem/progenitor regions of the bulge and SHG in telogen HFs (Figures. 11D and 12). Its role could be postulated from evaluation of another miRNA, miR-125b, which has been shown to modulate SC activities and fine tune SC activation/quiescence during HF cycling. MiR-125b is expressed in early bulge cells and targets *VDR*, a promotor of anagen stage of HF cycling. Furthermore, gain and loss of function studies revealed miR-125b to repress SC differentiation, whilst depilation of HFs in miR-125b overexpression mouse model failed to re-grow HFs (Zhang et al., 2011). In addition, similarly to miR-148a, miR-29a/b1 was shown to be highly expressed during telogen stage of HF cycling, and overexpression of miR-29a/b1 during telogen or anagen resulted in shortened HFs and eventual hair loss (Ge et al., 2019). We believe that miR-148a may have a similar effect as miR-125b and miR-29a/b1 in HFs, in regulating SC quiescence/activation based on their spatiotemporal expression pattern in healthy skin and HFs. Furthermore, we speculate that elevated levels (induced overexpression) of miR-148a may also lead to failure of HF development, which requires further investigation.

Taken together, our data suggests a dual role for miR-148a during skin and HF development due to its specific spatiotemporal expression patterns. We postulate that miR-148a in the epidermis acts as a molecular switch between proliferative basal cells

into a terminal differentiation program. In the HF, miR-148a may act as a repressor of SC activation, limiting HF-SC activation, proliferation, and differentiation.

4.2 Rock1 and Elf5 Are Direct Targets of MiRNA-148a

MicroRNAs function as post-transcriptional regulators by binding to the 3'-UTR of target genes, preventing their translation into proteins (Yi and Fuchs, 2010). To identify gene targets of miR-148a, and elucidate its potential regulatory pathway in skin, we performed overexpression of miR-148a in PMEKs and further downstream analyses. Through analysis of RNA-seq data of miR-148a overexpression in PMEKs and overlapping of potential gene targets of miR-148a from online databases, we identified 43 potential gene targets of miR-148a (Figure. 13). Of these 43 genes, subsequent validation by RT-qPCR of the top, highly conserved genes between human and mice and with a known role in epithelial tissue, revealed only Rock1 and Elf5 as significantly changed in expression following modulation of miR-148a in PMEKs. This was validated at protein level by Western blot (Figure. 14). Through dual luciferase reporter assay, our study identified targets Rock1 and Elf5 as genuine miR-148a targets (Figure 15), which helps to elucidate the potential role of miR-148a during skin development and HF cycling. In addition, fluorescent *in situ* hybridisation with simultaneous immunostaining revealed miR-148a, Rock1 and Elf5 are co-expression in the bulge and SHG of telogen HFs, whilst expression was mutually exclusive in the epidermis (Figure. 15).

This inverse expression pattern observed in the epidermis between miR-148a, and its gene targets is common in many tissue types due to miRNA degradation of their target mRNAs (Stark et al., 2005, Bartel, 2009). However, co-expression of miR-148a and

its targets was also observed (Figure. 15). Of note, miRNAs and their targets tend to be mutually exclusive in neighbouring cells and tissues (Wang et al., 2019a) as we observe with miR-148a in the epidermis (basal *versus* suprabasal). However, miRNAs and their target mRNA co-expression have also been observed in a cell and tissue dependent manner (Liu and Kohane, 2009). These demonstrate that miRNAs can form diverse networks of gene regulation and can act as 'buffers' of gene expression by fine tuning different cellular processes upon developmental cues (Farh et al., 2005, Ebert and Sharp, 2012).

The mainly mutually exclusive expression of Rock1 and Elf5 to miR-148a in the epidermis indicates that Rock1 and Elf5 may have a functional role required for basal cell proliferation, whereas miR-148a inhibition of Rock1 and Elf5 in the suprabasal epidermal layers, functions to restrict proliferation and promote terminal differentiation. MiR-148a functions to buffer the activity of Rock1 and Elf5 suggesting a dual functionality of miR-148a is dependent on its spatiotemporal expression and its target genes in the skin and HFs. Of interest, Rock1 is a downstream effector of GTPase Rho. Rock1 regulates downstream genes that are involved in a variety of cellular processes. Lim kinases (Limk1 and Limk2) are Rock1 substrates. Limk2 has been shown to be expressed in the basal layer of the epidermis, functioning to maintain adhesion to the basement membrane and prevent terminal differentiation. Limk1 has been shown to be expressed in the upper spinous and granular layers of the epidermis, inhibiting cofilin and promoting epidermal differentiation and compaction of differentiated layers (Honma et al., 2006). In addition, Rock signalling component Rac1 co-localises with Limk2 in the basal layer of the epidermis, suggesting that Rock signalling is required to prevent terminal differentiation and maintain proliferation in this region. Rock signalling has also been shown to phosphorylate Limk1, which in

turn inhibits cofilin-mediated actin depolymerisation, maintaining healthy and homeostatic epidermal stratification program (Honma et al., 2006). MiR-148a regulation of Rock1 may serve as a switch between proliferating basal cells into terminally differentiating suprabasal cells, however, more research is required to confirm this mechanism.

Studies with inducible *Rock1* knockout mouse embryonic fibroblasts have shown that inhibition of Rock1 improved actin cytoskeletal stability and reduced cell detachment through decreased MLC2 phosphorylation and maintained cofilin phosphorylation (inhibition) (Shi et al., 2013). Through a similar mechanism, Rock1 may function to promote detachment and migration in skin and HFs. Promotion of bulge and SHG cell detachment/adhesion and migration is an integral part of initiation of anagen stage of HF cycling and these processes are inhibited during telogen stage of HF cycling (Blanpain and Fuchs, 2009).

Rock1 has not been previously categorised in epidermal or HF-SCs, however, Rock1 has been shown to promote embryonic SC colony formation, and maintenance of an undifferentiated state (Chang et al., 2010). Additionally, Rock1 signalling is thought to elevate stem/progenitor cell functions by its prevention of apoptosis of human embryonic SCs, and inhibition of Rock signalling by administration of Y-27632 Rock inhibitor led to enhanced survival of intestinal crypt SCs and neuronal precursor cells (Watanabe et al., 2007, Koyanagi et al., 2008, Sato et al., 2009, Centonze et al., 2022). Rock inhibitor Y-27632 has also been shown to maintain HF-SC stemness and self-renewal (An et al., 2018). However, inhibition of Rock signalling was shown to promote differentiation and proliferation of bone marrow SCs into keratinocyte-like cells, suggesting that Rock signalling provides a mechanism for SC differentiation and lineage commitment (Li et al., 2015). Therefore, miR-148a regulation of Rock1 may

serve as a regulator of SC quiescence/activation in HF cycling. Of note, miR-148a is known to regulate Rock1 in gastric cancer cell lines and tissue, with inhibition of Rock1 resulted in a decrease in cell migration and invasion (Zheng et al., 2011). Together, these studies suggest how miR-148a may contribute to prevention of stem/progenitor cell activation (detachment/migration) in HFs, through inhibition of Rock1 in these stem/progenitor cell regions.

In the epidermis, miR-148a regulation of Rock1 may function to promote differentiation processes as keratinocytes transition from basal to suprabasal. Whereas, in the HF, negative regulation of Rock1 by miR-148a may function to maintain quiescence and self-renewal capacity of HF-SCs and their progeny. These studies show several functional roles of Rock1, and in turn suggest how miR-148a regulation of Rock1 is important for normal and healthy skin and HFs development and homeostasis, which is dependent on their spatiotemporal expression patterns.

Similarly, Elf5 is expressed in the bulge and SHG stem/progenitor regions of telogen HFs (Figure. 15), and in the IRS and ORS of HFs (Choi et al., 2008, Singh et al., 2019). The function of Elf5 in skin and HFs is currently unknown, however, Elf5 has been shown to be a key regulator of stem/progenitor cells in other epithelial tissues, such as the mammary gland (Chakrabarti et al., 2012b, Choi et al., 2009). Elf5 functions in mammary gland include regulating stem/progenitor cell fates, with *Elf5*-null mice resulting in accumulation of basal/luminal (Krt8⁺/Krt14⁺) cells with dual identity and also to promote differentiation during alveologenesis (Oakes et al., 2008, Chakrabarti et al., 2012b). In the kidney, Elf5 functions to promote principal cell lineage commitment by activation of promoters for principal cell genes, *Aqp2* and *Avpr2*. While Notch signalling has been shown to promote principal cell lineage commitment through Elf5, highlighting that Elf5 has a crucial role in network of lineage commitment

promoting genes and transcription factors in the kidney (Grassmeyer et al., 2017). These studies reveal that Elf5 functions as a key regulator of stem/progenitor cell commitment for specific lineages during specific developmental cues in other epithelial tissue development, which may be sustained in skin and HF development.

We postulate that due to the dynamic expression patterns of miR-148a and Elf5 within stem/progenitor populations of the skin and HF (Figure. 15, bulge, SHG and basal layer of the epidermis), suggest that miR-148a *via* tight regulation of Elf5 is a key determining factor of SC fate and lineage commitment in the bulge and SHG region, as well as maintaining healthy, homeostatic differentiation processes in the epidermis.

4.3 MiRNA-148a Alters Proliferation and Differentiation Programs in Primary Mouse Epidermal Keratinocytes, *In Vitro*

MiRNAs, through their gene targets, fine tune cellular processes in response to developmental signals. Here, we reveal that, miR-148a inhibits proliferation of PMEKs and cells accumulate in the S phase of cell cycling after miR-148a overexpression, *in vitro* (Figure. 16). MiR-148a also affects differentiation processes in skin with modulation of miR-148a in calcium induced differentiation assay revealed that miR-148a inhibits differentiation of PMEKs, *in vitro* (Figure. 17). Subsequent investigation as to whether overexpression of miR-148a could prevent the nuclear translocation of Rock1 and Elf5 during in calcium induced differentiation of PMEKs revealed that Rock1 and Elf5 were indeed prevented from translocating to the nucleus, indicating that modulation of differentiation processes in PMEKs by miR-148a occurs through its regulation of Rock1 and Elf5 (Figure. 18).

To our knowledge, our study is the first to demonstrate miR-148a effects on cell proliferation in PMEKs, revealing an accumulation of PMEKs in S-G2/M transition phase of cell cycle after overexpression of miR-148a in PMEKs (Figure. 16C), a potential keratinocyte mitotic checkpoint *via* miR-148a. In addition, our data showed an up-and/or downregulation of *Cdk1* and *Cks1 β* after modulation of miR-148a expression in PMEKs (Figures. 17A-B). Inhibition of *Cdk1* and *Cks1 β* have been shown to arrest cell cycle at S-G2 transition in somatic cells during embryogenesis (Martinsson-Ahlzén et al., 2008). While, *Cks1 β* has also been shown to also promote cell growth and metastasis in cancers (Shi et al., 2020). Furthermore, we observe expression changes of *Ccne1*, *Cdk16*, *Ccnb2* and *Ccnd1/2* after modulation of miR-148a expression in PMEKs (Figure. 16A-B). Inhibition of *Cdk16* has been shown to reduce proliferation of squamous cell carcinoma cell lines by G2/M arrest, and inhibition of *Ccnb2* has been shown to reduce mouse embryonic fibroblasts in M phase and inhibit cellular proliferation (Yanagi et al., 2017, Wu et al., 2010b). Interestingly, overexpression of *Ccnd1* in differentiated epidermal cells induces re-programming into SC-like cells with high colony forming ability (Zhao et al., 2016). MiR-148a regulation of *Ccnd1* in particular, may play a role in restricting proliferation of terminally differentiating keratinocytes during skin development and epidermal stratification. Furthermore, miR-148a regulation of *Ccnd1* may help to maintain SC quiescence in the HFs, whilst promoting SC maintenance and self-renewal. While our study did not investigate *Ccnd1* specifically, these studies indicate a potential mechanism of miR-148a regulation of proliferation and SC maintenance *via* *Ccnd1* which needs to be explored further in skin.

Of note, miR-148a has been implicated in previous studies to modulate proliferation in various cancer tissues and cell lines suggesting a common role of miR-148a as an

anti-proliferative regulator. MiR-148a has been shown to reduce proliferation in cervical cancer by targeting DNA methyl transferase 1 (*DNMT1*) (Chen et al., 2021). Proliferation is also inhibited in cutaneous squamous cell carcinoma by miR-148a modulation of MAPK pathway (Luo et al., 2015). In esophageal squamous cell carcinoma (ESCC), miR-148a is downregulated alongside a reduction of protein levels of KLF4, SOX2, OCT4 and NANOG, whose genes are known to promote 'stemness' (Qi and Pei, 2007, Wei et al., 2009, Tan et al., 2020). In addition, miR-148a was shown to inhibit proliferation, migration and invasion in human ESCC cell lines by targeting activin receptor type-1 (*ACVR1*) (Tan et al., 2020). In oral squamous cell carcinoma (OSCC), miR-148a was downregulated. Overexpression of miR-148a in SCC-9 cells inhibited migration, invasion, and proliferation, whereas inhibition of miR-148a, enhanced these through regulation of human leukocyte antigen-G (*HLA-G*) (Zhang et al., 2019). Lastly, in gastric cancer, miR-148a was shown to inhibit proliferation and metastasis by targeting *SMAD2* (Wang et al., 2013b). These studies highlight that miR-148a acts as a tumour suppressor and our data suggests that miR-148a may be crucial in regulating proliferation in normal healthy tissue cells and preventing initiation and development of tumorigenesis.

Also, as miR-148a is a well-established proliferative regulator, we attempted to determine if miR-148a modulation of cell proliferation may also occur through regulation of Rock1 and Eif5 (Figure. 16). After modulation of miR-148a, *in vitro*, we observed changes in proliferative processes (Figure. 16), however, we did not observe any changes in proliferation after inhibition of miR-148a, *in vivo* (Figure. 22D-F). Rock signalling has been shown to regulate cell proliferation in lung tumour and melanoma mouse models, with deletion of *Rock1/2* in mice resulted in cell cycle arrest and downregulation of Cdk1 and Cks1 expression (Kümper et al., 2016). While, miR-148a

has also been shown to target *Cdk1* directly in cervical cancer cells (Wang et al., 2020). These indicate that through regulation of Rock1, miR-148a functions as a tumour suppressor, modulating cell proliferation through a potential novel miR-148a-Rock1/Cdk1 mechanism. Evidence of this mechanism has largely been discovered in cancer models; further investigation would be required to establish this as a potential anti-tumorigenic mechanism *via* miR-148a during skin development.

Of note, Elf5 has been shown to modulate proliferation programs in various other tissues and pathologies. In human breast cancer cells, Elf5 was found to interact with acetyltransferase p300, where acetylation of Elf5 led to its degradation. Inhibition of cell proliferation was observed in breast cancer cells after Elf5 acetylation, by inhibition of CCND1 (Li et al., 2021). MiRNA regulation of genes by acetylation has previously been observed, for example, miR-455 promotes chondrogenesis by enhancing acetylation of histone 3 by targeting histone deacetylases (Chen et al., 2016). Through this mechanism, cell proliferation programs in skin and HFs may be regulated by a potential indirect miR-148a acetylation of Elf5, although further research is required to confirm this.

In addition to proliferation, our data revealed that modulation of miR-148a activities affects differentiation of PMEKs (Figures. 18 and 22A-C). This is consistent with previous data demonstrating that miR-148a promotes differentiation and suppresses apoptosis in skeletal muscle cells (Yin et al., 2020). In another study, miR-148a has been shown to mediate Notch signalling to promote the differentiation of monocytes (Huang et al., 2017). Our data shows mutually exclusive expression of miR-148a and Rock1 in the epidermis (suprabasal *versus* basal) (Figure. 15B Panel (i)). Of note, inhibition of Rock1 has been shown to inhibit human keratinocyte terminal differentiation (McMullan et al., 2003) which is also consistent with our data in PMEKs

(Figure. 17). MiR-148a has been shown to target Rock1 in myoblasts and inhibition of Rock1 resulted in an increase in differentiation (Zhang et al., 2012). During epidermal stratification, proliferation of basal progenitors is suppressed, whilst terminal differentiation is activated (Fuchs, 2007). MiR-148a may contribute to commitment to terminal differentiation by functioning to suppress proliferation of keratinocytes, thereby promoting terminal differentiation program, in part by regulating Rock1.

Furthermore, Elf5 has been previously categorised in regulating differentiation processes during mammary gland development (Oakes et al., 2008, Chakrabarti et al., 2012b), and in other tissues. In trophoblast cells, overexpression of Elf5 resulted in an increase in differentiation through co-occupancy of Tfp2c at differentiation associated gene promoters. Moreover, a certain threshold of Elf5 expression was found to be required for maintenance of trophoblast cells and proliferative processes, with a critical expression threshold promoting cells to differentiate (Latos et al., 2015). In turn, Tfp2 has also been shown to promote differentiation of trophoblast cells by inhibiting OCT4 (Krendl et al., 2017). In embryonic SCs, overexpression of Elf5 can promote differentiation into blood cells, while Elf5 in combination with other transcription factors can lead to differentiation into other cell types (Yamamizu et al., 2013). We postulate that miR-148a tight regulation of Elf5 may function to regulate differentiation and maintain normal processes during skin and HF development and homeostasis.

4.4 Inhibition of MiRNA-148a Accelerates Telogen-Anagen Transition, and Modifies Stem Cell Activity, *In Vitro* and *In Vivo*

The effect of miR-148a on SCs *in vitro*, was performed by colony forming assay. Inhibition of miR-148a in isolated bulge SCs revealed an increase in colony size and number of bulge SCs compared to controls, *in vitro* (Figure. 19). The possible phenotypic effects of miR-148a on stem/progenitor cell populations in skin and HFs were investigated by pharmacological inhibition of miR-148a. Our data revealed an acceleration of telogen to anagen transition in anti-miR-148a treated skins compared to controls. An increase in anagen stage III HFs in anti-miR-148a treated skins were observed compared to predominantly anagen stage II in control treated skins, whilst a thickening of the skin was also observed in anti-miR-148a treated skins compared to controls (Figure. 20). Immunofluorescent analysis revealed a significant increase in activity of stem/progenitor marker Krt15 in anti-miR-148a treated skins compared to controls (Figure. 21).

The accelerated telogen-anagen transition we observe after inhibition of miR-148a (Figure. 20) suggests that miR-148a may function to prevent SC activation, proliferation, migration, and differentiation, required for anagen stage initiation of HF cycling. Our data shows that stem/progenitor marker Krt15 is upregulated in stem/progenitor regions of the bulge, SHG and in the epidermis after inhibition of miR-148a, *in vivo* (Figure. 21), indicating an abnormal activation of stem/progenitor cells within the epidermis and HFs, potentially responsible for the acceleration of telogen-anagen transition by reduction of modulation by miR-148a.

The hair cycle is a tightly regulated process of gene activation and silencing. The telogen stage of HF cycling is a period of rest and SC quiescence, in which we observe miR-148a expression in the SC bulge region (Figures. 11D (i) and 12A-B and 15B). We subsequently isolated bulge SCs and performed a colony forming assay, which showed that miR-148a inhibition in isolated bulge SCs, leads to an increase in colony size and number, *in vitro* (Figure. 19).

This data indicates that miR-148a may play a role in maintaining SC quiescence and repression of proliferative/differentiation processes during telogen stage of HF cycling. We speculate that this may potentially occur through miR-148a regulation of *Ccnd1*, which has been shown to re-program differentiated epidermal cells into SC-like cells with high colony forming capacity (Zhao et al., 2016). However, additional experiments will be required to confirm this.

The role of miR-148a in modulating SC activation has been observed in other cells. MiR-148a promotes differentiation of embryonic SCs into mesenchymal SCs (Giraud-Triboult et al., 2011). In mesenchymal stromal cells, a multipotent SC progenitor, miR-148a was found to be downregulated during osteogenic differentiation (Manochantr et al., 2017). Together, these indicate that miR-148a may play a role in stem/progenitor maintenance/activation and may have a similar role in maintenance of SC populations in HF-SC regions in the skin and HFs.

The potential role of miR-148a in stem/progenitor cell populations in HFs can be evaluated by other miRNAs, which have been shown to play an important functional role in telogen stage of HF cycling. In goat HFs, thirty-five miRNAs were found to be upregulated in telogen stage compared to anagen stage, with miR-148a, miR-335, and miR-34b being some of the most highly upregulated (Liu et al., 2018). Inhibition

of miR-335 was shown to promote differentiation, and overexpression inhibited proliferation and migration in human mesenchymal SCs (Tomé et al., 2011). Secondly, miR-34b has been shown to suppress cell cycle progression in myoblasts (Wang et al., 2019b). Whilst in the skin, the miR-34 family was shown to be regulated by p63 to maintain proliferation in basal cells of the epidermis. The miR-34 family are expressed in the suprabasal layers of the epidermis and contribute to commitment of terminal differentiation from proliferative basal cells (Antonini et al., 2010). These suggest that miR-148a regulation of stem/progenitor populations in the skin and HF may be part of a wider gene regulatory network to fine tune the control of healthy, homeostatic skin development and HF cycling, through modulating various gene targets, however further research is required to elucidate the wider network.

4.5 Inhibition of MiRNA-148a Leads to Increased Activity of Rock1 and Elf5, *In Vivo*.

After we determined the effects of modulation of miR-148a on Rock1, Elf5 and proliferation and differentiation processes in PMEKs, *in vitro* (Figures. 17-18), we examined whether these effects were sustained *in vivo*. After pharmacological inhibition of miR-148a in mouse skin, immunofluorescent analysis revealed an increase in fluorescence of differentiation marker Krt1 in the epidermis compared to control treated skins. However, no increase in fluorescence was observed for proliferation marker Ki67 between anti-miR-148a and control treated skins (Figure. 22). Moreover, immunofluorescent analysis of Rock1 and Elf5 revealed an increase in fluorescence in the epidermis, hair bulb, bulge region and ORS in anti-miR-148a treated skins compared to control treated skins (Figure. 23).

The functional importance of Elf5 has not been characterised in the skin or HFs. However, Elf5 has been shown to be a master regulator of stem/progenitor populations and cellular processes in the control of a closely related tissue of the skin, the mammary gland (Zhou et al., 2005, Choi et al., 2009, Chakrabarti et al., 2012b). Knockout studies of Elf5 in mammary gland resulted in loss of Stat5 through direct targeting, resulting in inhibition of alveogenesis (Choi et al., 2009). Stat5 is a component of the Jak/Stat signalling pathway which has been shown to have regulatory roles in cell proliferation, differentiation and migration in a variety of cells and tissues (Williams, 2000, Andl et al., 2004a, Amoyel and Bach, 2012, Jang and Baik, 2013). Of note, in the skin, Stat5 expression originating in the DP has been shown to induce anagen, with knockout models in mice resulting in delayed anagen re-entry (Legrand et al., 2016). In other studies, topological pharmacological inhibition of JAK/STAT pathway in mice and human dermal papilla cells (including patients with alopecia) resulted in anagen onset and subsequent hair growth (Harel et al., 2015, Kim et al., 2020). Of interest, miR-148a is predicted to target various protein tyrosine phosphatase (PTP) receptors in online databases TargetScan (<http://www.targetscan.org>), miRanda (<http://microrna.sanger.ac.uk>) and miRDB (<http://mirdb.org/>). PTPs function to regulate the Jak/Stat pathway, and have been shown to play functional roles in disease pathogenesis (Böhmer and Friedrich, 2014). For example, in glioblastoma multiforme, PTP-receptor delta (PTPRD) was found to be frequently inactivated. Furthermore, PTPRD was found to dephosphorylate Stat3 and result in decrease in cell proliferation (Rahaman et al., 2002, Veeriah et al., 2009). In addition, PTPRA has been shown to be upregulated in some breast cancers and result in decrease in tumour growth (Ardini et al., 2000). These show that PTPRs function in a network in modulation of tumorigenesis and cell proliferation and may

have a similar functional role in skin. We speculate that miR-148a modulation of Jak/Stat pathway through Elf5 or PTP mechanism in stem/progenitor populations could maintain SC quiescence during telogen stage of HF cycling, while aberrant expression of Elf5-Jak/stat pathway after inhibition of miR-148a may be responsible for the accelerated telogen-anagen transition we observe (Figure. 20). However, additional studies will need to be carried out to determine this potential mechanism.

Interestingly, Rock1 is also implicated in the Jak/Stat pathway. Rock1 was shown to activate Jak2 in hypothalamic leptin signalling (Huang et al., 2012). Whilst, in carcinoma-associated fibroblasts, Rock signalling has been shown to activate Stat3, regulating actomyosin contractility in tumour cells (Sanz-Moreno et al., 2011). The Jak/Stat3 pathway has been shown to be essential in skin tumour development with inhibition of Stat3 resulting in decreased proliferation and reduction of targets Ccnd1 and c-Myc (Pedranzini et al., 2004). Myc has been shown to be essential in epidermal differentiation processes and expressed in the basal layer of the epidermis and in proliferative areas of the HF, with activation in SC regions leading to SC depletion (Waikel et al., 2001, Watt et al., 2008). In addition, miR-148a was also shown to regulate Stat3 and subsequent proliferation and invasion of non-small cell lung carcinomas and also in papillary thyroid cancer cells (He and Xue, 2017, Xu et al., 2017). MiR-148a regulation of Rock1 and in turn potentially regulating Jak/Stat3 pathway (directly/indirectly), may provide a mechanism for regulation of a switch from proliferative basal to terminally differentiating suprabasal keratinocytes, along-side regulation of SC quiescence through reduction of the Rock1-Jak/Stat3 pathway. Further experimentation through transcriptomic and proteomic analysis of Jak/Stat signalling components after inhibition/overexpression of Rock1/Elf5, would indicate a link between miR-148a-Rock1/Elf5 and Jak/Stat signalling in the skin. *In vitro* and *in*

vivo inhibition and functional analysis of Jak/Stat pathway would give an insight whether Jak/Stat signalling is a key player in the control of HF homeostasis through modulation of Rock1/Elf5. We have identified miR-148a modulation of Rock1 and Elf5 provides a key regulatory pathway in the homeostatic control of skin. Further work to elucidate the wider regulatory pathway could provide biomarkers and therapeutic targets in the treatment and/or research of dermatological conditions such as dermatitis, skin cancers or wound healing.

5.0

Conclusion

In this project, a novel role of miR-148a in skin development and HF cycling has been determined with far reaching implications for dermatological and SC research. The following conclusions can be made based on this study:

1. miR-148a exhibits distinct expression pattern in the skin with highest expression observed during telogen stage of HF cycling. In the epidermis of telogen skin, miR-148a is expressed in the differentiated suprabasal layers, in the HF during telogen stage of HF cycling, miR-148a is expressed in the stem/progenitor cell populations of the bulge and SHG.
2. RNA sequencing analysis, target prediction tools and validation by RT-qPCR, Western blot and Luciferase reporter assay, *Rock1* and *Elf5* were confirmed as genuine direct targets of miR-148a in keratinocytes.
3. MiR-148a inhibits proliferation and differentiation processes in PMEKs, in part, through tight regulation of *Rock1* and *Elf5*, *in vitro*.
4. Pharmacological inhibition of miR-148a resulted in acceleration of telogen-anagen transition and an increase in activity of stem/progenitor cell populations in skin and HFs, *in vivo*.
5. Inhibition of miR-148a increased colony forming capacity of isolated HF-SCs after inhibition of miR-148a expression, *in vitro*.
6. Pharmacological inhibition of miR-148a modulates cellular differentiation and leads to elevated expression of *Rock1* and *Elf5* expression in skin and HFs, *in vivo*.

Taken together, we propose a dual role of miR-148a in skin. In the epidermis, miR-148a functions to reduce the proliferative potential of basal stem/progenitor cell populations and commitment to terminal differentiation. In the HF, miR-148a functions to maintain quiescence in stem/progenitor cell populations. We believe these roles of miR-148a in skin and HFs is due, in part, to tight regulation of Rock1 and Elf5 (Figure. 15). Of note, Rock1 and Elf5 have not been functionally analysed in the skin and HF and their targets are currently unknown. Identification of their targets may provide an insight to a potential indirect regulatory mechanism of miR-148a for normal skin and HF development, cycling and homeostasis, which requires further investigation. Our proposed mechanism can be observed in Figure 24. This study identifies a previously unidentified miRNA in the control of homeostasis within the skin. We believe we have identified potential new therapeutic/diagnostic markers in skin and a route for further research in the control of epidermal SCs and treatment of various skin disorders.

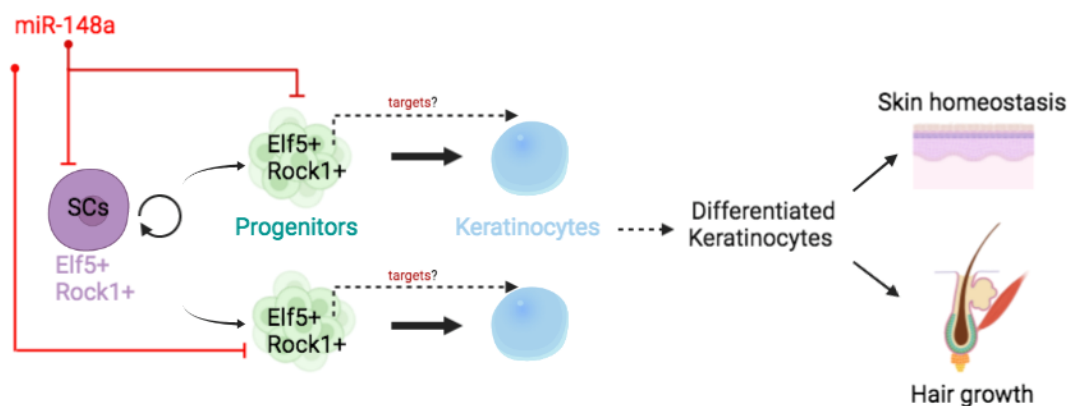


Figure 24. Working Model: The Mechanism of Action of MiR-148a in Modulating Stem/Progenitor Cells during Skin development and Hair Follicle Cycling

A working model of the potential mechanisms of miR-148a on stem/progenitor cell populations. MiR-148a modulation of stem/progenitor differentiation and proliferation programs helps to maintain SC quiescence and epidermal development, through regulation of Rock1 and Elf5 required for normal skin development and HF cycling.

6.0

Future directions

To continue this research, we would aim to categorise the role of Rock1 and Elf5 in skin development and HF cycling. Along-side this, understanding the role of miR-148a in controlling wound healing would provide further understanding of the modulation of stem/progenitor cell populations by miR-148a. We would perform the following experiments:

- Transgenic knockout of miR-148a with subsequent pharmacological inhibition of Rock1/Elf5 to confirm whether the phenotype observed in our study can be rescued from inhibition of miR-148a alone. This would provide clearer mechanistic evidence of miR-148a functions in skin *via* regulation of Rock1 and Elf5.
- Transgenic knockout of *Rock1/Elf5* to determine the regulatory processes governed by Rock1 and Elf5.
 - Histological, immunofluorescent and pathway analysis during skin development, hair cycling and wound healing.
- ChIP sequencing to identify binding site associated with Elf5 and elucidate pathways that are regulated by Elf5 as this would allow the identification of indirect targets of miR-148a *via* Elf5 (Figure. 24).
- Lineage tracing of Rock1 and Elf5 to elucidate their functional role throughout skin and HF development, homeostasis and cycling, and identify progenitor cell populations.

- To investigate whether the Jak/Stat pathway is involved with miR-148a-Elf5/Rock1 mediated regulation in skin involving:
 - RNA-sequencing after overexpression/inhibition of Rock1 and Elf5 in PMEKs.
 - RT-qPCR analysis of Jak/Stat pathway components following modulation of activities of miR-148a, Elf5 and Rock1 in PMEKs.
 - Jak/Stat inhibition/overexpression in PMEKs to determine any effect of differentiation and proliferation assays, *in vitro*.

7.0

Appendix

Appendix 1. MicroRNA Microarray.

- 1.1 MicroRNA microarray examines all microRNAs and their expression levels in a biological sample. This is completed as anti-miRNA probes are conjugated to the wells of a microarray plate and are fluorescently conjugated. With addition of total RNA, miRNAs hybridize to the anti-miRNAs and fluoresce, which is measured and given as a relative expression level microarray profile (Thomson et al., 2007).

Appendix 2. Cell Culture and Transfection.

- 2.1 Primary epidermal mouse keratinocytes (PMEKs) were isolated as outlined by Lichti and authors (Lichti et al., 2008). No calcium EMEM was used as keratinocytes are highly sensitive to calcium concentration, which causes them to differentiate. Calcium was removed from heat inactivated fetal bovine serum by chelation process using BT chelex 100 resin. 100 g of chelex resin was dissolved in 450 ml H₂O and titrated to pH 7.4 before filtering through filter paper (5-13 µm pore size). The resin slurry was then added to a 500 ml bottle of heat inactivated fetal bovine serum and mixed at room temperature for 3 hours. The mix was then filtered through filter paper, resin slurry discarded and re-filtered. Chelated heat inactivated fetal bovine serum was filtered through 0.2 µm filter before use in cell culture. Chelex resin removes

calcium from solution by ion exchange. At pH 7.4, chelex resin binds to Ca^{2+} ions by its charged carboxylic acid groups, which is filtered out of solution using filter paper.

2.2 Selection of keratinocytes from other cells in the skin was firstly conducted by trypsin-EDTA digestion of the dermis and isolation of the epidermis. Collagen coated cell culture plates allow for attachment of viable keratinocytes, Lastly, hydrocortisone, cholera toxin and epidermal growth factor aid keratinocyte proliferation, out competing contaminating dermal fibroblasts and melanocytes *in vitro* (Rheinwald and Green, 1975). In rat keratinocytes, Insulin and hydrocortisone are essential for attachment and sustained proliferation (Vaughan et al., 1981). Supplementation of EMEM media was based on the protocol from Dlugosz and authors (Dlugosz et al., 1995).

2.3 Cells were transfected at 70% confluence to maximize transfection efficiency with either miRNA mimic/inhibitor/control or plasmid. MiRNA mimics have the same sequence as endogenous miRNA with chemical modifications to ensure the guide strand is selected in the RISC. MiRNA inhibitors are single stranded oligonucleotides and have a sequence complimentary to the target miRNA, binding to and preventing its activity. MiRNA controls do not bind to any known miRNAs/target mRNAs. The transfection volumes depended on the plate size being used (Table 8).

Table 8. Volumes of Reagents for Cell Transfection Using MiRNAs or Plasmids in Different Sized Cell Culture Plates.

Plate type	Lipofectamine 3000 (µl)	MiRNA (20µM stocks) (µl)	Plasmid (µg)	OptiMEM (µl)
96 well	0.2	1	0.1	100
12 well	2.5	3	1.25	300
60mm dish	5	10	5.75	1000

Lipofectamine 3000 reagent was mixed with OptiMEM and 200nM miRNA mimic/inhibitor/control or plasmid was mixed with OptiMEM in separate tubes and incubated at room temperature for 5 minutes. The OptiMEM-lipofectamine mix was added to the OptiMEM miRNA mimic/inhibitor/control/plasmid mix and incubated at room temperature for 15 minutes. Lipofectamine is a lipid-based cation and so liposomes form surrounding the miRNA/plasmids with lipid subunits forming positively charged surface. The liposomes are attracted to the target cells' negatively charged lipid bilayers, increasing attraction, and delivery of the miRNA/plasmid into the cell. Cells are transfected using reduced serum OptiMEM as proteins found in serum can interfere with the complexes formed between lipofectamine and miRNA, reducing transfection efficiency. After incubation, cell media was removed and cells washed 3 times with PBS, after which, transfection medium was pipette onto the cells and cells incubated at their appropriate cell culture conditions for 4 hours. After 4 hours, the transfection mixture was removed, cells washed rinsed with PBS, replaced with media, and cultured for 48 hours. 48 hours post transfection, cells were used for further analysis.

Appendix 3. Cell Cycle Analysis by Flow Cytometry.

3.1 Flow cytometry by propidium iodide (PI) staining was used to determine the percentage of cells in each phase of cell cycling. PMEKs were grown and treated in 60mm dishes and pooled together before flow cytometric analysis. Fixing cells with 70% (v/v) ethanol at -20°C causes cell dehydration and precipitation of proteins as well as permeabilization to allow entry of PI. PI binds to the major groove of double stranded DNA and is excited at 535 nm with an emission wavelength of 615 nm. The amount of binding is directly proportional to the fluorescence measured, the more double stranded DNA present, the higher the fluorescence. PI also binds to RNA, because of this, RNase treatment is required to degrade RNA, so only difference in quantity of DNA is measured as cells are fixed at different stages of mitosis.

Appendix 4. Transcriptomic Analysis of Total RNA.

4.1 RNA was collected from adherent cells by first removing media and washing cells three times with PBS. Cells were collected and lysed using TRIzol reagent with subsequent rigorous vortexing. TRIzol reagent is a guanidine thiocyanate chaotropic salt solution that can be used to isolate RNA, DNA and protein from a single sample. It lyses cells and causes disruption of hydrogen bonds with water, allowing negatively charged DNA and RNA to bind via salt bridges to the negatively charged silica membrane at low pH and high salt concentrations, whereas protein does not. It also inhibits RNase and DNase activity by enzyme denaturation. RNA was extracted from TRIzol solution using Direct-Zol RNA MiniPrep kit. Reagents were prepared by adding the

appropriate volume of ethanol to the pre-wash and wash buffers (as per manufacturers instruction) and DNase I powder is reconstituted to 6 U/ml. All centrifuge steps are performed at 16,000 x g at room temperature (RT). Firstly, equal volume of 100% (w/w) ethanol was added to the TRIzol sample and mixed thoroughly. Nucleic acids are insoluble in ethanol and will bind to the silica-based column matrix once centrifuged through. The TRIzol-ethanol mix was added to a Zymo-spin IIC column and centrifuged. The flow through was discarded. Next, 400 µl of RNA wash buffer was added to the column and centrifuged. The flow through was discarded. DNase treatment was conducted at this stage by adding 5 µl of DNase I to 75 µl of DNA digestion buffer and pipette directly onto the column matrix and incubated at room temperature for 15 minutes. This digests the DNA, leaving RNA in the column matrix. Next, 400 µl of RNA PreWash was added to the column and centrifuged. The flow through was discarded and the step repeated. This wash buffer functions to remove any small, degraded DNA and contains a low concentration of chaotropic salts. Next, 700 µl of RNA Wash buffer was added to the tube and centrifuged for 1 minute to ensure complete removal of the wash buffer. This wash buffer contained a higher ethanol concentration and functions to remove any residual salts left on the column. contaminating salts will affect downstream applications. Lastly, 30 µl of DNase/RNase free water was added directly to the column matrix and centrifuged into a new DNase/RNase free microcentrifuge tube to elute the RNA in low salt conditions. RNA is soluble in water so will dissolve from the column matrix. RNA is quantified using NanoDrop 8000, using the same vial of DNase/RNase free water used for elution as the blank. The NanoDrop is a UV

spectrophotometer and the Beer-Lambert law to calculate the concentration of RNA. Nucleic acids absorb UV light at 260 nm whereas proteins absorb at 280nm. A 260/280 ratio of approximately 2.0 is considered RNA without protein contaminants. Salts involved in the RNA isolation process absorb UV at 230 nm. A 260/230 ratio of approximately 2.0 is considered RNA without salt contaminants. The 260/280 ratio is higher in RNA than DNA (approx. 1.8) due to the presence of uracil. RNA was evaluated for integrity by gel electrophoresis. 800 ng of RNA was run on a 1% (w/v) TAE gel and imaged using SybrSafe dye on the iBright FL1000 (Figure 25).

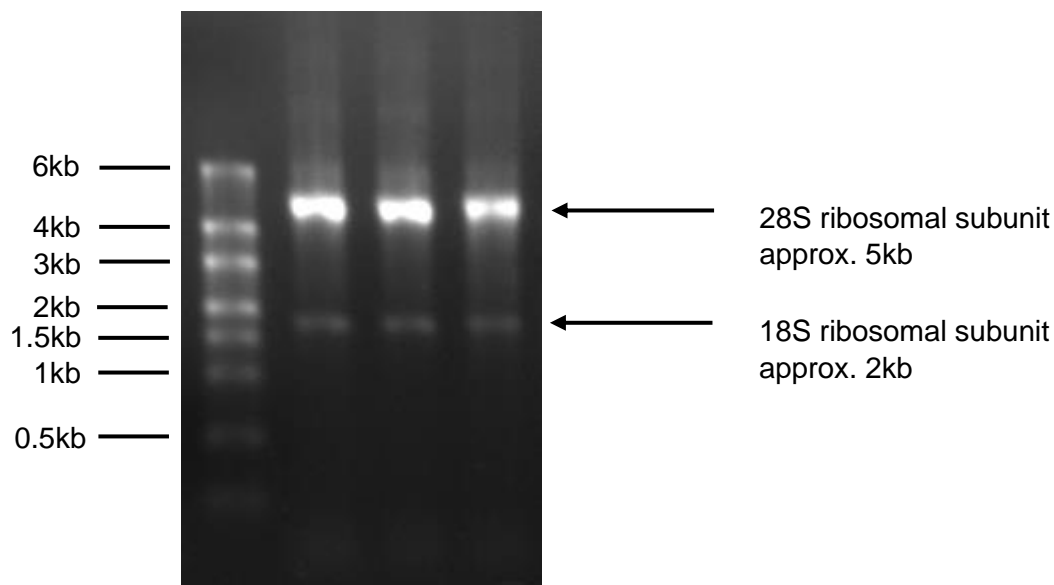


Figure 25. *Example of an RNA Integrity Analysis by Gel Electrophoresis.*

800ng of RNA was run on a 1% (w/v) TAE gel with SybrSafe and imaged. Intact RNA is observed to have two bands. One at approximately 5 kb and 2 kb, with the 5 kb band twice as bright. These are the RNA ribosomal subunits 28S and 18S respectively. RiboRuler high range RNA ladder used and imaged using iBright FL1000.

4.2 Complimentary DNA (cDNA) synthesis was performed using qPCR BIO cDNA synthesis kit. RNA is converted to cDNA due to increased stability and protection from abundant RNases, and for using DNA polymerase to amplify DNA in the subsequent qPCR. Conversion of RNA into cDNA excludes non-coding introns in DNA, leaving only coding regions. cDNA synthesis was performed by making up the following reaction mixtures. 4 µl of 5x cDNA synthesis mix, 1 µl of Reverse Transcriptase, 100 ng total RNA and DNase/RNase free water up to 20 µl. The 5x cDNA synthesis mix contains anchored oligo(dT) and random hexamer primers, 15 mM MgCl₂, 5 mM dNTPs and enhancers and stabilizers. Anchored oligo(dT)s contains a sequence of thymine nucleotides which serve as primers to RNA, annealing to the poly(A) tail and contains a Guanine, Cytosine or Adenine nucleotide at the 3' end which ensures the primer binds to the 5' end of the poly(A) tail of RNA. Random hexamers are 6-9 bases long and anneal at several different points along the RNA sequence. In combination, these primers increase transcription efficiency and can therefore increase RT-qPCR sensitivity. MgCl₂ is required to enhance the activity of reverse transcriptase by binding to negatively charged phosphate groups on the RNA (through Mg²⁺ ions), linearising secondary folding/binding structures. Deoxyribonucleic triphosphates (dNTPs) provide the building blocks of cDNA as it is synthesized, consisting of each of the four bases – adenine, thymine, cytosine, and guanine. The cDNA synthesis reaction mixture underwent the following cycling conditions using a T-100 Thermal Cycler: 42°C for 30 minutes followed by 85°C for 10 minutes. 42°C is the optimal working condition for reverse transcriptase, primer annealing and extension or the

template. At 85°C, the Reverse Transcriptase is denatured so it will not interfere with the following RT-qPCR, affecting results.

4.3 Real-time quantitative PCR (RT-qPCR) was performed using SYBR Green chemistry. SYBR Green binds to double stranded DNA and as more copies of the target gene are made, the fluorescence increases. The following reaction mixtures were made: 5 µl SYBR GreenBlue Mix + ROX, 0.4 µl (10 µM) Forward primer, 0.4 µl (10 µM) Reverse primer, 1 µl cDNA, 3.2 µl nuclease free water. SYBR GreenBlue mix + ROX contains dNTPs, DNA polymerase and ROX as a reference fluorescent against SYBR green dye. dNTPs provide 'building blocks' for the amplification of DNA. Amplification was performed at the following conditions: 95°C for 2 minutes – to fully denature the double stranded cDNA template, followed by 40 cycles of denaturation (95°C for 5 seconds), annealing, and elongation (optimised primer temperature for 30 seconds). Primer annealing temperature is determined experimentally by completing RT-qPCR reactions for untreated cDNA samples at different temperatures. The resulting melt curve is analysed and the temperature giving a single, tall, distinct peak is used in future experiments. Running PCR products on a 1% (w/v) agarose gel to determine expected product size was also employed. Negative control reactions where cDNA is synthesised without Reverse transcriptase is used to evaluate any amplification caused by genomic DNA (gDNA) contamination of the RNA samples. Fluorescence is relative to Actin (*Actb*) expression. Fluorescence is given as a Ct value, the cycle number at which fluorescence exceeds the threshold or background fluorescence. The lower the Ct value, the more starting amount of a certain

gene. Primers were designed using prediction tools that predict only the gene of interest using (<https://primer3.ut.ee/>), (<https://genome.ucsc.edu/>) and (<https://www.ncbi.nlm.nih.gov/tools/primer-blast/>). NCBI primer blast evaluates how self-complimentary the primers are, indicating the potential for primer dimers, a low score alongside using prediction tools stated gives a good indication of primer specificity.

Appendix 5. Transcriptomic Analysis of TaqMan Targets.

- 5.1 TaqMan cDNA was synthesised from total RNA. MicroRNAs are converted to cDNA using a stem-loop primer which binds to the mature miRNA. The following reaction master mixtures were made: 0.15 µl 100mM dNTPs, 1 µl 50 U/µl Reverse transcriptase, 1.5 µl 10X reverse transcription buffer, 0.19µl 20 U/µl RNase inhibitor and 4.16 µl Nuclease free H₂O. 3µl of the specific 5X stem-loop primer and 5 µl of total RNA (containing 5 ng of RNA) was added to each master mix. Reaction mixes are then incubated at 16°C for 30 minutes (for primer annealing), followed by 42°C for 30 minutes (optimal temperature for Reverse transcriptase and template extension) and then 85°C for 5 minutes (to degrade the Reverse transcriptase).
- 5.2 TaqMan qPCR was performed using the following reaction mixture for a 96 well plate: 1 µl 20X TaqMan small RNA assay, 10 µl TaqMan universal mix II (no UNG), 7.67 µl Nuclease free H₂O and 1.33 µl cDNA template. Each sample was completed in duplicates. The TaqMan universal master mix II (no UNG) contains free dNTP nucleotides, buffer, Taq polymerase to amplify the

cDNA, and passive ROX dye for normalisation of fluorescence of TaqMan probes. Uracil-N-glycosylase (UNG) functions to prevent carry over contamination from previous PCR reactions by degradation of uracil containing contaminant products. However, good lab practise and fresh tubes should prevent this. TaqMan small RNA assay contain dual labelled probes for specific miRNAs with a reporter dye attached to the 5' end and a quencher dye attached to the 3' end of the probe. When the probes are located close to one another, the quencher suppresses the fluorescence of the reporter dye. A minor groove binder (MGB) moiety is also incorporated to allow for short probes, suitable for tagging miRNAs. Forward and reverse primers are also contained. The reaction mixture underwent the following cycling conditions: 95°C for 10 minutes for polymerase activation, followed by 40 cycles of 95°C for 15 seconds and 60°C for 60 seconds for strand denaturation, primer annealing and strand extension. During annealing, the TaqMan probe and primers anneal to the cDNA. During extension, Taq polymerase extends from the primers using dNTPs and cleaves the labelled probes, separating the reporter and quencher dye, allowing fluorescence to be detected. As more copies of the target miRNA are made, fluorescence increases. Fluorescence is normalised to U6 snRNA expression, a small nuclear component of spliceosome formation (Didychuk et al., 2018), which is highly and consistently expressed in skin.

Appendix 6. Proteomic Analysis by Western Blot.

6.1 Before protein collection, cell media was removed and washed three times with PBS. This is to wash any contaminating proteins away that are present in the media. RIPA lysis buffer contains buffer to maintain pH to prevent protein degradation, detergent to solubilise the proteins, and salts to maintain ionic structure of proteins. Protein quantification by bicinchoninic acid (BCA) assay was completed using Micro BCA Protein assay kit. Bovine serum albumin (BSA) of stock solution 10 mg/ml was used to create serial dilutions from 10 mg/ml to 0.08 mg/ml. Volumes were made up equal with RIPA buffer. Protein lysate samples were diluted, 1:2, 1:4 and 1:10 with RIPA buffer and pipette into a 96-well flat bottom plate. Using Micro BCA protein assay kit, 100 μ l of reagent 'MA' is mixed with 96 μ l reagent 'MB' and 4 μ l of reagent 'MC' for each well and pipette into the protein test wells. Plates are incubated at 37°C for 2 hours before reading absorbance at 562 nm using CALRIOSStar plate reader. Cu^{2+} ions in the reaction mix are reduced by protein to Cu^{1+} which forms complex with BCA in an alkaline environment resulting in a purple colour that absorbance at 562 nm can be measured (Smith et al., 1985). The absorbance of known protein concentration standards were plot and a line of best fit was drawn. The unknown samples were interpolated against the calibration curve and estimated protein concentration was obtained (Figure 26).

Protein concentration versus absorbance
calibration curve

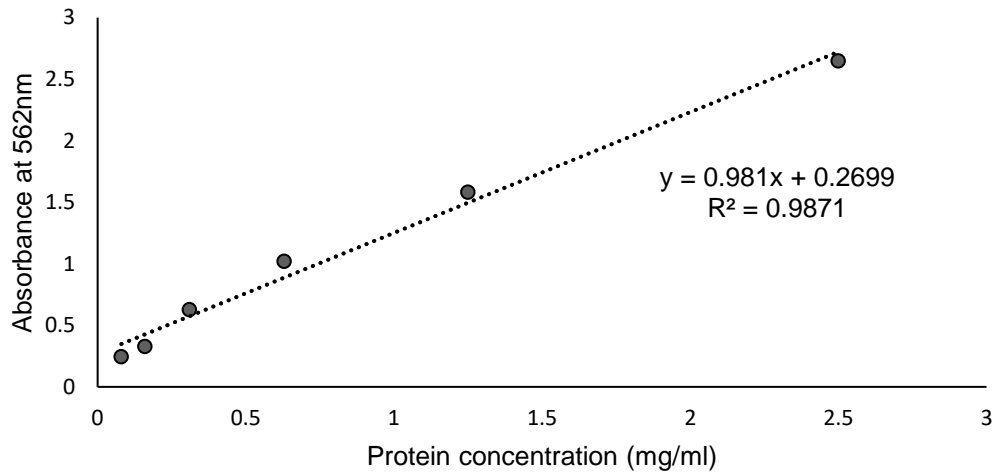


Figure 26. *Example of a BCA Calibration Plot for Determining Protein Concentration.*

A BCA assay is conducted including proteins of known concentrations ranging from 2.5 mg/ml – 0.08 mg/ml are plot against their absorbance reading at 562 nm. The resulting line of best fit equation is used for calculating the concentration of an unknown protein samples using their absorbance reading. R^2 value indicates how close the absorbance values are to the line of best fit – the variance. An R^2 value of 1 shows no variance and a perfect fit. The equation is used to estimate the protein concentration of an unknown sample using its absorbance. The equation is solved for X with Y being the absorbance reading.

- 6.2 Sodium dodecyl sulphate-polyacrylamide gel electrophoresis (SDS-PAGE) is a method to separate protein by molecular weight. SDS is a detergent with a hydrophobic tail and hydrophilic head. SDS strips the outer shell of water molecules and linearises proteins by hydrophobic interactions, leaving a denatured, linear protein with a negative charge. A charge difference at one end of the polyacrylamide gel causes migration of the negatively charged proteins towards the positive electrode. Longer proteins move through the gel more slowly than shorter proteins, giving separation by molecular weight. Gels

were made using BIO-RAD mini-protein tetra cell system. The gels were made in two parts, the lower resolving gel for protein separation, and the upper stacking gel, for protein loading. The resolving gel was made using the following reagents for a 10% gel: 4.0 ml of 30% (w/w) Acrylamide/bis solution, 3.0 ml of 4X lower buffer (1.5 M Tris-base, 0.4% (w/v) SDS, pH8.8), 4.9 ml H₂O, 75 µl APS and 10 µl TEMED. For a different percentage gel to resolve proteins of varying molecular weight, the volume of acrylamide and H₂O are amended with the final volume remaining the same as for 10% gel. Volume of acrylamide is changed to 3.0 ml, 4.8 ml and 6 ml, and H₂O is changed to 5.9 ml, 4.1 ml and 2.9 ml for a 7.5%, 12% and 15% gel respectively. The higher percentage gel resolves proteins of lower molecular weight. The stacking gel remains 4% regardless of the resolving gel percentage. The 4% stacking gel was made using the following reagents: 0.65 ml of 30% (w/w) Acrylamide/bis solution, 1.25 ml 4X upper buffer (0.5 M Tris-base, 0.4% (w/v) SDS, pH6.8), 3.075 ml H₂O, 25 µl APS and 5 µl TEMED. The resolving gel was pipette into a gel chamber (leaving enough room for the stacking gel and comb) and 1 ml of isopropanol was pipette on top. 30 minutes later, once the resolving gel had set, the isopropanol was removed and allowed to evaporate. The stacking gel was pipette on top followed by addition of the comb. After 30 minutes, once set, the comb was removed, and the gel placed in a gel tank with 1X running buffer (25 mM tris-base, 0.192 M glycine, 3.5 mM SDS, pH7.4).

The samples were prepared with addition of 5 µl 4X sample buffer (0.25 M Tris-HCl, 0.28 M SDS, 40% (v/v) glycerol), 0.5 µl 2-Mercaptoethanol and made up to 20 µl with RIPA buffer. The samples were then heated at 98°C for

10 minutes. 2-Mercaptoethanol functions to break disulphide bonds in the tertiary structure of proteins that can affect the migration of the proteins. Heating the sample also aids protein denaturation and breakdown of any proteases. SDS maintains the protein a uniform negative charge, so the proteins migrate towards the positive electrode. The gel was run at 120V for approximately 90 minutes, or until the dye front has reached the end of the gel. The SDS is negatively charged and functions to maintain proteins in a linear form and maintain overall negative charge across the protein so the only variable of the protein as they migrate across the gel is the molecular weight.

6.3 Transfer of proteins to membrane was conducted by wet transfer method. A transfer stack was made from positive to negative electrode: 2xs 2.5 mm thick filter papers followed by 0.45 µm nitrocellulose membrane, the protein gel, and lastly, 2xs 2.5 mm thick filter papers. A roller was used to expel any bubbles between the layers that would affect protein transfer. The transfer stack was placed in a transfer tank and submerged in ice cold transfer buffer (0.192 M glycine, 25 mM tris-base, 20% (v/v) methanol), packed around with ice and run at 90V for 90 minutes until the proteins have transferred to the membrane which were visualised using ponceau stain (5% (v/v) acetic acid, 0.1% (w/v) ponceau) (Figure. 27). The cold temperature prevents overheating and potential damaging of proteins. Methanol functions to dissociate SDS from the protein and absorption of protein onto the membrane.

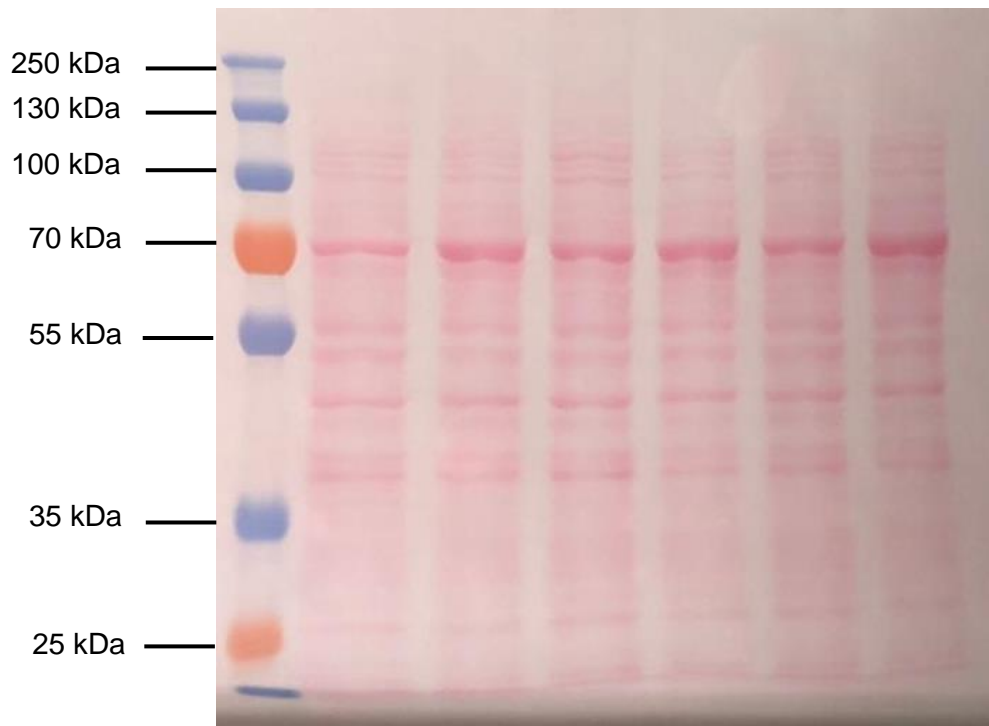


Figure 27. *Example of a Ponceau Stained Protein Transferred Nitrocellulose Membrane.*

Once the proteins have transferred to the nitrocellulose membrane, the membrane is incubated for two minutes with ponceau stain before washing the excess off with ddH₂O. Ponceau bind reversibly to positively charged amino acids on proteins allowing for visualisation of successful protein transfer and an indication of equal loading before antibody staining.

- 6.4 The transferred protein membrane was blocked with 5% (w/v) milk in TBST for 1 hour at room temperature. The milk proteins bind to non-specific proteins, reducing background when visualising. The blocked membrane was then incubated with primary antibody in 1% (w/v) milk in TBST overnight at 4°C. The primary antibody binds to the protein of interest. The following day, the membranes were washed five times for 5 minutes with TBST. Next, horseradish peroxidase conjugated antibodies in 1% (w/v) milk in TBST were

incubated with the membrane for 1 hour at room temperature, followed by five washes for 5 minutes with TBST. The horseradish peroxidase antibodies are developed against the same species as the primary antibody and so will only bind to the primary antibody. The protein was visualised using enhanced chemiluminescence system SuperSignal West Pico kit. 500 µl of SuperSignal West Pico PLUS Luminol/Enhancer Solution and 500 µl SuperSignal West Pico PLUS Stable Peroxide Solution were mixed and pipette onto the membrane and incubated for 5 minutes before visualisation using iBright FL1000 GelDoc Imager. The horseradish peroxidase tagged to the secondary antibodies oxidises luminol to 3-aminophthalate which emits light that can be detected at 425 nm.

6.5 Nuclear vs cytoplasmic protein extraction was performed using NE-PER Nuclear and cytoplasmic extraction reagents. Adherent cells grown in 60 mm dishes were collected by trypsinization with 0.25% (w/v) Trypsin-EDTA, generally giving a packed cell volume of 20 µl following centrifugation at 500 x g. 200 µl of CER I buffer was added to each packed cell pellet, vortexed vigorously and incubated on ice for 10 minutes. 11 µl of CER II buffer was added and vigorously vortexed before centrifugation at 16,000 x g for 5 minutes. CER I and CER II buffers lyse the cell membrane but leaves the nuclei intact. The nuclear pellet was then suspended in 100 µl NER buffer and vortex every 5 minutes for 40 mins on ice. Both cytoplasmic and nuclear protein lysates underwent BCA assay and subsequent Western blot.

Appendix 7. *In Situ* Hybridization.

7.1 *In situ* hybridization utilizes colour change to detect miRNA spatiotemporal expression patterns in tissue sections. Acetylation of fixed tissue sections functions to reduce non-specific background signal by neutralising positive charges in the tissue and glass slide (Princivalle et al., 2012). Permeabilization of tissue was then conducted to solubilise the fixed cells to allow probes to reach their targets. Following permeabilization, slides were incubated with hybridization buffer which contains salt buffers alongside yeast RNA and heparin, both acting to reduce background signal and increase target specificity (Singh and Jones, 1984). Double-Digoxigenin (DIG) labelled probes (hsa-miR-148a-3p miRCURY LNA detection probe) were used specific to the target of interest. DIG is a non-radioactive method of detection. Double DIG probes have a DIG molecule bound to the 3' and 5' end of the probe, allowing for more binding sites for anti-DIG antibodies and a higher signal to background ratio. Through locked nucleic acid (LNA) structure, the probes exhibit high thermal stability upon perfect base pairing of the target. LNA technology can aid sensitivity by discriminating between single nucleotide changes in highly similar miRNAs. The double DIG label attached to the probe provides a higher signal when visualising due to additional binding site for AP linked antibodies. The tissue was incubated at the predetermined hybridisation temperature for 16-18h. potential hybridisation temperature can be determined by reducing the melting temperature given on probe data sheet by approx. 20-18°C due to the deionized formamide destabilization of double stranded molecules (Blake and Delcourt, 1996, Farrell, 2010), but optimal hybridization temperature must be experimentally determined for best results.

The following day the slides were washed. Levamisole in wash buffer functions to bind to endogenous alkaline phosphatase, reducing non-specific background signal. Slides were incubated with anti-DIG alkaline phosphatase (AP) conjugated antibody at pre optimised dilution (approx. 1:1000 for low expressing miRNAs to 1:2500 for high expressing miRNAs) at room temperature for 2 hours. After washing and incubation with NTMT staining buffer, the samples were incubated with BM purple for 12-96 hours at RT until a desired colour reaction has occurred. BM purple substrate reacts with AP to produce a purple-coloured precipitate. Nuclear fast red is used as a counter stain to stain cell nuclei red, together showing the complete structure of the tissue section.

7.2 Fluorescent *in situ* hybridization (FISH) utilises the same fundamental process as *in situ* hybridization with a few modifications. Instead of using alkaline phosphatase tagged anti-DIG antibody, rhodamine tagged anti-DIG antibody was used. Rhodamine is a fluorescent marker with an emission of 568 nm. This negates colour development time when using BM purple as the fluorescent rhodamine can be visualised after 1 hour incubation. It also allows co-staining antibodies with different emission spectra, a fundamental application of FISH.

Appendix 8. RNA Sequencing Analysis.

8.1 RNA sequencing data was analysed using Galaxy web platform (<https://usegalaxy.org/>). The RNA sequencing data has been deposited to

GEO Datasets with the following accession number: GSE197862. For analysis: The data was aligned to *Mus musculus* genome (mm9) using Hisat2 (version 2.2.1) (Kim et al., 2015) with mapping quality (Phred score) set to >30, allowing an error or 0.1%. Genes were counted using FeatureCounts (version 2.0.1) (Liao et al., 2014), and then differential gene expression analysis was performed by DESeq2 (version 2.11.40.7) (Love et al., 2014) and the resulting output sorted with significance $*P < 0.05$. The heatmap was produced using Heatmap2 (3.1.1) and gene ontology was assessed using GOEnrichment (version 2.0.1). The differential expressed gene list was then sorted by expression level compared to controls (average of $n=3$). This data was then overlapped with online miRNA target prediction tools to refine our target gene list to give 43 potential gene targets of miR-148a. Percentage of similarity between mouse and human genes was assessed by NCBI homologue (<https://www.ncbi.nlm.nih.gov/homologene/>).

Table 9. 43 potential gene targets of miR-148a were identified from overlapping of analysed RNA-seq data and online target prediction tools.

Gene symbol	Accession number	Expression level	P value	Percentage Homology between mouse and human
Dynll2	NM_026556	0.81655	0.00138215	97.8
Rab10	NM_016676	0.43973	0.006483	95.3
Rmnd5a	NM_024288	0.51768	0.000375	95.1
Ptges3	NM_019766	0.65226	0.01218438	95.0
Rab14	NM_026697	0.86911	0.00430008	94.4
Rock1	NM_009071	0.81003	0.00982357	92.0

Stx3	NM_152220	0.82185	1.48E-06	91.8
Ythdc2	NM_001163013	0.83512	8.30E-05	91.3
Tbl1xr1	NM_030732	0.77985	6.92E-07	91.2
Atxn7l1	NM_028139	0.80868	0.01177215	91.1
Sos1	NM_009231	0.84467	0.02493209	91.1
Dyrk2	NM_001014390	0.54666	0.02734482	90.8
Tmed7	NM_025698	0.77670	0.00052898	90.8
Ywhab	NM_018753	0.74636	0.03941289	90.7
Btbd3	NM_145534	0.80771	5.32E-05	90.7
Wnt10b	NM_011718	0.60175	0.00170011	90.2
Tnrc6c	NM_198022	0.74672	0.0009881	90.1
Klf5	NM_009769	0.57879	1.60E-08	89.9
Chd7	NM_001277149	0.74508	0.04007672	89.9
Slc2a1	NM_011400	0.71758	4.12E-10	89.5
Prickle2	NM_001134460	0.85677	0.01490624	89.5
Hecw2	NM_001001883	0.88179	0.04509484	89.4
Rab12	NM_024448	0.62497	0.00010101	89.3
Ube2d1	NM_145420	0.62590	7.63E-07	89.3
Sbf2	NM_177324	0.82114	0.00124393	89.0
Gpr137c	NM_027518	0.18994	1.84E-20	88.8
Klf4	NM_010637	0.88910	0.01386642	88.5
Uba6	NM_172712	0.75934	2.35E-07	88.2
Chd1	NM_007690	0.68441	0.04546082	88.0
Gpatch8	NM_001159492	0.76258	0.00607488	87.8
Klf6	NM_011803	0.80318	0.00893694	87.8

Itga11	NM_176922	0.56667	1.67E-05	86.8
Osbp11	NM_176840	0.73272	1.44E-09	86.7
Adamts19	NM_175506	0.85175	0.00616249	86.6
Met	NM_008591	0.80327	5.99E-08	86.4
Zdhhc7	NM_133967	0.39462	0.002814	85.9
Mmp15	NM_008609	0.30996	2.31E-28	85.2
Dock6	NM_177030	0.67926	2.67E-08	84.7
Prnp	NM_001278256	0.64051	0.00078513	84.1
Mdfic	NM_175088	0.73773	1.12E-07	83.9
Ap4e1	NM_175550	0.72860	2.23E-06	83.8
Rassf8	NM_027760	0.61594	0.00025408	83.0
Arhgap20	NM_175535	0.83735	0.00720285	82.2

Appendix 9. Generation of MiR-148a Binding Site Clones.

9.1 The first stage of generating clones incorporating miR-148a binding site was to generate PCR products incorporating this site for later input into plasmids. Phusion Flash High-Fidelity PCR Master Mix is used for generation of PCR products from C57BL/6 primary mouse epidermal keratinocytes (PMEKs) genomic DNA. Genomic DNA (gDNA) was extracted using Quick-DNA Miniprep Plus kit. Untreated PMEKs were collected using 0.25% (w/v) trypsin-EDTA, centrifuged and washed with PBS. PMEKs pellet was then re-suspended in 200 µl Cell buffer and 20 µl Proteinase K before mixing and incubation for 10 minutes at 55°C. This lyses the cells and digests proteins. 220 µl of genomic binding buffer was then added to the digested sample and mixed. Genomic binding buffer is guanidine thiocyanate chaotropic salt and

works as outlined in appendices 4.1. All following centrifuge steps were performed at 12,000 x g at room temperature. The digested sample was added to a Zymo-Spin IIC-CLR column and centrifuges for 1 minute and flow through discarded. 400 µl of DNA pre-wash buffer was added to the column and centrifuged for 1 minute followed by 700 µl of gDNA wash buffer, discarding the flow through each time. The DNA was eluted in 40 µl DNA elution buffer by centrifugation for 1 minute and quantified using NanoDrop 8000 for subsequent use. Primers were designed either side of the miR-148a binding site within the 3'UTR of Rock1 and Elf5 using tools outlined in appendices 4.3. Restriction enzymes XhoI was added to the forward primer and NotI to the reverse primer so they could be cloned between these sites in psiCHECK-2 plasmid. The PCR reaction mix was generated as follows: 10 µl 2X Phusion Flash PCR master mix, 2 µl (5 µM) forward primer, 2 µl (5 µM) reverse primer, 50 ng gDNA, up to 20 µl with H₂O. The PCR reaction underwent the following cycling conditions: 98°C for 10 seconds, followed by 30 cycles of 90°C for 1 second, gradient annealing temperature for 5 seconds (can use online prediction tool can be used to estimate primer annealing temperature), 72°C for 15 seconds and a final extension of 72°C for 1 minute. The PCR mix was then run on a 1% (w/v) TAE gel and the band of interest was visualised using SybrSafe on a transilluminator. The PCR product size for Elf5 was 204 bp and for Rock1, 271 bp. PCR product was extracted from the gel using Nucleospin Gel and PCR clean-up kit. The band of interest was excised and placed in a tube with NTI buffer, 200 µl for every 100 mg of gel and the gel dissolved for 5-10 minutes at 50°C. DNA was then bound to a silica spin-through tube by centrifugation. DNA binds to the silica membrane

in the presence of chaotropic salts as outlined in appendices 4.1. The silica membrane was washed twice with NT3 buffer – an ethanoic wash buffer to remove contaminants soluble in ethanol. The purified DNA was then eluted in slightly alkaline buffer to re-establish the ‘water shell’ around the nucleic acid and break the bonds with the silica membrane. Concentration and purity of DNA PCR products was evaluated using NanoDrop 8000.

9.2 PCR products incorporating the miR-148a binding site was cloned into psiCHECK-2 plasmid by a multifaceted approach. Firstly, linearizing psiCHECK-2 plasmid by double digestion with NotI and XhoI to linearize the plasmid and create ‘sticky ends’ to the 5’ and 3’ end of the plasmid. For double digestion with NotI and XhoI restriction enzymes, the following reaction mixture was made: 1 µg plasmid, 2 µl NEB Cutsmart buffer, 2 µl BSA, 0.5 µl (10 U) NotI, 0.5 µl (10 U) XhoI, up to 20 µl H₂O. BSA in the reaction mixture reduced the enzyme lost to binding to pipette or tube surfaces by stabilising the enzymes. The mixture was flick-mixed and incubated for 1 hour at 37°C followed by 65°C for 20 minutes. 65°C is required to inactivate the enzymes. The digested psiCHECK-2 plasmid was then run on a 1% (w/v) TAE gel with SybrSafe and a band of approximately 6250 bp was excised and underwent gel extraction as outlined in appendices 9.1. The PCR products generated by Phusion Flash High-Fidelity PCR Master Mix generates blunt ends, ‘sticky ends’ incorporating a sequence over-hang will increase cloning efficiency into psiCHECK-2. Blunt PCR products are cloned into pCR-Blunt plasmid using Zero Blunt PCR Cloning Kit. A 10:1 molar ratio of PCR product to plasmid vector was used. The following reaction mixture was made: 1 µl (25 ng) pCR-

Blunt plasmid, 14.58 ng Elf5 PCR product (204 bp) or 19.35 ng Rock1 PCR product, 2 µl 5X ExpressLink T4 DNA ligase buffer, 1 µl ExpressLink T4 DNA ligase (5 U/µl), H₂O up to 10 µl. The amount of PCR product insert was calculated using the following equation:

$$X \text{ ng insert} = \frac{(\text{molar ratio})(\text{base pairs of PCR product})(25 \text{ ng pCR-Blunt plasmid})}{(3500 \text{ pCR-Blunt base pairs})}$$

The reaction mixture was incubated at room temperature for 15 minutes. The ligated pCR-Blunt vector and PCR insert were cloned into DH5α competent *E.coli*. Firstly, the *E.coli* was thawed on ice for 30 minutes. Next, 50 µl of *E.coli* was pipette to a new tube with 5 ng ligated pCR-Blunt – PCR insert plasmid, mixed gently and heat-shock at 42°C for 20 seconds before incubating on ice for 2 minutes. This permeabilises the *E.coli* membrane for the plasmid to enter the cells. 500 µl of SOC media was added to the *E.coli* mix and incubated in an orbital shaker at 37°C for 1 hour. The SOC media mix was plated on an agar plate supplemented with 50 µg/ml Kanamycin and incubated at 37°C overnight. The following day, colonies were selected and placed in 10 ml LB broth media supplemented with 50 µg/ml Kanamycin overnight at 37°C. The following day the bacteria was pelleted by centrifugation at 5,000 x g and bacterial plasmid DNA was extracted using NucleoSpin plasmid mini kit as per the following protocol: Prior to starting, 1 ml of RNase A is added to buffer A1 which makes sure only DNA is eluted. Absolute ethanol was added to wash buffer A4 to 20% (v/v) ethanol content. Post bacterial pelleting, 250 µl of re-suspension buffer A1 was added to the bacterial pellet and mixed. Next, 250 µl of lysis buffer A2 was added to the bacterial and incubated at room temperature for 5 minutes. Lysis buffer A2 contains sodium dodecyl sulphate

(SDS) which disrupts cell membranes and denatures proteins by forming hydrophobic interactions with membrane lipid bilayers and proteins. 300 µl of inactivation buffer A3 was added and gently mixed by inversion. The lysate was then clarified by centrifugation at 11,000 x g for 5 minutes. The clear lysate was then loaded into a NucleoSpin column and collection tube, which contains a binding silica membrane and centrifuged at 11,000 x g for 1 minutes before flow through was discarded. The neutralisation buffer contains guanidine hydrochloride, a chaotropic salt and works to bind DNA to the silica membrane as described in appendices 4.1. The bound DNA was then washed with 600 µl of wash buffer A4, centrifuged at 11,000 x g and flow through discarded. The purified plasmid was eluted using 50 µl of Elution buffer AE and quantified using NanoDrop 8000. The purified plasmid was then double digested with NotI and XhoI restriction enzymes as previously outlined. The digested plasmid was run on a 1% (w/v) TAE agarose gel and PCR products gel extracted as outlined in appendices 9.1. Both psiCHECK-2 plasmid and PCR product inserts have sequence overhangs which increases ligation efficiency. Double digested PCR product and psiCHECK-2 plasmid were ligated using T4 DNA ligase (NEB, USA). A 3:1 molar ratio of PCR insert to psiCHECK-2 plasmid was used. The following reaction mixture was made: 2 µl T4 DNA ligase buffer (10X), 100 ng of psiCHECK-2 vector, 9.79 ng Elf5 PCR product insert or 13.01 ng Rock1 PCR product insert, 1 µl T4 DNA ligase, H₂O up to 20 µl. The amount of insert was calculated using the following equation:

$$X \text{ ng insert} = \frac{(\text{molar ratio})(\text{base pairs of PCR product})(100 \text{ ng psiCHECK-2 plasmid})}{(6250 \text{ pCR-Blunt base pairs})}$$

The reaction mixture was incubated at 16°C overnight followed by 65°C for 10 minutes. Ligated plasmids were transformed into competent *E.coli* as previously outlined and spread on agar plates supplemented with 50 µg/ml Ampicillin and incubated at 37°C overnight. The following day, colonies were selected, expanded and DNA extracted using NucleoSpin plasmid mini kit. Purified plasmids were double digested with NotI and XhoI and run on 1% (w/v) TAE gel as previously outlined to confirm PCR product incorporation into psiCHECK-2 plasmid.

Appendix 10. Generation of MiR-148a Binding Site Mutated Clones.

10.1 Q5 site-directed mutagenesis kit was used to generate mutated miR-148a binding sites. Back-to-back primers were designed binding to the psiCHECK-2-*Elf5/Rock1* plasmids, incorporating a 6-base substitution in the miR-148a binding sequence using (<https://nebasechanger.neb.com/>). The following reaction mixture was made to generate mutated psiCHECK-2-*Elf5/Rock1* plasmids: 12.5 µl Q5 Hot Start High-Fidelity 2x master mix, 1.25 µl Forward primer (10 µM), 1.25 µl Reverse primer (10 µM), 25 ng psiCHECK-2-*Elf5/Rock1* plasmid DNA, up to 25 µl H₂O. The reaction mixture underwent the following cycling conditions: 98°C for 30 seconds (denaturation) followed by 25 cycles of 98°C for 10 seconds, 56°C (psiCHECK-2-*Elf5*) or 58°C (psiCHECK-2-*Rock1*) for 20 seconds (primer annealing) and 72°C for 2.5 minutes (extension) followed by a final extension of 72°C for 2 minutes. The mutated sequences then underwent kinase, ligase and DpnI (KLD) treatment. The kinase phosphorylates the 5' ends of the generated sequences, the ligase ligates the sequence into a circular plasmid and DpnI degrades the original

template sequence. DpnI discriminates between the PCR generated sequence and the template sequence by recognition of methyl groups on the A of GATC elements. The template plasmid has been transformed with DH5 α *E.coli*, which methylates elements of the genome to protect the genetic material from being degraded by endogenous endonucleases. The PCR product generated using the Q5 site-directed mutagenesis kit do not contain methylated groups and so will not be degraded by DpnI. The following reaction mixture was made: 1 μ l PCR product, 5 μ l KLD reaction buffer (2X), 1 μ l KLD enzyme mix (10X), 3 μ l H₂O. The reaction mix was incubated at room temperature for 5 minutes. The mutated plasmids were then transformed into DH5 α *E.coli* as described in appendices 9.2 (100 μ l of SOC media with heat shocked *E.coli* was plated supplemented with 50 μ g/ml ampicillin to avoid formation of a lawn of colonies) and colonies were selected, digested, and checked on a gel as described in appendices 9.1 and 9.2.

Appendix 11. Validation of Clones by Sanger Sequencing.

11.1 Sanger sequencing is required to check if the insert is indeed ligated into the plasmid but also that the insert is the correct orientation and includes no unintentional mutations. The plasmid undergoes extension with DNA polymerase, primer and free nucleotides. Along with the free nucleotides are modified versions that halt the strand extension due to a lack of hydroxyl group on the 3' carbon. The template is separated into 4 separate reactions, one for each modified base, and then run on an agarose gel. The smaller fragments will run furthest on the gel and the base sequence can be read off from

smallest band to largest (Sanger et al., 1977). A more up to date version is the modified nucleotides are labelled with a particular fluorophore depending on the base. Fragments are separated by capillary gel electrophoresis and a laser reads of the terminating base from one reaction mixture. The PCR fragments are aligned in size order on a chromatograph, giving the sequence much quicker than the traditional method (Prober et al., 1987, Swerdlow and Gesteland, 1990). The result of sequencing is a chromatogram which is split into four colours, one per base. The resulting peaks and their colour indicate the base which has been read. Peaks should be single, high, and distinct, an example of which can be observed in Figure 28. Sanger sequencing is accurate to approximately 1kb, so using a primer close to the cloning site/site of interest and with only a single priming site are important considerations.

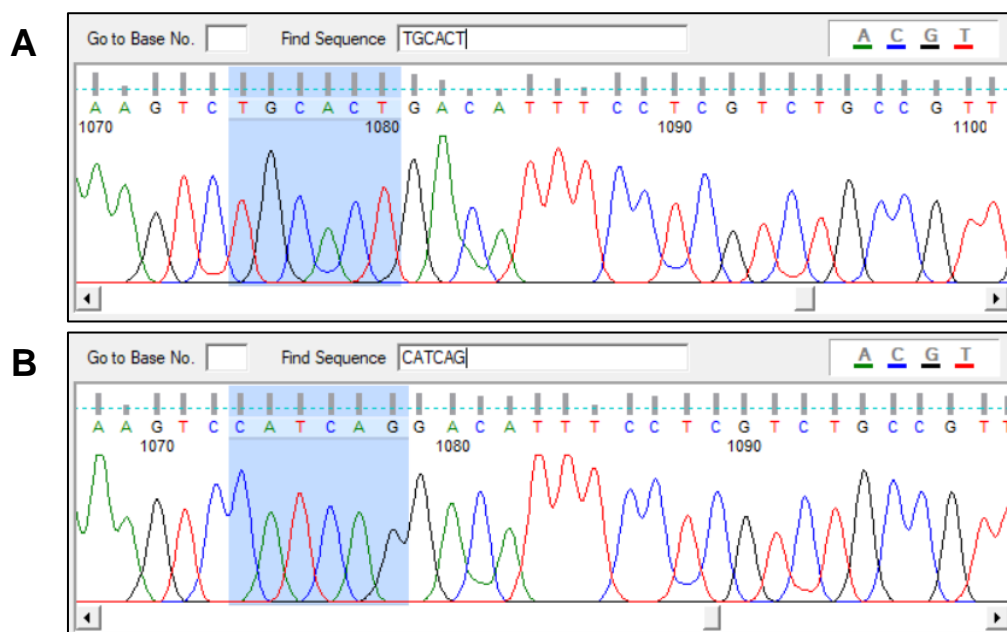


Figure 28. *A Chromatogram of Sanger Sequenced PsiCHECK-2 Cloned with MiR-148a Binding Site from Elf5 3'UTR and its Corresponding Mutation.*

(A-B) A chromatogram following sanger sequencing of PsiCHECK-2 cloned plasmids. Each base is indicated by a colour: Adenine (green), guanine (black), cytosine (blue) and thymine (red). The tall peaks indicate pure and intact DNA, good primer specificity, and correct concentrations of products used. **(A)** A chromatogram of PsiCHECK-2 cloning site. Highlighted sequence shows cloned miR-148a binding site from E1f5 3'UTR. **(B)** A chromatogram of PsiCHECK-2 cloning site following site-directed mutagenesis. Highlighted sequence shows mutated miR-148a binding site from E1f5 3'UTR.

Appendix 12. Luciferase Bioluminescence Reporter Assay.

12.1 PsiCHECK-2 plasmid was used for luciferase reporter assay as it contains a cloning site downstream of the *Renilla* stop codon. *Renilla* luciferase activity is used as a primary reporter gene which is normalised to *Firefly* luciferase activity. Dual-Glo Luciferase assay system was used to measure *Renilla* and firefly luminescence. HaCaTs were co-transfected with 100 ng psiCHECK-2-*E1f5/Rock1* or mutated psiCHECK-2-*E1f5/Rock1* with 200 nM miR-148a mimic or miR control in a 96 well white bioluminescence plate. These plates are white sided, that reflect light and increase the signal when reading bioluminescence. 24 hours post transfection, 75 µl of Dual-Glo luciferase reagent is added to 75 µl of media with the transfected HaCaT cells and incubated at room temperature for 15 minutes before reading firefly luciferase activity at 560 nm. 75 µl of Dual-Glo Stop & Glo luciferase reagent was then added to the HaCaT cells and incubated at room temperature for 15 minutes before reading *Renilla* luciferase activity at 480 nm. Firefly and *Renilla* luciferase activity was measured using a CLARIOStar plate reader. Luciferase activity was calculated relative to firefly luciferase activity and untransfected

HaCaTs, giving background bioluminescence. MiR-148a binding site in cloned into the 3' end of *Renilla* translational stop sequence, fusing it with *Renilla*. When miRNA-148a binds to the cloned binding site mRNA, it is cleaved and reduces *Renilla* luminescence. MiR control or mutated binding site sequence will not cause a reduction in *Renilla* luminescence. Firefly luciferase activity is activated by beetle luciferin, ATP, Mg²⁺ and O₂ which are present in the Dual-Glo luciferase reagent. *Renilla* requires coelenterate luciferin. Dual-Glo Stop & Glo luciferase reagent also quenches firefly activity before activating *Renilla* luciferase.

Appendix 13. Pharmacological Inhibition of MiR-148a *In Vivo*.

13.1 20 µM of atelocollagen was mixed with 20 µM synthetic miR-148a inhibitor (anti-miR-148a) or miRNA negative control and delivered by injection into three points in the dorsal skin, subcutaneously. Atelocollagen is a liquid at 4°C allowing for injection but solidifies at 30°C, allowing targeted area for release of siRNAs, and sustained delivery as atelocollagen breaks down (Minakuchi et al., 2004, Takeshita et al., 2005, Mardaryev et al., 2010). This delivery system slowly releases synthetic miR-148a inhibitor over time providing a sustained inhibition of miR-148a in the skin.

Appendix 14. Alkaline Phosphatase Staining for Morphological Analysis.

14.1 Alkaline phosphatase staining is a histochemical staining method for staining cells a deep red colour and identification of morphology of tissue sections.

New fuchsin is used as the chromogen as it precipitates in the presence of alkaline phosphatase. The tissue sections are counter stained with haematoxylin, a nucleic acid stain giving a light pink colour to the tissue.

Appendix 15. Immunofluorescent Analysis.

15.1 Immunofluorescent analysis using tissue or cells follows the same basic principle. Blocking with fetal calf serum and goat or donkey serum contains antibodies that will bind to non-specific antigens on the cells/tissue which reduces background signal for the specific test antibody. A serum of the same host species as the secondary antibody makes sure that the secondary antibody only binds to the primary antibody and not non-specific antigens, reducing background signal. BSA in the blocking buffer also reduces non-specific binding to proteins in the sample and saturates any exposed slide or plate that could interfere with antibody binding. Once blocked, the primary antibody binds to a specific antigen. The secondary antibody which is fluorescently tagged will bind to the primary antibody which can then be imaged with a fluorescent microscope. Washes between incubation steps removes excess and unbound antibody, making sure each incubation step binds efficiently to bound antibody and removes excess when imaging, reducing background signal.

Appendix 16. Fluorescence activated cell sorting of hair Follicle Bulge Stem Cells.

16.1 Fluorescence activated cell sorting (FACS) is the mechanism of sorting cell populations based on fluorescent antibody binding. 7–9-week-old C57BL/6

dorsal and ventral mouse skin was used to extract hair follicle bulge stem cells and suprabasal keratinocytes. Antibodies: Ly-6A/E (Stem cell antigen 1 (Sca-1)), CD34 and CD49f ($\alpha 6$) were used to stain cells. Sca-1 and CD49f are both fluorescently conjugated, Sca-1 is FITC conjugated so has an emission peak of 525 nm and CD49f is phycoerythrin conjugated with an emission peak of 574 nm. CD34 is not fluorescently tagged but is biotin tagged. Allophycocyanin (APC) streptavidin secondary antibody is used which binds to biotin, with an emission peak of 660 nm. CD34 alongside CD49f has been shown to be specific markers of hair follicle bulge stem cells (Trempe et al., 2003). Sca-1 is not expressed in bulge stem cell region but is expressed in basal stem cells in the epidermis thus differentiating between bulge and basal stem cells (Triebl et al., 2004). Combinations of antibody binding were isolated giving the different sorted populations: HF bulge SCs ($CD34^+/CD49f^{High}/Sca-1^-$) and junctional cells ($CD34^-/CD49f^{Low}/Sca-1^-$). DAPI (25 ng/ml) was added prior to running to stain exposed nucleic acid of dead cells, making sure only viable cells were sorted. DAPI has an emission peak of 457 nm. Along-side the sample run, individual samples with single test antibodies were used to align the lasers before running the sorting sample.

Appendix 17. Lentiviral Production and Transduction of Hair Follicle Bulge Stem Cells.

- 17.1 Lentiviruses are packaged in HEK293T cells using plasmids for either control or miR-148a inhibition (Scrambled shRNA control in pGFP-C-shLenti shRNA Vector control or MiRZIP-148a anti-miR-148a microRNA construct). The

plasmids have a puromycin resistance gene and so colony amplification/selection was completed as described in appendices 9.2 with 50 µg/ml puromycin. Once heat-shocked into *E.coli* bacteria, Ampicillin was used to select for positive clones. Scrambled plasmids take an siRNA sequence and then are rearranged so they do not target any known genes. MiR-148a inhibition is caused by antagomirs which are oligonucleotides that are complimentary to miR-148 which prevents its binding activity. The antiMiR-148a insert is driven by H1 RNA promoter for amplification with RNA polymerase III. The lentiviral plasmids contain a copGFP insert driven by CMV promoter which causes transduced cells to fluoresce GFP, allowing visualisation of successfully transduced cells. The plasmids including the gene for the specific virus targets are co-transfected with a packaging plasmid which contains key genes: *Gag*, used for viral assembly and matrix proteins synthesis, the *Pol* gene codes for RNA polymerase, *RNase H* and *Integrase*, required for amplification and integration of viral DNA, and *Env*, which codes for surface glycoproteins. Transfected together, the mature, complete viral particles are made by the cells and can be collected for transduction experiments. HEK293T cells are used due to their high lentiviral production efficiency due to the presence of SV40 T-antigen (Gama-Norton et al., 2011). Turbofectin is a cationic polymer that produces complexes with the plasmid DNA, aiding transfection by producing a charge attraction between the plasmid and the target cell surface membrane. Once the cells have been transfected and media changed, the transfected cells produce viral particles which are collected 24- and 48-hours post media change. The viral particle rich media was then precipitated to collect concentrated viral particles.

80µg/ml polybrene and 80 µg/ml CSC were added directly to the viral media and incubated overnight, shaking at 4°C. The following day, the media was centrifuged at 10,000 x g for 30 minutes at 4°C before re-suspension in 1% original volume using DMEM complete media. Polybrene, a cationic polymer and CSC, an anionic polymer form large complexes around viral particles which can be pelleted by ultracentrifugation (Le Doux et al., 2001, Landázuri and Le Doux, 2006).

17.2 Lentiviral titration is the mechanism for working out the concentration of virus for use in downstream lentiviral transduction. qPCR lentiviral titration kit was used to complete lentiviral titration. Standard control DNA was dilution by serial dilutions to obtain 1/100 - 1/100,000 dilutions for creation of a standard curve. 2 µl of viral sample was added to 18 µl virus lysis buffer and incubated at room temperature for 3 minutes. The following reaction mix was made up per standard/test sample. 10 µl BlasTaq 2X qPCR titre master mix, 2 µl primer mix, 2 µl viral lysate with each test sample and standard conducted in triplicates. BlasTaq 2X qPCR titre master mix contains a fluorescent dye which binds to double stranded DNA, the more DNA present, the higher the fluorescence. The reaction mixture underwent the following cycling conditions: 42°C for 20 minutes (RNA reverse transcription) 95°C for 10 minutes (enzyme activation) followed by 30 cycles of 95°C for 15 seconds (denaturation) and 60°C for 1 minute (primer annealing and extension). Ct values of standard dilutions were plot against the viral titre and a logarithmic regression curve was made. Unknown viral titres were interpolated on to the standard curve using the equation $y=m\ln(x)+b$ where m is the slope of the line, y is the Ct

value and b is the y intercept. Concentration is given in viral infectious units per ml.

- 17.3 Feeder cells are required for stem cell growth as they produce growth factors and provide a matrix in which stem cells can adhere to. 3T3 cells are either gamma-irradiated or mitomycin C (MMC) treated to prevent proliferation of the feeder cells at approximately 80% confluency. This leaves enough room for stem cells to adhere with close proximity to feeder cells for paracrine and physical interactions. MMC treatment was chosen due to its cost-effectiveness, ease of use and ability to stop proliferation (Ponchio et al., 2000). Optimal concentration of MMC was determined by testing 2, 4, 6, 8 and 10µg/ml with a two-hour incubation based on previously reported concentration for 3T3 cells (Nowak and Fuchs, 2009). Treated cells were imaged using IncuCyte S3 live cell analysis instrument over a course of 5 days to determine whether the confluence changed. The lowest concentration of MMC where confluency did not change was selected as MMC at too high concentrations can be cytotoxic. MMC arrests cell proliferation by covalently linking DNA, preventing DNA replication but not affecting protein synthesis, keeping cells viable for several weeks (Llames et al., 2015).
- 17.4 The multiplicity of infection (MOI) is the ratio between viral particles and infection targets. Viral volume for a given MOI was calculated using the following equation:

$$\text{MOI} = \frac{\text{Viral titer} \times \text{Virus volume}}{\text{Total cell number}}$$

An MOI of 20 was chosen and tested for infection efficiency. Too low MOI can result in too few viral particles per cell and so low transduction efficiency, too high MOI can lead to cytotoxicity and cell death. Polybrene is a positively charged polymer which increases lentiviral transduction efficiency by neutralising the charge repulsion between the lentiviral particles (virions) and cell surface membrane. Efficiency of transduction was assessed by GFP imaging using IncuCyte S3 live cell analysis instrument.

Appendix 18. Statistical Analysis.

- 18.1 The $\Delta\Delta\text{Ct}$ method of analysis relies on a reference gene expression level or control fluorescence level. For RT-qPCR, for each sample, house-keeping reporter *Actin* (*Actb*), expression is subtracted from the value of any other gene analysed giving a normalised expression (ΔCt), before normalised control sample was subtracted away from test sample giving $\Delta\Delta\text{Ct}$. *Actin* does not change in expression between treated samples. Fold difference was calculated by the equation $2^{\Delta\Delta\text{Ct}}$ and relative the control sample with a fold difference of 1. For luciferase reporter assay the house-keeping reporter is Firefly luciferase activity. In immunofluorescence, relative arbitrary fluorescence units for Elf5 and Rock1 was normalised to DAPI arbitrary fluorescence units.
- 18.2 Unpaired student's *t*-test was used for analysis of relative expression or relative fluorescence intensity in RT-qPCR data, Immunocytochemistry, and

luciferase reporter assay. The student's *t*-test is a parametric test used for calculating significance *p*-value based on two sets of normally distributed data. Data was normalised by logarithmic transformation so a parametric test can be used. The statistical significance of the difference between the two data sets is given as a *P* value; **P*<0.05 meaning there is a 95% chance the difference between two samples is true and the hypothesis can be accepted. ***P*<0.01 there is a 99% chance the difference between two samples is true, and ****P*<0.001 there is a 99.9% chance the difference between two samples is true.

8.0

References

- ABDELFATTAH, A. M., PARK, C. & CHOI, M. Y. 2014. Update on non-canonical microRNAs. *Biomol Concepts*, 5, 275-87.
- ABE, Y. & TANAKA, N. 2017. Roles of the Hedgehog Signaling Pathway in Epidermal and Hair Follicle Development, Homeostasis, and Cancer. *J Dev Biol*, 5.
- AHMED, M. I., ALAM, M., EMELIANOV, V. U., POTERLOWICZ, K., PATEL, A., SHAROV, A. A., MARDARYEV, A. N. & BOTCHKAREVA, N. V. 2014. MicroRNA-214 controls skin and hair follicle development by modulating the activity of the Wnt pathway. *J Cell Biol*, 207, 549-67.
- AHMED, M. I., MARDARYEV, A. N., LEWIS, C. J., SHAROV, A. A. & BOTCHKAREVA, N. V. 2011. MicroRNA-21 is an important downstream component of BMP signalling in epidermal keratinocytes. *J Cell Sci*, 124, 3399-404.
- AHMED, M. I., PICKUP, M. E., RIMMER, A. G., ALAM, M., MARDARYEV, A. N., POTERLOWICZ, K., BOTCHKAREVA, N. V. & BOTCHKAREV, V. A. 2019. Interplay of MicroRNA-21 and SATB1 in Epidermal Keratinocytes during Skin Aging. *J Invest Dermatol*, 139, 2538-2542.e2.
- AMOH, Y., LI, L., KATSUOKA, K., PENMAN, S. & HOFFMAN, R. M. 2005. Multipotent nestin-positive, keratin-negative hair-follicle bulge stem cells can form neurons. *Proc Natl Acad Sci U S A*, 102, 5530-4.
- AMOYEL, M. & BACH, E. A. 2012. Functions of the Drosophila JAK-STAT pathway: Lessons from stem cells. *Jakstat*, 1, 176-83.
- AN, L., LING, P., CUI, J., WANG, J., ZHU, X., LIU, J., DAI, Y., LIU, Y., YANG, L. & DU, F. 2018. ROCK inhibitor Y-27632 maintains the propagation and characteristics of hair follicle stem cells. *Am J Transl Res*, 10, 3689-3700.
- ANDL, C. D., MIZUSHIMA, T., OYAMA, K., BOWSER, M., NAKAGAWA, H. & RUSTGI, A. K. 2004a. EGFR-induced cell migration is mediated predominantly by the JAK-STAT pathway in primary esophageal keratinocytes. *Am J Physiol Gastrointest Liver Physiol*, 287, G1227-37.
- ANDL, T., AHN, K., KAIRO, A., CHU, E. Y., WINE-LEE, L., REDDY, S. T., CROFT, N. J., CEBRA-THOMAS, J. A., METZGER, D., CHAMBON, P., LYONS, K. M., MISHINA, Y., SEYKORA, J. T., CRENSHAW, E. B., 3RD & MILLAR, S. E. 2004b. Epithelial Bmpr1a regulates differentiation and proliferation in postnatal hair follicles and is essential for tooth development. *Development*, 131, 2257-68.
- ANDL, T., MURCHISON, E. P., LIU, F., ZHANG, Y., YUNTA-GONZALEZ, M., TOBIAS, J. W., ANDL, C. D., SEYKORA, J. T., HANNON, G. J. & MILLAR, S. E. 2006. The miRNA-processing enzyme dicer is essential for the morphogenesis and maintenance of hair follicles. *Curr Biol*, 16, 1041-9.
- ANDL, T., REDDY, S. T., GADDAPARA, T. & MILLAR, S. E. 2002. WNT signals are required for the initiation of hair follicle development. *Dev Cell*, 2, 643-53.
- ANTONINI, D., RUSSO, M. T., DE ROSA, L., GORRESE, M., DEL VECCHIO, L. & MISSERO, C. 2010. Transcriptional repression of miR-34 family contributes to p63-mediated cell cycle progression in epidermal cells. *J Invest Dermatol*, 130, 1249-57.
- ARDINI, E., AGRESTI, R., TAGLIABUE, E., GRECO, M., AIELLO, P., YANG, L. T., MÉNARD, S. & SAP, J. 2000. Expression of protein tyrosine phosphatase alpha (RPTPalpha) in human breast cancer correlates with low tumor grade, and inhibits tumor cell growth in vitro and in vivo. *Oncogene*, 19, 4979-87.

- ATIT, R., SGAIER, S. K., MOHAMED, O. A., TAKETO, M. M., DUFORT, D., JOYNER, A. L., NISWANDER, L. & CONLON, R. A. 2006. β -catenin activation is necessary and sufficient to specify the dorsal dermal fate in the mouse. *Developmental Biology*, 296, 164-176.
- BACCARINI, A., CHAUHAN, H., GARDNER, T. J., JAYAPRAKASH, A. D., SACHIDANANDAM, R. & BROWN, B. D. 2011. Kinetic analysis reveals the fate of a microRNA following target regulation in mammalian cells. *Curr Biol*, 21, 369-76.
- BAINS, W. 2013. Transglutaminase 2 and EGGL, the protein cross-link formed by transglutaminase 2, as therapeutic targets for disabilities of old age. *Rejuvenation Res*, 16, 495-517.
- BARRANDON, Y. & GREEN, H. 1987. Three clonal types of keratinocyte with different capacities for multiplication. *Proc Natl Acad Sci U S A*, 84, 2302-6.
- BARTEL, D. P. 2009. MicroRNAs: target recognition and regulatory functions. *Cell*, 136, 215-33.
- BERNSTEIN, E., KIM, S. Y., CARMELL, M. A., MURCHISON, E. P., ALCORN, H., LI, M. Z., MILLS, A. A., ELLEDGE, S. J., ANDERSON, K. V. & HANNON, G. J. 2003. Dicer is essential for mouse development. *Nat Genet*, 35, 215-7.
- BESSON, V., KYRYACHENKO, S., JANICH, P., BENITAH, S. A., MARAZZI, G. & SASSOON, D. 2017. Expression Analysis of the Stem Cell Marker Pw1/Peg3 Reveals a CD34 Negative Progenitor Population in the Hair Follicle. *Stem Cells*, 35, 1015-1027.
- BICKENBACH, J. R., GREER, J. M., BUNDMAN, D. S., ROTHNAGEL, J. A. & ROOP, D. R. 1995. Loricrin expression is coordinated with other epidermal proteins and the appearance of lipid lamellar granules in development. *J Invest Dermatol*, 104, 405-10.
- BLAKE, R. D. & DELCOURT, S. G. 1996. Thermodynamic Effects of Formamide on DNA Stability. *Nucleic Acids Research*, 24, 2095-2103.
- BLANPAIN, C. & FUCHS, E. 2009. Epidermal homeostasis: a balancing act of stem cells in the skin. *Nat Rev Mol Cell Biol*, 10, 207-17.
- BLANPAIN, C., LOWRY, W. E., GEOGHEGAN, A., POLAK, L. & FUCHS, E. 2004. Self-renewal, multipotency, and the existence of two cell populations within an epithelial stem cell niche. *Cell*, 118, 635-48.
- BLANPAIN, C., LOWRY, W. E., PASOLLI, H. A. & FUCHS, E. 2006. Canonical notch signaling functions as a commitment switch in the epidermal lineage. *Genes Dev*, 20, 3022-35.
- BORCHERT, G. M., LANIER, W. & DAVIDSON, B. L. 2006. RNA polymerase III transcribes human microRNAs. *Nat Struct Mol Biol*, 13, 1097-101.
- BOROWIEC, A. S., DELCOURT, P., DEWAILLY, E. & BIDAUX, G. 2013. Optimal differentiation of in vitro keratinocytes requires multifactorial external control. *PLoS One*, 8, e77507.
- BOTCHKAREV, V. A., BOTCHKAREVA, N. V., NAKAMURA, M., HUBER, O., FUNA, K., LAUSTER, R., PAUS, R. & GILCHREST, B. A. 2001a. Noggin is required for induction of the hair follicle growth phase in postnatal skin. *Faseb j*, 15, 2205-14.
- BOTCHKAREV, V. A., BOTCHKAREVA, N. V., ROTH, W., NAKAMURA, M., CHEN, L. H., HERZOG, W., LINDNER, G., MCMAHON, J. A., PETERS, C., LAUSTER, R., MCMAHON, A. P. & PAUS, R. 1999. Noggin is a mesenchymally derived stimulator of hair-follicle induction. *Nat Cell Biol*, 1, 158-64.
- BOTCHKAREV, V. A. & FLORES, E. R. 2014. p53/p63/p73 in the epidermis in health and disease. *Cold Spring Harb Perspect Med*, 4.
- BOTCHKAREV, V. A., KOMAROVA, E. A., SIEBENHAAR, F., BOTCHKAREVA, N. V., SHAROV, A. A., KOMAROV, P. G., MAURER, M., GUDKOV, A. V. & GILCHREST, B. A. 2001b. p53 Involvement in the control of murine hair follicle regression. *Am J Pathol*, 158, 1913-9.
- BOTCHKAREV, V. A. & SHAROV, A. A. 2004. BMP signaling in the control of skin development and hair follicle growth. *Differentiation*, 72, 512-26.
- BRODERSEN, P. & VOINNET, O. 2009. Revisiting the principles of microRNA target recognition and mode of action. *Nat Rev Mol Cell Biol*, 10, 141-8.

- BROWNELL, I., GUEVARA, E., BAI, C. B., LOOMIS, C. A. & JOYNER, A. L. 2011. Nerve-derived sonic hedgehog defines a niche for hair follicle stem cells capable of becoming epidermal stem cells. *Cell Stem Cell*, 8, 552-65.
- BUFFOLI, B., RINALDI, F., LABANCA, M., SORBELLINI, E., TRINK, A., GUANZIROLI, E., REZZANI, R. & RODELLA, L. F. 2014. The human hair: from anatomy to physiology. *Int J Dermatol*, 53, 331-41.
- BUKOWSKA, J., KOPCEWICZ, M., WALENDZIK, K. & GAWRONSKA-KOZAK, B. 2018. Foxn1 in Skin Development, Homeostasis and Wound Healing. *Int J Mol Sci*, 19.
- BYRNE, C., TAINSKY, M. & FUCHS, E. 1994. Programming gene expression in developing epidermis. *Development*, 120, 2369-83.
- BÖHMER, F. D. & FRIEDRICH, K. 2014. Protein tyrosine phosphatases as wardens of STAT signaling. *Jakstat*, 3, e28087.
- CADDY, J., WILANOWSKI, T., DARIDO, C., DWORKIN, S., TING, S. B., ZHAO, Q., RANK, G., AUDEN, A., SRIVASTAVA, S., PAPENFUSS, T. A., MURDOCH, J. N., HUMBERT, P. O., PAREKH, V., BOULOS, N., WEBER, T., ZUO, J., CUNNINGHAM, J. M. & JANE, S. M. 2010. Epidermal wound repair is regulated by the planar cell polarity signaling pathway. *Dev Cell*, 19, 138-47.
- CAI, J., LEE, J., KOPAN, R. & MA, L. 2009. Genetic interplays between Msx2 and Foxn1 are required for Notch1 expression and hair shaft differentiation. *Dev Biol*, 326, 420-30.
- CASTILHO, R. M., SQUARIZE, C. H., CHODOSH, L. A., WILLIAMS, B. O. & GUTKIND, J. S. 2009. mTOR mediates Wnt-induced epidermal stem cell exhaustion and aging. *Cell Stem Cell*, 5, 279-89.
- CENTONZE, G., CENTONZE, S., PONZONE, L. & CALAUTTI, E. 2022. ROCK 'n TOR: An Outlook on Keratinocyte Stem Cell Expansion in Regenerative Medicine via Protein Kinase Inhibition. *Cells*, 11.
- CETERA, M., LEYBOVA, L., JOYCE, B. & DEVENPORT, D. 2018. Counter-rotational cell flows drive morphological and cell fate asymmetries in mammalian hair follicles. *Nat Cell Biol*, 20, 541-552.
- CHAKRABARTI, R., HWANG, J., ANDRES BLANCO, M., WEI, Y., LUKAČIŠIN, M., ROMANO, R. A., SMALLEY, K., LIU, S., YANG, Q., IBRAHIM, T., MERCATALI, L., AMADORI, D., HAFFTY, B. G., SINHA, S. & KANG, Y. 2012a. Elf5 inhibits the epithelial-mesenchymal transition in mammary gland development and breast cancer metastasis by transcriptionally repressing Snail2. *Nat Cell Biol*, 14, 1212-22.
- CHAKRABARTI, R., WEI, Y., ROMANO, R. A., DECOSTE, C., KANG, Y. & SINHA, S. 2012b. Elf5 regulates mammary gland stem/progenitor cell fate by influencing notch signaling. *Stem Cells*, 30, 1496-508.
- CHANG, T. C., CHEN, Y. C., YANG, M. H., CHEN, C. H., HSING, E. W., KO, B. S., LIOU, J. Y. & WU, K. K. 2010. Rho kinases regulate the renewal and neural differentiation of embryonic stem cells in a cell plating density-dependent manner. *PLoS One*, 5, e9187.
- CHATTERJEE, S., FASLER, M., BÜSSING, I. & GROSSHANS, H. 2011. Target-mediated protection of endogenous microRNAs in *C. elegans*. *Dev Cell*, 20, 388-96.
- CHATTERJEE, S. & GROSSHANS, H. 2009. Active turnover modulates mature microRNA activity in *Caenorhabditis elegans*. *Nature*, 461, 546-9.
- CHEN, D., JARRELL, A., GUO, C., LANG, R. & ATIT, R. 2012. Dermal β -catenin activity in response to epidermal Wnt ligands is required for fibroblast proliferation and hair follicle initiation. *Development*, 139, 1522-33.
- CHEN, J. & CHUONG, C. M. 2012. Patterning skin by planar cell polarity: the multi-talented hair designer. *Exp Dermatol*, 21, 81-5.
- CHEN, Q., WANG, Y., DANG, H. & WU, X. 2021. MicroRNA-148a-3p inhibits the proliferation of cervical cancer cells by regulating the expression levels of DNMT1 and UTF1. *Oncol Lett*, 22, 617.

- CHEN, W., CHEN, L., ZHANG, Z., MENG, F., HUANG, G., SHENG, P. & LIAO, W. 2016. MicroRNA-455-3p modulates cartilage development and degeneration through modification of histone H3 acetylation. *Biochim Biophys Acta*, 1863, 2881-2891.
- CHENDRIMADA, T. P., GREGORY, R. I., KUMARASWAMY, E., NORMAN, J., COOCH, N., NISHIKURA, K. & SHIEKHATTAR, R. 2005. TRBP recruits the Dicer complex to Ago2 for microRNA processing and gene silencing. *Nature*, 436, 740-4.
- CHI, W., WU, E. & MORGAN, B. A. 2013. Dermal papilla cell number specifies hair size, shape and cycling and its reduction causes follicular decline. *Development*, 140, 1676-83.
- CHI, W. Y., ENSHELL-SEIFFERS, D. & MORGAN, B. A. 2010. De novo production of dermal papilla cells during the anagen phase of the hair cycle. *J Invest Dermatol*.
- CHIANG, H. R., SCHOENFELD, L. W., RUBY, J. G., AUYEUNG, V. C., SPIES, N., BAEK, D., JOHNSTON, W. K., RUSS, C., LUO, S., BABIARZ, J. E., BLELLOCH, R., SCHROTH, G. P., NUSBAUM, C. & BARTEL, D. P. 2010. Mammalian microRNAs: experimental evaluation of novel and previously annotated genes. *Genes Dev*, 24, 992-1009.
- CHOI, J. H., JUN, J. H., KIM, J. H., SUNG, H. J. & LEE, J. H. 2014. Synergistic effect of interleukin-6 and hyaluronic acid on cell migration and ERK activation in human keratinocytes. *J Korean Med Sci*, 29 Suppl 3, S210-6.
- CHOI, Y. S., CHAKRABARTI, R., ESCAMILLA-HERNANDEZ, R. & SINHA, S. 2009. Elf5 conditional knockout mice reveal its role as a master regulator in mammary alveolar development: failure of Stat5 activation and functional differentiation in the absence of Elf5. *Dev Biol*, 329, 227-41.
- CHOI, Y. S., CHENG, J., SEGRE, J. & SINHA, S. 2008. Generation and analysis of Elf5-LacZ mouse: unique and dynamic expression of Elf5 (ESE-2) in the inner root sheath of cycling hair follicles. *Histochem Cell Biol*, 129, 85-94.
- CHOI, Y. S., ZHANG, Y., XU, M., YANG, Y., ITO, M., PENG, T., CUI, Z., NAGY, A., HADJANTONAKIS, A. K., LANG, R. A., COTSARELIS, G., ANDL, T., MORRISEY, E. E. & MILLAR, S. E. 2013. Distinct functions for Wnt/ β -catenin in hair follicle stem cell proliferation and survival and interfollicular epidermal homeostasis. *Cell Stem Cell*, 13, 720-33.
- CIANFEROTTI, L., COX, M., SKORIJA, K. & DEMAY, M. B. 2007. Vitamin D receptor is essential for normal keratinocyte stem cell function. *Proc Natl Acad Sci U S A*, 104, 9428-33.
- CICHOREK, M., WACHULSKA, M., STASIEWICZ, A. & TYMIŃSKA, A. 2013. Skin melanocytes: biology and development. *Postepy Dermatol Alergol*, 30, 30-41.
- CLAVEL, C., GRISANTI, L., ZEMLA, R., REZZA, A., BARROS, R., SENNETT, R., MAZLOOM, A. R., CHUNG, C. Y., CAI, X., CAI, C. L., PEVNY, L., NICOLIS, S., MA'AYAN, A. & RENDL, M. 2012. Sox2 in the dermal papilla niche controls hair growth by fine-tuning BMP signaling in differentiating hair shaft progenitors. *Dev Cell*, 23, 981-94.
- CLAYTON, K., VALLEJO, A. F., DAVIES, J., SIRVENT, S. & POLAK, M. E. 2017. Langerhans Cells- Programmed by the Epidermis. *Front Immunol*, 8, 1676.
- COTSARELIS, G. 2006. Epithelial stem cells: a folliculocentric view. *J Invest Dermatol*, 126, 1459-68.
- COTSARELIS, G., SUN, T. T. & LAVKER, R. M. 1990. Label-retaining cells reside in the bulge area of pilosebaceous unit: implications for follicular stem cells, hair cycle, and skin carcinogenesis. *Cell*, 61, 1329-37.
- CUI, C. Y. & SCHLESSINGER, D. 2015. Eccrine sweat gland development and sweat secretion. *Exp Dermatol*, 24, 644-50.
- CUI, C. Y., YIN, M., SIMA, J., CHILDRESS, V., MICHEL, M., PIAO, Y. & SCHLESSINGER, D. 2014. Involvement of Wnt, Eda and Shh at defined stages of sweat gland development. *Development*, 141, 3752-60.
- DALE, B. A., HOLBROOK, K. A., KIMBALL, J. R., HOFF, M. & SUN, T. T. 1985. Expression of epidermal keratins and filaggrin during human fetal skin development. *J Cell Biol*, 101, 1257-69.
- DASGUPTA, R. & FUCHS, E. 1999. Multiple roles for activated LEF/TCF transcription complexes during hair follicle development and differentiation. *Development*, 126, 4557-68.

- DASZCZUK, P., MAZUREK, P., PIECZONKA, T. D., OLCZAK, A., BORYŃ Ł, M. & KOBIELAK, K. 2020. An Intrinsic Oscillation of Gene Networks Inside Hair Follicle Stem Cells: An Additional Layer That Can Modulate Hair Stem Cell Activities. *Front Cell Dev Biol*, 8, 595178.
- DEVENPORT, D. & FUCHS, E. 2008. Planar polarization in embryonic epidermis orchestrates global asymmetric morphogenesis of hair follicles. *Nat Cell Biol*, 10, 1257-68.
- DIDYCHUK, A. L., BUTCHER, S. E. & BROW, D. A. 2018. The life of U6 small nuclear RNA, from cradle to grave. *Rna*, 24, 437-460.
- DJURANOVIC, S., NAHVI, A. & GREEN, R. 2012. miRNA-mediated gene silencing by translational repression followed by mRNA deadenylation and decay. *Science*, 336, 237-40.
- DLUGOSZ, A. A., GLICK, A. B., TENNENBAUM, T., WEINBERG, W. C. & YUSPA, S. H. 1995. Isolation and utilization of epidermal keratinocytes for oncogene research. *Methods Enzymol*, 254, 3-20.
- DRISKELL, R. R., CLAVEL, C., RENDL, M. & WATT, F. M. 2011. Hair follicle dermal papilla cells at a glance. *J Cell Sci*, 124, 1179-82.
- DRISKELL, R. R., GIANGRECO, A., JENSEN, K. B., MULDER, K. W. & WATT, F. M. 2009. Sox2-positive dermal papilla cells specify hair follicle type in mammalian epidermis. *Development*, 136, 2815-23.
- DRISKELL, R. R., LICHTENBERGER, B. M., HOSTE, E., KRETZSCHMAR, K., SIMONS, B. D., CHARALAMBOUS, M., FERRON, S. R., HERAULT, Y., PAVLOVIC, G., FERGUSON-SMITH, A. C. & WATT, F. M. 2013. Distinct fibroblast lineages determine dermal architecture in skin development and repair. *Nature*, 504, 277-281.
- DUVERGER, O. & MORASSO, M. I. 2009. Epidermal patterning and induction of different hair types during mouse embryonic development. *Birth Defects Res C Embryo Today*, 87, 263-72.
- EBERT, M. S. & SHARP, P. A. 2012. Roles for microRNAs in conferring robustness to biological processes. *Cell*, 149, 515-24.
- ELBASHIR, S. M., HARBORTH, J., LENDECKEL, W., YALCIN, A., WEBER, K. & TUSCHL, T. 2001. Duplexes of 21-nucleotide RNAs mediate RNA interference in cultured mammalian cells. *Nature*, 411, 494-8.
- ELLIS, T., GAMBARDELLA, L., HORCHER, M., TSCHANZ, S., CAPOL, J., BERTRAM, P., JOCHUM, W., BARRANDON, Y. & BUSSLINGER, M. 2001. The transcriptional repressor CDP (Cutl1) is essential for epithelial cell differentiation of the lung and the hair follicle. *Genes Dev*, 15, 2307-19.
- ENSHELL-SEIJFFERS, D., LINDON, C., KASHIWAGI, M. & MORGAN, B. A. 2010. β -catenin Activity in the Dermal Papilla Regulates Morphogenesis and Regeneration of Hair. *Developmental Cell*, 18, 633-642.
- ESQUELA-KERSCHER, A. & SLACK, F. J. 2006. Oncomirs - microRNAs with a role in cancer. *Nat Rev Cancer*, 6, 259-69.
- FARH, K. K., GRIMSON, A., JAN, C., LEWIS, B. P., JOHNSTON, W. K., LIM, L. P., BURGE, C. B. & BARTEL, D. P. 2005. The widespread impact of mammalian MicroRNAs on mRNA repression and evolution. *Science*, 310, 1817-21.
- FARRELL, R. E. 2010. Chapter 13 - Practical Nucleic Acid Hybridization. In: FARRELL, R. E. (ed.) *RNA Methodologies (Fourth Edition)*. San Diego: Academic Press.
- FERGUSON, B. M., BROCKDORFF, N., FORMSTONE, E., NGYUEN, T., KRONMILLER, J. E. & ZONANA, J. 1997. Cloning of Tabby, the murine homolog of the human EDA gene: evidence for a membrane-associated protein with a short collagenous domain. *Hum Mol Genet*, 6, 1589-94.
- FESSING, M. Y., MARDARYEV, A. N., GDULA, M. R., SHAROV, A. A., SHAROVA, T. Y., RAPISARDA, V., GORDON, K. B., SMORODCHENKO, A. D., POTERLOWICZ, K., FERONE, G., KOHWI, Y., MISSERO, C., KOHWI-SHIGEMATSU, T. & BOTCHKAREV, V. A. 2011. p63 regulates Satb1 to control tissue-specific chromatin remodeling during development of the epidermis. *J Cell Biol*, 194, 825-39.

- FESTA, E., FRETZ, J., BERRY, R., SCHMIDT, B., RODEHEFFER, M., HOROWITZ, M. & HORSLEY, V. 2011. Adipocyte lineage cells contribute to the skin stem cell niche to drive hair cycling. *Cell*, 146, 761-71.
- FIRE, A., XU, S., MONTGOMERY, M. K., KOSTAS, S. A., DRIVER, S. E. & MELLO, C. C. 1998. Potent and specific genetic interference by double-stranded RNA in *Caenorhabditis elegans*. *Nature*, 391, 806-11.
- FOITZIK, K., LINDNER, G., MUELLER-ROEVER, S., MAURER, M., BOTCHKAREVA, N., BOTCHKAREV, V., HANDJISKI, B., METZ, M., HIBINO, T., SOMA, T., DOTTO, G. P. & PAUS, R. 2000. Control of murine hair follicle regression (catagen) by TGF-beta1 in vivo. *Faseb j*, 14, 752-60.
- FOLGUERAS, ALICIA R., GUO, X., PASOLLI, H. A., STOKES, N., POLAK, L., ZHENG, D. & FUCHS, E. 2013. Architectural Niche Organization by LHX2 Is Linked to Hair Follicle Stem Cell Function. *Cell Stem Cell*, 13, 314-327.
- FORNI, M. F., TROMBETTA-LIMA, M. & SOGAYAR, M. C. 2012. Stem cells in embryonic skin development. *Biol Res*, 45, 215-22.
- FRANCES, D. & NIEMANN, C. 2012. Stem cell dynamics in sebaceous gland morphogenesis in mouse skin. *Dev Biol*, 363, 138-46.
- FRANK, F., SONENBERG, N. & NAGAR, B. 2010. Structural basis for 5'-nucleotide base-specific recognition of guide RNA by human AGO2. *Nature*, 465, 818-22.
- FUCHS, E. 2007. Scratching the surface of skin development. *Nature*, 445, 834-42.
- FUCHS, E. & GREEN, H. 1980. Changes in keratin gene expression during terminal differentiation of the keratinocyte. *Cell*, 19, 1033-42.
- FUCHS, E. & HORSLEY, V. 2008. More than one way to skin. *Genes Dev*, 22, 976-85.
- FUCHS, E. & RAGHAVAN, S. 2002. Getting under the skin of epidermal morphogenesis. *Nat Rev Genet*, 3, 199-209.
- FUCHS, E. & WEBER, K. 1994. Intermediate filaments: structure, dynamics, function, and disease. *Annu Rev Biochem*, 63, 345-82.
- GAMA-NORTON, L., BOTEZATU, L., HERRMANN, S., SCHWEIZER, M., ALVES, P. M., HAUSER, H. & WIRTH, D. 2011. Lentivirus production is influenced by SV40 large T-antigen and chromosomal integration of the vector in HEK293 cells. *Hum Gene Ther*, 22, 1269-79.
- GE, M., LIU, C., LI, L., LAN, M., YU, Y., GU, L., SU, Y., ZHANG, K., ZHANG, Y., WANG, T., LIU, F., LI, M., XIONG, L., WANG, K., HE, T., DAI, Y., ZHAO, Y., LI, N., YU, Z. & MENG, Q. 2019. miR-29a/b1 Inhibits Hair Follicle Stem Cell Lineage Progression by Spatiotemporally Suppressing WNT and BMP Signaling. *Cell Rep*, 29, 2489-2504.e4.
- GE, Y., GOMEZ, N. C., ADAM, R. C., NIKOLOVA, M., YANG, H., VERMA, A., LU, C. P., POLAK, L., YUAN, S., ELEMENTO, O. & FUCHS, E. 2017. Stem Cell Lineage Infidelity Drives Wound Repair and Cancer. *Cell*, 169, 636-650.e14.
- GENANDER, M., COOK, P. J., RAMSKÖLD, D., KEYES, B. E., MERTZ, A. F., SANDBERG, R. & FUCHS, E. 2014. BMP signaling and its pSMAD1/5 target genes differentially regulate hair follicle stem cell lineages. *Cell Stem Cell*, 15, 619-33.
- GERBER, P. A., BUHREN, B. A., SCHRUMPF, H., HOMEY, B., ZLOTNIK, A. & HEVEZI, P. 2014. The top skin-associated genes: a comparative analysis of human and mouse skin transcriptomes. *Biol Chem*, 395, 577-91.
- GIRAUD-TRIBOULT, K., ROCHON-BEAUCOURT, C., NISSAN, X., CHAMPON, B., AUBERT, S. & PIÉTU, G. 2011. Combined mRNA and microRNA profiling reveals that miR-148a and miR-20b control human mesenchymal stem cell phenotype via EPAS1. *Physiol Genomics*, 43, 77-86.
- GLAICH, O., PARIKH, S., BELL, R. E., MEKAHEL, K., DONYO, M., LEADER, Y., SHAYEVITCH, R., SHEINBOIM, D., YANNAI, S., HOLLANDER, D., MELAMED, Z., LEV-MAOR, G., AST, G. & LEVY, C. 2019. DNA methylation directs microRNA biogenesis in mammalian cells. *Nat Commun*, 10, 5657.
- GRASSMEYER, J., MUKHERJEE, M., DERISO, J., HETTINGER, C., BAILEY, M., SINHA, S., VISVADER, J. E., ZHAO, H., FOGARTY, E. & SURENDRAN, K. 2017. Elf5 is a principal cell lineage specific

- transcription factor in the kidney that contributes to Aqp2 and Avpr2 gene expression. *Dev Biol*, 424, 77-89.
- GRECO, V., CHEN, T., RENDL, M., SCHOBBER, M., PASOLLI, H. A., STOKES, N., DELA CRUZ-RACELIS, J. & FUCHS, E. 2009. A two-step mechanism for stem cell activation during hair regeneration. *Cell Stem Cell*, 4, 155-69.
- GRIMSON, A., FARH, K. K., JOHNSTON, W. K., GARRETT-ENGELE, P., LIM, L. P. & BARTEL, D. P. 2007. MicroRNA targeting specificity in mammals: determinants beyond seed pairing. *Mol Cell*, 27, 91-105.
- GRITLI-LINDE, A., HALLBERG, K., HARFE, B. D., REYAHY, A., KANNIUS-JANSON, M., NILSSON, J., COBOURNE, M. T., SHARPE, P. T., MCMAHON, A. P. & LINDE, A. 2007. Abnormal hair development and apparent follicular transformation to mammary gland in the absence of hedgehog signaling. *Dev Cell*, 12, 99-112.
- HA, M. & KIM, V. N. 2014. Regulation of microRNA biogenesis. *Nat Rev Mol Cell Biol*, 15, 509-24.
- HAMILTON, A. J. & BAULCOMBE, D. C. 1999. A species of small antisense RNA in posttranscriptional gene silencing in plants. *Science*, 286, 950-2.
- HAMMOND, S. M. 2015. An overview of microRNAs. *Adv Drug Deliv Rev*, 87, 3-14.
- HAMMOND, S. M., BOETTCHER, S., CAUDY, A. A., KOBAYASHI, R. & HANNON, G. J. 2001. Argonaute2, a link between genetic and biochemical analyses of RNAi. *Science*, 293, 1146-50.
- HAN, C. & WANG, W. 2018. MicroRNA-129-5p suppresses cell proliferation, migration and invasion via targeting ROCK1 in osteosarcoma. *Mol Med Rep*, 17, 4777-4784.
- HAN, J., LEE, Y., YEOM, K. H., KIM, Y. K., JIN, H. & KIM, V. N. 2004. The Drosha-DGCR8 complex in primary microRNA processing. *Genes Dev*, 18, 3016-27.
- HAN, J., LEE, Y., YEOM, K. H., NAM, J. W., HEO, I., RHEE, J. K., SOHN, S. Y., CHO, Y., ZHANG, B. T. & KIM, V. N. 2006. Molecular basis for the recognition of primary microRNAs by the Drosha-DGCR8 complex. *Cell*, 125, 887-901.
- HANDJISKI, B. K., EICHMÜLLER, S., HOFMANN, U., CZARNETZKI, B. M. & PAUS, R. 1994. Alkaline phosphatase activity and localization during the murine hair cycle. *Br J Dermatol*, 131, 303-10.
- HANSEN, L. S., COGGLE, J. E., WELLS, J. & CHARLES, M. W. 1984. The influence of the hair cycle on the thickness of mouse skin. *Anat Rec*, 210, 569-73.
- HAREL, S., HIGGINS, C. A., CERISE, J. E., DAI, Z., CHEN, J. C., CLYNES, R. & CHRISTIANO, A. M. 2015. Pharmacologic inhibition of JAK-STAT signaling promotes hair growth. *Sci Adv*, 1, e1500973.
- HE, M. & XUE, Y. 2017. MicroRNA-148a suppresses proliferation and invasion potential of non-small cell lung carcinomas via regulation of STAT3. *Oncotargets Ther*, 10, 1353-1361.
- HEBERT, J. M., ROSENQUIST, T., GOTZ, J. & MARTIN, G. R. 1994. FGF5 as a regulator of the hair growth cycle: evidence from targeted and spontaneous mutations. *Cell*, 78, 1017-25.
- HEITMAN, N., SENNETT, R., MOK, K. W., SAXENA, N., SRIVASTAVA, D., MARTINO, P., GRISANTI, L., WANG, Z., MA'AYAN, A., ROMPOLAS, P. & RENDL, M. 2020. Dermal sheath contraction powers stem cell niche relocation during hair cycle regression. *Science*, 367, 161-166.
- HENNINGS, H., MICHAEL, D., CHENG, C., STEINERT, P., HOLBROOK, K. & YUSPA, S. H. 1980. Calcium regulation of growth and differentiation of mouse epidermal cells in culture. *Cell*, 19, 245-54.
- HEO, I., JOO, C., CHO, J., HA, M., HAN, J. & KIM, V. N. 2008. Lin28 mediates the terminal uridylation of let-7 precursor MicroRNA. *Mol Cell*, 32, 276-84.
- HIGGINS, C. A., CHEN, J. C., CERISE, J. E., JAHODA, C. A. & CHRISTIANO, A. M. 2013. Microenvironmental reprogramming by three-dimensional culture enables dermal papilla cells to induce de novo human hair-follicle growth. *Proc Natl Acad Sci U S A*, 110, 19679-88.
- HIGGINS, C. A., WESTGATE, G. E. & JAHODA, C. A. 2009. From telogen to exogen: mechanisms underlying formation and subsequent loss of the hair club fiber. *J Invest Dermatol*, 129, 2100-8.
- HONMA, M., BENITAH, S. A. & WATT, F. M. 2006. Role of LIM kinases in normal and psoriatic human epidermis. *Mol Biol Cell*, 17, 1888-96.

- HORSLEY, V., ALIPRANTIS, A. O., POLAK, L., GLIMCHER, L. H. & FUCHS, E. 2008. NFATc1 balances quiescence and proliferation of skin stem cells. *Cell*, 132, 299-310.
- HORSLEY, V., O'CARROLL, D., TOOZE, R., OHINATA, Y., SAITOU, M., OBUKHANYCH, T., NUSSENZWEIG, M., TARAKHOVSKY, A. & FUCHS, E. 2006. Blimp1 defines a progenitor population that governs cellular input to the sebaceous gland. *Cell*, 126, 597-609.
- HSU, Y. C., LI, L. & FUCHS, E. 2014. Emerging interactions between skin stem cells and their niches. *Nat Med*, 20, 847-56.
- HSU, Y. C., PASOLLI, H. A. & FUCHS, E. 2011. Dynamics between stem cells, niche, and progeny in the hair follicle. *Cell*, 144, 92-105.
- HU, H. Y., YAN, Z., XU, Y., HU, H., MENZEL, C., ZHOU, Y. H., CHEN, W. & KHAITOVICH, P. 2009. Sequence features associated with microRNA strand selection in humans and flies. *BMC Genomics*, 10, 413.
- HU, M. S., BORRELLI, M. R., HONG, W. X., MALHOTRA, S., CHEUNG, A. T. M., RANSOM, R. C., RENNERT, R. C., MORRISON, S. D., LORENZ, H. P. & LONGAKER, M. T. 2018a. Embryonic skin development and repair. *Organogenesis*, 14, 46-63.
- HU, Y., CONVERSE, C., LYONS, M. C. & HSU, W. H. 2018b. Neural control of sweat secretion: a review. *Br J Dermatol*, 178, 1246-1256.
- HUANG, F., ZHAO, J. L., WANG, L., GAO, C. C., LIANG, S. Q., AN, D. J., BAI, J., CHEN, Y., HAN, H. & QIN, H. Y. 2017. miR-148a-3p Mediates Notch Signaling to Promote the Differentiation and M1 Activation of Macrophages. *Front Immunol*, 8, 1327.
- HUANG, H., KONG, D., BYUN, K. H., YE, C., KODA, S., LEE, D. H., OH, B. C., LEE, S. W., LEE, B., ZABOLOTNY, J. M., KIM, M. S., BJØRBAEK, C., LOWELL, B. B. & KIM, Y. B. 2012. Rho-kinase regulates energy balance by targeting hypothalamic leptin receptor signaling. *Nat Neurosci*, 15, 1391-8.
- HUELSKEN, J., VOGEL, R., ERDMANN, B., COTSARELIS, G. & BIRCHMEIER, W. 2001. beta-Catenin controls hair follicle morphogenesis and stem cell differentiation in the skin. *Cell*, 105, 533-45.
- HUH, S. H., NÄRHI, K., LINDFORS, P. H., HÄÄRÄ, O., YANG, L., ORNITZ, D. M. & MIKKOLA, M. L. 2013. Fgf20 governs formation of primary and secondary dermal condensations in developing hair follicles. *Genes Dev*, 27, 450-8.
- ICHIHARA, A., JINNIN, M., YAMANE, K., FUJISAWA, A., SAKAI, K., MASUGUCHI, S., FUKUSHIMA, S., MARUO, K. & IHN, H. 2011. microRNA-mediated keratinocyte hyperproliferation in psoriasis vulgaris. *Br J Dermatol*, 165, 1003-10.
- IIDA, M., IHARA, S. & MATSUZAKI, T. 2007. Hair cycle-dependent changes of alkaline phosphatase activity in the mesenchyme and epithelium in mouse vibrissal follicles. *Dev Growth Differ*, 49, 185-95.
- ITO, M., KIZAWA, K., HAMADA, K. & COTSARELIS, G. 2004. Hair follicle stem cells in the lower bulge form the secondary germ, a biochemically distinct but functionally equivalent progenitor cell population, at the termination of catagen. *Differentiation*, 72, 548-57.
- JAHODA, C. A., HORNE, K. A. & OLIVER, R. F. 1984. Induction of hair growth by implantation of cultured dermal papilla cells. *Nature*, 311, 560-2.
- JAHODA, C. A. B., REYNOLDS, A. J. & OLIVER, R. F. 1993. Induction of Hair Growth in Ear Wounds by Cultured Dermal Papilla Cells. *Journal of Investigative Dermatology*, 101, 584-590.
- JAKS, V., BARKER, N., KASPER, M., VAN ES, J. H., SNIPPERT, H. J., CLEVERS, H. & TOFTGÅRD, R. 2008. Lgr5 marks cycling, yet long-lived, hair follicle stem cells. *Nat Genet*, 40, 1291-9.
- JANG, Y. N. & BAIK, E. J. 2013. JAK-STAT pathway and myogenic differentiation. *Jakstat*, 2, e23282.
- JENSEN, K. B., COLLINS, C. A., NASCIMENTO, E., TAN, D. W., FRYE, M., ITAMI, S. & WATT, F. M. 2009. Lrig1 Expression Defines a Distinct Multipotent Stem Cell Population in Mammalian Epidermis. *Cell Stem Cell*, 4, 427-439.

- JENSEN, U. B., YAN, X., TRIEL, C., WOO, S. H., CHRISTENSEN, R. & OWENS, D. M. 2008. A distinct population of clonogenic and multipotent murine follicular keratinocytes residing in the upper isthmus. *J Cell Sci*, 121, 609-17.
- JO, M. H., SHIN, S., JUNG, S. R., KIM, E., SONG, J. J. & HOHNG, S. 2015. Human Argonaute 2 Has Diverse Reaction Pathways on Target RNAs. *Mol Cell*, 59, 117-24.
- KADAJA, M., KEYES, B. E., LIN, M., PASOLLI, H. A., GENANDER, M., POLAK, L., STOKES, N., ZHENG, D. & FUCHS, E. 2014. SOX9: a stem cell transcriptional regulator of secreted niche signaling factors. *Genes Dev*, 28, 328-41.
- KANNO, H., KUBO, A., YOSHIZUMI, T., MIKAMI, T. & MAEGAWA, J. 2013. Isolation of multipotent nestin-expressing stem cells derived from the epidermis of elderly humans and TAT-VHL peptide-mediated neuronal differentiation of these cells. *Int J Mol Sci*, 14, 9604-17.
- KARLSSON, L., BONDJERS, C. & BETSHOLTZ, C. 1999. Roles for PDGF-A and sonic hedgehog in development of mesenchymal components of the hair follicle. *Development*, 126, 2611-21.
- KAUFMAN, C. K., ZHOU, P., PASOLLI, H. A., RENDL, M., BOLOTIN, D., LIM, K. C., DAI, X., ALEGRE, M. L. & FUCHS, E. 2003. GATA-3: an unexpected regulator of cell lineage determination in skin. *Genes Dev*, 17, 2108-22.
- KAWAHARA, Y., ZINSHTEYN, B., CHENDRIMADA, T. P., SHIEKHATTAR, R. & NISHIKURA, K. 2007. RNA editing of the microRNA-151 precursor blocks cleavage by the Dicer-TRBP complex. *EMBO Rep*, 8, 763-9.
- KHVOROVA, A., REYNOLDS, A. & JAYASENA, S. D. 2003. Functional siRNAs and miRNAs exhibit strand bias. *Cell*, 115, 209-16.
- KIM, D., LANGMEAD, B. & SALZBERG, S. L. 2015. HISAT: a fast spliced aligner with low memory requirements. *Nat Methods*, 12, 357-60.
- KIM, J. E., LEE, Y. J., PARK, H. R., LEE, D. G., JEONG, K. H. & KANG, H. 2020. The Effect of JAK Inhibitor on the Survival, Anagen Re-Entry, and Hair Follicle Immune Privilege Restoration in Human Dermal Papilla Cells. *Int J Mol Sci*, 21.
- KIMURA-UEKI, M., ODA, Y., OKI, J., KOMI-KURAMOCHI, A., HONDA, E., ASADA, M., SUZUKI, M. & IMAMURA, T. 2012. Hair cycle resting phase is regulated by cyclic epithelial FGF18 signaling. *J Invest Dermatol*, 132, 1338-45.
- KLOEPPER, J. E., ERNST, N., KRIEGER, K., BODÓ, E., BÍRÓ, T., HASLAM, I. S., SCHMIDT-ULLRICH, R. & PAUS, R. 2014. NF- κ B activity is required for anagen maintenance in human hair follicles in vitro. *J Invest Dermatol*, 134, 2036-2038.
- KOBIELAK, K., PASOLLI, H. A., ALONSO, L., POLAK, L. & FUCHS, E. 2003. Defining BMP functions in the hair follicle by conditional ablation of BMP receptor IA. *J Cell Biol*, 163, 609-23.
- KOBIELAK, K., STOKES, N., DE LA CRUZ, J., POLAK, L. & FUCHS, E. 2007. Loss of a quiescent niche but not follicle stem cells in the absence of bone morphogenetic protein signaling. *Proc Natl Acad Sci U S A*, 104, 10063-8.
- KONNO, M., KOSEKI, J., ASAI, A., YAMAGATA, A., SHIMAMURA, T., MOTOOKA, D., OKUZAKI, D., KAWAMOTO, K., MIZUSHIMA, T., EGUCHI, H., TAKIGUCHI, S., SATOH, T., MIMORI, K., OCHIYA, T., DOKI, Y., OFUSA, K., MORI, M. & ISHII, H. 2019. Distinct methylation levels of mature microRNAs in gastrointestinal cancers. *Nat Commun*, 10, 3888.
- KOROSEC, A., FRECH, S., GESSLBAUER, B., VIERHAPPER, M., RADTKE, C., PETZELBAUER, P. & LICHTENBERGER, B. M. 2019. Lineage Identity and Location within the Dermis Determine the Function of Papillary and Reticular Fibroblasts in Human Skin. *J Invest Dermatol*, 139, 342-351.
- KOSTER, M. I., DAI, D., MARINARI, B., SANO, Y., COSTANZO, A., KARIN, M. & ROOP, D. R. 2007. p63 induces key target genes required for epidermal morphogenesis. *Proc Natl Acad Sci U S A*, 104, 3255-60.
- KOSTER, M. I., KIM, S., MILLS, A. A., DEMAYO, F. J. & ROOP, D. R. 2004. p63 is the molecular switch for initiation of an epithelial stratification program. *Genes Dev*, 18, 126-31.

- KOSTER, M. I. & ROOP, D. R. 2004. Genetic pathways required for epidermal morphogenesis. *Eur J Cell Biol*, 83, 625-9.
- KOSTER, M. I. & ROOP, D. R. 2007. Mechanisms regulating epithelial stratification. *Annu Rev Cell Dev Biol*, 23, 93-113.
- KOYANAGI, M., TAKAHASHI, J., ARAKAWA, Y., DOI, D., FUKUDA, H., HAYASHI, H., NARUMIYA, S. & HASHIMOTO, N. 2008. Inhibition of the Rho/ROCK pathway reduces apoptosis during transplantation of embryonic stem cell-derived neural precursors. *J Neurosci Res*, 86, 270-80.
- KREBSBACH, P. H. & VILLA-DIAZ, L. G. 2017. The Role of Integrin $\alpha 6$ (CD49f) in Stem Cells: More than a Conserved Biomarker. *Stem Cells Dev*, 26, 1090-1099.
- KRENDL, C., SHAPOSHNIKOV, D., RISHKO, V., ORI, C., ZIEGENHAIN, C., SASS, S., SIMON, L., MÜLLER, N. S., STRAUB, T., BROOKS, K. E., CHAVEZ, S. L., ENARD, W., THEIS, F. J. & DRUKKER, M. 2017. GATA2/3-TFAP2A/C transcription factor network couples human pluripotent stem cell differentiation to trophoderm with repression of pluripotency. *Proc Natl Acad Sci U S A*, 114, E9579-e9588.
- KRIEG, T. & AUMAILLEY, M. 2011. The extracellular matrix of the dermis: flexible structures with dynamic functions. *Exp Dermatol*, 20, 689-95.
- KRIEGER, K., MILLAR, S. E., MIKUDA, N., KRAHN, I., KLOPPER, J. E., BERTOLINI, M., SCHEIDEREIT, C., PAUS, R. & SCHMIDT-ULLRICH, R. 2018. NF- κ B Participates in Mouse Hair Cycle Control and Plays Distinct Roles in the Various Pelage Hair Follicle Types. *J Invest Dermatol*, 138, 256-264.
- KUBO, A., NAGAO, K., YOKOUCHI, M., SASAKI, H. & AMAGAI, M. 2009. External antigen uptake by Langerhans cells with reorganization of epidermal tight junction barriers. *J Exp Med*, 206, 2937-46.
- KÜMPER, S., MARDAKHEH, F. K., MCCARTHY, A., YEO, M., STAMP, G. W., PAUL, A., WORBOYS, J., SADOK, A., JØRGENSEN, C., GUICHARD, S. & MARSHALL, C. J. 2016. Rho-associated kinase (ROCK) function is essential for cell cycle progression, senescence and tumorigenesis. *Elife*, 5, e12994.
- LAMBERT, N. J., GU, S. G. & ZAHLER, A. M. 2011. The conformation of microRNA seed regions in native microRNPs is prearranged for presentation to mRNA targets. *Nucleic Acids Research*, 39, 4827-4835.
- LANDÁZURI, N. & LE DOUX, J. M. 2006. Complexation with chondroitin sulfate C and Polybrene rapidly purifies retrovirus from inhibitors of transduction and substantially enhances gene transfer. *Biotechnol Bioeng*, 93, 146-58.
- LATOS, P. A., SIENERTH, A. R., MURRAY, A., SENNER, C. E., MUTO, M., IKAWA, M., OXLEY, D., BURGE, S., COX, B. J. & HEMBERGER, M. 2015. Elf5-centered transcription factor hub controls trophoblast stem cell self-renewal and differentiation through stoichiometry-sensitive shifts in target gene networks. *Genes Dev*, 29, 2435-48.
- LAURIKKALA, J., MIKKOLA, M. L., JAMES, M., TUMMERS, M., MILLS, A. A. & THESLEFF, I. 2006. p63 regulates multiple signalling pathways required for ectodermal organogenesis and differentiation. *Development*, 133, 1553-63.
- LE DOUX, J. M., LANDAZURI, N., YARMUSH, M. L. & MORGAN, J. R. 2001. Complexation of retrovirus with cationic and anionic polymers increases the efficiency of gene transfer. *Hum Gene Ther*, 12, 1611-21.
- LECHLER, T. & FUCHS, E. 2005. Asymmetric cell divisions promote stratification and differentiation of mammalian skin. *Nature*, 437, 275-80.
- LEE, D., PROWSE, D. M. & BRISSETTE, J. L. 1999. Association between mouse nude gene expression and the initiation of epithelial terminal differentiation. *Dev Biol*, 208, 362-74.
- LEE, R. C., FEINBAUM, R. L. & AMBROS, V. 1993. The *C. elegans* heterochronic gene *lin-4* encodes small RNAs with antisense complementarity to *lin-14*. *Cell*, 75, 843-54.
- LEE, Y., AHN, C., HAN, J., CHOI, H., KIM, J., YIM, J., LEE, J., PROVOST, P., RÅDMARK, O., KIM, S. & KIM, V. N. 2003. The nuclear RNase III Drosha initiates microRNA processing. *Nature*, 425, 415-9.

- LEE, Y., HUR, I., PARK, S. Y., KIM, Y. K., SUH, M. R. & KIM, V. N. 2006. The role of PACT in the RNA silencing pathway. *Embo j*, 25, 522-32.
- LEE, Y., JEON, K., LEE, J. T., KIM, S. & KIM, V. N. 2002. MicroRNA maturation: stepwise processing and subcellular localization. *Embo j*, 21, 4663-70.
- LEE, Y., KIM, M., HAN, J., YEOM, K. H., LEE, S., BAEK, S. H. & KIM, V. N. 2004. MicroRNA genes are transcribed by RNA polymerase II. *Embo j*, 23, 4051-60.
- LEGRAND, J. M. D., ROY, E., ELLIS, J. J., FRANCOIS, M., BROOKS, A. J. & KHOSROTEHRANI, K. 2016. STAT5 Activation in the Dermal Papilla Is Important for Hair Follicle Growth Phase Induction. *J Invest Dermatol*, 136, 1781-1791.
- LEGUÉ, E. & NICOLAS, J. F. 2005. Hair follicle renewal: organization of stem cells in the matrix and the role of stereotyped lineages and behaviors. *Development*, 132, 4143-54.
- LI, E. R., OWENS, D. M., DJIAN, P. & WATT, F. M. 2000. Expression of involucrin in normal, hyperproliferative and neoplastic mouse keratinocytes. *Exp Dermatol*, 9, 431-8.
- LI, J., JIANG, T. X., HUGHES, M. W., WU, P., YU, J., WIDELITZ, R. B., FAN, G. & CHUONG, C. M. 2012. Progressive alopecia reveals decreasing stem cell activation probability during aging of mice with epidermal deletion of DNA methyltransferase 1. *J Invest Dermatol*, 132, 2681-90.
- LI, S., ZHENG, X., NIE, Y., CHEN, W., LIU, Z., TAO, Y., HU, X., HU, Y., QIAO, H., QI, Q., PEI, Q., CAI, D., YU, M. & MOU, C. 2018. Defining Key Genes Regulating Morphogenesis of Apocrine Sweat Gland in Sheepskin. *Front Genet*, 9, 739.
- LI, X., LI, S., LI, B., LI, Y., AMAN, S., XIA, K., YANG, Y., AHMAD, B. & WU, H. 2021. Acetylation of ELF5 suppresses breast cancer progression by promoting its degradation and targeting CCND1. *NPJ Precis Oncol*, 5, 20.
- LI, Z., HAN, S., WANG, X., HAN, F., ZHU, X., ZHENG, Z., WANG, H., ZHOU, Q., WANG, Y., SU, L., SHI, J., TANG, C. & HU, D. 2015. Rho kinase inhibitor Y-27632 promotes the differentiation of human bone marrow mesenchymal stem cells into keratinocyte-like cells in xeno-free conditioned medium. *Stem Cell Res Ther*, 6, 17.
- LIAO, Y., SMYTH, G. K. & SHI, W. 2014. featureCounts: an efficient general purpose program for assigning sequence reads to genomic features. *Bioinformatics*, 30, 923-30.
- LICHTI, U., ANDERS, J. & YUSPA, S. H. 2008. Isolation and short-term culture of primary keratinocytes, hair follicle populations and dermal cells from newborn mice and keratinocytes from adult mice for in vitro analysis and for grafting to immunodeficient mice. *Nat Protoc*, 3, 799-810.
- LIM, X. & NUSSE, R. 2013. Wnt signaling in skin development, homeostasis, and disease. *Cold Spring Harb Perspect Biol*, 5.
- LISSE, T. S., SAINI, V., ZHAO, H., LUDERER, H. F., GORI, F. & DEMAY, M. B. 2014. The vitamin D receptor is required for activation of cWnt and hedgehog signaling in keratinocytes. *Mol Endocrinol*, 28, 1698-706.
- LIU, H. & KOHANE, I. S. 2009. Tissue and process specific microRNA-mRNA co-expression in mammalian development and malignancy. *PLoS One*, 4, e5436.
- LIU, J., CARMELL, M. A., RIVAS, F. V., MARSDEN, C. G., THOMSON, J. M., SONG, J. J., HAMMOND, S. M., JOSHUA-TOR, L. & HANNON, G. J. 2004. Argonaute2 is the catalytic engine of mammalian RNAi. *Science*, 305, 1437-41.
- LIU, S., ZHANG, H. & DUAN, E. 2013. Epidermal development in mammals: key regulators, signals from beneath, and stem cells. *Int J Mol Sci*, 14, 10869-95.
- LIU, Y., LYLE, S., YANG, Z. & COTSARELIS, G. 2003. Keratin 15 promoter targets putative epithelial stem cells in the hair follicle bulge. *J Invest Dermatol*, 121, 963-8.
- LIU, Z., YANG, F., ZHAO, M., MA, L., LI, H., XIE, Y., NAI, R., CHE, T., SU, R., ZHANG, Y., WANG, R., WANG, Z. & LI, J. 2018. The intragenic mRNA-microRNA regulatory network during telogen-anagen hair follicle transition in the cashmere goat. *Sci Rep*, 8, 14227.
- LLAMES, S., GARCÍA-PÉREZ, E., MEANA, Á., LARCHER, F. & DEL RÍO, M. 2015. Feeder Layer Cell Actions and Applications. *Tissue Eng Part B Rev*, 21, 345-53.

- LOCK, F. E. & HOTCHIN, N. A. 2009. Distinct roles for ROCK1 and ROCK2 in the regulation of keratinocyte differentiation. *PLoS One*, 4, e8190.
- LOPEZ-PAJARES, V., YAN, K., ZARNEGAR, B. J., JAMESON, K. L. & KHAVARI, P. A. 2013. Genetic pathways in disorders of epidermal differentiation. *Trends Genet*, 29, 31-40.
- LOVE, M. I., HUBER, W. & ANDERS, S. 2014. Moderated estimation of fold change and dispersion for RNA-seq data with DESeq2. *Genome Biol*, 15, 550.
- LU, C. & FUCHS, E. 2014. Sweat gland progenitors in development, homeostasis, and wound repair. *Cold Spring Harb Perspect Med*, 4.
- LU, C. P., POLAK, L., ROCHA, A. S., PASOLLI, H. A., CHEN, S. C., SHARMA, N., BLANPAIN, C. & FUCHS, E. 2012. Identification of stem cell populations in sweat glands and ducts reveals roles in homeostasis and wound repair. *Cell*, 150, 136-50.
- LUO, Q., LI, W., ZHAO, T., TIAN, X., LIU, Y. & ZHANG, X. 2015. Role of miR-148a in cutaneous squamous cell carcinoma by repression of MAPK pathway. *Arch Biochem Biophys*, 583, 47-54.
- LYLE, S., CHRISTOFIDOU-SOLOMIDOU, M., LIU, Y., ELDER, D. E., ALBELDA, S. & COTSARELIS, G. 1998. The C8/144B monoclonal antibody recognizes cytokeratin 15 and defines the location of human hair follicle stem cells. *J Cell Sci*, 111 (Pt 21), 3179-88.
- M'BONEKO, V. & MERKER, H. J. 1988. Development and morphology of the periderm of mouse embryos (days 9-12 of gestation). *Acta Anat (Basel)*, 133, 325-36.
- MACRAE, I. J., MA, E., ZHOU, M., ROBINSON, C. V. & DOUDNA, J. A. 2008. In vitro reconstitution of the human RISC-loading complex. *Proc Natl Acad Sci U S A*, 105, 512-7.
- MACRAE, I. J., ZHOU, K., LI, F., REPIC, A., BROOKS, A. N., CANDE, W. Z., ADAMS, P. D. & DOUDNA, J. A. 2006. Structural basis for double-stranded RNA processing by Dicer. *Science*, 311, 195-8.
- MANOCHANTR, S., MARUPANTHORN, K., TANTRAWATPAN, C., KHEOLAMAI, P., TANTIKANLAYAPORN, D. & SANGUANJIT, P. 2017. The Effects of BMP-2, miR-31, miR-106a, and miR-148a on Osteogenic Differentiation of MSCs Derived from Amnion in Comparison with MSCs Derived from the Bone Marrow. *Stem Cells Int*, 2017, 7257628.
- MARDARYEV, A. N., AHMED, M. I., VLAHOV, N. V., FESSING, M. Y., GILL, J. H., SHAROV, A. A. & BOTCHKAREVA, N. V. 2010. Micro-RNA-31 controls hair cycle-associated changes in gene expression programs of the skin and hair follicle. *Faseb j*, 24, 3869-81.
- MARDARYEV, A. N., LIU, B., RAPISARDA, V., POTERLOWICZ, K., MALASHCHUK, I., RUDOLF, J., SHAROV, A. A., JAHODA, C. A., FESSING, M. Y., BENITAH, S. A., XU, G. L. & BOTCHKAREV, V. A. 2016. Cbx4 maintains the epithelial lineage identity and cell proliferation in the developing stratified epithelium. *J Cell Biol*, 212, 77-89.
- MARDARYEV, A. N., MEIER, N., POTERLOWICZ, K., SHAROV, A. A., SHAROVA, T. Y., AHMED, M. I., RAPISARDA, V., LEWIS, C., FESSING, M. Y., RUENGER, T. M., BHAWAN, J., WERNER, S., PAUS, R. & BOTCHKAREV, V. A. 2011. Lhx2 differentially regulates Sox9, Tcf4 and Lgr5 in hair follicle stem cells to promote epidermal regeneration after injury. *Development*, 138, 4843-52.
- MARTINEZ, J. & TUSCHL, T. 2004. RISC is a 5' phosphomonoester-producing RNA endonuclease. *Genes Dev*, 18, 975-80.
- MARTINO, P. A., HEITMAN, N. & RENDL, M. 2021. The dermal sheath: An emerging component of the hair follicle stem cell niche. *Exp Dermatol*, 30, 512-521.
- MARTINSSON-AHLZÉN, H. S., LIBERAL, V., GRÜNENFELDER, B., CHAVES, S. R., SPRUCK, C. H. & REED, S. I. 2008. Cyclin-dependent kinase-associated proteins Cks1 and Cks2 are essential during early embryogenesis and for cell cycle progression in somatic cells. *Mol Cell Biol*, 28, 5698-709.
- MCELWEE, K. J., KISSLING, S., WENZEL, E., HUTH, A. & HOFFMANN, R. 2003. Cultured peribulbar dermal sheath cells can induce hair follicle development and contribute to the dermal sheath and dermal papilla. *J Invest Dermatol*, 121, 1267-75.
- MCGOWAN, K. M., TONG, X., COLUCCI-GUYON, E., LANGA, F., BABINET, C. & COULOMBE, P. A. 2002. Keratin 17 null mice exhibit age- and strain-dependent alopecia. *Genes Dev*, 16, 1412-22.

- MCMULLAN, R., LAX, S., ROBERTSON, V. H., RADFORD, D. J., BROAD, S., WATT, F. M., ROWLES, A., CROFT, D. R., OLSON, M. F. & HOTCHIN, N. A. 2003. Keratinocyte differentiation is regulated by the Rho and ROCK signaling pathway. *Curr Biol*, 13, 2185-9.
- MEDLEY, J. C., PANZADE, G. & ZINOVYEVA, A. Y. 2021. microRNA strand selection: Unwinding the rules. *Wiley Interdiscip Rev RNA*, 12, e1627.
- MEIJER, H. A., SMITH, E. M. & BUSHHELL, M. 2014. Regulation of miRNA strand selection: follow the leader? *Biochem Soc Trans*, 42, 1135-40.
- MESLER, A. L., VENIAMINOVA, N. A., LULL, M. V. & WONG, S. Y. 2017. Hair Follicle Terminal Differentiation Is Orchestrated by Distinct Early and Late Matrix Progenitors. *Cell Rep*, 19, 809-821.
- METZGER, D. E., XU, Y. & SHANNON, J. M. 2007. Elf5 is an epithelium-specific, fibroblast growth factor-sensitive transcription factor in the embryonic lung. *Dev Dyn*, 236, 1175-92.
- MI, S., CAI, T., HU, Y., CHEN, Y., HODGES, E., NI, F., WU, L., LI, S., ZHOU, H., LONG, C., CHEN, S., HANNON, G. J. & QI, Y. 2008. Sorting of small RNAs into Arabidopsis argonaute complexes is directed by the 5' terminal nucleotide. *Cell*, 133, 116-27.
- MILLAR, S. E. 2002. Molecular mechanisms regulating hair follicle development. *J Invest Dermatol*, 118, 216-25.
- MILLS, A. A., ZHENG, B., WANG, X. J., VOGEL, H., ROOP, D. R. & BRADLEY, A. 1999. p63 is a p53 homologue required for limb and epidermal morphogenesis. *Nature*, 398, 708-13.
- MILNER, Y., KASHGARIAN, M., SUDNIK, J., FILIPPI, M., KIZOULIS, M. & STENN, K. 2002. Exogen, Shedding Phase of the Hair Growth Cycle: Characterization of a Mouse Model. *Journal of Investigative Dermatology*, 119, 639-644.
- MINAKUCHI, Y., TAKESHITA, F., KOSAKA, N., SASAKI, H., YAMAMOTO, Y., KOUNO, M., HONMA, K., NAGAHARA, S., HANAI, K., SANO, A., KATO, T., TERADA, M. & OCHIYA, T. 2004. Atelocollagen-mediated synthetic small interfering RNA delivery for effective gene silencing in vitro and in vivo. *Nucleic Acids Res*, 32, e109.
- MISKA, E. A., ALVAREZ-SAAVEDRA, E., ABBOTT, A. L., LAU, N. C., HELLMAN, A. B., MCGONAGLE, S. M., BARTEL, D. P., AMBROS, V. R. & HORVITZ, H. R. 2007. Most Caenorhabditis elegans microRNAs are individually not essential for development or viability. *PLoS Genet*, 3, e215.
- MOESTRUP, K. S., ANDERSEN, M. S. & JENSEN, K. B. 2017. Isolation and In Vitro Characterization of Epidermal Stem Cells. *Methods Mol Biol*, 1553, 67-83.
- MOK, K. W., SAXENA, N., HEITMAN, N., GRISANTI, L., SRIVASTAVA, D., MURARO, M. J., JACOB, T., SENNETT, R., WANG, Z., SU, Y., YANG, L. M., MA'AYAN, A., ORNITZ, D. M., KASPER, M. & RENDL, M. 2019. Dermal Condensate Niche Fate Specification Occurs Prior to Formation and Is Placode Progenitor Dependent. *Dev Cell*, 48, 32-48.e5.
- MOLL, R., DIVO, M. & LANGBEIN, L. 2008. The human keratins: biology and pathology. *Histochem Cell Biol*, 129, 705-33.
- MORIYAMA, M., DURHAM, A. D., MORIYAMA, H., HASEGAWA, K., NISHIKAWA, S., RADTKE, F. & OSAWA, M. 2008. Multiple roles of Notch signaling in the regulation of epidermal development. *Dev Cell*, 14, 594-604.
- MORRIS, R. J., LIU, Y., MARLES, L., YANG, Z., TREMPUS, C., LI, S., LIN, J. S., SAWICKI, J. A. & COTSARELIS, G. 2004. Capturing and profiling adult hair follicle stem cells. *Nat Biotechnol*, 22, 411-7.
- MORRISON, K. M., MIESEGAES, G. R., LUMPKIN, E. A. & MARICICH, S. M. 2009. Mammalian Merkel cells are descended from the epidermal lineage. *Dev Biol*, 336, 76-83.
- MULLER-ROVER, S., HANDJISKI, B., VAN DER VEEN, C., EICHMULLER, S., FOITZIK, K., MCKAY, I. A., STENN, K. S. & PAUS, R. 2001. A comprehensive guide for the accurate classification of murine hair follicles in distinct hair cycle stages. *J Invest Dermatol*, 117, 3-15.
- MUSTONEN, T., PISPA, J., MIKKOLA, M. L., PUMMILA, M., KANGAS, A. T., PAKKASJÄRVI, L., JAATINEN, R. & THESLEFF, I. 2003. Stimulation of ectodermal organ development by Ectodysplasin-A1. *Dev Biol*, 259, 123-36.

- MYUNG, P. S., TAKEO, M., ITO, M. & ATIT, R. P. 2013. Epithelial Wnt ligand secretion is required for adult hair follicle growth and regeneration. *J Invest Dermatol*, 133, 31-41.
- MÜLLER-RÖVER, S., TOKURA, Y., WELKER, P., FURUKAWA, F., WAKITA, H., TAKIGAWA, M. & PAUS, R. 1999. E- and P-cadherin expression during murine hair follicle morphogenesis and cycling. *Exp Dermatol*, 8, 237-46.
- NAGOSA, S., LEESCH, F., PUTIN, D., BHATTACHARYA, S., ALTSHULER, A., SERROR, L., AMITAI-LANGE, A., NASSER, W., ABERDAM, E., ROULEAU, M., TATTIKOTA, S. G., POY, M. N., ABERDAM, D. & SHALOM-FEUERSTEIN, R. 2017. microRNA-184 Induces a Commitment Switch to Epidermal Differentiation. *Stem Cell Reports*, 9, 1991-2004.
- NAKAGAWA, O., FUJISAWA, K., ISHIZAKI, T., SAITO, Y., NAKAO, K. & NARUMIYA, S. 1996. ROCK-I and ROCK-II, two isoforms of Rho-associated coiled-coil forming protein serine/threonine kinase in mice. *FEBS Lett*, 392, 189-93.
- NGUYEN, B. C., LEFORT, K., MANDINOVA, A., ANTONINI, D., DEVGAN, V., DELLA GATTA, G., KOSTER, M. I., ZHANG, Z., WANG, J., TOMMASI DI VIGNANO, A., KITAJEWSKI, J., CHIORINO, G., ROOP, D. R., MISSERO, C. & DOTTO, G. P. 2006a. Cross-regulation between Notch and p63 in keratinocyte commitment to differentiation. *Genes Dev*, 20, 1028-42.
- NGUYEN, H., RENDL, M. & FUCHS, E. 2006b. Tcf3 governs stem cell features and represses cell fate determination in skin. *Cell*, 127, 171-83.
- NISHIMURA, E. K., JORDAN, S. A., OSHIMA, H., YOSHIDA, H., OSAWA, M., MORIYAMA, M., JACKSON, I. J., BARRANDON, Y., MIYACHI, Y. & NISHIKAWA, S. 2002. Dominant role of the niche in melanocyte stem-cell fate determination. *Nature*, 416, 854-60.
- NISHIMURA, E. K., SUZUKI, M., IGRAS, V., DU, J., LONNING, S., MIYACHI, Y., ROES, J., BEERMANN, F. & FISHER, D. E. 2010. Key roles for transforming growth factor beta in melanocyte stem cell maintenance. *Cell Stem Cell*, 6, 130-40.
- NITHYA, S., RADHIKA, T. & JEDDY, N. 2015. Loricrin - an overview. *J Oral Maxillofac Pathol*, 19, 64-8.
- NORAMLY, S., FREEMAN, A. & MORGAN, B. A. 1999. beta-catenin signaling can initiate feather bud development. *Development*, 126, 3509.
- NORUM, J. H., BERGSTRÖM, Å., ANDERSSON, A. B., KUIPER, R. V., HOELZL, M. A., SØRLIE, T. & TOFTGÅRD, R. 2015. A conditional transgenic mouse line for targeted expression of the stem cell marker LGR5. *Dev Biol*, 404, 35-48.
- NOWAK, J. A. & FUCHS, E. 2009. Isolation and culture of epithelial stem cells. *Methods Mol Biol*, 482, 215-32.
- NOWAK, J. A., POLAK, L., PASOLLI, H. A. & FUCHS, E. 2008. Hair follicle stem cells are specified and function in early skin morphogenesis. *Cell Stem Cell*, 3, 33-43.
- NÄRHI, K., JÄRVINEN, E., BIRCHMEIER, W., TAKETO, M. M., MIKKOLA, M. L. & THESLEFF, I. 2008. Sustained epithelial beta-catenin activity induces precocious hair development but disrupts hair follicle down-growth and hair shaft formation. *Development*, 135, 1019-28.
- O'BRIEN, J., HAYDER, H., ZAYED, Y. & PENG, C. 2018. Overview of MicroRNA Biogenesis, Mechanisms of Actions, and Circulation. *Front Endocrinol (Lausanne)*, 9, 402.
- O'CARROLL, D. & SCHAEFER, A. 2013. General principals of miRNA biogenesis and regulation in the brain. *Neuropsychopharmacology*, 38, 39-54.
- OAKES, S. R., NAYLOR, M. J., ASSELIN-LABAT, M. L., BLAZEK, K. D., GARDINER-GARDEN, M., HILTON, H. N., KAZLAUSKAS, M., PRITCHARD, M. A., CHODOSH, L. A., PFEFFER, P. L., LINDEMAN, G. J., VISVADER, J. E. & ORMANDY, C. J. 2008. The Ets transcription factor Elf5 specifies mammary alveolar cell fate. *Genes Dev*, 22, 581-6.
- OSHIMA, H., ROCHAT, A., KEDZIA, C., KOBAYASHI, K. & BARRANDON, Y. 2001. Morphogenesis and renewal of hair follicles from adult multipotent stem cells. *Cell*, 104, 233-45.
- OSHIMORI, N. & FUCHS, E. 2012. Paracrine TGF- β signaling counterbalances BMP-mediated repression in hair follicle stem cell activation. *Cell Stem Cell*, 10, 63-75.
- OUSPENSKAIA, T., MATOS, I., MERTZ, A. F., FIORE, V. F. & FUCHS, E. 2016. WNT-SHH Antagonism Specifies and Expands Stem Cells prior to Niche Formation. *Cell*, 164, 156-169.

- OZATA, D. M., GAINETDINOV, I., ZOCH, A., O'CARROLL, D. & ZAMORE, P. D. 2019. PIWI-interacting RNAs: small RNAs with big functions. *Nat Rev Genet*, 20, 89-108.
- PALADINI, R. D., SALEH, J., QIAN, C., XU, G. X. & RUBIN, L. L. 2005. Modulation of hair growth with small molecule agonists of the hedgehog signaling pathway. *J Invest Dermatol*, 125, 638-46.
- PALAZZO, E., KELLETT, M. D., CATAISSON, C., BIBLE, P. W., BHATTACHARYA, S., SUN, H. W., GORMLEY, A. C., YUSPA, S. H. & MORASSO, M. I. 2017. A novel DLX3-PKC integrated signaling network drives keratinocyte differentiation. *Cell Death Differ*, 24, 717-730.
- PAN, Y., LIN, M. H., TIAN, X., CHENG, H. T., GRIDLEY, T., SHEN, J. & KOPAN, R. 2004. gamma-secretase functions through Notch signaling to maintain skin appendages but is not required for their patterning or initial morphogenesis. *Dev Cell*, 7, 731-43.
- PANTELEYEV, A. A. 2018. Functional anatomy of the hair follicle: The Secondary Hair Germ. *Exp Dermatol*, 27, 701-720.
- PANTELEYEV, A. A., JAHODA, C. A. & CHRISTIANO, A. M. 2001. Hair follicle predetermination. *J Cell Sci*, 114, 3419-31.
- PARK, J. E., HEO, I., TIAN, Y., SIMANSHU, D. K., CHANG, H., JEE, D., PATEL, D. J. & KIM, V. N. 2011. Dicer recognizes the 5' end of RNA for efficient and accurate processing. *Nature*, 475, 201-5.
- PARK, M. S., PHAN, H. D., BUSCH, F., HINCKLEY, S. H., BRACKBILL, J. A., WYSOCKI, V. H. & NAKANISHI, K. 2017. Human Argonaute3 has slicer activity. *Nucleic Acids Res*, 45, 11867-11877.
- PARKER, J. S., PARIZOTTO, E. A., WANG, M., ROE, S. M. & BARFORD, D. 2009. Enhancement of the seed-target recognition step in RNA silencing by a PIWI/MID domain protein. *Mol Cell*, 33, 204-14.
- PAUS, R. & COTSARELIS, G. 1999. The biology of hair follicles. *N Engl J Med*, 341, 491-7.
- PAUS, R., MÜLLER-RÖVER, S., VAN DER VEEN, C., MAURER, M., EICHMÜLLER, S., LING, G., HOFMANN, U., FOITZIK, K., MECKLENBURG, L. & HANDJISKI, B. 1999. A comprehensive guide for the recognition and classification of distinct stages of hair follicle morphogenesis. *J Invest Dermatol*, 113, 523-32.
- PEDRANZINI, L., LEITCH, A. & BROMBERG, J. 2004. Stat3 is required for the development of skin cancer. *J Clin Invest*, 114, 619-22.
- PENA, J. C., KELEKAR, A., FUCHS, E. V. & THOMPSON, C. B. 1999. Manipulation of outer root sheath cell survival perturbs the hair-growth cycle. *Embo j*, 18, 3596-603.
- PLIKUS, M., WANG, W. P., LIU, J., WANG, X., JIANG, T. X. & CHUONG, C. M. 2004. Morpho-regulation of ectodermal organs: integument pathology and phenotypic variations in K14-Noggin engineered mice through modulation of bone morphogenic protein pathway. *Am J Pathol*, 164, 1099-114.
- PLIKUS, M. V. 2012. New activators and inhibitors in the hair cycle clock: targeting stem cells' state of competence. *J Invest Dermatol*, 132, 1321-4.
- PLIKUS, M. V., MAYER, J. A., DE LA CRUZ, D., BAKER, R. E., MAINI, P. K., MAXSON, R. & CHUONG, C. M. 2008. Cyclic dermal BMP signalling regulates stem cell activation during hair regeneration. *Nature*, 451, 340-4.
- PONCHIO, L., DUMA, L., OLIVIERO, B., GIBELLI, N., PEDRAZZOLI, P. & ROBUSTELLI DELLA CUNA, G. 2000. Mitomycin C as an alternative to irradiation to inhibit the feeder layer growth in long-term culture assays. *Cytotherapy*, 2, 281-6.
- PORTER, R. M., CORDEN, L. D., LUNNY, D. P., SMITH, F. J., LANE, E. B. & MCLEAN, W. H. 2001. Keratin K6irs is specific to the inner root sheath of hair follicles in mice and humans. *Br J Dermatol*, 145, 558-68.
- PRINCIVALLE, A. P., PARKER, R. M., DOVER, T. J. & BARNES, N. M. 2012. Detection of mRNA encoding receptors by in situ and Northern hybridization. *Methods Mol Biol*, 897, 261-302.
- PROBER, J. M., TRAINOR, G. L., DAM, R. J., HOBBS, F. W., ROBERTSON, C. W., ZAGURSKY, R. J., COCUZZA, A. J., JENSEN, M. A. & BAUMEISTER, K. 1987. A system for rapid DNA sequencing with fluorescent chain-terminating dideoxynucleotides. *Science*, 238, 336-41.

- PROKSCH, E., BRANDNER, J. M. & JENSEN, J. M. 2008. The skin: an indispensable barrier. *Exp Dermatol*, 17, 1063-72.
- PUMMILA, M., FLINIAUX, I., JAATINEN, R., JAMES, M. J., LAURIKKALA, J., SCHNEIDER, P., THESLEFF, I. & MIKKOLA, M. L. 2007. Ectodysplasin has a dual role in ectodermal organogenesis: inhibition of Bmp activity and induction of Shh expression. *Development*, 134, 117-25.
- QI, H. & PEI, D. 2007. The magic of four: induction of pluripotent stem cells from somatic cells by Oct4, Sox2, Myc and Klf4. *Cell Res*. England.
- RAHAMAN, S. O., HARBOR, P. C., CHERNOVA, O., BARNETT, G. H., VOGELBAUM, M. A. & HAQUE, S. J. 2002. Inhibition of constitutively active Stat3 suppresses proliferation and induces apoptosis in glioblastoma multiforme cells. *Oncogene*, 21, 8404-13.
- RAHMANI, W., ABBASI, S., HAGNER, A., RAHARJO, E., KUMAR, R., HOTTA, A., MAGNESS, S., METZGER, D. & BIERNASKIE, J. 2014. Hair follicle dermal stem cells regenerate the dermal sheath, repopulate the dermal papilla, and modulate hair type. *Dev Cell*, 31, 543-58.
- RAMALINGAM, P., PALANICHAMY, J. K., SINGH, A., DAS, P., BHAGAT, M., KASSAB, M. A., SINHA, S. & CHATTOPADHYAY, P. 2014. Biogenesis of intronic miRNAs located in clusters by independent transcription and alternative splicing. *Rna*, 20, 76-87.
- RAY, S. & LECHLER, T. 2011. Regulation of asymmetric cell division in the epidermis. *Cell Div*.
- REDDY, S., ANDL, T., BAGASRA, A., LU, M. M., EPSTEIN, D. J., MORRISEY, E. E. & MILLAR, S. E. 2001. Characterization of Wnt gene expression in developing and postnatal hair follicles and identification of Wnt5a as a target of Sonic hedgehog in hair follicle morphogenesis. *Mech Dev*, 107, 69-82.
- REINHART, B. J., SLACK, F. J., BASSON, M., PASQUINELLI, A. E., BETTINGER, J. C., ROUGVIE, A. E., HORVITZ, H. R. & RUVKUN, G. 2000. The 21-nucleotide let-7 RNA regulates developmental timing in *Caenorhabditis elegans*. *Nature*, 403, 901-6.
- RENDL, M., POLAK, L. & FUCHS, E. 2008. BMP signaling in dermal papilla cells is required for their hair follicle-inductive properties. *Genes Dev*, 22, 543-57.
- REZZA, A., SENNETT, R., TANGUY, M., CLAVEL, C. & RENDL, M. 2015. PDGF signalling in the dermis and in dermal condensates is dispensable for hair follicle induction and formation. *Exp Dermatol*, 24, 468-70.
- RHEE, H., POLAK, L. & FUCHS, E. 2006. Lhx2 maintains stem cell character in hair follicles. *Science*, 312, 1946-9.
- RHEINWALD, J. G. & GREEN, H. 1975. Serial cultivation of strains of human epidermal keratinocytes: the formation of keratinizing colonies from single cells. *Cell*, 6, 331-43.
- RICHARDSON, R. & HAMMERSCHMIDT, M. 2018. The role of Rho kinase (Rock) in re-epithelialization of adult zebrafish skin wounds. *Small GTPases*, 9, 230-236.
- RIPPA, A. L., KALABUSHEVA, E. P. & VOROTELYAK, E. A. 2019. Regeneration of Dermis: Scarring and Cells Involved. *Cells*, 8.
- RISHIKAYSH, P., DEV, K., DIAZ, D., QURESHI, W. M., FILIP, S. & MOKRY, J. 2014. Signaling involved in hair follicle morphogenesis and development. *Int J Mol Sci*, 15, 1647-70.
- RISSLAND, O. S., HONG, S. J. & BARTEL, D. P. 2011. MicroRNA destabilization enables dynamic regulation of the miR-16 family in response to cell-cycle changes. *Mol Cell*, 43, 993-1004.
- RITTIÉ, L., STOLL, S. W., KANG, S., VOORHEES, J. J. & FISHER, G. J. 2009. Hedgehog signaling maintains hair follicle stem cell phenotype in young and aged human skin. *Aging Cell*, 8, 738-51.
- ROMANO, R. A., BIRKAYA, B. & SINHA, S. 2007. A functional enhancer of keratin14 is a direct transcriptional target of deltaNp63. *J Invest Dermatol*, 127, 1175-86.
- ROMANO, R. A., SMALLEY, K., LIU, S. & SINHA, S. 2010. Abnormal hair follicle development and altered cell fate of follicular keratinocytes in transgenic mice expressing DeltaNp63alpha. *Development*, 137, 1431-9.
- RUBY, J. G., JAN, C. H. & BARTEL, D. P. 2007. Intronic microRNA precursors that bypass Drosha processing. *Nature*, 448, 83-6.

- RÜCKERT, R., LINDNER, G., BULFONE-PAUS, S. & PAUS, R. 2000. High-dose proinflammatory cytokines induce apoptosis of hair bulb keratinocytes in vivo. *Br J Dermatol*, 143, 1036-9.
- SAKUMA, T. H. & MAIBACH, H. I. 2012. Oily skin: an overview. *Skin Pharmacol Physiol*, 25, 227-35.
- SANDILANDS, A., SUTHERLAND, C., IRVINE, A. D. & MCLEAN, W. H. 2009. Filaggrin in the frontline: role in skin barrier function and disease. *J Cell Sci*, 122, 1285-94.
- SANGER, F., NICKLEN, S. & COULSON, A. R. 1977. DNA sequencing with chain-terminating inhibitors. *Proc Natl Acad Sci U S A*, 74, 5463-7.
- SANZ-MORENO, V., GAGGIOLI, C., YEO, M., ALBRENGUES, J., WALLBERG, F., VIROS, A., HOOPER, S., MITTER, R., FÉRAL, C. C., COOK, M., LARKIN, J., MARAIS, R., MENEGUZZI, G., SAHAI, E. & MARSHALL, C. J. 2011. ROCK and JAK1 signaling cooperate to control actomyosin contractility in tumor cells and stroma. *Cancer Cell*, 20, 229-45.
- SATO, N., LEOPOLD, P. L. & CRYSTAL, R. G. 1999. Induction of the hair growth phase in postnatal mice by localized transient expression of Sonic hedgehog. *J Clin Invest*, 104, 855-64.
- SATO, T., VRIES, R. G., SNIPPERT, H. J., VAN DE WETERING, M., BARKER, N., STANGE, D. E., VAN ES, J. H., ABO, A., KUJALA, P., PETERS, P. J. & CLEVERS, H. 2009. Single Lgr5 stem cells build crypt-villus structures in vitro without a mesenchymal niche. *Nature*, 459, 262-5.
- SAXENA, N., MOK, K. W. & RENDL, M. 2019. An updated classification of hair follicle morphogenesis. *Exp Dermatol*, 28, 332-344.
- SCHMIDT, B. & HORSLEY, V. 2012. Unravelling hair follicle-adipocyte communication. *Exp Dermatol*, 21, 827-30.
- SCHMIDT-ULLRICH, R., AEBISCHER, T., HÜLSKEN, J., BIRCHMEIER, W., KLEMM, U. & SCHEIDEREIT, C. 2001. Requirement of NF-kappaB/Rel for the development of hair follicles and other epidermal appendices. *Development*, 128, 3843-53.
- SCHMIDT-ULLRICH, R. & PAUS, R. 2005. Molecular principles of hair follicle induction and morphogenesis. *Bioessays*, 27, 247-61.
- SCHMIDT-ULLRICH, R., TOBIN, D. J., LENHARD, D., SCHNEIDER, P., PAUS, R. & SCHEIDEREIT, C. 2006. NF-kappaB transmits Eda A1/EdaR signalling to activate Shh and cyclin D1 expression, and controls post-initiation hair placode down growth. *Development*, 133, 1045-57.
- SCHNEIDER, M. R. 2012. MicroRNAs as novel players in skin development, homeostasis and disease. *Br J Dermatol*, 166, 22-8.
- SCHNEIDER, M. R. & PAUS, R. 2014. Deciphering the functions of the hair follicle infundibulum in skin physiology and disease. *Cell Tissue Res*, 358, 697-704.
- SCHNEIDER, M. R., SCHMIDT-ULLRICH, R. & PAUS, R. 2009. The hair follicle as a dynamic miniorgan. *Curr Biol*, 19, R132-42.
- SCHWARZ, D. S., HUTVÁGNER, G., DU, T., XU, Z., ARONIN, N. & ZAMORE, P. D. 2003. Asymmetry in the assembly of the RNAi enzyme complex. *Cell*, 115, 199-208.
- SCHWEIZER, J., LANGBEIN, L., ROGERS, M. A. & WINTER, H. 2007. Hair follicle-specific keratins and their diseases. *Exp Cell Res*, 313, 2010-20.
- SENNETT, R. & RENDL, M. 2012. Mesenchymal-epithelial interactions during hair follicle morphogenesis and cycling. *Semin Cell Dev Biol*, 23, 917-27.
- SENNETT, R., WANG, Z., REZZA, A., GRISANTI, L., ROITERSHTEIN, N., SICCHIO, C., MOK, K. W., HEITMAN, NICHOLAS J., CLAVEL, C., MA'AYAN, A. & RENDL, M. 2015. An Integrated Transcriptome Atlas of Embryonic Hair Follicle Progenitors, Their Niche, and the Developing Skin. *Developmental Cell*, 34, 577-591.
- SEQUEIRA, I. & NICOLAS, J. F. 2012. Redefining the structure of the hair follicle by 3D clonal analysis. *Development*. England.
- SERRE, C., BUSUTTIL, V. & BOTTO, J. M. 2018. Intrinsic and extrinsic regulation of human skin melanogenesis and pigmentation. *Int J Cosmet Sci*, 40, 328-347.
- SHI, C., ZHANG, M., TONG, M., YANG, L., PANG, L., CHEN, L., XU, G., CHI, X., HONG, Q., NI, Y., JI, C. & GUO, X. 2015. miR-148a is Associated with Obesity and Modulates Adipocyte Differentiation of Mesenchymal Stem Cells through Wnt Signaling. *Sci Rep*, 5, 9930.

- SHI, J., WU, X., SURMA, M., VEMULA, S., ZHANG, L., YANG, Y., KAPUR, R. & WEI, L. 2013. Distinct roles for ROCK1 and ROCK2 in the regulation of cell detachment. *Cell Death Dis*, 4, e483.
- SHI, W., HUANG, Q., XIE, J., WANG, H., YU, X. & ZHOU, Y. 2020. CKS1B as Drug Resistance-Inducing Gene-A Potential Target to Improve Cancer Therapy. *Front Oncol*, 10, 582451.
- SHWARTZ, Y., GONZALEZ-CELEIRO, M., CHEN, C. L., PASOLLI, H. A., SHEU, S. H., FAN, S. M., SHAMSI, F., ASSAAD, S., LIN, E. T., ZHANG, B., TSAI, P. C., HE, M., TSENG, Y. H., LIN, S. J. & HSU, Y. C. 2020. Cell Types Promoting Goosebumps Form a Niche to Regulate Hair Follicle Stem Cells. *Cell*, 182, 578-593.e19.
- SINGH, L. & JONES, K. W. 1984. The use of heparin as a simple cost-effective means of controlling background in nucleic acid hybridization procedures. *Nucleic Acids Res*, 12, 5627-38.
- SINGH, S., ELENIO, E., LEU, N. A., ROMANO, R. A., VAUGHAN, A. E., DERISO, J., SURENDRAN, K. & CHAKRABARTI, R. 2019. A new Elf5(Cre) (ERT) (2-) (GFP) BAC transgenic mouse model for tracing Elf5 cell lineages in adult tissues. *FEBS Lett*, 593, 1030-1039.
- SLEZAK-PROCHAZKA, I., KLUIVER, J., DE JONG, D., KORTMAN, G., HALSEMA, N., POPPEMA, S., KROESEN, B. J. & VAN DEN BERG, A. 2013. Cellular localization and processing of primary transcripts of exonic microRNAs. *PLoS One*, 8, e76647.
- SLOMINSKI, A., WORTSMAN, J., PLONKA, P. M., SCHALLREUTER, K. U., PAUS, R. & TOBIN, D. J. 2005. Hair follicle pigmentation. *J Invest Dermatol*, 124, 13-21.
- SMART, I. H. 1970. Variation in the plane of cell cleavage during the process of stratification in the mouse epidermis. *Br J Dermatol*, 82, 276-82.
- SMITH, P. K., KROHN, R. I., HERMANSON, G. T., MALLIA, A. K., GARTNER, F. H., PROVENZANO, M. D., FUJIMOTO, E. K., GOEKE, N. M., OLSON, B. J. & KLENK, D. C. 1985. Measurement of protein using bicinchoninic acid. *Anal Biochem*, 150, 76-85.
- SNIPPERT, H. J., HAEGEBARTH, A., KASPER, M., JAKS, V., VAN ES, J. H., BARKER, N., VAN DE WETERING, M., VAN DEN BORN, M., BEGTHEL, H., VRIES, R. G., STANGE, D. E., TOFTGÅRD, R. & CLEVERS, H. 2010. Lgr6 marks stem cells in the hair follicle that generate all cell lineages of the skin. *Science*, 327, 1385-9.
- SONKOLY, E., STÅHLE, M. & PIVARCSI, A. 2008. MicroRNAs and immunity: novel players in the regulation of normal immune function and inflammation. *Semin Cancer Biol*, 18, 131-40.
- SORRELL, J. M. & CAPLAN, A. I. 2004. Fibroblast heterogeneity: more than skin deep. *J Cell Sci*, 117, 667-75.
- SRIVASTAVA, A., NIKAMO, P., LOHCHAROENKAL, W., LI, D., MEISGEN, F., XU LANDÉN, N., STÅHLE, M., PIVARCSI, A. & SONKOLY, E. 2017. MicroRNA-146a suppresses IL-17-mediated skin inflammation and is genetically associated with psoriasis. *J Allergy Clin Immunol*, 139, 550-561.
- SRIVASTAVA, A. K., PISPA, J., HARTUNG, A. J., DU, Y., EZER, S., JENKS, T., SHIMADA, T., PEKKANEN, M., MIKKOLA, M. L., KO, M. S., THESLEFF, I., KERE, J. & SCHLESSINGER, D. 1997. The Tabby phenotype is caused by mutation in a mouse homologue of the EDA gene that reveals novel mouse and human exons and encodes a protein (ectodysplasin-A) with collagenous domains. *Proc Natl Acad Sci U S A*, 94, 13069-74.
- ST-JACQUES, B., DASSULE, H. R., KARAVANOVA, I., BOTCHKAREV, V. A., LI, J., DANIELIAN, P. S., MCMAHON, J. A., LEWIS, P. M., PAUS, R. & MCMAHON, A. P. 1998. Sonic hedgehog signaling is essential for hair development. *Curr Biol*, 8, 1058-68.
- STACEY, D. W. 2003. Cyclin D1 serves as a cell cycle regulatory switch in actively proliferating cells. *Curr Opin Cell Biol*, 15, 158-63.
- STARK, A., BRENNECKE, J., BUSHATI, N., RUSSELL, R. B. & COHEN, S. M. 2005. Animal MicroRNAs confer robustness to gene expression and have a significant impact on 3'UTR evolution. *Cell*, 123, 1133-46.
- STRUTT, D. 2001. Planar polarity: getting ready to ROCK. *Curr Biol*, 11, R506-9.
- SUZUKI, S., OTA, Y., OZAWA, K. & IMAMURA, T. 2000. Dual-mode regulation of hair growth cycle by two Fgf-5 gene products. *J Invest Dermatol*, 114, 456-63.

- SWERDLOW, H. & GESTELAND, R. 1990. Capillary gel electrophoresis for rapid, high resolution DNA sequencing. *Nucleic Acids Res*, 18, 1415-9.
- TADEU, A. M. & HORSLEY, V. 2013. Notch signaling represses p63 expression in the developing surface ectoderm. *Development*, 140, 3777-86.
- TAGANOV, K. D., BOLDIN, M. P., CHANG, K. J. & BALTIMORE, D. 2006. NF-kappaB-dependent induction of microRNA miR-146, an inhibitor targeted to signaling proteins of innate immune responses. *Proc Natl Acad Sci U S A*, 103, 12481-6.
- TAKEDA, N., JAIN, R., LEOEUF, M. R., PADMANABHAN, A., WANG, Q., LI, L., LU, M. M., MILLAR, S. E. & EPSTEIN, J. A. 2013. Hopx expression defines a subset of multipotent hair follicle stem cells and a progenitor population primed to give rise to K6+ niche cells. *Development*, 140, 1655-64.
- TAKESHITA, F., MINAKUCHI, Y., NAGAHARA, S., HONMA, K., SASAKI, H., HIRAI, K., TERATANI, T., NAMATAME, N., YAMAMOTO, Y., HANAI, K., KATO, T., SANO, A. & OCHIYA, T. 2005. Efficient delivery of small interfering RNA to bone-metastatic tumors by using atelocollagen in vivo. *Proceedings of the National Academy of Sciences of the United States of America*, 102, 12177-12182.
- TAN, G. C., CHAN, E., MOLNAR, A., SARKAR, R., ALEXIEVA, D., ISA, I. M., ROBINSON, S., ZHANG, S., ELLIS, P., LANGFORD, C. F., GUILLOT, P. V., CHANDRASHEKRAN, A., FISK, N. M., CASTELLANO, L., MEISTER, G., WINSTON, R. M., CUI, W., BAULCOMBE, D. & DIBB, N. J. 2014. 5' isomiR variation is of functional and evolutionary importance. *Nucleic Acids Res*, 42, 9424-35.
- TAN, Y., LU, X., CHENG, Z., PAN, G., LIU, S., APIZIAI, P., WANG, H., ZHANG, J. & ABULIMITI, Y. 2020. miR-148a Regulates the Stem Cell-Like Side Populations Distribution by Affecting the Expression of ACVR1 in Esophageal Squamous Cell Carcinoma. *Oncotargets Ther*, 13, 8079-8094.
- TARUTANI, M., NAKAJIMA, K., UCHIDA, Y., TAKAISHI, M., GOTO-INOUE, N., IKAWA, M., SETOU, M., KINOSHITA, T., ELIAS, P. M., SANO, S. & MAEDA, Y. 2012. GPHR-dependent functions of the Golgi apparatus are essential for the formation of lamellar granules and the skin barrier. *J Invest Dermatol*, 132, 2019-25.
- TEN DIJKE, P. & ARTHUR, H. M. 2007. Extracellular control of TGFbeta signalling in vascular development and disease. *Nat Rev Mol Cell Biol*, 8, 857-69.
- TETA, M., CHOI, Y. S., OKEGBE, T., WONG, G., TAM, O. H., CHONG, M. M., SEYKORA, J. T., NAGY, A., LITTMAN, D. R., ANDL, T. & MILLAR, S. E. 2012. Inducible deletion of epidermal Dicer and Drosha reveals multiple functions for miRNAs in postnatal skin. *Development*, 139, 1405-16.
- THARAKAN, S., PONTIGGIA, L., BIEDERMANN, T., BOTTCHEH-HABERZETH, S., SCHIESTL, C., REICHMANN, E. & MEULI, M. 2010. Transglutaminases, involucrin, and loricrin as markers of epidermal differentiation in skin substitutes derived from human sweat gland cells. *Pediatr Surg Int*, 26, 71-7.
- THOLPADY, S. S., DEGEORGE, B. R., JR. & CAMPBELL, C. A. 2014. The effect of local rho-kinase inhibition on murine wound healing. *Ann Plast Surg*, 72, S213-9.
- THOMAS, M. F., ABDUL-WAJID, S., PANDURO, M., BABIARZ, J. E., RAJARAM, M., WOODRUFF, P., LANIER, L. L., HEISSMEYER, V. & ANSEL, K. M. 2012. Eri1 regulates microRNA homeostasis and mouse lymphocyte development and antiviral function. *Blood*, 120, 130-42.
- THOMSON, J. M., PARKER, J. S. & HAMMOND, S. M. 2007. Microarray Analysis of miRNA Gene Expression. *Methods in Enzymology*. Academic Press.
- TIMIS, T. L. & ORASAN, R. I. 2018. Understanding psoriasis: Role of miRNAs. *Biomed Rep*, 9, 367-374.
- TING-BERRETH, S. A. & CHUONG, C. M. 1996. Sonic Hedgehog in feather morphogenesis: induction of mesenchymal condensation and association with cell death. *Dev Dyn*, 207, 157-70.
- TOBIN, D. J. 2006. Biochemistry of human skin--our brain on the outside. *Chem Soc Rev*, 35, 52-67.
- TOBIN, D. J., GUNIN, A., MAGERL, M., HANDIJSKI, B. & PAUS, R. 2003. Plasticity and cytokinetic dynamics of the hair follicle mesenchyme: implications for hair growth control. *J Invest Dermatol*, 120, 895-904.

- TOMÉ, M., LÓPEZ-ROMERO, P., ALBO, C., SEPÚLVEDA, J. C., FERNÁNDEZ-GUTIÉRREZ, B., DOPAZO, A., BERNAD, A. & GONZÁLEZ, M. A. 2011. miR-335 orchestrates cell proliferation, migration and differentiation in human mesenchymal stem cells. *Cell Death Differ*, 18, 985-95.
- TONG, X. & COULOMBE, P. A. 2006. Keratin 17 modulates hair follicle cycling in a TNF α -dependent fashion. *Genes Dev*, 20, 1353-64.
- TREIBER, T., TREIBER, N. & MEISTER, G. 2018. Author Correction: Regulation of microRNA biogenesis and its crosstalk with other cellular pathways. *Nat Rev Mol Cell Biol*. England.
- TREMPUS, C. S., MORRIS, R. J., BORTNER, C. D., COTSARELIS, G., FAIRCLOTH, R. S., REECE, J. M. & TENNANT, R. W. 2003. Enrichment for living murine keratinocytes from the hair follicle bulge with the cell surface marker CD34. *J Invest Dermatol*, 120, 501-11.
- TRIEL, C., VESTERGAARD, M. E., BOLUND, L., JENSEN, T. G. & JENSEN, U. B. 2004. Side population cells in human and mouse epidermis lack stem cell characteristics. *Exp Cell Res*, 295, 79-90.
- TUMBAR, T., GUASCH, G., GRECO, V., BLANPAIN, C., LOWRY, W. E., RENDL, M. & FUCHS, E. 2004. Defining the epithelial stem cell niche in skin. *Science*, 303, 359-63.
- TUMMALA, R. & SINHA, S. 2006. Differentiation-specific transcriptional regulation of the ESE-2 gene by a novel keratinocyte-restricted factor. *J Cell Biochem*, 97, 766-81.
- TÓTH, B. I., OLÁH, A., SZÖLLOSI, A. G., CZIFRA, G. & BÍRÓ, T. 2011. "Sebocytes' makeup": novel mechanisms and concepts in the physiology of the human sebaceous glands. *Pflugers Arch*, 461, 593-606.
- VALENCIA-SANCHEZ, M. A., LIU, J., HANNON, G. J. & PARKER, R. 2006. Control of translation and mRNA degradation by miRNAs and siRNAs. *Genes Dev*, 20, 515-24.
- VAUGHAN, F. L., KASS, L. L. & UZMAN, J. A. 1981. Requirement of hydrocortisone and insulin for extended proliferation and passage of rat keratinocytes. *In Vitro*, 17, 941-6.
- VEERIAH, S., BRENNAN, C., MENG, S., SINGH, B., FAGIN, J. A., SOLIT, D. B., PATY, P. B., ROHLE, D., VIVANCO, I., CHMIELECKI, J., PAO, W., LADANYI, M., GERALD, W. L., LIAU, L., CLOUGHESY, T. C., MISCHEL, P. S., SANDER, C., TAYLOR, B., SCHULTZ, N., MAJOR, J., HEGUY, A., FANG, F., MELLINGHOFF, I. K. & CHAN, T. A. 2009. The tyrosine phosphatase PTPRD is a tumor suppressor that is frequently inactivated and mutated in glioblastoma and other human cancers. *Proc Natl Acad Sci U S A*, 106, 9435-40.
- VENIAMINOVA, N. A., VAGNOZZI, A. N., KOPINKE, D., DO, T. T., MURTAUGH, L. C., MAILLARD, I., DLUGOSZ, A. A., REITER, J. F. & WONG, S. Y. 2013. Keratin 79 identifies a novel population of migratory epithelial cells that initiates hair canal morphogenesis and regeneration. *Development*, 140, 4870-80.
- VIDAL, V. P., CHABOISSIER, M. C., LÜTZKENDORF, S., COTSARELIS, G., MILL, P., HUI, C. C., ORTONNE, N., ORTONNE, J. P. & SCHEDL, A. 2005. Sox9 is essential for outer root sheath differentiation and the formation of the hair stem cell compartment. *Curr Biol*, 15, 1340-51.
- VILLANI, R. M., AKYUZ, M. D., NIESSEN, M. T. & NIESSEN, C. M. 2013. Analysis of bulge stem cells from the epidermis using flow cytometry. *Methods Mol Biol*, 989, 33-43.
- WAIKEL, R. L., KAWACHI, Y., WAIKEL, P. A., WANG, X. J. & ROOP, D. R. 2001. Deregulated expression of c-Myc depletes epidermal stem cells. *Nat Genet*, 28, 165-8.
- WAN, X., CHENG, Q., PENG, R., MA, Z., CHEN, Z., CAO, Y. & JIANG, B. 2014. ROCK1, a novel target of miR-145, promotes glioma cell invasion. *Mol Med Rep*, 9, 1877-82.
- WANG, A. B., ZHANG, Y. V. & TUMBAR, T. 2017. Gata6 promotes hair follicle progenitor cell renewal by genome maintenance during proliferation. *Embo j*, 36, 61-78.
- WANG, C., SHAO, S., DENG, L., WANG, S. & ZHANG, Y. 2020. LncRNA SNHG12 regulates the radiosensitivity of cervical cancer through the miR-148a/CDK1 pathway. *Cancer Cell Int*, 20, 554.
- WANG, D., ZHANG, Z., O'LOUGHLIN, E., WANG, L., FAN, X., LAI, E. C. & YI, R. 2013a. MicroRNA-205 controls neonatal expansion of skin stem cells by modulating the PI(3)K pathway. *Nat Cell Biol*, 15, 1153-63.

- WANG, L. C., LIU, Z. Y., GAMBARDELLA, L., DELACOUR, A., SHAPIRO, R., YANG, J., SIZING, I., RAYHORN, P., GARBER, E. A., BENJAMIN, C. D., WILLIAMS, K. P., TAYLOR, F. R., BARRANDON, Y., LING, L. & BURKLY, L. C. 2000. Regular articles: conditional disruption of hedgehog signaling pathway defines its critical role in hair development and regeneration. *J Invest Dermatol*, 114, 901-8.
- WANG, N., ZHENG, J., CHEN, Z., LIU, Y., DURA, B., KWAK, M., XAVIER-FERRUCIO, J., LU, Y. C., ZHANG, M., RODEN, C., CHENG, J., KRAUSE, D. S., DING, Y., FAN, R. & LU, J. 2019a. Single-cell microRNA-mRNA co-sequencing reveals non-genetic heterogeneity and mechanisms of microRNA regulation. *Nat Commun*, 10, 95.
- WANG, S. H., LI, X., ZHOU, L. S., CAO, Z. W., SHI, C., ZHOU, C. Z., WEN, Y. G., SHEN, Y. & LI, J. K. 2013b. microRNA-148a suppresses human gastric cancer cell metastasis by reversing epithelial-to-mesenchymal transition. *Tumour Biol*, 34, 3705-12.
- WANG, Y., JURANEK, S., LI, H., SHENG, G., WARDLE, G. S., TUSCHL, T. & PATEL, D. J. 2009. Nucleation, propagation and cleavage of target RNAs in Ago silencing complexes. *Nature*, 461, 754-61.
- WANG, Z., ZHANG, X., LI, Z., ABDALLA, B. A., CHEN, Y. & NIE, Q. 2019b. MiR-34b-5p Mediates the Proliferation and Differentiation of Myoblasts by Targeting IGFBP2. *Cells*, 8.
- WATANABE, K., UENO, M., KAMIYA, D., NISHIYAMA, A., MATSUMURA, M., WATAYA, T., TAKAHASHI, J. B., NISHIKAWA, S., MUGURUMA, K. & SASAI, Y. 2007. A ROCK inhibitor permits survival of dissociated human embryonic stem cells. *Nat Biotechnol*, 25, 681-6.
- WATT, F. M. 2002. Role of integrins in regulating epidermal adhesion, growth and differentiation. *Embo j*, 21, 3919-26.
- WATT, F. M., FRYE, M. & BENITAH, S. A. 2008. MYC in mammalian epidermis: how can an oncogene stimulate differentiation? *Nat Rev Cancer*.
- WEI, T., ORFANIDIS, K., XU, N., JANSON, P., STÅHLE, M., PIVARCSI, A. & SONKOLY, E. 2010. The expression of microRNA-203 during human skin morphogenesis. *Exp Dermatol*. Denmark.
- WEI, Z., YANG, Y., ZHANG, P., ANDRIANAKOS, R., HASEGAWA, K., LYU, J., CHEN, X., BAI, G., LIU, C., PERA, M. & LU, W. 2009. Klf4 interacts directly with Oct4 and Sox2 to promote reprogramming. *Stem Cells*, 27, 2969-78.
- WILLIAMS, J. G. 2000. STAT signalling in cell proliferation and in development. *Curr Opin Genet Dev*, 10, 503-7.
- WILSON, P. A. & HEMMATI-BRIVANLOU, A. 1995. Induction of epidermis and inhibition of neural fate by Bmp-4. *Nature*, 376, 331-3.
- WILSON, S. I., RYDSTRÖM, A., TRIMBORN, T., WILLERT, K., NUSSE, R., JESSELL, T. M. & EDLUND, T. 2001. The status of Wnt signalling regulates neural and epidermal fates in the chick embryo. *Nature*, 411, 325-30.
- WINTER, J., JUNG, S., KELLER, S., GREGORY, R. I. & DIEDERICHS, S. 2009. Many roads to maturity: microRNA biogenesis pathways and their regulation. *Nat Cell Biol*, 11, 228-34.
- WOO, W. M. & ORO, A. E. 2011. SnapShot: hair follicle stem cells. *Cell*, 146, 334-334.e2.
- WOO, W. M., ZHEN, H. H. & ORO, A. E. 2012. Shh maintains dermal papilla identity and hair morphogenesis via a Noggin-Shh regulatory loop. *Genes Dev*, 26, 1235-46.
- WOODLEY, D. T. 2017. Distinct Fibroblasts in the Papillary and Reticular Dermis: Implications for Wound Healing. *Dermatol Clin*, 35, 95-100.
- WU, P., ZHANG, Y., XING, Y., XU, W., GUO, H., DENG, F., MA, X. & LI, Y. 2019. The balance of Bmp6 and Wnt10b regulates the telogen-anagen transition of hair follicles. *Cell Commun Signal*, 17, 16.
- WU, S., HUANG, S., DING, J., ZHAO, Y., LIANG, L., LIU, T., ZHAN, R. & HE, X. 2010a. Multiple microRNAs modulate p21Cip1/Waf1 expression by directly targeting its 3' untranslated region. *Oncogene*, 29, 2302-8.
- WU, T., ZHANG, X., HUANG, X., YANG, Y. & HUA, X. 2010b. Regulation of cyclin B2 expression and cell cycle G2/m transition by menin. *J Biol Chem*, 285, 18291-300.

- WU, Y., LIU, L., BIAN, C., DIAO, Q., NISAR, M. F., JIANG, X., BARTSCH, J. W., ZHONG, M., HU, X. & ZHONG, J. L. 2018. MicroRNA let-7b inhibits keratinocyte differentiation by targeting IL-6 mediated ERK signaling in psoriasis. *Cell Commun Signal*, 16, 58.
- XHEMALCE, B., ROBSON, S. C. & KOUZARIDES, T. 2012. Human RNA methyltransferase BCDIN3D regulates microRNA processing. *Cell*, 151, 278-88.
- XING, Y., MA, X., GUO, H., DENG, F., YANG, J. & LI, Y. 2016. Wnt5a Suppresses β -catenin Signaling during Hair Follicle Regeneration. *Int J Med Sci*, 13, 603-10.
- XING, Y. Z., WANG, R. M., YANG, K., GUO, H. Y., DENG, F., LI, Y. H., YE, J. X., HE, L., LIAN, X. H. & YANG, T. 2013. Adenovirus-mediated Wnt5a expression inhibits the telogen-to-anagen transition of hair follicles in mice. *Int J Med Sci*, 10, 908-14.
- XU, Y., HAN, Y. F., ZHU, S. J., DONG, J. D. & YE, B. 2017. miRNA-148a inhibits cell growth of papillary thyroid cancer through STAT3 and PI3K/AKT signaling pathways. *Oncol Rep*, 38, 3085-3093.
- YAMAMIZU, K., PIAO, Y., SHAROV, A. A., ZSIROS, V., YU, H., NAKAZAWA, K., SCHLESSINGER, D. & KO, M. S. 2013. Identification of transcription factors for lineage-specific ESC differentiation. *Stem Cell Reports*, 1, 545-59.
- YANAGI, T., HATA, H., MIZUNO, E., KITAMURA, S., IMAFUKU, K., NAKAZATO, S., WANG, L., NISHIHARA, H., TANAKA, S. & SHIMIZU, H. 2017. PCTAIRE1/CDK16/PCTK1 is overexpressed in cutaneous squamous cell carcinoma and regulates p27 stability and cell cycle. *J Dermatol Sci*, 86, 149-157.
- YANG, A., SCHWEITZER, R., SUN, D., KAGHAD, M., WALKER, N., BRONSON, R. T., TABIN, C., SHARPE, A., CAPUT, D., CRUM, C. & MCKEON, F. 1999. p63 is essential for regenerative proliferation in limb, craniofacial and epithelial development. *Nature*, 398, 714-8.
- YANG, J. S., MAURIN, T., ROBINE, N., RASMUSSEN, K. D., JEFFREY, K. L., CHANDWANI, R., PAPAPETROU, E. P., SADELAIN, M., O'CARROLL, D. & LAI, E. C. 2010. Conserved vertebrate mir-451 provides a platform for Dicer-independent, Ago2-mediated microRNA biogenesis. *Proc Natl Acad Sci U S A*, 107, 15163-8.
- YI, R. & FUCHS, E. 2010. MicroRNA-mediated control in the skin. *Cell Death Differ*, 17, 229-35.
- YI, R., O'CARROLL, D., PASOLLI, H. A., ZHANG, Z., DIETRICH, F. S., TARAKHOVSKY, A. & FUCHS, E. 2006. Morphogenesis in skin is governed by discrete sets of differentially expressed microRNAs. *Nat Genet*, 38, 356-62.
- YI, R., PASOLLI, H. A., LANDTHALER, M., HAFNER, M., OJO, T., SHERIDAN, R., SANDER, C., O'CARROLL, D., STOFFEL, M., TUSCHL, T. & FUCHS, E. 2009. DGCR8-dependent microRNA biogenesis is essential for skin development. *Proc Natl Acad Sci U S A*, 106, 498-502.
- YI, R., POY, M. N., STOFFEL, M. & FUCHS, E. 2008. A skin microRNA promotes differentiation by repressing 'stemness'. *Nature*, 452, 225-9.
- YI, R., QIN, Y., MACARA, I. G. & CULLEN, B. R. 2003. Exportin-5 mediates the nuclear export of pre-microRNAs and short hairpin RNAs. *Genes Dev*, 17, 3011-6.
- YIN, H., HE, H., CAO, X., SHEN, X., HAN, S., CUI, C., ZHAO, J., WEI, Y., CHEN, Y., XIA, L., WANG, Y., LI, D. & ZHU, Q. 2020. MiR-148a-3p Regulates Skeletal Muscle Satellite Cell Differentiation and Apoptosis via the PI3K/AKT Signaling Pathway by Targeting Meox2. *Front Genet*, 11, 512.
- YU, K. R., YANG, S. R., JUNG, J. W., KIM, H., KO, K., HAN, D. W., PARK, S. B., CHOI, S. W., KANG, S. K., SCHÖLER, H. & KANG, K. S. 2012. CD49f enhances multipotency and maintains stemness through the direct regulation of OCT4 and SOX2. *Stem Cells*, 30, 876-87.
- ZHANG, H., KOLB, F. A., JASKIEWICZ, L., WESTHOF, E. & FILIPOWICZ, W. 2004. Single processing center models for human Dicer and bacterial RNase III. *Cell*, 118, 57-68.
- ZHANG, H., NAN, W., WANG, S., ZHANG, T., SI, H., YANG, F. & LI, G. 2016. Epidermal Growth Factor Promotes Proliferation and Migration of Follicular Outer Root Sheath Cells via Wnt/ β -Catenin Signaling. *Cell Physiol Biochem*, 39, 360-70.
- ZHANG, J., HE, X. C., TONG, W. G., JOHNSON, T., WIEDEMANN, L. M., MISHINA, Y., FENG, J. Q. & LI, L. 2006. Bone morphogenetic protein signaling inhibits hair follicle anagen induction by restricting epithelial stem/progenitor cell activation and expansion. *Stem Cells*, 24, 2826-39.

- ZHANG, J., YING, Z. Z., TANG, Z. L., LONG, L. Q. & LI, K. 2012. MicroRNA-148a promotes myogenic differentiation by targeting the ROCK1 gene. *J Biol Chem*, 287, 21093-101.
- ZHANG, L., STOKES, N., POLAK, L. & FUCHS, E. 2011. Specific microRNAs are preferentially expressed by skin stem cells to balance self-renewal and early lineage commitment. *Cell Stem Cell*, 8, 294-308.
- ZHANG, S., TANG, Q., XU, F., XUE, Y., ZHEN, Z., DENG, Y., LIU, M., CHEN, J., LIU, S., QIU, M., LIAO, Z., LI, Z., LUO, D., SHI, F., ZHENG, Y. & BI, F. 2009a. RhoA regulates G1-S progression of gastric cancer cells by modulation of multiple INK4 family tumor suppressors. *Mol Cancer Res*, 7, 570-80.
- ZHANG, Y., JIN, X. & WANG, J. 2019. miR-148a modulates the viability, migration and invasion of oral squamous cell carcinoma cells by regulating HLA-G expression. *Mol Med Rep*, 20, 795-801.
- ZHANG, Y., TOMANN, P., ANDL, T., GALLANT, N. M., HUELSKEN, J., JERCHOW, B., BIRCHMEIER, W., PAUS, R., PICCOLO, S., MIKKOLA, M. L., MORRISEY, E. E., OVERBEEK, P. A., SCHEIDEREIT, C., MILLAR, S. E. & SCHMIDT-ULLRICH, R. 2009b. Reciprocal requirements for EDA/EDAR/NF-kappaB and Wnt/beta-catenin signaling pathways in hair follicle induction. *Dev Cell*, 17, 49-61.
- ZHAO, A., YANG, L., MA, K., SUN, M., LI, L., HUANG, J., LI, Y., ZHANG, C., LI, H. & FU, X. 2016. Overexpression of cyclin D1 induces the reprogramming of differentiated epidermal cells into stem cell-like cells. *Cell Cycle*, 15, 644-53.
- ZHAO, Y., WANG, F., CHEN, S., WAN, J. & WANG, G. 2017. Methods of MicroRNA Promoter Prediction and Transcription Factor Mediated Regulatory Network. *Biomed Res Int*, 2017, 7049406.
- ZHENG, B., LIANG, L., WANG, C., HUANG, S., CAO, X., ZHA, R., LIU, L., JIA, D., TIAN, Q., WU, J., YE, Y., WANG, Q., LONG, Z., ZHOU, Y., DU, C., HE, X. & SHI, Y. 2011. MicroRNA-148a suppresses tumor cell invasion and metastasis by downregulating ROCK1 in gastric cancer. *Clin Cancer Res*, 17, 7574-83.
- ZHOU, J., CHEHAB, R., TKALCEVIC, J., NAYLOR, M. J., HARRIS, J., WILSON, T. J., TSAO, S., TELLIS, I., ZAVARSEK, S., XU, D., LAPINSKAS, E. J., VISVADER, J., LINDEMAN, G. J., THOMAS, R., ORMANDY, C. J., HERTZOG, P. J., KOLA, I. & PRITCHARD, M. A. 2005. Elf5 is essential for early embryogenesis and mammary gland development during pregnancy and lactation. *Embo j*, 24, 635-44.
- ZHOU, J., NG, A. Y., TYMMS, M. J., JERMIIN, L. S., SETH, A. K., THOMAS, R. S. & KOLA, I. 1998. A novel transcription factor, ELF5, belongs to the ELF subfamily of ETS genes and maps to human chromosome 11p13-15, a region subject to LOH and rearrangement in human carcinoma cell lines. *Oncogene*, 17, 2719-32.
- ZHOU, L., XU, Z., REN, X., CHEN, K. & XIN, S. 2016. MicroRNA-124 (MiR-124) Inhibits Cell Proliferation, Metastasis and Invasion in Colorectal Cancer by Downregulating Rho-Associated Protein Kinase 1(ROCK1). *Cell Physiol Biochem*, 38, 1785-95.
- ZHU, X. J., LIU, Y., DAI, Z. M., ZHANG, X., YANG, X., LI, Y., QIU, M., FU, J., HSU, W., CHEN, Y. & ZHANG, Z. 2014. BMP-FGF signaling axis mediates Wnt-induced epidermal stratification in developing mammalian skin. *PLoS Genet*, 10, e1004687.